Title
Improvements, Validation, and Applications of a Metaheuristic Optimization Method for Neutron Spectra Tailoring at the National Ignition Facility

Author
BOGETIC, SANDRA

Publication Date
2020

Peer reviewed|Thesis/dissertation

Improvements, Validation, and Applications of a Metaheuristic Optimization Method for Neutron Spectra Tailoring at the National Ignition Facility

by

Sandra Bogetic

A dissertation submitted in partial satisfaction of the

requirements for the degree of

Doctor of Philosophy

in

Engineering — Nuclear Engineering

in the

Graduate Division

of the

University of California, Berkeley

Committee in charge:

Professor Jasmina Vujić, Chair
Professor Lee Bernstein
Professor Phillip Colella
Dr. Lucile Dauffy

Spring 2020

Improvements, Validation, and Applications of a Metaheuristic Optimization Method for Neutron Spectra Tailoring at the National Ignition Facility

Abstract

Improvements, Validation, and Applications of a Metaheuristic Optimization Method for Neutron Spectra Tailoring at the National Ignition Facility

by

Sandra Bogetic

Doctor of Philosophy in Engineering — Nuclear Engineering

University of California, Berkeley

Professor Jasmina Vujić, Chair

Gnowee/COEUS v1.0 is a metaheuristic software package that has been developed at the University of California, Berkeley (UC Berkeley), in collaboration with Lawrence Livermore National Laboratory (LLNL), to design optimized Energy Tuning Assemblies (ETA). ETAs are designed in order to modify the neutron source spectrum and produce an objective spectrum given a large set of constraints and changeable variables. The software package is based on a general-purpose metaheuristic optimization algorithm, Gnowee, which uses COEUS to couple the algorithm to the the Monte Carlo N-Particle (MCNP) radiation transport package. The initial successful application, of the software package, was the design of a conical ETA to spectrally shape a simplified monoenergetic 14.1 MeV neutron point source to a thermonuclear and prompt fission neutron spectrum for technical nuclear forensics (TNF) purposes. Like TNF, many other applications in the nuclear engineering field require neutron energy distributions that cannot be obtained with currently available neutron sources. With an increased demand in neutron beam applications, numerous facilities, including the NIF, are interested in employing an accurate and efficient optimization design methodology, such as Gnowee/COEUS, to tailor available neutron spectra and intensity for specific requirements. The dissertation research included the following steps: (a) development of a fast and efficient optimization methodology and software package for tailoring neutron energy, (b) identification of the neutron transport simulation code package to be coupled with the optimization part, (c) experimental validation of optimization software package (d) applying the optimization package for specific ETA designs, and (e) performing simple experiments on specific ETA designs.

This dissertation describes further efforts made in developing and efforts that have been made in generating a generalized, problem independent Gnowee/COEUS v2.0. The new software package includes the ability to design an ETA within a high fidelity model of a neutron producing facility, with realistic source configurations, a wider range of possible

optimization functions, and a larger set of possible variables and constraints. The first part of the dissertation describes the improved COEUS v2.0 and the possibilities of applying the code to design ETAs within LLNL's National Ignition Facility (NIF) Target Chamber (TC). The improved modeling of the NIF TC environment by a set of Monte Carlo and deterministic codes is described, including the modeling and characterization of its system components and instrumentation, including Diagnostic Instrument Manipulator (DIM) 90-78, Target and Diagnostic Manipulator (TANDM) 90-348, SNOUT and large Target Option Activation Device (HTOADs) used for validation and ETA experiments. In addition, a detailed description of the activation foils used to cover a large range of neutron energy spectra is included, as well as the analysis and the unfolding techniques of the obtained experimental results. The second part of the dissertation focuses on the improvements and experimental validation of the full 3-D Monte Carlo model of the NIF Target Chamber. A discussion about various system errors and material uncertainties that could explain certain differences in modeling and experimental results is included. This thesis shows the ability of the newly developed software package to shape the NIF's high neutron flux output of a mainly monoenergetic 14.1 MeV neutron source peak, to an energy range including 8 to 10 MeV for integral benchmarking applications, or to highly peaked 8 or 10 keV spectra for a Boron Neutron Capture Therapy (BNCT) application. The final results provide a powerful demonstration of the tailoring capabilities of Gnowee/COEUS v2.0. This could allow various neutron producing facilities, such as the NIF, to expand their user base in various nuclear science and engineering applications, including detector characterization and calibration, study of radiation damage to various materials, cross section measurements for neutron activation studies, or medical applications such as BNCT or isotope separation.

To my late father,
I wish you were here to see what I've accomplished and what I'm planning for my future.

Contents

List of Figures

List of Tables

Acknowledgments

I would like to express my sincerest gratitude and thanks to everyone that has been involved in the completion of my Ph.D. degree. I would especially like to thank my advisor, Jasmina Vujić, for the opportunities she has given me as a student, and whose support, guidance, generosity and inclusiveness has made my experience at UC Berkeley the most enriching period in my life.

I also owe a debt of gratitude to Dr. Lucile Dauffy for her constant support, scientific guidance and enthusiastic encouragement on my research paths. I would also like to thank her for being a friend as well as a mentor. I thank both her and her husband for looking out for my future well being as well.

The thesis has been carried out in the framework of a collaboration and financial support with Lawrence Livermore National Laboratories. To all LLNL researchers that I collaborated with, I owe you a great debt for your invaluable contribution to this research. In particular, I am grateful to Dr. Dawn Shaughnessy for the years of funding my research and for her constant encouragement and inclusion. The experimental work would not have been possible without the assistance of the excellent radiochemistry group, who provided instrumentation and donated their knowledge and work for the experiments. Special thanks to Dr. Narek Gharibyan and Dr. Ken Moody, for their willingness to generously donate their time to help me, it has been very much appreciated. Also, the NIF campaign experiments were only possible thanks to the help and guidance of Dr. Charles Yeamans, to whom I owe a big debt for all the NIF scoping study and design process. Dr. Charles Yeamans provided valuable NIF shot planning expertise and without him the experimental part of this dissertation would not have been possible. I was fortunate enough to take part in 4 experimental campaigns at NIF and to have the opportunity to study some of the analyzed portions of the data. I am in debt for the incredible experience I gain from participating in those campaigns, both in terms of research fields that were not of my initial focus as radiochemistry, detectors, etc., and especially in opportunity to learn various necessary steps in designing, approving, building and performing actual experiments in a prestigious facility as NIF.

I owe a debt of gratitude to Dr. James Bevins, who provided me with the initial version of his optimization code and with his experience. Despite not being on my committee, Dr. James Bevins was incredibly valuable throughout this research and a key factor to my ability to understand and learn about optimization, neutron tailoring and fielding neutron activation experiments. I am fortunate to have had this opportunity to learn from him and his work during my time at UCB. I am in debt for his willingness to share his wealth of knowledge and to help me when I was stumped.

I have also been supported by a great dissertation and qualifying committee, which has contributed to my development and learning in ways above and beyond what I reasonably could have expected. Dr. Lee Bernstein was a great source of ideas, physics knowledge, and incredible positivity. A big thank you goes also to Dr. Ehud Greenspan, without whom I might not have had the opportunity to learn about the great Department of Nuclear Engineering at UC Berkeley, and who have taught me how to be a researcher.

Thanks should also be given to Dr. Bethany Goldblum and the whole Nuclear Science and Security Consortium (NSSC) team, who allowed me to be an affiliate member. Dr. Bethany Goldblum and the rest of NSSC team highly enriched my knowledge and given me directions for my present and future career.

Thank you to everyone who has provided support and counsel throughout my academic career. I would like to thank Kirsten Wimple for answering all of my Berkeley relating questions and

for helping navigate the bureaucratic system at UC Berkeley and always remaining calm and supportive.

I cannot possibly thank all of the students and friends who helped me with the studies, the research and with the moral support throughout those years at UC Berkeley. Thank you, everyone, for all that time spent together that made my stay in Berkeley an amazing experience. The friends I met here have created a "home away from home" for me.

And *ultimum sed grave quam primum* I thank my great family for being on my side. I am grateful for my mother, my sister and my late father's endless support and for investing in my education and development through the years of my endeavors.

Most of all, I couldn't have survived through all those challenging years without my husband Florian Soom and I am grateful for all the encouragement, patience, support and help he continually shows me. All love to my daughter who over the past years, has grown into a funny, smart and caring girl which makes our life endlessly interesting.

This work was performed under the auspices of the U.S Department of Energy by Lawrence Livermore National Laboratory under contract DE-AC52-07NA27344. This work was funded by the Laboratory Directed Research and Development Program at LLNL under project tracking code 16-SI-01. This material is based upon work supported by the National Science Foundation Graduate Research Fellowship, Grant No. NSF 11-582. The thesis has been approved with an IM number LLNL-TH-810566.

The work has been also supported by the Department of Energy National Nuclear Security Administration through the Nuclear Science and Security Consortium, Award Numbers DE-NA0000979 and DE- NA0003180. This report was prepared as an account of work sponsored by an agency of the United States Government. Neither the United States Government nor any agency thereof, nor any of their employees, makes any warranty, express or limited, or assumes any legal liability or responsibility for the accuracy, completeness, or usefulness of any information, apparatus, product, or process disclosed, or represents that its use would not infringe privately owned rights. Reference herein to any specific commercial product, process, or service by trade name, trademark, manufacturer, or otherwise does not necessarily constitute or imply its endorsement, recommendation, or favoring by the United States Government or any agency thereof. The views and opinions of authors expressed herein do not necessarily state or reflect those of the United States Government or any agency thereof. This research uses Savio computational cluster provided by the Berkeley Research Computing program at the University of California, Berkeley (supported by the UC Berkeley Chancellor, Vice Chancellor for Research, and Chief Information Officer).

Chapter 1

Introduction

Utilization of neutrons [1] is important for many applications across a broad range of industries including, but not limited to, nuclear forensics, the medical field, oil well drilling, and geochronology [2]. Specifically, numerous research fields are interested in employing an accurate and efficient methodology to tailor available neutron spectra and intensity requirements to their specific application needs. Many applications in the nuclear engineering field require, in fact, neutron energy distributions that cannot be obtained with current neutron sources, and with an increased demand in neutron production applications, the development of multiple compact Beam Shaping Assemblies (BSA) in pre-existing facilities is needed.

Basically, neutrons are neutral and there is the need to use neutron interactions with matter (scattering) in order to extract particular energy range, or force the neutrons to go in particular directions. BSAs are an example of highly advanced employment of neutron filters and moderation for the purpose of spectral modification in the location of interest. The complexity of such assemblies comes from the physics of neutrons and their interactions with matter. Neutrons have mass but are uncharged particles, and therefore they do not participate in the electromagnetic interactions and their direction and velocity cannot be modified with electromagnetic fields. Unlike charged particles, which practically continuously lose energy in small portions, neutrons experience rare collisions with atoms, in which they can lose either all or a large part of their energy [3]. In order to tailor neutron energy spectra, one must rely on neutron interactions with materials. Summary of neutron interactions with matter is given in Chapter 2. Thus, in order to design neutron beam shaping assemblies that consist of combination of materials, it is also necessary to know how those interactions with specific materials change with changes in neutron energies.

The lack of a coherent, coordinated approach to tackling such a difficult problem as designing customized BSA at least partially explains why state-of-the-art spectral modification techniques have not advanced significantly over the last several decades. An example of the importance of having an improved methodology for BSA designs is given by the past research in the Neutron Capture Therapy (NCT) [4]. One of the main reasons for the failed clinical trials of the 1990s for the Boron NCT (BNCT) was related to the less-than optimal neutron beam characteristics [5]. Thus, there is an increasing need to optimize the neutron beam in

order to satisfy improved patient-tailored neutrons for BNCT.

Section 1.1 introduces the scope and motivation for this work, as well as a discussion of the previous work upon which this thesis is based, thus contextualizing and highlighting the impact of this dissertation within the scope of the collaboration between University of California, Berkeley (UC Berkeley) and Lawrence Livermore National Laboratory (LLNL) [6]. Moreover, Section 1.2 presents an overview of the structure of this dissertation.

1.1 Scope of the Work and Overview

The National Ignition Facility (NIF) [7] at LLNL uses laser inertial confinement [8],[9] to drive Deuterium-Tritium (D-T) fusion reaction producing a very high flux output, approximately 10^{15} /10^{16} neutrons in 4π in $\sim$100 ps, providing a mainly monoenergetic 14.1 MeV source peak [7],[10]. Tailoring such a strong neutron source spectrum would lead to unique applications such as detector characterization and calibrations, for a study of radiation damage to various materials, for cross section measurements, for neutron activation studies, or for medical applications such as Boron Neutron Capture Therapy or isotope separation. In order to expand those capabilities and to open up the facility for different users and applications there is the need for an efficient, high fidelity easy to use design framework, where besides performing a high fidelity modeling of the NIF facility and shot there is a good tailoring of the neutron flux for the needed application. Thus, exists the need to provide automatically optimized assemblies that produces customized exit neutron spectra, but ideally also optimize the number of neutrons going in particular direction within particular energy range. Those assemblies are defined here as Energy Tuning Assemblies (ETAs) in contrast to the early BSAs. The problem space to design ETAs is large and many dimensional and there are multiple competing neutron interactions with widely varying and often rapid changes in probability of occurrence. If done appropriately, the application of optimization to the ETA design processes can be extended to cover a broad set of design problems to generate nearly ideal solutions as seen in Figure 1.1.

Such research endeavors involving the design and building of preliminary ETA designs are thus of significant interest in many fields in nuclear science and engineering and entails multidisciplinary research: (1) understanding of neutron interactions with various materials, (2) determining nuclear data uncertainties in complex models, (3) choosing appropriate neutron transport simulation codes, (4) developing optimization methodologies, (5) developing set of experiments, (6) performing initial experimental testing to verify and validate the simulation model, (7) designing, licensing and implementing ETA for particular application.

Initial development of a metaheuristic optimization software for designing ETAs was a part of James Bevins dissertation [6], and included collaboration between the UC Berkeley and LLNL.

The initial metaheuristic optimization methodology developed by Dr. James Bevins, consists of two software packages: Gnowee [14], a general-purpose metaheuristic optimization algorithm, and COEUS [12], which couples Gnowee to a radiation transport solver to auto-

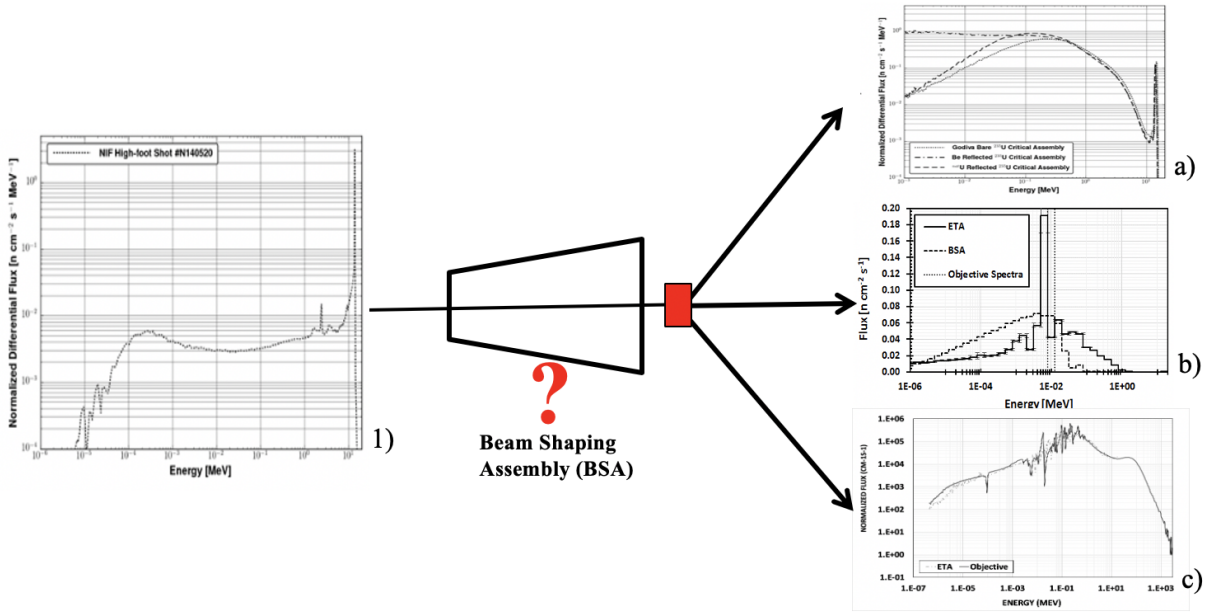

Figure 1.1: Schematic of the required actions necessary to design energy tuning assemblies (ETA) in order to produce custom neutron energy spectra. 1) Represents the 14.1 MeV flux generated by the D-T reaction at the NIF [11], a) b) and c) pictures three examples of shaped spectra that can be generated with the appropriate optimized ETA: a fission spectrum [6],[12], a 10 keV peaked spectrum, and an exotic meteorite spectrum [13].

matically generate an Energy Tuning Assemblies (ETA) design given a set of constrains and an objective spectrum. Both software packages (henceforth referred to as Gnowee/COEUS) are available on GitHub[15]. Gnowee/COEUS performs an efficient search for neutron ETAs, enabling modifications of the characteristic neutron spectra in the NIF to mimic desired neutron sources in terms of energy and intensity characteristics. The first application for which the code has been developed is presented in the Section 1.1.1, while detailed description of the software is presented is Chapter 4.

The objective of this thesis is to further develop, validate, and apply the newly developed optimization methodology, Gnowee/COEUS, to provide various accurate and multiple neutron tailored spectra for some of the above mentioned applications. Particularly, the focus is to introduce various ETAs at the NIF, where such an approach is needed to provide accurate modeling in a reasonable amount of CPU time for day-by-day whole-modeling calculations on available parallel machines utilizing fewer than one hundred cores, which corresponds to the computational resource that typical nuclear engineering laboratories and companies currently possess. Researchers with access to supercomputers at LLNL, in particular, would also appreciate the ability to perform more rapid computational modeling with reduced processing times.

The improved optimization methodology would then be used to generate the appropriate

stack-up assemblies by introducing multiple objective functions for the various flux. Information on the collaboration with LLNL for the dissertation is presented in Section 1.1.2.

1.1.1 Previous Experiences with Gnowee/COEUS

Gnowee/COEUS was initially developed to generate realistic synthetic fission and activation products through irradiation of samples with a combined thermonuclear and prompt fission neutron spectrum (TN+PFNS) as part of the thesis by Dr. James Bevins [6]. The Gnowee/COEUS run generated and computed 4500 designs over the course of only 76 hours to design the ETA of interest. Details on the Gnowee/COEUS software are given in Chapter 4. The resulting optimized ETA designed and the comparison of the objective and achieved neutron spectrum are shown in Figure 1.2.

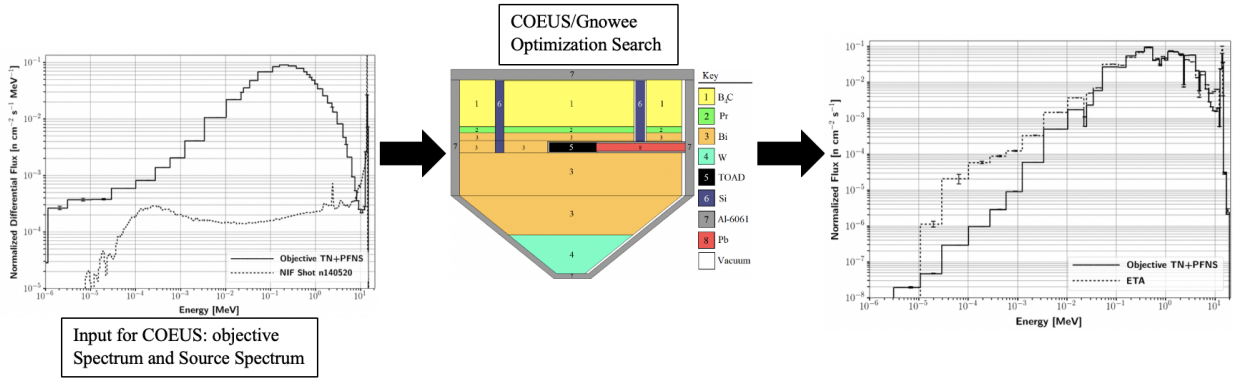

Figure 1.2: First Gnowee/COEUS application for thermonuclear plus prompt fission neutron spectrum for sample irradiation: Design of the nearly optimum ETA production of synthetic fission and activation products and the shaped flux in the sample cavity. Figures taken from [6], [12].

In Figure 1.2 the first left picture illustrates the objective spectrum and the 14.1 MeV source spectrum of the NIF, which are provided to Gnowee/COEUS. The optimization software is then run to provide the ideal ETA which recreates the objective spectrum. The third picture on the right represents the spectrum recreated by the ETA of choice and shows the differences with the objective TN+PFNS spectrum. Comparing the objective and ETA neutron spectra, the ETA accomplished a significant shift from a 14.1 MeV mono-energetic source and matched the overall objective neutron spectrum well. The areas of disagreement, <10 keV and 6-12 MeV, represent a low fraction (∼2-3%) of the overall spectrum. The differences <10 keV were driven by the weight constraints on the system, and the ones at the 6-12 MeV region were driven by known modeling errors associated with using bare critical assemblies to derive a representative TN+PFNS.

These promising initial modeled results represent a step forward in being able to design customizable neutron energy spectra for a variety of applications. From here, increasing

interest exists on the part of UC Berkeley and LLNL to continue in this line of studies for developing a coherent, coordinated and validated approach to tackling the difficult problem of neutron spectra modification techniques, which is the main goal of this dissertation.

1.1.2 LLNL Project

The NIF currently contains the world's largest laser utilized to create inertial confinement fusion [7]. Optics convert a weak laser pulse with an energy of a billionth of a Joule into 192 laser beams that have a total of 4 million joules of energy. The target is comprised of a tiny capsule of a frozen deuterium and tritium mixture, and is surrounded by a hohlraum, a small cylinder made of a high-Z material. Lasers enter the hohlraum from the top and bottom and heat its inner surface to high temperatures allowing uniform X-rays to be released. These X-rays then heat up the outer layer of the D-T capsule causing the surface to ablate and the rest of the capsule to implode. The compression of the fuel releases shock waves that travel to the center of the fuel pellet and condenses it even further. This forms a hot spot in the center that allows fusion reactions to occur. This entire process is illustrated in Figure 1.3.

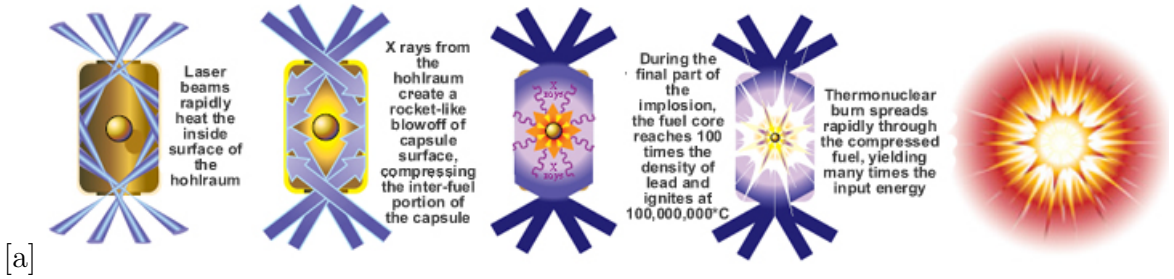

[a]

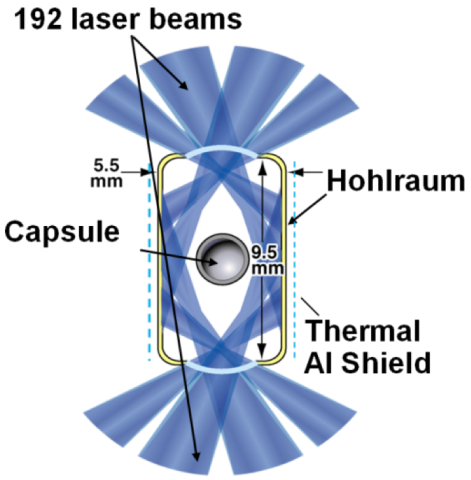

[b]

Figure 1.3: a) Illustration of inertial confinement fusion at the NIF; b) Schematic of the indirect drive fusion [16].

This reaction produces a very high neutron flux output, approximately $10^{15}/10^{16}$ neutrons, produced in 4π, in $\sim$100 ps by the D-T reactions described by Eq. 1.1:

$$ {}^{2}_{1}H + {}^{3}_{1}H \Rightarrow {}^{4}_{2}He + {}^{1}_{0}n + 17.59MeV, \tag{1.1} $$

where D-T fusion produces an alpha particle and a neutron, with the Q value of the reaction 17.59 MeV. The neutron gets the most of the available reaction energy, so that the D-T reaction provides a mainly monoenergetic source of neutrons with a peak at 14.1 MeV. There is also a less intense part of the neutron spectrum at lower energies. The neutron spectrum is furthermore shifted to lower energies at later times when neutrons scatter in the different instruments inside the target chamber for several 100's of nanoseconds. The source spectrum is then different at each location and time after implosion. With such a strong neutron source, wide range of potential applications would be possible if an efficient methodology could be developed to tailor neutron spectra to specific needs. Expanding its capacities to multiple applications is of significant interest for the NIF community.

This thesis research project was completed within the Nuclear and Chemical Sciences Division at LLNL under the directorship of Dr. Dawn Shaughnessy [17], in the nuclear forensic program, with the task of designing of platforms for tailored neutron outputs and moderated spectra at the NIF. Furthermore, this work introduces a justification for simpler nuclear energy-oriented experiments to be performed at the NIF, such as the one presented in the previous Section. In fact, the ETA design for the TN+PFNS showed promising results for a device that though very heavy, is within the broad envelop for the instrumentation in the NIF chamber with some careful engineering.

The research work performed at the NIF consisted of three steps: (1) modifications and expansions of Gnowee/COEUS, (2) experimental verification and validation of the modeling and simulation, and (3) design of ETAs for specific applications. The second step has been performed at the NIF, and the possible ETA designed for future application are specific for the NIF.

This research work has provided an opportunity to develop simplified procedures to perform NIF experiments quickly that could be useful for various nuclear science and engineering applications. The NIF facility was used to validate the modeling framework developed as a part of this dissertation. As a result, the experimental procedure and modeling methodology introduced through this dissertation has significant potential impact for future experiments to be performed at the NIF.

1.2 Dissertation Outline

Chapter 2 presents the theoretical background behind the proposed modeling methodologies used for the optimization software, Gnowee/COEUS, and to predict fluxes and reaction rates at the NIF. This chapter briefly covers the basis of the neutron interaction with matter, introduces the neutron transport equation and the main numerical methods used to solve the transport problem, which the proposed software are based upon. Additionally, this chapter

describes the main concepts of nuclear data and the importance of considering appropriate uncertainties.

Chapter 3 describes the modeling technique used specifically for this research effort to design and model the experimental infrastructures at the NIF. This Chapter gives a brief introduction to the set of external code packages used jointly with Gnowee/COEUS to perform neutron transport simulations (MCNP and ADVANTG [18],[19]), and determine uncertainties in nuclear data (SCALE) [20]. Chapter 3 also includes the arguments behind each software choice and details, the software approximations and how uncertainties are treated. To blindly rely on software is bad practice in most instances, especially state-of-the-art software for the nuclear applications, without fully understanding how it works and its limitations.

Chapter 4 presents the optimization methodology, the main focus of this research. This chapter begins with an overview of the initial version of Gnowee/COEUS, highlighting the motivation and the theory behind the metaheuristic algorithm. Next, the limitation of the first version are introduced and the second part of the chapter focuses on the efforts to improve and further develop the software. Chapter 4 concludes by summarizing the software usefulness for facilities like the NIF and provides a user-friendly description on how the software is used and run.

Preliminary experiments performed at the NIF for validation and application of the modeling software, as introduced in Chapters 3 and 4, are described in detail in Chapters 5 and 6. Chapter 5 begins with an overview of the experimental setup inside the NIF target chamber.

Chapter 6 further presents the chosen detection methodologies for the active interrogation, specifically the activation foils [21] and CVD detectors [22], and provides a description on how the detector data are processed.

Chapter 7 introduces the anticipated results of the simulation of the experiments presented in Chapter 5 and 6. Next, this chapter presents the results of the measurements during the shots and compares them with the simulations. This chapter discusses both how the experimental data are processed and how well the modeling methodologies predict the measurements. Finally, this chapter details how the information about the system is combined with the experimental data to produce a proof-of-concept platform for modeling capabilities at the NIF.

Equipped with the full modeling experience from work in Chapter 7, Chapter 8 presents designs and models for ETAs within the NIF to tailor the D-T spectrum for a series of applications, proposing a series of experiments and shot configurations for the ETA of interest. There is a certain beauty to the depth and scope achievable with such physically large, mechanically intricate, and computationally powerful device that is NIF in fields of nuclear engineering that have been overlooked with time.

Finally, Chapter 9 summarizes the conclusions and lays out a plan for future work. The chapter hypothesizes what impact this method might have at nuclear laboratory like LLNL. Additionally, this chapter ends with the state of the developed system and of the work being continued. Suggestions are also made as to how the optimization method might be extended, as well as on new experiments that can be performed at NIF or at other facilities.

Chapter 2

Background

This chapter presents the foundations of the dominant physical mechanisms behind all of the simulations as well as experiments carried out in this work.

Basic principles of the nuclear reactions featured in this work are discussed in Section 2.1. Section 2.2 presents the nuclear data library where all of the fundamental principles governing different nuclear interactions between neutrons and absorbing materials are collected. Section 2.2.3 explains the principle of the experiments needed for validation of the modeling capabilities of the optimization software. In Section 2.3 the transport equation governing the principle of such neutron interactions is described. Understanding what mechanisms drive the neutrons within the materials is critical in order to recognize the ultimate accuracy of the model and to most accurately interpret its results.

2.1 Neutron Interactions

Neutrons were first discovered by Chadwick in 1932 [1]. Almost 100 years after this discovery, neutrons are being used in a variety of applications, ranging from medicine to nuclear weapons, spanning over a wide spectrum of sciences and technologies in the fields of biology, material science, explosive detection, fission and fusion, to name a few. As the understanding of neutrons and their interactions with matter continues to grow, so will their diverse applications in such fields.

All neutrons are emitted as fast neutrons and lose kinetic energy by collision until they are absorbed. Free neutrons are unstable and decay in a vacuum by β decay with a half-life of 615 s. Neutrons have a rest mass similar to that of protons and are electrically neutral. Therefore, they do not interact with electrons but undergo elastic or inelastic scattering with nuclei or nuclear reactions. Neutron interaction mechanisms with matter serve as a physical constraint to spectral shaping of a neutron flux spectrum. Neutron interactions can act to moderate, absorb, or even emit more neutrons. The major reaction mechanisms available in the range of the fast to thermal energies that are relevant to nuclear weapon environments are elastic scattering, inelastic scattering, radiative capture, and the release

of 'x' neutrons (n,xn) through neutron evaporation. A diagram summarizing the important neutron reactions is shown in Figure 2.1. This section provides an overview of the basics of neutron interaction [2].

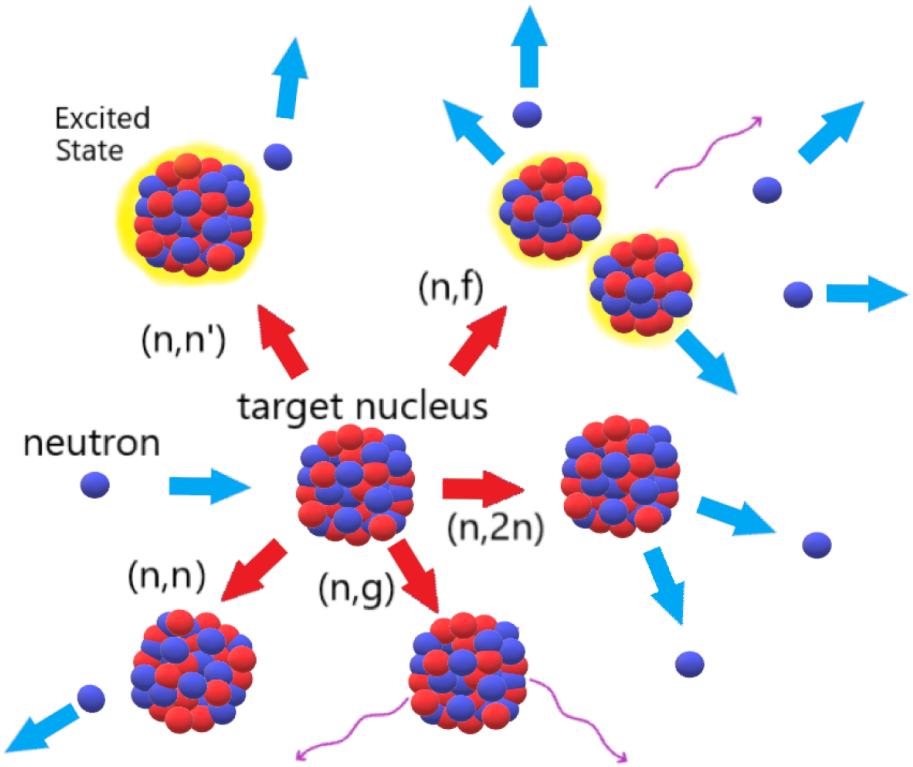

Figure 2.1: Schematic of the type of important neutron reactions.

- **Scattering**. In scattering reactions a neutron "bounces off" a nucleus. They change a neutron's direction and energy, but do not terminate its progression through matter. Scattering reactions can be further broken down into elastic and inelastic types [23]:
  - **Elastic scattering.** This type of interaction is analogous to the idealized interaction between billiard balls. In this situation, the neutron strikes the nucleus of an atom and is elastically scattered and the nucleus remains in the ground state during the interaction. This interaction is abbreviated by the symbol (n,n).
  - **Inelastic scattering.** This process is identical to elastic scattering except that the nucleus is left in an excited state, and later decays by the emission of γ. The symbol for inelastic scattering is (n,n').
- **Absorption.** A heavy target nucleus absorbs an incoming neutron. After an absorption, a secondary radiation will be emitted, this radiation can then be generally

detected. There are many types of different absorption reactions, which are categorized by how the compound nucleus behaves, *i.e.* the number and type of secondary products it produces as it de-excites. Some reactions do not produce any secondary particles, and the neutron is captured. Others produce secondary neutrons, like (n,2n) reactions where the neutron is absorbed, but the excited compound nucleus decays to a ground state by emitting two neutrons. Fission is also classified as an absorption reaction since a compound nucleus is formed, but in this case the compound nucleus splits instead of relaxing to another state [24]. Based by the secondary radiation produced there are different type of absorption:

- **Radiative capture.** The neutron is captured by the nucleus, and γ radiation or electromagnetic radiation are emitted. This interaction type is denoted as (n,γ).
- **Charged-particle reactions**. The neutron is absorbed by the nucleus and a charged particle, such as an α or proton, is emitted. The symbols of these reactions are (n,α), (n,p), etc.
- **Neutron-producing reactions.** Denoted as (n, 2n), (n, 3n), these reactions occur only with energetic neutrons, whereby one neutron is absorbed by the nucleus and two or more neutrons are emitted. This process can also proceed via the emission of a single neutron with the nucleus being left in an excited state. This process is quantum mechanically indistinguishable from the inelastic process described above.
- **Fission.** Neutron colliding may cause the nucleus to split apart, *i.e.* to undergo fission, denoted as (n,f).

The relative probabilities of the occurrence of these various types of neutron interactions change dramatically with neutron energy [24]. The probabilities for individual reactions occurring are expressed in terms of cross sections.

Cross sections are classified in two types: microscopic and macroscopic. Microscopic cross sections, represented by σ (lower case Greek letter sigma), have units of area and describe the individual nucleus interaction probabilities in terms of the apparent "size" of the reaction. They are often expressed in units of barns (b), where 1 barn is equivalent to 10^{-24} cm^2. Macroscopic cross sections, represented by Σ (Greek capital sigma), take into account the density of nuclei, and describe the interaction probability per unit length along a neutron's direction of travel. The sum of the microscopic cross sections for all possible interactions is known as the total microscopic cross section σ_t.

A useful parameter for calculations of trajectories of neutrons in matter is the mean free path, λ_t, here denoted, for a specific neutron energy, as [24]:

$$\lambda_t = \frac{1}{\Sigma_t}. \tag{2.1}$$

The mean free path is especially useful for Monte Carlo (MC) simulations (Chapter 3) and it is characterized as the average distance traveled by a moving particle (neutron) in a

target medium between interactions with the target material. The collision probability per unit time, τ_t, defined as the mean time, is denoted as:

$$\tau_t = \frac{1}{\nu \Sigma_t}. \tag{2.2}$$

Alternatively:

$$\frac{\lambda_t}{\nu} = \frac{1}{\nu \Sigma_t} = \tau_t, \tag{2.3}$$

where ν is the frequency of collisions.

With the exception of elastic scattering at low neutron energies and non-elastic scattering at energies in excess of 10-20 MeV, most of the neutron reactions upon striking a target nucleus proceed in two steps. First, the incident neutron coalesces with the target nucleus to form a compound nucleus. The compound nucleus then decays in a number of ways. Figure 2.2, 2.3 and 2.4 show the energy dependence of reaction types for some of the most common elements, of different atomic weights, seen in this thesis from the Evaluated Nuclear Data File library [25].

In the past in order to ensure the requested neutron beam parameters at an exit port, a proper spectrum shifter system, or Beam Shaping Assembly (BSA), was necessary. As an example, complex BSA have been designed for Boron Neutron Capture Therapy (BNCT) application, where the assemblies need to include four parts, namely the epithermal spectrum shifter, the reflector for epithermal neutrons (*i.e.* neutrons with energy 1 eV - 10 keV)and some absorber/beam delimiter for low energy (*i.e.*, thermal, $<$ 1 eV) neutrons and shielding for γ radiation produced both in the neutron converter and during the neutron beam tailoring. The neutron spectrum shifter, the core of the system, has to slow down the fast neutrons yielded by the source, *e.g.* having energy larger than 10 keV, in a selected way without increasing the fraction of thermal neutrons in order to get a net accumulation in the epithermal energy range. A reflector has to be included to either limit the neutron losses or scatter neutrons toward the beam port, while further improving the quality of the beam. Thus, the difficulties and poor efficiency in applying enumerative methodologies to design BSA: a lot of variables come into play for the neutron interactions. As the energy of neutrons is reduced through scattering interactions (neutron thermalization/moderation), all neutron interactions increase in probability and neutron capture interactions become more important.

The goal in this work is to automatically generate Energy Tuning Assemblies (ETAs) with an optimization software which take into considerations all the variables that affect the neutron energy and the number of neutrons at a specific energy.

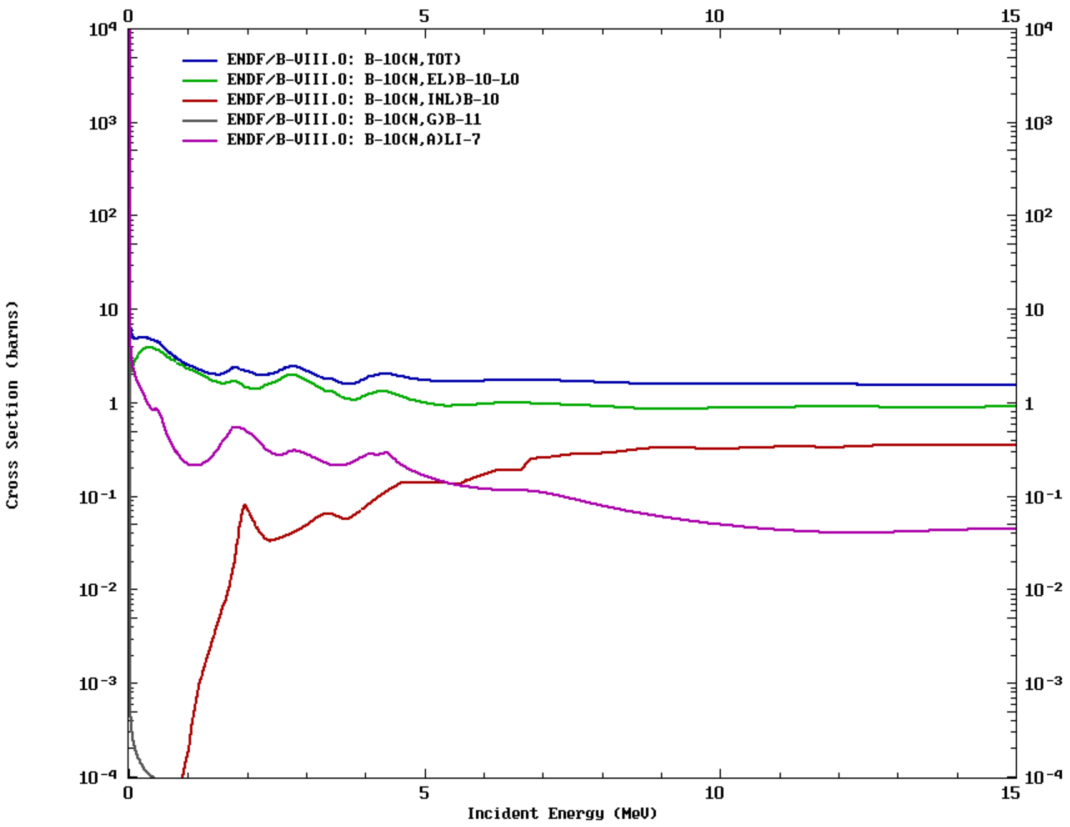

Figure 2.2: The energy dependence of some reactions in ^{10}B [26].

2.1.1 Neutron Scattering

Tailoring neutron spectra of neutron sources (spectrum) like the National Ignition Facility (NIF) involves mainly down-scattering 14.1 MeV neutrons. In the 10-15 MeV energy region, on most high-Z materials (n,2n) is bigger in this energy range than (n,n') and in low-Z materials (n,pn) and (n,n) dominate, but overall the scattering, especially the elastic one, is the largest reactions. The scattering reaction is helpful as it is important to try to reduce the absorption reactions and the production of other particles like γ rays. Generally, a neutron scattering reaction occurs when a target nucleus emits a single neutron after a neutron-nucleus interaction. Scattering cross sections include elastic and inelastic scattering.

2.1.1.1 Elastic Scattering

Elastic scattering is the most important and frequent process for slowing down neutrons. The neutrons are moderated *via* elastic collisions in which a neutron merely bounces off of a nucleus. As it is a very important process in neutron moderation, elastic scattering will be analyzed in greater detail than other forms of scattering in the following section.

At each scattering site, the neutron loses energy and is thereby moderated or slowed

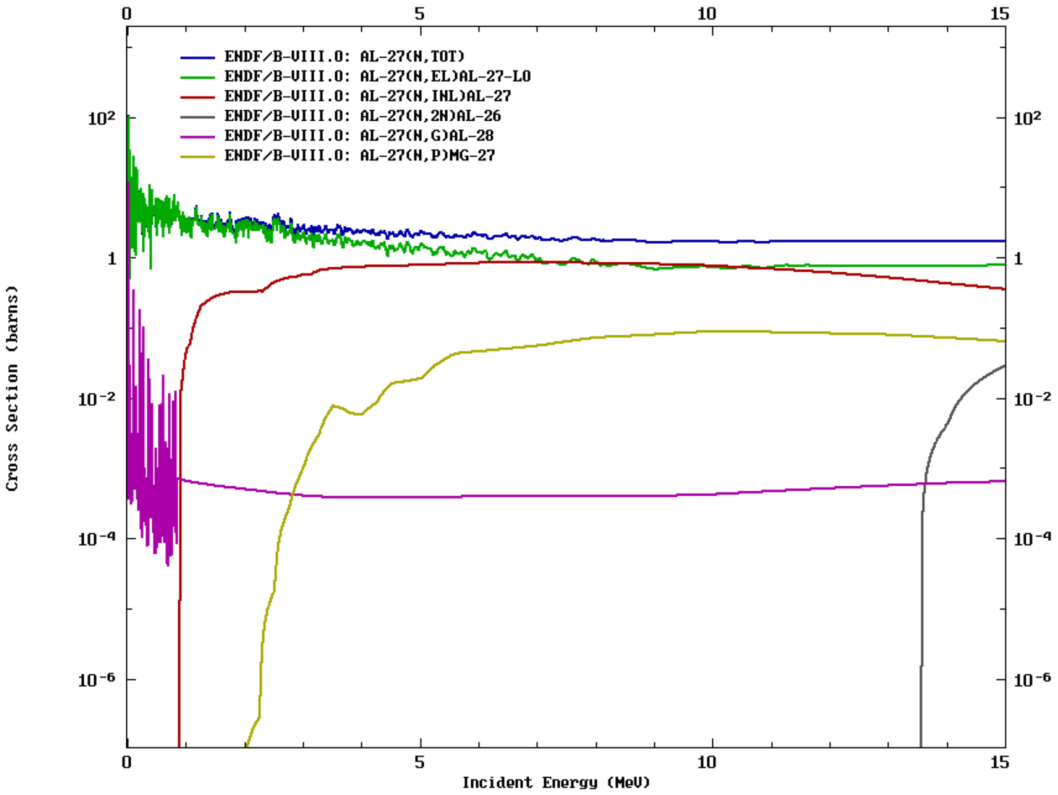

Figure 2.3: The energy dependence of some reactions in ^{27}Al [26].

to lower energy. In an elastic scattering reaction between a neutron and a target nucleus, no energy is transferred into nuclear excitation. Elastic scattering conserves both the momentum and the kinetic energy of the reacting particles and occurs when the neutron does not enter the nucleus, but bounces off its potential field or if the neutron is absorbed and re-emitted from the compound nucleus without leaving any excitation energy in the nucleus (*e.g.* compound elastic). Since there is only a single exiting particle, elastic scattering is a two-body interaction and the kinematics are constrained by conservation of momentum and total energy. This may be modeled as a billiard ball-like collision between a neutron and a nucleus. When a neutron is elastically scattered from a nucleus at rest, the nucleus recoils from the site of collision.

The maximum energy that a neutron of mass M and kinetic energy E_n can transfer to a nucleus of mass m in a single (head-on) elastic collision is given by Eq.2.4:

$$Q_{max} = \frac{4mME_n}{(m+M)^2}. \tag{2.4}$$

Setting M=*1*, it is possible to calculate the maximum fraction of a neutrons energy that can be lost in a collision with nuclei of different atomic-mass numbers m. For ordinary hydrogen, because the proton and neutron masses are approximately equal, the neutron

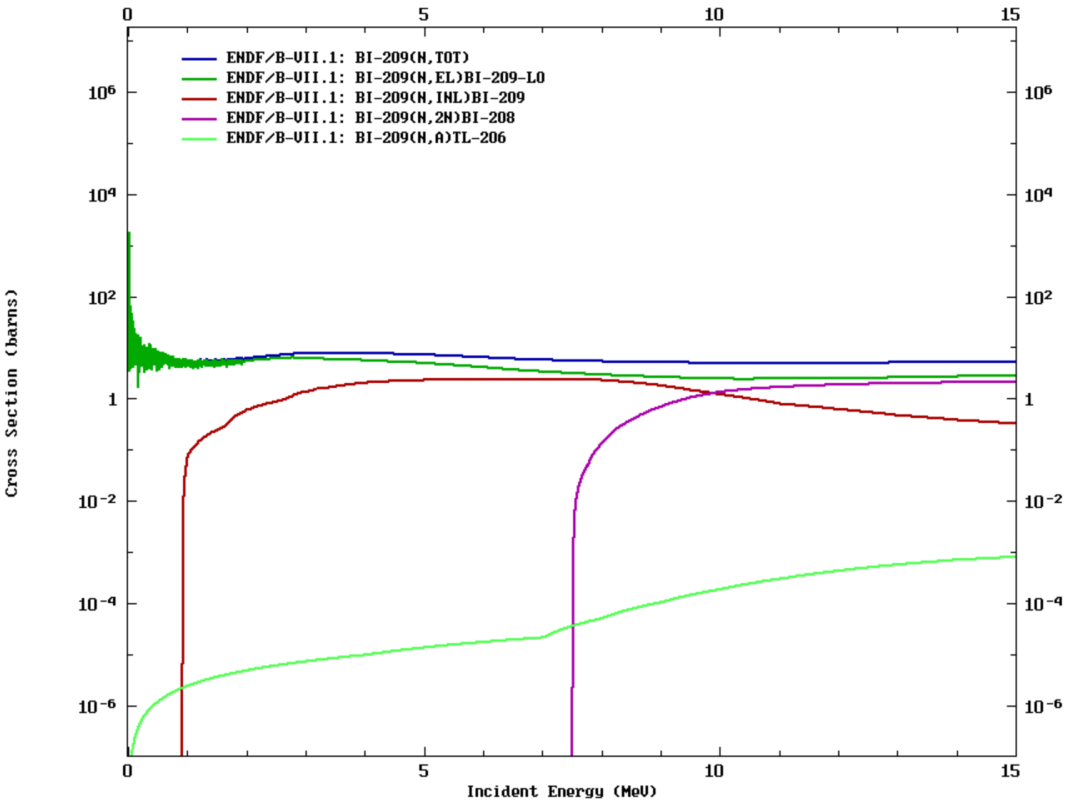

Figure 2.4: The energy dependence of some reactions in ^{209}Bi [26].

can lose all of its kinetic energy in a head-on, billiard-ball-like collision. As the nuclear mass increases, one can see how the efficiency of a material per collision for moderating neutrons grows progressively worse. As a rule of thumb, the average energy lost per collision is approximately one-half the maximum. An interesting consequence of the equality of the masses in neutron-proton scattering is that the particles separate at right angles after collision as seen in the lab frame, when the collision is non relativistic. Figure 2.5 a) represents a neutron of mass M and momentum MV approaching a stationary nucleus of mass m. After collision, in Figure 2.5 b), the nucleus and neutron, respectively, have momenta mv and MV. The conservation of momentum requires that the sum of the vectors, mv+MV, be equal to the initial momentum vector MV, as shown in Figure 2.5 c). Since kinetic energy is conserved, we have:

$$\frac{1}{2}MV^2 = \frac{1}{2}mv'^2 + \frac{1}{2}MV'^2. \tag{2.5}$$

If M=m, then V^2= v^2+V^2, which implies the Pythagorean theorem for the triangle in (c). Therefore, v' and V' are at right angles. A selected group of elastic scattering cross-sections relevant to the application in the ETA design are shown in Figure 2.6.

The energy range spanned by neutrons slowing down is extremely large, ranging from 20

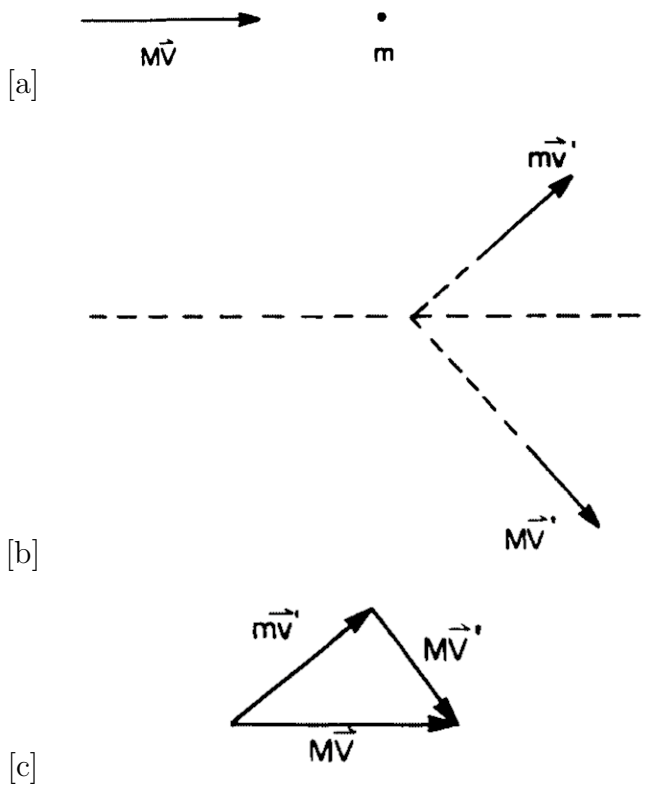

Figure 2.5: Kinetics of neutron elastic scattering [27].

MeV down to 5 MeV. Thus, a neutron tends to lose a fraction of its incident energy rather than a fixed amount of energy in elastic scattering proving how much more effective low mass number nuclei are at moderating fast neutrons.

If the goal is to down-scatter the 14.1 MeV neutrons to match various energy ranges, mid- to high-A materials provide more fine-tuned control over the neutron population for elastic scattering reactions and are likely to be better suited to this application. High-A materials offer actual advantage, in the 10-15 MeV energy region, the trend is towards higher elastic scattering cross sections with increasing atomic mass, as shown in Figure 2.4. Additionally, the overall trend is for increasing atom density with increasing Z. Therefore, higher A materials will scatter the D-T fusion neutrons more frequently. Low-A materials would be undesirable due to fewer scatters required for thermalization.

2.1.1.2 Inelastic Scattering

Inelastic scattering is the other type of scattering a neutron can undergo, but in this case kinetic energy is no longer conserved. Energy is transferred to or from an internal state of the target nucleus. This amount of energy, Q, is typically defined to be positive for reactions where energy is given to the neutron and target nucleus, *i.e.* Q is positive when the sum of

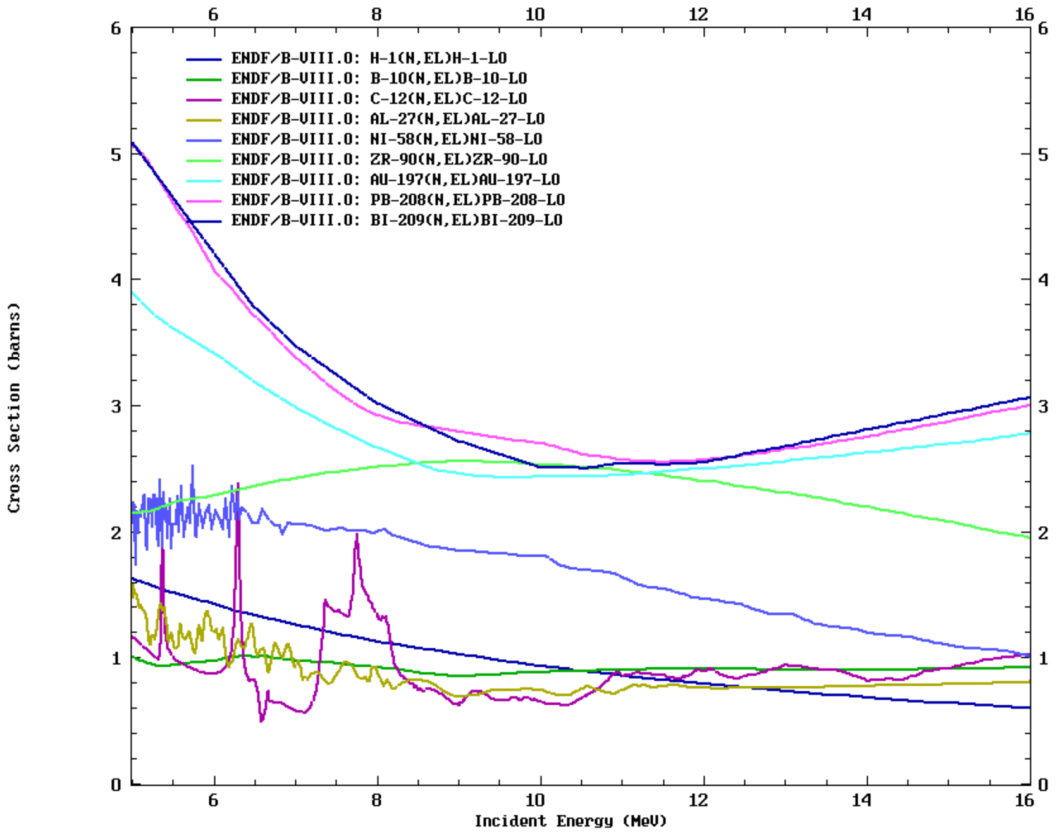

Figure 2.6: Comparison of the elastic scattering cross-sections for materials common in the experiments here presented, of several isotopes spanning various atomic masses [26].

the particles' kinetic energies is greater after the reaction than before. Therefore, Q values for inelastic scattering are negative, since energy is always lost to an internal state of the nucleus. In neutron-nucleus collisions, the target nucleus can be excited to a higher energy state than its ground state if the colliding neutron has a high enough energy to do so. If the colliding neutron has enough energy (*e.g.* 50 keV) and the collision excites the nucleus, a discrete amount of energy is lost to the reaction. These excited states typically do not have long half lives, and a γ ray, or other form of energetic radiation, is emitted when the nucleus relaxes to its ground state. This type of reaction is called inelastic level scattering because an excited energy level becomes occupied by the target nucleus.

In comparison to elastic scattering reactions, formulating an expression for the average energy loss of inelastic scattering reactions is not a trivial matter, since such a reaction depends on the energy levels within the target nucleus. Inelastic scattering, however, occurs only above a certain threshold energy. Thus, minimum energy needed for the neutron to excite the target nucleus is referred to as the threshold energy. This threshold energy is higher than the energy of the first excited state of a target nucleus (due to the laws of conservation of energy) and it is given by Eq. 2.6.

$$E_t = (\frac{A+1}{A}) * \epsilon_1, \tag{2.6}$$

where E_t is known as the inelastic threshold energy and ϵ_1 is the energy of the first excited state. Therefore the inelastic scattering cross section, σ_i is zeroed up to some threshold energy; hence, inelastic scattering is said to be a *threshold reaction*. Generally speaking, the energy at which the first excited state is found decreases with increasing mass number, and as a consequence, σ_i is non-zero over a larger energy region for heavier nuclei than for lighter nuclei.

Figure 2.7 shows the energy levels in ^{115}In, which is often used as an activation foil for flux monitoring, as seen in Chapter 6, due to the large cross section at < 1 MeV, extensive experimental experience at the NIF, the 54 minute half-life of ^{116m}In, which lends itself to multiple laboratory experiments in a condensed period of time. Indium metastable isomeric states have applications in foil activation experiments used for neutron spectrum unfolding, where it may take some time to start measuring the foil activity.

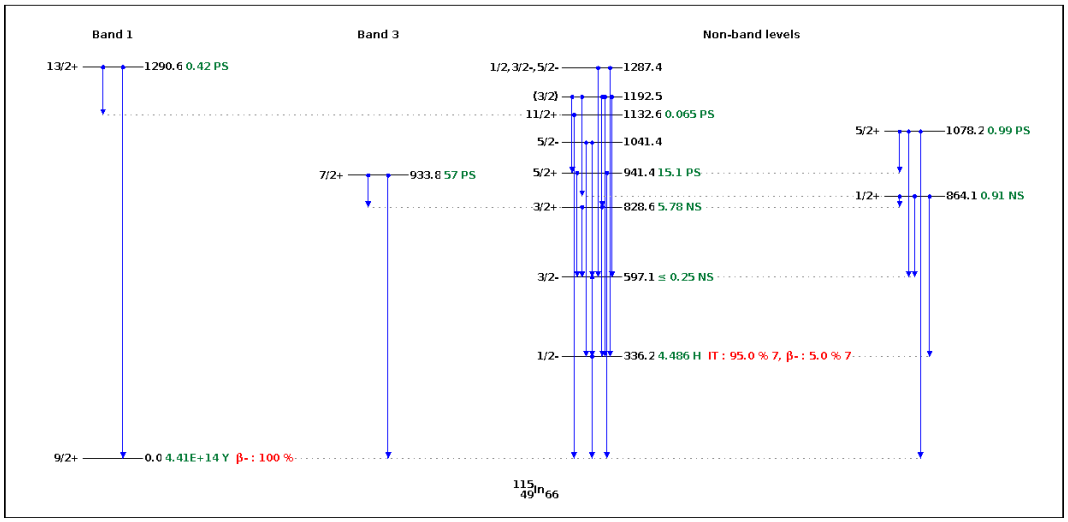

Figure 2.7: The energy levels of ^{115}In energy and decay mode diagram truncated at 1.3 MeV. Plots produced using [26].

Inelastic scattering is extremely important in heavy mass nuclei, in which slowing down by elastic scattering is negligible. Additionally, neutrons generally lose more energy per collision with high-Z isotopes if the interaction is inelastic compared to elastic scattering. The energy that would normally be conserved in an elastic collision is reduced in the conservation equations by the energy of the excited state populated. The overall trends are a decrease in the energy of the lowest lying state and an increase in the number of states with increasing Z. The increase in the number of states translates to a general increase in the inelastic scattering cross section for high-Z materials, but these global trends are subject to significant local deviations due to shell and nuclear structure effects. The differentiation of the cross-section

and variable energy loss can be exploited to fine tune the spectral shaping of the 100s of keV to several MeV range. However, there is little differentiation of the inelastic cross section in the 14.1 MeV range, which would be important for depopulation of the D-T fusion peak.

High-Z materials will still maintain an advantage due to increased reaction rates from a generally higher atom density. In contrast to elastic scattering, this gain in reaction rate for high-Z materials is not necessarily offset by a reduction in the energy loss per reaction.

Examples of inelastic scattering cross-sections are shown in Figure 2.8, materials that are frequently seen in ETA or experiments at the NIF, as ^{27}Al, a lighter isotope or ^{56}Fe, then heavier examples as ^{209}Bi and ^{208}Pb. These cross-sections indicate the energy levels of the nuclei itself. Iron is for example also a good moderator at high energies due to its high inelastic scattering cross section above 860 keV, which can be used beneficially to decrease the fast component of the neutron flux, to the advantage of the epithermal one. Iron has instead a less-pronounced (n,2n) reaction and a higher absorption cross section than materials as lead. Figure 2.8 shows iron inelastic cross sections.

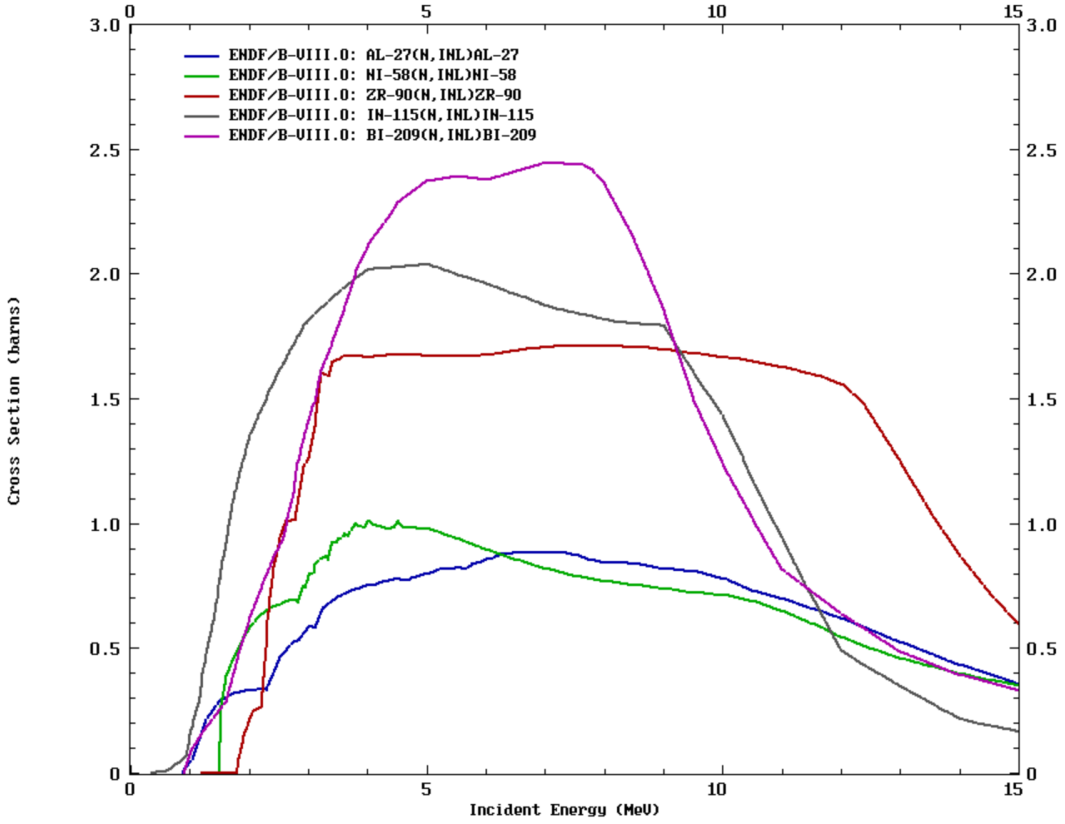

Figure 2.8: Comparison of the inelastic scattering cross-sections for materials common in the experiments here presented, of several isotopes spanning various atomic weights [26].

Calculations of spectra of inelastically scattered neutrons are performed within the framework of models of equilibrium and pre-equilibrium decay of excited nuclei and direct interac-

tion. There is, in fact, the possibility for an intermediate process known as pre-equilibrium in which the struck nucleon makes a few collisions with other target nucleons before ejection [28]. These are generally smaller reaction than compound nuclear reactions for the energy considered in this thesis, but they are not negligible. While the pre-equilibrium process are not described here at length, it is important to know that the pre-equilibrium reactions are "built-in" to the evaluated cross sections, thanks to codes like TALYS [28].

2.1.2 Absorption

Other possible reactions needed to be taken into consideration are radiative capture (or absorption), fission and multi-particle emission. As no fissile material is present in the experiments conducted, fission reactions will not be considered here. However, since optimization of this method to every material is possible, they would need to be kept in consideration in such a case where fissile material is present [2]. Unlike scattering reactions, where the energy and direction of the neutron is changed but continues to transport, absorption remove free neutrons from the system.

Absorption reaction can be important in building ETAs in order to filter neutrons, when specific neutron ranges are negatively affecting the spectrum, as in the BNCT case where neutrons above 40 keV are dangerous or thermal neutron, where it is required to have materials with increasing absorption cross section for decreasing neutron energies which would make an excellent thermal neutron filter.

This category encompasses all the other reactions neutrons undergo. This includes: reactions that produce secondary neutrons in some amount and reactions that do not. Those that do not may still produce other particles, like alpha particles, tritions, protons, etc. Since these do not produce secondary neutrons, however, they are basically equivalent to capture reactions from a neutron transport standpoint. Even though they aren't strictly capture reactions, they can contribute significantly to an isotope's absorption of neutrons.

2.1.2.1 (n,x)

In such reactions [2], n represents neutron, and x represents any particle like neutron, proton, deuteron, α particle, etc. or a combination of such particles. This expression represents a neutron interaction with a nuclide resulting in emission of the particle(s) represented by x. Important examples include ^{10}B(n,α) in boron neutron capture therapy and ^{3}He(n,p) in neutron detection. Boron is used, for example, as the most common element added to low-Z materials in neutron shielding, as it is a very strong absorber of low energy neutrons, and in safety and control systems in thermal-spectrum reactors. An example Figure 2.2 a) shows the (n,α) in ^{10}B.

The (n,xn) reactions require a threshold energy to separate the neutron from the original nucleus, appropriately called the neutron separation energy. Neutron separation energies for stable nuclei are on the order of 1 to 10 MeV. Increasing the incident neutron energy allows for the evaporation of more neutrons from the nucleus [29],[2]. Of all the reactions that

produce secondary neutrons, the (n,2n) reaction is most significant because it has the lowest threshold energy [29]. These reactions are called neutron evaporation or also multiplicity reactions [2],[29]. At higher incident neutron energies, (n,3n) and even (n,4n) can become possible. Other particle combinations are possible as well, such as (n,nγ), and these reactions act like an inelastic scatter interaction where the relationship between scattering angle and energy no longer applies due to there being three bodies to distribute energy to instead of only two.

The cross-section threshold is generally lower for higher atomic mass isotopes, which have neutrons that are not as tightly bound to the nucleus. In the context of spectral shaping, (n,xn) reactions are significant for two reasons. First, the interaction increases the total neutron population by sacrificing a high energy neutron. Second, the neutron energies are lower post-reaction because the reaction is required to overcome the potential barrier and losses through γ emission. The lowered neutron energy is beneficial for building up lower energy neutron populations. Additionally, this reaction mechanism has applications in foil activation experiments for determining the high energy neutron population. Higher-A materials also tend to have higher overall cross-sections at MeV energies. This, combined with higher atom densities, results in the most favorable combination of reaction rate and energy loss of any neutron interaction mechanism available in the 14.1 MeV energy range.

Example (n,2n) reactions are shown in Figure 2.9. The (n,2n) reaction occurring in materials such as lead, bismuth and iron can be advantageous when high-energy neutrons, such as those emitted by the D-T reaction, are available; however, the (n,2n) reactions occur only for neutrons with energies higher than 5 MeV. The (n,2n) cross sections for these materials are very high for neutron energies higher than 10 MeV, and the neutrons emitted by these reactions are of much lower energy and are useful to enhance the number of neutrons from the D-T neutron source.

2.1.2.2 Radiative Capture (n,γ)

Radiative capture reactions [2] involve absorption of neutrons followed by emission of γ rays. In contrary to the (n,2n) reaction, (n,γ) reactions can occur with neutrons of all energy levels and is a very important reaction in radiation protection and in reactor physics, as important nuclides have very large capture cross sections (*i.e.* resonances) at low energies. At low energies (below approximately 1 keV, isotope dependent) the absorption cross-section follows the *1/v* law, so the probability increases with the inverse of the square root of E_n [23].

Radiative capture is an important absorption reaction mechanism in a few ways. Neutron shielding therefore usually includes a material to slow down neutrons and a material to then absorb the slow neutrons. Important capture nuclides include Boron, Cadmium, and Gadolinium.

As previously mentioned, the (n,γ) reactions are used to clean-up any low energy neutrons resulting from over-thermalization of the spectrum and are useful as diagnostic tools to measure the spectrum generated through activation analysis, which is discussed further in

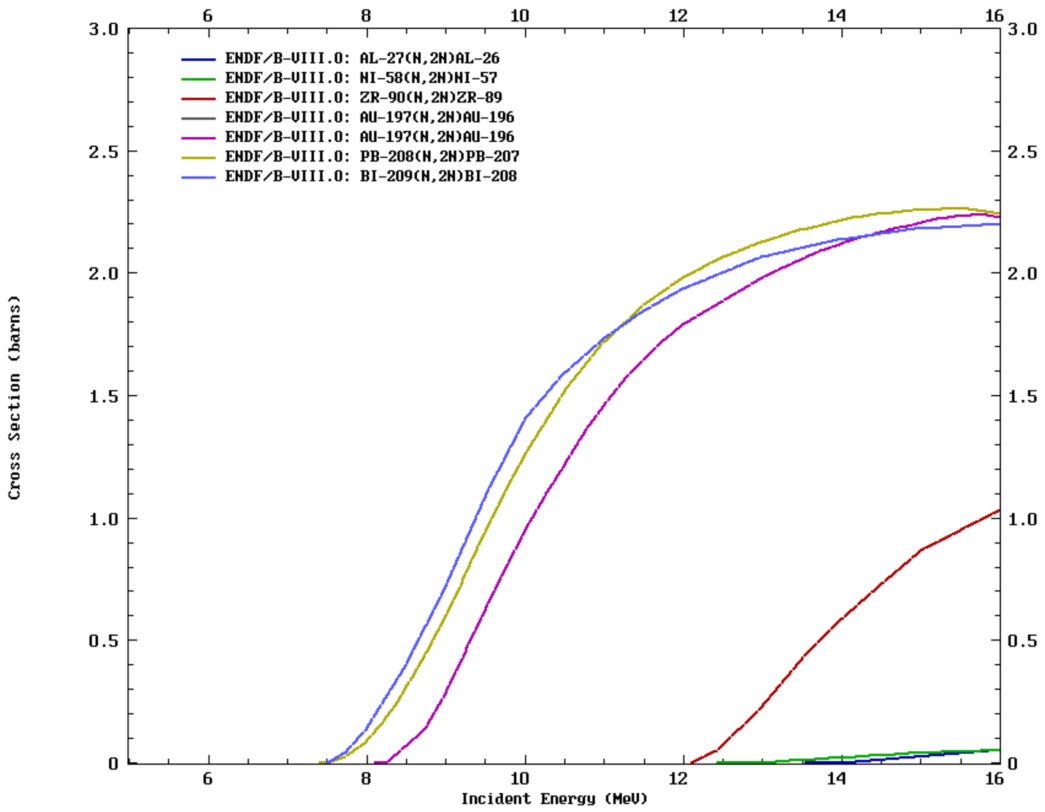

Figure 2.9: Comparison of the inelastic scattering cross-sections for materials common in the experiments here presented, of several isotopes spanning various atomic weights [26].

Chapter 6 with examples of cross section plots. The (n,γ) reactions are of interest to foil activation experiments, specifically for determining the thermal spectrum. The resonance structure of the cross-section in the epithermal region can also be used to generate a unique response. Radiative capture is generally undesirable for spectral shaping, acting as a poison to the neutron economy. Fortunately, the 14.1 MeV source inside the NIF, is not largely impacted by radiative capture until the neutrons have been moderated. It should be noted that radiative capture produces γ rays that have the potential to be detrimental for certain experiments. For example, for an experiment involving patients or delicate technology, the γ rays that the radiative capture produces are detrimental to the patient. Thus, production of γ might even cause the need for γ shielding or to optimize in order to include it in the ETA of interest.

2.2 Nuclear Data

Neutron reaction information is identified as a probability distribution recorded within the nuclear data library. Nuclear data are of interest for in nuclear physics, testing theoretical

models, designing experiments, analyzing experimental data, etc. The quality of the results of simulating and building specific flux neutron spectra stand from the quality of the nuclear data that are provided.

2.2.1 Nuclear Data File Libraries

Cross section data compiled by the United States is distributed by the Department of Energy in Evaluated Nuclear Data Files (ENDF) [25] as well as similar files produced by European, Japanese, Russian and Chinese nuclear data organizations. For the purposes of this thesis we will be focusing exclusively on cross sections from ENDF. ENDF is maintained by the National Nuclear Data Center (NNDC) [26] in the United States. There are many other evaluated libraries in the world, such as the Japanese Evaluated Nuclear Data Library (JENDL) [30] and the Joint Evaluated Fission and Fusion File (JEFF) [31]. The ENDF files contain data for nuclear decay, photons, atomic relaxation, fission yields, thermal neutron scattering, and charged particle reactions as well as neutron reactions. The data files are called "evaluated" because a group of experts decides, or evaluates, what data is included in them. The data includes theoretical calculations of cross sections based on well developed models guided by experimental data [25]. They also decide how to represent regimes that haven't been measured yet by comparing simulation results to experiments. The first data released was ENDF/B-I in 1968 and the latest set is ENDF/B-VIII, which was released in 2019 [32]. The data is written in a standard format that dates back to when the data was stored on magnetic tapes, and data entries are sometimes referred to as "tapes" to this day. Many MC codes read ACE (a compact ENDF) -formatted data rather than the original ENDF file and most transport codes need the data in tabular format. This is why transport codes normally use ACE-formatted data files. ACE files contain ENDF data processed in to appropriate energy- and angle-differential bins and contain not only cross sections, but also angle and energy distributions used in scattering and fission. ENDF assigns a number to each type of reaction called the MT number.

Data may be the most important part of the simulation; it is what ties the calculations to reality. There are also application-specific evaluated libraries, which focus on certain reactions and observables that are of greater interest to their application. They may also make use of application-specific validation methods and measurements, like the International Reactor Dosimetry File (IRDF) [33] which has recently been superseded by the International Reactor Dosimetry and Fusion File (IRDFF-II) [34]. Structure information can be found in the Evaluated Nuclear Structure Data File (ENSDF)[35], which is also maintained by the NNDC [26].

The source providers of nuclear data are responsible for ensuring the quality of the nuclear data that they generate; for example, the National Nuclear Data Center is responsible for simple formatting and physical testing of nuclear reaction data files in the ENDF library on behalf of the Cross Section Working Group (CSEWG) [36], and the US Nuclear Data Program performs similar tests on the nuclear structure data files in the ENSDF library. The result is a collection of nuclear data files which are partially complete, originating from

different eras, and of which the quality is only known to the evaluator (who, especially in this branch of nuclear science, may be retired). The new ENDF/B-VIII.0, evaluated nuclear reaction data library, fully incorporates the new IAEA standards, it includes improved thermal neutron scattering data, and uses new evaluated data from the CIELO project [37].

For this reason, it is imperative that for each calculation made, the nuclear data library used for the simulation and the associated uncertainties are declared. While certain cross sections used could be produced in-house, it is important to ensure proper configuration for the neutron simulation software used. The cross-section data used in transport codes have specific characteristics. Libraries include two different types of cross-section information:

- **Macroscopic data**. Experimental results from arrangements in which the dominant feature is neutron transport, *i.e.* multiple encounters of neutrons with nuclei which produce a series of velocity changes and, in certain important instances, new sources of neutrons.

- **Microscopic data**. Experimental results, generally cross sections, from arrangements in which single encounters of neutrons with nuclei predominate.

Complete nuclear data libraries, such as TENDL [38], also include covariance matrices for many isotopes, particles, energies, reaction channels and secondary quantities which are important for uncertainties and uncertainty propagation evaluation. The information of covariance data have been scarce in the past; the first comprehensive effort was undertaken for ENDF/B-IV at the end of the 1970s. Subsequently however, no major effort was made until the 1990s when scattered data were provided for few isotopes and reaction rates for different files (dosimetry, fusion, JEFF, ENDF). Most recently, ENDF/B-VII.1 and JENDL-4 evaluated data files provided covariance data for the most important isotopes and reactions.

There is a series of unevaluated databases as well, which compile experimental data and calculations that are used to guide the evaluation process. The EXFOR (EXchange FORmat) database [39] stores information about reaction experiments of cross sections, outgoing particles, multiplicities, fission product yields, and more. EXFOR started as a consistent format that was used to exchange nuclear measurement results between different data centers.

2.2.2 Nuclear Data Shortcomings

Regardless of many decades invested in cross section library development, all data libraries contain approximations, inaccuracies that may be rooted in experimental errors or simple shortcomings of the experimental techniques which inhibit a full interpretation of the complete physical picture. Nuclear data libraries could be further improved with improvements in nuclear theory and relevant experiments. Even though theoretical progress has been made as far as the predictability of neutron cross-section models, measurements are still indispensable to meet tight design requirements for reduced uncertainties. Those inaccuracies

produce discrepancies when comparing simulated results and experimental measurements. In addition, the analysis and interpretation of experimental data relies on sophisticated MC simulations that use a variety of nuclear structures and decay data, which could lead to even more shortcomings. Nuclear data uncertainties affect all the transport codes: uncertainties in cross-sections, angular distributions, neutron multiplicities and fission spectra imply uncertainties in the neutron flux and the neutron energy spectrum. Nuclear data uncertainty quantification is still a developing field, which is demonstrated by the fact that covariance data sometimes significantly change even from one release of a nuclear data library to the other.

In the most recent ENDF library release (ENDF/B-VIII.0 [32]) reference, some time was devoted to the status of the covariances in the library, *i.e.* the statistics on the evaluations were updated. It was showed that of the total 557 isotope evaluations, the majority (375) still do not have covariances associated with the evaluation. The lack of uncertainties means that the users of the data have no indication of the confidence in the evaluation. These statistics are improving, as all new evaluations are expected to have associated covariances as time goes on, but there is still work to be done. In this context, high-quality data are needed for simulations [40].

For this reason, new efforts are made to build costly differential experiments for cross section measurements, but an easier route and available at the NIF is to design simple integral experiments in order to assess and isolate uncertainties that come from the nuclear data itself as described in the following section. For example, diagnosing shortcomings for reactions in elastic and inelastic neutron scattering can be done with semi-integral data. The need for more semi-integral and differential experiments are driven by application and science needs that are raising. In particular, the need for the understanding of the new benchmarking experiments in order to separate the various effects and achieve an understanding of some of the basic phenomena. More advanced benchmarking can be performed by comparing results from simulations, ENDF files for example, to results from high-fidelity integral experiments.

There could also be inconsistencies in the cross section evaluations for elements between various libraries both for the cross section and the corresponding uncertainties, which reflects the lack of understanding of this reaction, with uncertainties that are greater than 10% over most of the energy region. In an example in Figure 2.10, the evaluation of ^{27}Al inelastic scattering from three major libraries are shown.

2.2.3 Integral Validation Experiments

In this section, fundamental definitions of integral and validation experiments are presented, which are both necessary to address current challenges associated with recent advances in nuclear engineering modeling simulation, on which this work is focused.

Validation means assessing the physics modeling accuracy using experimental data [41],[42]. The validation process includes two sides: (1) the modeling activities, where the models are developed, the predictive calculations are made and the uncertainties assessed; and (2) the experimental activities which include experimental design, defining initial and boundary con-

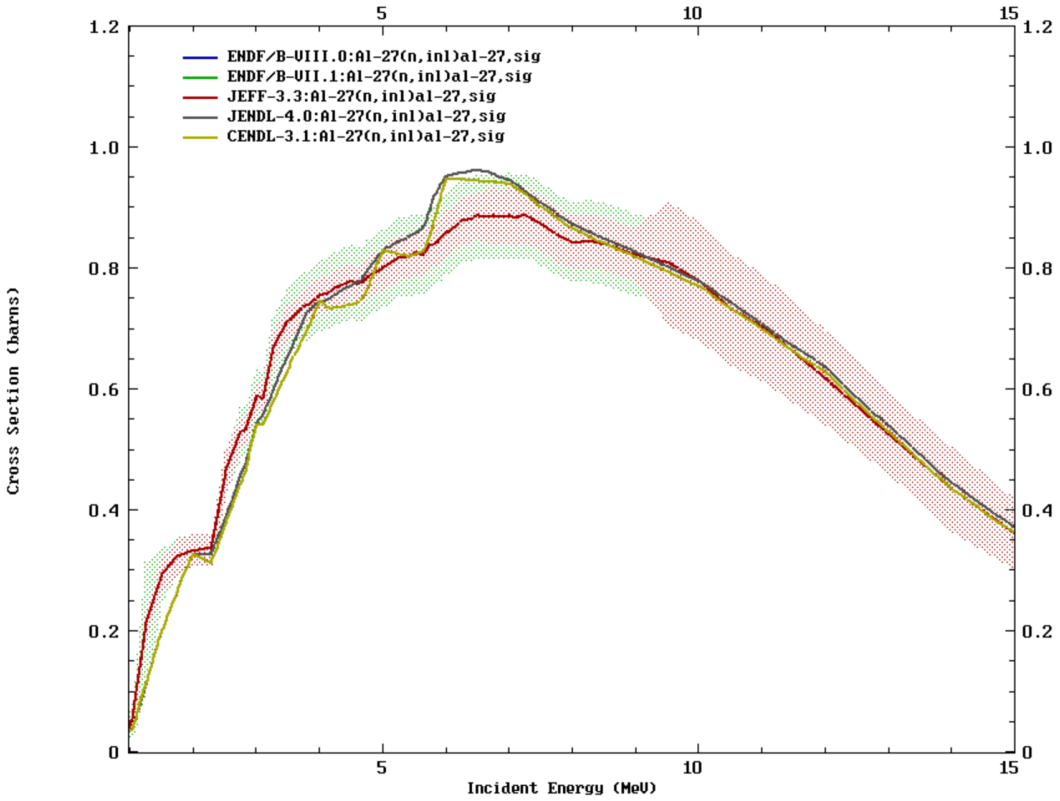

Figure 2.10: Evaluations of ^{27}Al inelastic scattering from some major libraries, with the ENDF/B-VIII.0 uncertainties shown in the green band and the JEFF-3.3 in red. The large uncertainties reflect the lack of data for the inelastic and elastic reactions for this isotope, and covers the discrepancies between the libraries with differences too between the two bands of ENDF/B-VIII.0 and JEFF-3.3 [26].

ditions, measuring the responses and the experimental uncertainties identified. The tactical goal of the validation analysis is the identification and quantification of the uncertainties and errors in the computational model and in the experimental measurements. The set of validation experiments are performed to increase confidence in the quantitative predictive capability of the computational model and to assess uncertainty estimations.

Validation experiments are used to assess the accuracy of the reaction model used to obtain the microscopic cross sections. The simulation methodologies, described in Chapter 3 and 4, are used as predictive capabilities and it is required to have information on the certainty of the prediction, which should rely on a physics-based extrapolation, as opposed to statistical extrapolation.

Both differential and integral measurements provide a set of necessary complementary information about the nuclear data. The two complementary sources of information can be of use for nuclear data evaluations: (1) in a differential measurements the neutron source often involves a particle accelerator and the outcome is the cross section value, σ_E; and (2)

in an integral measurement the neutron source is a broader energy spectrum source such as a nuclear reactor or a facility like the NIF, and the outcome is the effective cross section (e.g. energy-integrated), $\overline{\sigma}$ evaluated in Eq. 2.7.

$$\overline{\sigma} = \frac{\int_0^\infty \sigma(E)\phi(E)dE}{\int_0^\infty \phi(E)dE} = \textit{Effective cross section.} \tag{2.7}$$

Historically, the first data used for reactor physics applications were mainly integral, since differential techniques either did not exist or were not sufficiently accurate. The first integral reactor physics experiment was Fermi's exponential pile, constructed to demonstrate that a self-sustained chain reaction was possible.

Integral experiments are those investigated here to validate and study different material of interest as to assess parameters such as nuclear data and to assess the optimization performance. To validate the simulation performance the integral experiments are needed first to reduce uncertainties associated with input parameters and then to simply explore the basic phenomena.

Designing integral validation experiments depends upon the capability to detect possible systematic errors in the experiments [43], on the completeness of the covariance data, and on the drastic reduction of modeling errors. The uncertainty schematic identified and investigated for the NIF simulations is described in detail in Chapter 4; furthermore, Chapter 7 presents actual values to those uncertainties. The main approach described in the experiments of Chapter 5 relies on the existence or performance of selected integral experiments that provide information on elemental phenomena or on separated individual physics effects or on individual parameters of interest (*e.g.* individual cross sections). Integral measurements are measurements that require for their interpretation an integration of point-wise microscopic data over energy and/or space intervals that are not small compared to the range of interest. A specific type of integral experiment can be used to validate a particular neutron cross section with ample irradiation experiments.

2.3 Nuclear Transport

Neutron transport is the study of the motions and interactions of neutrons within materials. Nuclear scientists and engineers often need to know where neutrons are in an apparatus, what direction they are going and how quickly they are moving. A primary goal in neutron related design is the reliable prediction of neutron population production and loss rates. In order to fully describe neutron transport through media, describing neutron motion and neutron interactions with matter is necessary.

2.3.1 Neutron Transport Equation

Every Ph.D. dissertation in the field of nuclear engineering application and neutron transport will ultimately fall back upon the Boltzmann transport equation [24], and this one

is no exception! The Boltzmann equation describes the detailed neutron balance, *i.e.* the production and loss at every point in the phase space, *i.e.* the energy (E), position ($\underline{\mathbf{r}}$), direction ($\hat{\Omega}$) and time (t). The neutron transport equation is a conservation statement that conserves all energy and momentum of the neutron that is produced and is consumed, as neutrons are absorbed in the media or are scattered in the media. Each term represents a gain or a loss of a neutron, and the balance, in essence, claims that neutrons gained equals neutrons lost. This equation is commonly used to determine the behavior of nuclear reactor cores and experimental or industrial neutron beams. The Boltzmann transport equation used most frequently for engineering applications is given by Eq. 2.8 [24].

$$\begin{aligned}\frac{1}{v(E)}\frac{\partial}{\partial t}\psi(\underline{r},E,\hat{\Omega},t) = &\int_o^\infty dE' \int_{\hat{\Omega}} d\Omega' \Sigma_s(E'\to E,\hat{\Omega}'\to\hat{\Omega})\psi(\underline{r},E',\hat{\Omega}',t)\\ &+\frac{\chi_p(E)}{4\pi}\int_o^\infty dE' \int_{\hat{\Omega}} d\Omega' \nu_p(E')\Sigma_f(\underline{r},E')\psi(\underline{r},E',\hat{\Omega}',t)\\ &-\Sigma_t(\underline{r},E)\psi(\underline{r},E,\hat{\Omega},t) - \hat{\Omega}\cdot\nabla\psi(\underline{r},E,\hat{\Omega},t)\\ &+Q_{ext}(\underline{r},E,\hat{\Omega},t), \quad (2.8)\end{aligned}$$

in which:

- v is the neutron speed, which depends on energy E;
- $\psi(\overline{r},E,\hat{\Omega},t)$ is the angular flux density. It is called a "flux" because it represents a rate at which particles are passing through a surface and "angular" because it is angle-dependent. Since the reaction rates depend on this quantity, the neutron transport problem is usually written in terms of the angular flux density, which is then solved for instead of the neutron distribution:

  $$\psi(\underline{r},E,\hat{\Omega},t) = v(E)n(\underline{r},E,\hat{\Omega},t), \quad (2.9)$$

  where $n(\underline{r},E,\hat{\Omega},t)$ is the neutron distribution function.

  The scalar flux density (or simply the flux) is the angular flux that has been integrated over all angles. The relation between the angular and scalar fluxes is show in Eq. 2.10.

  $$\phi(\underline{r},E,t) = \int_{\hat{\Omega}} d\hat{\Omega}\psi(\underline{r},E,\hat{\Omega},t); \quad (2.10)$$

- Σ_t is the total macroscopic cross section given by:

  $$\Sigma_t(\underline{r},E,t) = \Sigma_s(\underline{r},E,t) + \Sigma_c(\underline{r},E,t) + \Sigma_f(\underline{r},E,t), \quad (2.11)$$

  where Σ_s, Σ_c, and Σ_f are respectively the macroscopic scattering, capture and fission cross section;

- Σ_s ($\underline{r}$,E'$\rightarrow$ E, $\hat{\Omega}' \rightarrow \hat{\Omega}$,t) is the macroscopic double differential scattering cross section, which gives us the macroscopic scattering cross section Σ_s ($\overline{r}$,E,t) over all directions $\hat{\Omega}'$ and energies E' of the outgoing neutrons:

$$\Sigma_s(\underline{r}, E, t) = \int_0^\infty \int_{4\pi} \Sigma_s(\underline{r}, E \rightarrow E', \hat{\Omega} \rightarrow \hat{\Omega}', t) d\hat{\Omega}' dE'; \tag{2.12}$$

- Q_{ext}($\underline{r}$,E,$\hat{\Omega}$,t) is the external neutron source, which is independent of the angular flux;

- χ_p is the fission spectrum, neutrons born from fission are not emitted at a single energy, and the fission spectrum describes the probability for a neutron to be emitted at a certain energy (it is a probability distribution function). For prompt neutron only in this case;

- ν_p(E) is average fission neutron yield;

- Σ_f($\underline{\mathbf{r}}$,E') is the macroscopic fission cross section. The fission reaction rate must be integrated over all other energies, E, and angles, $\hat{\Omega}$.

In the case of neutron generators as the NIF, the fission source is not taken into account in the Boltzmann equation only the external (D-T) source.

The neutron transport equation in this form is an integro-differential equation since it has both derivatives and integrals in it. Its spatial and temporal parts are differential, whereas its angular and energy parts are integral.

The solutions of interest from solving the neutron transport problem are the neutron flux and the reaction rates [24]. Both of those results are used as values for the comparison analysis between the experiments and the simulation. The measurement of the intensity of neutron radiation, expressed in units of neutrons/$(\mathrm{cm}^2 \cdot s)$, corresponds to the rate of flow of neutrons. Consider N particles that travel at speed v in one direction. It is the interaction probability per unit length, multiplying it by the speed gives the probability of interaction per second, or the collision rate. Since there are N particles, multiplying the collision rate by N gives the overall reaction rate, $Nv\Sigma$, of the particles in an infinite medium. If N is substituted for the neutron distribution function instead of a pulse, the expression becomes the reaction rate per distribution differential, or the reaction rate density, *R($\underline{r}$,E,$\hat{\Omega}$,t)*. This expression is shown in Eq. 2.13 and is the first building block of the explicit neutron balance equation. The reaction (*i.e.* interaction) rate knowledge of the neutron flux (ψ) and the material cross sections allows us to compute the rate of interactions.

$$R(\underline{r}, E, \hat{\Omega}, t) = v(E) n(\underline{r}, E, \hat{\Omega}, t) \Sigma(\underline{r}, E) = \psi(\underline{r}, E, \hat{\Omega}, t) \Sigma(\underline{r}, E). \tag{2.13}$$

The scalar flux is often the most interesting quantity as in in reactor physics. The scalar flux is seen in Eq. 2.10 and the the reaction rate for a reaction i that has no angular dependence is shown in Eq. 2.14 [24].

$$R_i(\underline{r}, E, t) = \int_{\hat{\Omega}} d\Omega \Sigma_i(\underline{r}, E)\psi(\underline{r}, E, \hat{\Omega}, t) = \Sigma_i(\underline{r}, E) \int_{\hat{\Omega}} d\Omega \psi(\underline{r}, E, \hat{\Omega}, t)$$
$$= \Sigma_i(\underline{r}, E)\phi(\underline{r}, E, t). \quad (2.14)$$

It is linear and relatively easy to solve for simple geometries and reaction parameters, but in order to capture all the relevant physics for real-world problems, complex geometries and energy-dependent reaction parameters must be used. Despite it's linearity, the neutron transport equation can be difficult to solve analytically because of the large, heterogeneous domains over which it must be solved and the complex energy dependence of the cross sections. The energy range of interest can span more then 12 orders of magnitude, from 1×10^{-11} to 1×10^{1} MeV and above, and the geometries involved can include millions of individual material regions containing many different mixtures of materials. Different techniques have been used to approach the problem: deterministic or MC based methodology. A complex neutron transport computation is required to predict the number of transmitted neutrons and their distributed energy. The latter methodologies and their associated codes used are described in Chapter 3.

2.4 Neutron Flux Tailoring

Understanding how neutrons interact with different materials, the differences in nuclear data libraries and the uncertainties and shortcoming are vital for properly moderating and tailoring the neutron spectra with complex beam shaping assemblies. Every tailoring methodology described in Chapter 4 relies on properly simulating the neutron path, the neutron energy variation within the environment considered and the materials inserted. All codes used for the simulations are developed to solve the Boltzmann transport equation and introduce a series of approximations and limitations the designer needs to consider and properly understand in order to trust the results and perform tailoring experiments.

All of the tailoring methodologies, those which are the state-of-the-art or those introduced with COEUS, encounter the same difficulties in increasing the uncertainties in the reaction products, in the neutron spectrum measurements, thereby limiting the quality of the data gathered.

The analyzed data in this research work will be compared with the simulated results to determine the ability to model beam shaping assemblies performance. Initial models have been developed and through this thesis research are updated in order to be made to fully propagate nuclear data uncertainties. This is performed within different MC models as described in Chapter 3. Understanding the effects of all the uncertainties and shortcoming can be used to gain insight into nuclear data issues where the model diverges from the actual beam shaping assembly performance. The initial planned integral experiments are then crucial as a development step for designing complex beam shaping assemblies. The

propagation of the nuclear data uncertainties into the modeled the NIF results would also be highly beneficial and worthwhile for future nuclear experiments.

Chapter 3

Neutronics Modeling Methodology

This chapter introduces both the methodology and the software employed for modeling the NIF neutron source and the surrounding environment used in COEUS.

The first part of the chapter discusses in details the deterministic and Monte Carlo methodologies. Also Denovo and the Monte Carlo N-Particle (MCNP) codes are introduced by describing the motivation behind choosing those two codes, how they work, and their limitations. Section 3.2 illustrates the uncertainties in the modeling methodologies and the techniques used to take them into consideration and how to possibly reduce them.

The actual simulations of the National Ignition Facility (NIF) environment in full 3D geometry will be presented in Chapter 7, focusing on the experiment simulation from Chapter 5. Chapter 8 will focus on the modeling of optimized Energy Tuning Assembly (ETA) using COEUS.

3.1 Neutron Transport Modeling

In Chapter 2 the Boltzmann neutron transport equation [24] is introduced as the chapter focuses on describing the computational methodologies used to solve this highly complex problem that cannot be solved analytically. Three methodologies have been identified as useful during this work to solve the transport problem. Those methodologies are described below [44].

- **Deterministic approach**, which discretizes all of the independent variables to obtain a set of coupled linear (not always guaranteed linear) algebraic equations, and develops a numerical method to solve them.
- **Probabilistic approach**, which follows the history of each relevant particle, based on the underlying probabilities for various types of interactions.
- **Hybrid methodology**, which is a combination of both methods above.

Both, the probabilistic methodologies, in our case specifically the Monte Carlo (MC) method, as well as the deterministic methodologies have been used here and for each of those methodologies different simulation software has been chosen.

3.1.1 Deterministic Methodology

In deterministic calculations, all the variables (space, energy, and angle) are discretized [45]. The spatial discretization is often based on structured Cartesian, hexagonal/triangular or cylindrical grids but can also be done with unstructured grids. The energy discretization is accomplished using a multi group approach and the angular discretization is based on a set of discrete directions (*e.g.*, discrete ordinates). The Boltzmann transport equation is solved deterministically for the average particle behavior which makes it computationally inexpensive, albeit memory intensive.

There are many deterministic methods, but here are mention only those that are widely used: the discrete ordinates method (first order equation, S_N method) [46], the method of characteristics (integral equation) [47], and the spherical harmonics method (second order equations) [48].

The deterministic methods introduce some approximations and simplifications [44]. The largest approximation is related to the discretization of continuous variables, and the computing accuracy depends on the size of the discretization mesh. A good example of this is the ray effect in deterministic codes based on the S_N method [48]. The discrete ordinate(s) method consists of a discretization of the angular variable $\hat{\Omega}$ in the Boltzmann equation so that neutrons will only travel in few specific directions. Thus, the accurate representation of neutron paths through the system might require very large number of directions, which could be prohibitively expensive. The ray effect itself is a particularly persistent spatial distortion of the scalar and angular flux which occurs mostly in 2D and 3D geometries with localized sources.

3.1.1.1 Denovo

An example of a deterministic (S_N) code solver used in this research is Denovo [49]. Denovo has been developed by Oak Ridge National Laboratory. It is a massively parallel, modern code created with a Cartesian grid for 2-D and 3-D geometries [49]. This modern code has solvers that take advantage of decades of research and experience in the development of deterministic codes. Denovo was developed to be used in parallel computing to enable solutions to very large problems. It also has an advanced visualization, run-time and development environment. A Denovo solver is used in this research as the solver within the Automated Variance Reduction Generator (ADVANTG) [19], described in Section 3.2.1.2.

3.1.2 Monte Carlo Methodology

While a deterministic code usually solves the integro-differential or integral form of the Boltzmann equation or a simplified equation mathematically, MC does not [44]. The MC methodology is capable of simulating the "true physics" of the problem without any approximation. MC methods are especially useful to employ in nuclear science studies due to the extremely large number of independent variables and complexity of the math involved in modeling and simulating macroscopic, real world scenarios. The process of MC particle transport can be described as a numerical simulation of the reality in which numerous particle histories are simulated to derive the statistical (*i.e.* average) behavior of the whole system through the use of the central limit theorem. In a MC methodology, the physics of the system is described through a probabilistic approach [44]: the cross-section are probabilities for a neutron to interact with a given nuclide, the angular distributions and energy spectra of secondary particles all give a probability for certain angles and energies. If a Monte Carlo simulation follows the physics of particle interactions accurately, such a direct simulation is known as the analog Monte Carlo. The MC simulation relies on the [44]:

- **Particle tracking**: by using ray-tracing through "exact" model of problem geometry to determine location of next particle collision or boundary crossing to different material.
- **Collision physics**: determination of the type of collision and consequences of that collision by sampling from various probability distributions represented as cross sections.
- **Tallies**: book-keeping, to record frequency of certain events during the simulation.

Theoretically, the MC numerical solutions need large number of CPUs, includes a long run time and the results have associated statistical uncertainties. However, MC methodology is easily parallelized and it takes advantage of the advancement in High Performance Computing (HPC) improvements and developments. This chapter is limited in describing the peculiarities of MC codes as they relate to our problem of simulating the full chamber of the NIF and the ETA optimization without going into detail about the mathematics behind the MC method itself.

3.1.2.1 Tally Estimators

The result of a basic MC simulation is a set of interaction points and corresponding set of particle tracks between the consecutive interaction points, a track length l, energy E and their corresponding weight w. Expected values of parameters like particle flux, current, etc. can be derived or tallied (as it is known in MC terminology) from this set of interaction points and tracks, either by demand of the user or by the code itself. An important MC tally estimator is the collision estimator which tallies a response function $g(x)$ at every collision in the cell or cells of interest. A variation on the collision estimator is the absorption estimator

which tallies a response function *g(x)* not at every collision but at every absorption event. In the case of a cell where a lot of particles passing through without interacting (such as a thin interface between two other cells as in an activation foil), these estimators are not very accurate. The track length estimator is another type of MC estimator that does not have the previous problem and that is often used in the most commonly used software, like MCNP to estimate the reaction rate and the total flux. The latter estimation actually uses the particles' track length to tally the averaged flux value of the response function *h(x)* and is therefore capable of giving results when the particles pass through the cell. For typical tallies, which may be volume-averaged or surface-averaged, the final estimate is the sample mean calculated as [50]:

$$\overline{x} = \frac{1}{N}\sum_{n=1}^{N} x_n, \tag{3.1}$$

where N is the number of particles/histories or batches and x_n is the estimate. The accuracy of the result is reported as the standard deviation of $\overline{x}$, which is also known as the standard error of the mean, and is denoted by:

$$\sigma_{\overline{x}} = \sqrt{\frac{1}{\sqrt{N(N-1)}}\sum_{n=1}^{N}(x_n - \overline{x})^2}. \tag{3.2}$$

It should be noted that Eq. 3.2 implies that the standard deviation of the mean always scales as $\frac{1}{\sqrt{N}}$ [50]. This means any calculation's variance of the mean will go to zero, *i.e.* the sample mean will converge to the true mean, as long it is run long enough and enough samples are collected, but that it will converge as $\frac{1}{\sqrt{N}}$, which is slow [50].

The standard deviation of $\overline{x}$ is a measure of variation in the results of multiple identical and independent simulations.

Since the central limit theorem states that the sample mean is normally distributed, we can make use of the well-know properties of the normal distribution, namely the confidence interval. The normal distribution has well-defined confidence intervals: 68% of the population will lie within a single standard deviation, σ, and 95.5% will lie within 2σ [51]. A more convenient form for the accuracy is the relative standard error (or relative statistical error) given by Eq. 3.3, which is for the 68% confidence level, and simply needs to be doubled for the 95% level [18].

$$Rel. \quad Err. = \frac{\sigma_{\overline{x}}}{\overline{x}}. \tag{3.3}$$

All outputs of any MC code, like MCNP [18], have the form:

$$\overline{x} \pm \sigma_{\overline{x}}. \tag{3.4}$$

The goal is to keep *Rel. Err.* as small as possible with as few histories as possible and generally must be less than 10% for meaningful results. Thus, increasing the number of

particle histories is often not enough to reduce the *Rel. Err.* This property of the relative error is the great weakness of the MC method, because, generally, many histories must be generated to obtain acceptable results leading to long running times. However, there are techniques, introduced in the MC based software, that are used to reduce statistical uncertainties and more details are given in Section 3.2.1.

3.1.2.2 MCNP

MCNP [18] has been developed at the Los Alamos National Laboratory (LANL) [52] during the Manhattan project [52] and it is a general-purpose MC Neutral Particle code that can be used for neutron, photon, electron, etc. or coupled particle transport and includes the capability to calculate eigenvalues for critical systems. The flexibility, wide adoption, extensive benchmarking, and test history make MCNP an ideal choice for the NIF modeling and for using it within the optimization COEUS software. Decades of documentation and experience and the fact that it is highly controlled and taken care of at LANL by a large community make it a very robust method. MCNP is under restriction from the Radiation Safety Information Computational Center (RSICC) [53]. The versions that are used for this thesis are both MCNP5 and MCNP6 [54].

MCNP treats an arbitrary three-dimensional configuration [18] of materials in geometric cells bounded by first- and second-degree surfaces. Pointwise cross-section data are used, and a large number of particles are tracked down depending on the interest of the user. For neutrons, all reactions given in a particular cross-section evaluation are accounted for. Those evaluations depend on outside information in the form of cross-section libraries (*e.g.* ENDF/B-VII [25], [55] or ENDF/B-VIII [32]), which are based on experimental values when available. The MCNP user submits an input file to the code package/suite, where simple predefined mathematical functions are used to build and describe the scenario simulated. These scenarios can vary widely in complexity, accuracy and precision, ranging from simple transmission of radiation through a single piece of material, to modeling and simulating an entire large-scale research facility like the NIF [56].

Several other MC codes have been developed over time in different research centers or Universities around the world: SCALE KENO [20], TRIPOLI [57], MONK (Oak Ridge National Laboratory, USA) [58], SERPENT (VTT Technical Research Center in Finland) [59], WARP (UC Berkeley, USA) [60], GEANT4 (CERN, Switzerland) [61], OpenMC (Massachusetts Institute of Technology, USA) [51], etc. Specifically, the SCALE code system is a widely used modeling and simulation suite for nuclear safety analysis and design that is developed, maintained, tested, and managed by the Reactor and Nuclear Systems Division (RNSD) at Oak Ridge National Laboratory (ORNL). SCALE provides an integrated framework with dozens of computational modules, including three deterministic solvers and three MC radiation transport solvers that could be selected based on the users' desired solution strategy. SCALE is another of the code described in this thesis is Section 3.2.3.

3.2 Uncertainties

In modeling and simulation, identification of uncertainties plays an important role in determining the accuracy of results. An uncertainty analysis of both experimental and simulation results allows better understanding of the confidence levels and reasons for possible discrepancies. There are two main sources of uncertainties in modeling and simulation: input data and simulation model. Examples in possible uncertainties in the input data: uncertainties in cross sections, uncertainties in material properties, geometry data, etc. Examples of modeling uncertainties are coming from various approximations incorporated into a particular modeling methodology or in a particular design process. High-fidelity simulation can provide a major benefit if it can reduce to the smallest amount the impact of uncertainties. Often, MCNP results are associated with statistical uncertainties alone. However, this research attempts to also provide uncertainty values from modeling approximations as well as from nuclear data.

3.2.1 Statistical Uncertainty of MC Simulations

When performing MCNP simulations, there is a possibility that not enough particles reach the region of interest due to leakage or absorption in the ETA geometry and this gives rise to issues in the uncertainty of the results since not enough events are registered. An example: if considering large ETA inside the NIF Target Chamber (TC), including very thin activation foils into the model could lead to very few neutrons interacting within the activation foils or even crossing an activation foil volume.

Thus, in case of complex geometries, MCNP can require several hundred to thousand computer hours to run in order to build up meaningful statistics detailing the requested results. The model can be improved by employing coding techniques and including additional mathematical structures. This is known as variance reduction (VR) [62], [63] and can have a significant effect on the quality of obtained statistics.

For this reason, often unbiased (or analog) MC [62] is not viable for the simulation of many real-world nuclear systems. The VR techniques modify the analog simulation process in such a way that they give the same average values as analog MC, while giving a variance (*i.e.* a statistical uncertainty) that is smaller than or at least equal to the analog case. As a result, such modified simulation processes can significantly speed-up a MC simulation.

3.2.1.1 Variance Reduction Techniques in MCNP

If in a complex environment, as the NIF, the VRs are not applied, it would quickly become impractical from a computing time standpoint to achieve any meaningful results.

In any VR technique, the simulation, hence the underlying distribution, is changed so that it produces fewer zero-score histories and becomes more concentrated about its mean. The variance of the mean will be less than that of the analog simulation. The VR techniques utilize biased sampling distributions to reduce the computer time required to obtain results

of sufficient precision. To preserve an unbiased estimate, the concept of particle weight (w) is introduced in Eq. 3.5.

$$w^0 p_{unbiased} = w^* p_{biased}, \tag{3.5}$$

where $p_{unbiased}$ is the actual physical probability distribution found in nature of the considered event sampled, and w^0 is the natural weight of the particles (usually unity). The biased probability is noted by p_{biased} with the corresponding weight, w^*, that accounts for such bias.

The weight of a particle track represents the relative contribution of that track to the final result. Examples of VR follow below.

1. **Population control methods**. These methods artificially increase/decrease the number of particles in spatial or energy regions that are important/unimportant to the tally score. Specific population control methods are listed below [64].

    - **Geometry splitting and Russian Roulette**. Geometry splitting is the easiest techniques to apply. Whenever a track enters a region with higher importance than the previous one, the particle track will be split in multiple tracks but each with a reduced weight. As a result, important particles are followed more often but the solution remains unchanged because of the conservation of particle weight. The reverse is also possible. This is useful as it does not require a particle to reach the detector location in order to add statistical value to the tally result. The original particle will continue its random walk throughout the problem until terminated.
    - **Energy splitting/Roulette**. Energy splitting and roulette is a means of biasing energy space. Although this feature is available in MCNP, its use is not recommended since the energy-dependent weight window does a better job.
    - **Weight cutoff**. Another common and simple variance reduction tool is the weight cutoff. A minimum weight is specified in each region below which Russian roulette is played. This avoids the loss of time following very low weight and, hence, unimportant particles. In MCNP, the weight cutoff is usually specified as proportional to the inverse cell importance in each geometric region.
    - **Weight windows**. This is a space-energy-dependent splitting/roulette technique where the number of particles increases in important regions. The splitting and roulette are used to maintain particle weights within a user-defined range, referred to as the weight window.

2. **Modified sampling methods**. The methods artificially increase the likelihood of events that increase the probability a particle reaches the tally region. Example of modified sampling methods included in MCNP are:

    - **Exponential transform**.

- **Implicit capture**.
- **Forced collisions**. Forced collision is a type of biasing allows for an increase in the number of collisions in the specified cells by dividing the incoming particle into an uncollided and collided particle. The collided particle is forced to collide in the cell while the uncollided exits with no interaction.
- **Bremsstrahlung biasing**.
- **Source direction and energy biasing**. Here the sample source from a biased pdf splits more particles in important regions. The particle weight is corrected by the ratio of the natural (unbiased) and biased probabilities.
- **Neutron induced photon production bias**.

3. **Partially deterministic methods**. These methods replace the random-walk process by a deterministic process (*e.g.*, exponential attenuation) to move particles from one region to another. In MCNP the following are available:

   - **Point and ring detector** (known as F5 tally in MCNP). This tool becomes very attractive as flux is being investigated in a region which particles (neutrons and photons) only reach with a low probability as the thin foils for foil activation detectors.
   - **DXTRAN sphere (DXT,DXC)**.
   - **Correlated sampling**.

An effective use of the VR proceeds with an iterative process that requires typically experience, knowledge, time, and effort from the designer and also skills in interpreting the MCNP output. If these parameters are well chosen, then the calculation should converge more quickly. Improper use can lead to unstable statistical behavior and unreliable/erroneous results.

3.2.1.2 Hybrid Methodology: MCNP/ADVANTG

The variance reduction in MCNP can be limiting and cannot vary based on the variation of the geometry of interest [64]. It is often important in the COEUS optimization to change the importance in order to have good statistics even in smaller parts of the NIF chamber and especially increased importance where the effect of scattered neutrons is felt. An alternative to using the VR methodology implemented in MCNP is to use a coupled hybrid methodology of MC and deterministic methodology [49]. The hybrid methods use fast, approximate deterministic calculations to accelerate highly accurate MC simulations. The method used in this work is the couple MCNP with ADVANTG, which is an automated tool for generating variance reduction parameters for fixed-source continuous-energy MC simulations based on approximate 3-D multigroup discrete ordinates adjoint transport solutions generated by Denovo. ADVANTG generates space and energy dependent mesh-based weight-window bounds [19].

ADVANTG automatically converts the continuous MCNP input to a discrete Denovo input, develops the variance reduction parameters, and outputs an updated MCNP and weight window input file [19]. ADVANTG has been applied to neutron, photon, and coupled neutron-photon simulations of real-world radiation shielding and detection scenarios. ADVANTG is compatible with all MCNP5 geometry features and can be used to accelerate cell tallies (F4, F6, F8), surface tallies (F1 and F2), point-detector tallies (F5), and mesh tallies (FMESH) [19]. ADVANTG implements the CADIS [65] method and the Forward-Weighted CADIS (FW-CADIS) method for generating variance reduction parameters [66],[67].

The need for ADVANTG comes from the flexibility of such software to modify the grid in the large space, it is user friendly and can be adapted with the variables of the MCNP in the optimization. For this reason, it is used in part of the MCNP modeling of the NIF as will be seen in Chapter 7 and especially coupled with MCNP in the optimization software COEUS.

3.2.2 Uncertainties in Modeling

The quantification of uncertainties is a crucial step in design and simulations. The uncertainty quantification drives requirements for modeling assessments, design margins definition and for the optimization of ETA. While uncertainty quantification in the case of existing experimental components at the NIF benefits from a large data base of experimental results, innovative designs for future shots at the NIF should rely on limited experiment data bases and on a number of past integral experiments that should be shown to be representative enough. In a preliminary design phase, the comparison of *a-priori* uncertainties (nuclear data and modeling) with the target accuracy, allows to define needs and priorities for calculation scheme improvement and uncertainty reduction. Integral experiments (as described in Chapters 5 and 6) have been performed in order to reduce uncertainties and to define new reduced *a-posteriori* uncertainties. Integral experiments used here are performed in a complex environment that is not completely a clean chamber as often items are introduced at the last minute and non predicted impurities can appear after the shots. In this case it impossible to avoid the risk of introducing error compensations, especially if introducing complex element like an ETA inside too.

It is better to envisage the experiments performed as a set of representative validation experiments where the goal is to have well-documented experimental uncertainties. The choice of integral experiments is done with specific results of interest that come from: identifying all the uncertainty effects to the final results. The choice of integral experiments is done with specific results of interest that come from:

- Performing a series of simpler experiments to validate separately different effects that influences the comparison of the measurements with the simulations, *e.g.* first validating the quality of the MCNP modeling for the background neutrons with an empty

SNOUT and HTOAD and record the room return in the NIF experiments; the measurements uncertainties for each shot, etc.

- Adding a material of interest at the time in order to single out the effects of cross section uncertainties in the material.
- Having a well-defined knowledge of the physics effects at different points in space and energy ranges recorded separately for each experiment, *e.g.* having a set of different neutron activation foils in different locations inside the NIF: closer to TCC. in the middle and at the end of the SNOUT and HTOAD. Also having different isotope samples in the foils too allow significant information at different point in the energy range of interest.

Once the above uncertainties are known, it will be possible to perform validation of the complex ETAs of interest, where the effects to the final results will be given by the uncertainties propagation of the cross section throughout the ETA. The goal is the user to have an ETA with provided only the resulting neutron spectra of interest with the uncertainties from the nuclear data uncertainty propagation as all the other effects will be accounted in the designing procedure.

3.2.2.1 Derivation of Uncertainty Forms

There are different types of uncertainties which need to be taken into consideration. The uncertainties can be divided in two categories described below.

- **Aleatory uncertainty** [41]. Aleatory uncertainties are due to inherent randomness. These are intrinsic and in principle not reducible uncertainties associated to random phenomena. Typical examples of aleatory uncertainties include geometrical description, environment conditions (*e.g.* in the NIF environment those can be the shot operating conditions,the changes post shot from initial configurations, etc.), tolerances in specifications, unexpected impurities in the materials used, etc. The aleatory uncertainty can be rigorously treated for propagation in the computer model.
- **Epistemic uncertainty** [41]. These type of uncertainties are due to lack of knowledge of the system and its parameters. A typical examples are cross sections. Reduction of the epistemic uncertainty can be performed when useful and relevant experimental information is available.

3.2.2.2 Sensitivity Calculation

Sensitivity analysis is performed at the NIF to understand the effects of each of the parameters causing uncertainties and how those influence the result. Sensitivity analysis and associated sensitivity coefficients can be used for different objectives: uncertainty estimates,

design optimization, determination of target accuracy requirements, adjustment of input parameters (data assimilation, model calibration), evaluations of the representativity of an experiment with respect to a reference design configuration. For example, the NIF experimental environment is highly complex and might contain materials, close to the instrumentation of interest, with uncertain relevant to nuclear properties. Those uncertainties in the surrounding materials might introduce a systematic uncertainty in the measurement results.

If this material with large data uncertainty is in close proximity to the target or detector, then even a small total mass of this material may be enough to cause a systematic uncertainty. An example is that if the operation of a detector is based on one or more uncertain nuclear observable, like the reaction cross sections of the foils materials described in Chapter 6, then a particularly significant systematic uncertainty may be present in results obtained. Uncertainties on the cross sections used in MC simulations imply a systematic uncertainty on every experimental result into which simulated data have been incorporated.

Several runs of the same problems are performed with different random input values, taken within the range of the specified uncertainty and associated distribution law, and then at the end the final results are statistically combined in order to determine the average value and the associated standard deviation. Sensitivity coefficients are also used in input parameter adjustments, where the coefficients are used within a fitting methodology (*e.g.* least square fit, Lagrange multipliers with most likelihood function, etc.) in order to reduce the discrepancies between measured and calculated results.

3.2.3 Uncertainties in the Model from Nuclear Data

The importance of nuclear data is often overlooked or outright ignored by many, although it encapsulates large parts of the physics behind the problem of particle transport. One can have the most robust codes in the world at their disposal, but if the nuclear data fed into those codes are lacking, the results themselves will be worthless.

Simulation tools like MCNP pay little attention to which library of nuclear data for particle transport calculations is used as the results do not provide information on the nuclear data uncertainties. A complex environment with multiple materials as in the NIF and the ETA would benefit of having fully propagated nuclear data uncertainties. One of the main sources of uncertainty is the input data like the cross sections. Several MC sampling methods have been created to capture the impact of nuclear data covariance on nuclear engineering problems, including SCALE Sampler [68], NUSS [69], SHARK-X [70], among others. Many collections of software package capable of performing these types of uncertainty quantification are not available for distribution or focus solely on reactors. Here the uncertainties are given only for neutron cross section data: no attempt is made to consider uncertainties on angular distributions, gamma-production data, secondary energy distributions, etc.

PTRAC in MCNP

Due to the inability of this methodology to introduce cross section uncertainties in the results, an implicit-capture MCNP simulation is needed. If an implicit-capture MCNP sim-

ulation is performed, a PTRAC output file is created [71] where the probabilistic weight of the tracks entering and exiting each event are provided. Since these weights depend on the cross section library used in the simulation, varying those weights allow to investigate the effects on the final results of the different cross section libraries and their uncertainties. The PTRAC file is used to plot particle tracks, which allows an overview of the type of interactions in the experimental environment. Using the PTRAC file to identify the nuclear data uncertainties is still limiting as it does not provide information on the transport uncertainties and is not efficient for propagating the uncertainties through multiple materials.

SCALE/SAMPLER

The SCALE Sampler module [20], [68] is used to assess the neutron transport response uncertainty. The uncertainty information is given by building a distribution of responses using the pre-built set of 252-group and 66-group nuclear data libraries sampled from ENDF/B-VII.1 [55] and the International Reactor Dosimetry and Fusion File (IRDFF) v.1.05 [72] consistent with the underlying nuclear data covariance. Sampler is a super-sequence that performs general uncertainty analysis by stochastically sampling uncertain parameters that can be applied to any type of SCALE calculation, propagating uncertainties throughout a computational sequence. Sampler treats uncertainties from two sources: nuclear data and input parameters. Sampler generates uncertainty in any result generated by any computational sequence through stochastic means by repeating numerous passes through the computational sequence, each with a randomly perturbed sample of the requested uncertain quantities.

The IRDFF nuclear cross sections are converted to SCALEs 252-group format [20], while the uncertainties are converted by linear interpolation of the midpoint bin energies. The Sampler values are collapsed at lower energy to create a 66-group structure. The Sampler results are then combined with statistical bootstrapping to provide a mean and uncertainty that included the systematic nuclear data uncertainty with statistical error included. Bootstrapping is a process of randomly selecting replacement data from a sampled distribution to create a probability distribution representative of the underlying distribution. Bootstrapping is used to create uncertainty bounds for the set of Sampler results. The reaction rates are determined in post processing by perturbing each Sampler reaction rate for each activation foil. Each of Samplers independent sample simulated fluences in each activation foil are convolved with the IRDFF nuclear data covariance sampled reaction cross-sections separately from the perturbation in SCALE. This methodology to re-sample the reaction rate for a response assumes that the nuclear data follows a correlated multivariate normal distribution [68], [73]. Multivariate normal distributions require an expectation value and a covariance matrix that is positive semi-definite. The resultant uncertainties from the Sampler multi-group neutron transport calculation are utilized to infer uncertainties in a continuous energy neutron transport simulation modeled in MCNP5. The impact of nuclear data covariances on the NIF and ETA simulated results is addressed for the neutron energy spectrum and foil activation rates.

Chapter 4

Optimization Methodology

This chapter describes the development of the Gnowee/COEUS optimization software, which began in 2016 [6] and, over the course of this research, was further expanded into an improved version [15]. Section 1.1.1 shows that the complexity of modifying a 14.1 MeV neutron spectra in order to generate artificial customized TN+PFNS spectrum leads to the reconsideration of the previous optimization methods. The latter, in fact, were not deemed suitable for such complex tailoring. Further extension and generalization of Gnowee/COEUS allowed for more flexibility in the choices of the number and type of variables, objective functions and constraints in designing Energy Tuning Assemblies (ETAs). Increasing the generalization of this software required most of the development efforts featured in this thesis work, as the improved version is designed to perform a high fidelity, fast-running simulation in order to tailor neutron spectra for multiple applications.

Section 4.1 introduces the motivation and nature of the software, and in Section 4.2 the code structure is described: first introducing the metaheuristic algorithm in Gnowee, then the design software, COEUS. The first part of this chapter is focused on the initial version of Gnowee/COEUS, including its limitations. The second part, Section 4.3, then focuses on of the thesis works efforts to improve the code and how the Version 2.0 (v2.0) of Gnowee/COEUS works, in addition to the consideration of possible applications. Chapter 7 will present the validation of the modeling capabilities of v2.0 and Chapter 8 will present a series of ETA design models introduced in the National Ignition Facility (NIF) environment, serving as and example of the modeling capability of the optimization software.

4.1 Motivation and Introduction of the Code

Optimization is a powerful tool for making decisions or developing designs given a design space, an objective and a set of constraints [74]. By using true optimization techniques, not parametric studies or expert intuition, better outcomes can be achieved often with less effort and time.

The benefits and drawbacks of enumerative (*i.e.* parametric) design approaches for com-

plicated neutron energy spectra tailoring designs are illustrated considering the extensive work that has gone into the BNCT application over the course of decades [5]. For example, the parametric design process tends to result in the investigation of limited geometries and materials, often based on those that had been applied for previous designs. The parametric approach is in fact described as a series of simulations where one or more parameters are varied individually to determine the best design where the correlations and inter-variable dependencies are not captured. Furthermore, this approach is also both manpower-intensive and problem-specific. Such limitations unnecessarily restrict the design space in ways that can drastically impact the overall performance of the design. The motivation for the development of metaheuristic optimization software, originating from the work by Dr. James Bevins [14], was a lack of satisfactory optimization methodologies in the nuclear world. The need of such effort is to have a generic and well-coherent methodology in order to design for different sources and optimization methodologies. By framing the design as a formal optimization problem, the design space can be expanded to materials and/or geometries that were not previously considered. Additionally, through the use of global or nearly global optimization techniques, designs developed will have the maximum possible performance under the constraints and objectives considered. Moreover, the hybrid metaheuristic optimization is significantly more advanced than the enumerative methodologies seen in the literature.

The manner of design of the ETA presented in Section 1.1.1 is a significant departure from the approach taken by current methodologies in the literature. In the past, even those applications which have sought complicated, multi-layered designs to achieve their objectives have used the parametric or deterministic approach. For complex optimization designs the deterministic methodology was often used as the optimal solutions are obtained through rigorous mathematical formulation of the problem where the convergence to local optimum is guaranteed and the results are repeatable. But as in the parametric studies, the solution is highly dependent on the starting point and is highly problem specific. In addition, this also requires mathematical formulation, all which makes it not an ideal approach for a generic neutron spectra tailoring software.

4.2 Gnowee/COEUS Version 1

The metaheuristic methodology used for Gnowee/COEUS can explore large design spaces efficiently and is relatively insensitive regarding the starting point. Furthermore, this methodology is limited to local optima trapping, the knowledge needed to be able to execute it is limited, the strategies are general and it is not problem specific. All of these aspects come handy for designing complex ETAs which are single or multi-objective, non-linear, constrained, continuous and discrete multi-modal optimization problems. The algorithm must also be coupled with a Black-box radiation transport code in order to evaluate the objective function for each design. All described aspects are indeed far too complex for standard enumerative and parametric techniques. If a particular methodology is to account for a large space of possible variables and constrains, even a search for optimal one-dimensional

ETA could lead to a prohibitive large number of possible permutations as shown in Eq. 4.1. Thus, the classic enumerative/parametric techniques will not work well if applied on large, multi-dimensional optimization problems.

$$P = (|M| \times |\rho| \times |IR| \times |OR| \times |Z_1| \times |Z_2|)^{|N|} \times |R_{foil}| \times |Z_{foil}|, \tag{4.1}$$

where:

- | | represents the number of allowed values for a given variable;
- M is the mass of the material;
- ρ is the density;
- IR and OR are the respective inner and outer radii of the ETA elements;
- Z_1 and Z_2 are the dimensions of the ETA (*e.g.* height and length);
- R_{foil} and Z_{foil} are the radius and height of the foils used inside the ETA for detecting the fluxes.

Specifically, the number of possible ETA designs that result from Eq. 4.1 can come to, for example, in a 1D ETA design to 3.94×10^{15} [6]. The goal of the new metaheuristic methodology is to enable future designs to be generated at a fraction of the cost in terms of manpower and research effort, thereby accelerating the pace of development in tailoring neutron spectra. The only significant drawback of the software is that finding global optimum is not inherently guaranteed and the results are not repeatable.

The structure of how Gnowee/COEUS are interfaced and how they interface with the radiation transport codes of choice is seen in Figure 4.1, and each of the software descriptions are presented in Section 4.2.1 and 4.2.2, respectively.

From the initial stages of the development, Gnowee/COEUS showed promising results for optimal tailoring of neutron spectra. Gnowee/COEUS Version 1 is fully operational on the UC Berkeley computing facility Savio. However, this version has limited applicability for a specific neutron spectra tailoring.

4.2.1 Metaheuristic Optimization Algorithm: Gnowee

Gnowee is a general-purpose hybrid metaheuristic optimization algorithm designed for rapid convergence to nearly globally optimum solutions for complex, constrained engineering problems with mixed-integer and combinatorial design vectors and high-cost, noisy, discontinuous, black box objective function evaluations [75], [76], [77]. The algorithm is developed as a modular, Python-based, open-source hybrid metaheuristic optimization framework [15]. Python is one of the most frequently used and flexible programming languages available today, running on all variants of UNIX, Windows, MS-DOS, MacOS, and many other operating

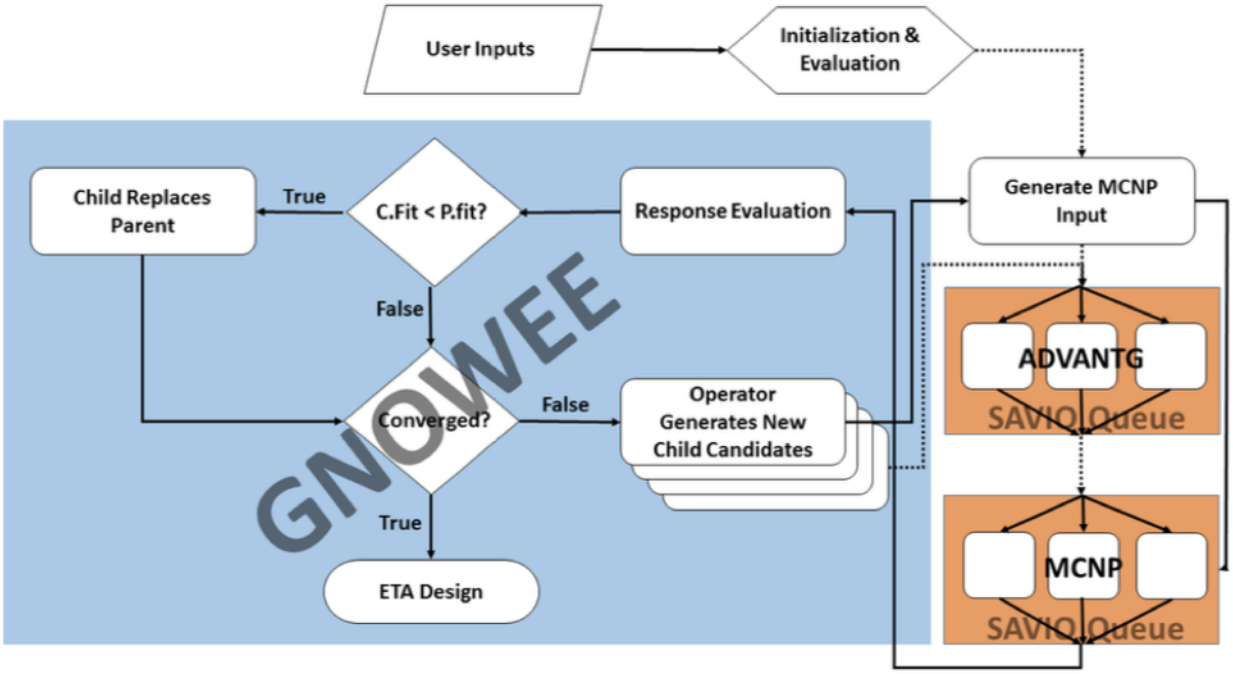

Figure 4.1: COEUS flowgorithm showing interfaces between Gnowee, radiation transport codes, and parallelization for HPC [6],[12].

systems. There are many potential applications for this novel algorithm even as standalone both within the nuclear community and beyond. The optimization problem can be stated according to Eq. 4.2.

$$\begin{aligned} Minimize: \quad \overrightarrow{x} \in \mathbb{R}^d \qquad & f_i(\overrightarrow{x}), \quad (i = 1, 2, \ldots, I)^T \\ Subject \quad to: \qquad & g_j(\overrightarrow{x}) \leq 0, \quad (j = 1, 2, \ldots, J) \\ & h_k(\overrightarrow{x}) = 0, \quad (k = 1, 2, \ldots, K). \end{aligned} \tag{4.2}$$

In Eq. 4.2 $f_i(\overrightarrow{x})$ is the objective function, I, J, and K are the number of objective functions, inequality, and equality constraints respectively, $\overrightarrow{x}$ is a n-dimensional vector in the design space and represents the candidate design solution given by $\overrightarrow{x} = (x_1, x_2, , x_n)^T \in \mathbb{R}^d$, where $\mathbb{R}^d$ is the design space. Functions $g(\overrightarrow{x})$ and $h(\overrightarrow{x})$are constraints the objective function is subject to, *i.e.* the constraints can be weight, the minimum number of neutrons reaching a detector or the minimum number of reactions in the foils. Optimization problems can be classified by sub-setting the mathematical formulation in ways that are illustrative to assessing the requirements for a given optimization algorithm. Some of the more general classifications are considered here: single objective (I = 1) versus multi-objective (I > 1); linear versus nonlinear objective function(s); differentiable versus derivative free objective function(s); unconstrained (J = K = 0) versus constrained (J, K > 0); continuous,

discrete, combinatorial, or mixed-integer (MI) design space (R_d); and uni-modal (convex) versus multi-modal (non-convex) fitness landscapes ($f(\overrightarrow{x})$) [14]. An ETA design is a single objective, non-linear, constrained, continuous and discrete, multi-modal optimization problem. The ETA designing (p) objective function is illustrated by Eq. 4.3 .

$$f_1(\overrightarrow{x}_p) = \sum_{g=1}^{G} \left(\frac{\phi_g^0 - \phi_g^D(\overrightarrow{x}_p)}{\phi_g^0} \right)^2 \times \frac{\phi_g^0}{\phi^0}, \tag{4.3}$$

where:

- $f_1(\overrightarrow{x}_p)$ is the objective function;
- $\overrightarrow{x_p}$ is the design vector of the variables corresponding to a candidate design p;
- ϕ^0 is the objective relevant fluence, ${\phi^0}_g$ is the fluence in a given bin g for the spectrum obtained from a candidate design;
- $\phi^D\ (\overrightarrow{x_p})$ is the spectra corresponding to candidate design, where p is the candidate design and g is the energy bin;

The design vector $\overrightarrow{x_p}$, contains all the variables that describe the candidate design of ETA. An example of constraint, seen in the TNF application example and that is recurring for ETA inserted at NIF, is the assembly weight. For this case Eq. 4.2 is:

$$g_1(\overrightarrow{x_p}) = \sum_{n=1}^{N} \rho_n V_n - W \leq 0, \tag{4.4}$$

where:

- ρ_n and V_n are the density and volume of the n^{th} component;
- W is the maximum system weight allowed.

Another constraint example can be the minimum number of any type of reactions inside a foil, *i.e.* important for statistical counting purpose, thus Eq. 4.2 is:

$$g_2(\overrightarrow{x_p}) = N_{reaction}^{min} - \phi_g^D(\overrightarrow{x}_p) V \Sigma_{reaction}^{foil} \leq 0, \tag{4.5}$$

where:

- N_{min} is the minimum number of reactions required;

- $\phi_g^D(\overrightarrow{x}_p)$ is the candidate designs relevant neutron fluence produced across the desired activation foil;
- V is the foil volume and $\Sigma_{reaction}$ is the macroscopic cross section of interest;
- $\Sigma_{reaction}^{foil}$ is the foil reaction of interest.

Alternative constraints are: the variable can be the actual size of the candidate design, the number of neutrons reaching a sample, etc. To express the complexity of an ETA design, Eq. 4.6 shows the possible variables of $\overrightarrow{x_p}$ for a 2-D ETA design.

$$\begin{aligned}\overrightarrow{x} = (Cell_1[M_1, \rho_1, IR_1, OR_1, Z1_1, Z2_1],\\ Cell_2[\ldots], \ldots, Cell_N[M_N, \rho_N, IR_N, OR_N, Z1_N, Z2_N], R_{foil}, Z_{foil}),\end{aligned} \tag{4.6}$$

where:

- M_i is the material for the i-th cell (discrete variable of size m, where m is the number of materials being considered);
- $\rho_{\ i}$ is the density corresponding to M_i (discrete variable of varying size depending on the allowable densities for a given material);
- IR_i, OR_i are the inner and outer radii, respectively (continuous variables);
- $Z1_i$, $Z2_i$ are the initial and final locations on Z, respectively (continuous variables);
- R_{foil} and Z_{foil} specify the foils location (continuous variable);
- N is the number of total cells in the geometry (integer variable). Each cell then contains one material, one density, one internal and external radius, two dimensions (length and width) and there could be N number of cell in the whole system.

Additionally, the location of the materials within the construct of each component or cell can be treated as a combinatorial variable such that the material ordering within the cells can be swapped. For such problems, the differences between the performance of the true global optimum result versus a nearly global optimum result is likely to be within the precision of the neutron transport code used and underlying data used. Furthermore, it is not useful to improve design precision beyond the point practicality for construction (*e.g.* consider machining tolerances and cost).

Gnowees framework is based on a set of diverse, robust heuristics that appropriately balance diversification and intensification strategies across a wide range of optimization problems. Within the metaheuristic framework, decision making is made through the inclusion, exclusion, and/or combination of different heuristics. Those implemented Gnowee heuristic operators constitute: the neighborhood search, hill climbing, accepting negative moves,

multi-start, adaptive memory programming, population-based search, intermediate search, directional search, and variable neighborhood search heuristics. It is possible to apply each of these heuristics to all continuous, integer, binary, and discrete variables. Those metaheuristic implementations are often stochastic, with a preponderance of implementations sampling from variations of uniform or normally distributed processes. An alternative is the Levy distribution, which also has a basis in animal foraging behavior [78]. The general algorithm for Gnowee is presented in Algorithm 1, and presented in Figure 4.2.

Algorithm 1: Gnowee Algorithm

Input : User defined objective function, f; constraints, g and h; design space, $\vec{x}$; and algorithm settings (see Table I)

begin
  $P.\vec{x} \leftarrow$ initialization(n) // P is the parent population of size n
  $P.fit \leftarrow$ population_update($P.\vec{x}$) // fit is the assessed fitness
  while *convergence criterion is not met* **do**
    $C.\vec{x} \leftarrow$ three_opt($P.\vec{x_x}$)
    $P.fit \leftarrow$ population_update($C.\vec{x}$)

    $C.\vec{x_c} \leftarrow$ cont_lévy_flight($P.\vec{x_c}$) // C is the child population and $\vec{x_c}$ is the subset of the design vector containing continuous variables
    $C.\vec{x_d} \leftarrow$ disc_lévy_flight($P.\vec{x_d}$) // $\vec{x_d}$ is the subset of the design vector containing discrete, integer, and binary variables
    $C.\vec{x_x} \leftarrow$ comb_lévy_flight($P.\vec{x_x}$) // $\vec{x_x}$ is the subset of the design vector containing combinatorial variables
    $P.fit \leftarrow$ population_update($C.\vec{x}$, mh) // mh indicates a Metropolis-Hastings algorithm is to be used

    $C.\vec{x} \leftarrow$ crossover($P.\vec{x_c}$, $P.\vec{x_d}$)
    $P.fit \leftarrow$ population_update($C.\vec{x}$)

    $C.\vec{x} \leftarrow$ scatter_search($P.\vec{x_c}$, $P.\vec{x_d}$)
    $P.fit \leftarrow$ population_update($C.\vec{x}$)

    $C.\vec{x} \leftarrow$ mutation($P.\vec{x_c}$, $P.\vec{x_d}$)
    $P.fit \leftarrow$ population_update($C.\vec{x}$)

    $C.\vec{x} \leftarrow$ inversion_crossover($P.\vec{x_c}$, $P.\vec{x_d}$, $P.\vec{x_x}$)
    $P.fit \leftarrow$ population_update($C.\vec{x}$)

    $C.\vec{x} \leftarrow$ two_opt($P.\vec{x_x}$)
    $P.fit \leftarrow$ population_update($C.\vec{x}$)

Figure 4.2: Gnowee Algorithm from Ref. [14].

For the sake of brevity, the operators of the algorithm in Figure 4.2 have been simplified. A summary of the selected operators follows, Ref. [14] provides a more detailed overview of each operator.

- **Initialization**. Gnowee enables the user to flexibly select initialization methodologies through random draws.

- **3-opt**. The 3-opt heuristic is ideal for the Gnowee algorithm as it is largely problem-independent, requires minimal, if any, knowledge of the problem and can be implemented rather generically.
- **Continuous Levy Flight**. Used to develop Markov chains that sample the design space, Levy have primarily been employed in Cuckoo Search (CS) [79] algorithms, but stochastic sampling of the search space is a commonly employed heuristic.
- **Discrete Levy Flight**. The Gnowee algorithm entails that one child is generated per-parent. The Metropolis-Hasting algorithm is employed to accept a fraction of the children that do not improve upon their parent's fitness.
- **Combinatorial Levy Flight**. Here, it is introduced as an inversion operator. Inversion operators are common in Genetic Algorithm (GA) implementations [80], and they have been adopted by other algorithms such as CS.
- **Crossover**. Crossover is a common feature of GA and Differential Evolution (DE) [81] algorithms implemented in a variety of manners. Variations of the crossover concept have been applied in Particle Swarm Optimization (PSO) [82] and CS algorithms, as well.
- **Scatter Search**. The scatter searches approach leverages the information of the population to build variable search spaces based on the relative fitness of selected population members.
- **Mutation**. Mutation is another foundation search heuristic of GA and DE algorithms that has been modified and adopted by a wide variety of other approaches.
- **Inversion and Crossover**. Inversion and crossover are used in GA and DE algorithms to copy portions of one parent into another to create a unique child.
- **Two-opt**. One of a family of heuristics introduced by Lin and Kernighan [83] that has been applied to a wide variety of different algorithms.
- **Population Update** [83]. The descriptions of the individual operators describe the population update procedures.

Search space mapping was not implemented as it generally requires discretization of the phase space. A balance was struck between directional search, which can increase the rate of convergence, and accepting negative moves, which can increase the global search capabilities, to accomplish a fast, nearly global convergence within the design criterion described more fully in Appendix A. To quantitatively capture the performance of a given algorithm, a Figure Of Merit (FOM) is defined in Eq. 4.7 and emphasizes the convergence rate and width of the functional evaluation distribution, whilst also penalizing prematurely-convergent algorithms

for poor fitness solutions. A smaller FOM value indicates better performance, which is the overall objective of the algorithm.

$$FOM = \frac{f_{avg}(\overrightarrow{x}) - f_{opt}}{f_{opt}} \times (N^{avg}_{f(\overrightarrow{x})} + 3\sigma_{avg}), \tag{4.7}$$

where:

- f_{avg} average function from the each design space evaluated;
- $\overrightarrow{x}$ design space, which contains all of the variables describing the system (ETA design);
- f_{opt} optimized function, input in the system from the user;
- $3\sigma_{avg}$ number of function evaluations, chosen to emphasize the importance of minimizing the total number of function evaluations;
- $N^{avg}_{f(\overrightarrow{x})}$ number of evaluations performed of the design space function.

The decision to implement the 3σ number of function evaluations emphasizes the importance of minimizing the overall total number of function evaluations, which is the key factor for the high-cost objective function evaluation applications for which Gnowee was designed. The Gnowee algorithm is neither input nor output specific, which makes its use advantageous for a wider range of applications without forcing the end user to perform any work or modifications within the software. In addition, the algorithm is problem as well as application independent.

A set of well-known and thoroughly-studied nuclear benchmarks currently does not exist for the purpose of testing optimization algorithms; therefore, the only way to verify the quality of the Gnowee algorithm is to compare it with several well-established metaheuristic algorithms on a set of eighteen benchmarks (continuous, mixed-integer and combinatorial) representing a wide range of types of engineering problems and solution space behaviors. Previously-published Gnowee framework and benchmark results [14] demonstrate that Gnowee has a superior flexibility and convergence characteristics over this diverse set of design spaces. This wide range of applicability will make the Gnowee algorithm desirable for many complex engineering applications.

4.2.2 Design Software: COEUS

The second part of the optimization software is COEUS, which provides an efficient capability to design and optimize ETAs for spectral shaping. COEUS provides the interface between Gnowee, the optimization algorithm, the radiation transport codes required to evaluate the ETA objective function and constraints, and the job scheduling system used to submit jobs on HPCs [84]. The radiation transport engine that is used for Version 1 (v1.0) of the optimization software is Denovo-MCNP, which are both described in Chapter 3.

The primary purpose of COEUS is to manage the interaction with Gnowee, to create MCNP inputs, to submit computing jobs, to read MCNP outputs, to update the population of various ETA designs and to determine the final results. COEUS takes advantage of the embarrassingly parallel nature of both Gnowee and MCNP to achieve efficient parallel computation through both Open MPI [52] and slave node tasking using the SLURM job scheduler [84]. In addition, COEUS must manage the creation of the ADVANTG inputs, submission of jobs, and reading of the ADVANTG outputs; however, these are essentially just extensions of the MCNP processes due to the tight integration between MCNP and ADVANTG.

In the v.1.0 of the software package, COEUS initializes surface and geometry objects to create a cylindrical/conical 2-D ETA geometry, which was initially used for NIF target chamber applications. The variables associated with each surface are then sampled by Gnowee. All of the surface and cell object updates and MCNP geometry logic are handled within each operator as needed for the variables under consideration for that particular operator. The MCNP parameters, surface, and cell objects are then passed to a function that generates an MCNP input for the new candidate design. However, nothing about COEUS or Gnowee requires the tight integration of the search operators and geometry update, and this can be handled in a much more generic, modular fashion. After each MCNP calculation, the specified MCNP tallies are read and used to calculate the objective function and constraints.

A significant improvement in efficiency is obtained by tying the statistical convergence of a design to the assessed fitness. If a current design is outside of the constraints imposed on the system or is a poor candidate, fewer particles are simulated to avoid wasting computational resources. As the fitness improves, the number of simulated particles is increased to reduce statistical uncertainty and ensure chosen designs are not statistical anomalies. Since the computational requirements change over time for a given parent (due to increases in accuracy for high fitness solutions) and operator (due to varying number of designs generated by an operator), this represents a very efficient use of HPC computing time, as only the number of nodes required at any given time are requested. COEUS holds a block of compute nodes and divides them up according to the needs of the individual threads. The threads would communicate *via* a bulletin board that would contain the design vectors for each thread in order to enable the information sharing required for some operators. In this construct, there is no requirement for the individual threads to be at the same operator or generation as another thread. When the optimization converges, each thread will be at a different generation and will have performed a different number of function evaluations than if they had moved in lockstep through the Gnowee algorithm. The understanding of the interaction of the heuristics with out-of-sync threads is further complicated by the fact that the best fitness threads will have higher numbers of particles (*i.e.* higher computational requirements) and take longer to run, unless some effort is spent on load balancing. COEUS builds the job scripts and submits slave jobs for each child generated by the current operator.

MCNPs task-based parallelization then provides the second level of parallelization within the allotted nodes and Central Processing Units (CPUs). COEUS monitors the submitted slave jobs waiting for their completion before moving to evaluate the objective function and

constraints. COEUS then continues to move through the algorithm with serial calculations in Gnowee and parallel calculations when evaluating ADVANTG or MCNP. This parallelization method has been successfully implemented on Savio [84], but it is not limited to Savio, as its implementation is flexible, compatible on a wide range of HPC assets. Additionally, the inputs required for the specific partition, user, or account are COEUS inputs, allowing for ease of use within a given architecture.

4.2.3 Limitations

Gnowee is not a problem specific algorithm and is highly generalized for various nuclear applications and other engineering problems. COEUS, on the other hand, has the limitation of being hard-coded as problem specific, using only MCNP-Denovo radiation transport code. For example, there is no possibility to adapt COEUS to design the ETA with geometries which are not conical, the variables available are only the ones corresponding to the assembly and not the surrounding environment. Further limitations are summarized below.

- The geometry uses pre-selected cylindrical/conic sections; therefore, the user is only allowed to change the dimensions and the number of material sections introduced. COEUS v1.0 is constructed in a series of modules which are required for each input file. In each input file only specific indications are given for: an already pre-constructed geometry; the strength of a point source; the objective spectrum, but not the type of objective function. Then the user provides just the parameters for the radiation transport code set, like the number of particles and the particle type.

- COEUS uses PyNE [85] to process material definitions and provide a basic material library. This is a cumbersome dependency for a limited benefit.

- The software optimizes ETA designs using a single objective function which is the neutron flux at the exit window of the assembly. The relevant design is chosen by comparing the objective neutron spectra and the resulting neutron spectra designed by the software. The tally specifications and corresponding tie to the objective and constraint functions are limited in v.1.0.

- Only a fixed-point source is permitted, and the user can only choose the strength and distance from the source.

- No nuclear data uncertainty is taken into consideration.

Unlike Gnowee, COEUS has many items that could be updated to improve its usability and applicability to problems outside of ETA design (or problems with similar geometries).

4.3 Further Improvements in COEUS

The aim is to develop a general-purpose nuclear engineering optimization code that is flexible enough to accommodate different transport engines, HPC architectures, modeled geometries, objective functions, and constraints. As a means to this end, this thesis project dedicated a significant effort in developing a general-purpose nuclear engineering optimization code, which will be henceforth referred to as: Gnowee/COEUS v.2.0. The reason behind the improved optimization process is the need for appropriate toolkits for tailoring spectra to fit the most applications taking advantage of all the advanced computational technology and computer hardware available. If successful, the new version of the optimization software package could be of great help for research and development work in many areas of nuclear science and engineering, particularly because of advanced validation and uncertainty quantification. All of the sections that are improved and now available in the v.2.0 of the software are described in this Section.

Firstly, this dissertation work was focused towards rewriting sections of COEUS in order to permit: any geometry, any type of objective function in different space location, as well as any source distribution in space and angle. In the new v.2.0 the previous MCNP setting, the objective spectrum and the source spectrum, are removed in addition to the MCNP utilities module and the ETA setting. Furthermore, the tight integration of the Gnowee operators and the MCNP geometry modification is separated. This was nearly performed initially, but the MCNP geometry logic piece was lacking till now. The new COEUS is by far less problem specific and is built as one single module with:

- An expanded geometry and variable option, within the limits of the neutron transport code of choice.
- An expanded range of constraints, and geometric options to let the user select N constraints, within the limits of the neutron transport of choice.
- Expanded capabilities by adding different types of objective functions and multi-objective.
- The possibility of different objectives and even multi-objectives.

For the optimized COEUS, a new input system has been introduced. The more greatly-expanded input system is generated for both MCNP and ADVANTG codes, the concept being that a standard MCNP-like input file will serve as the main input, with a special format used to identify inputs for variables to be sampled. A parser/reader in COEUS pulls the variable vector definition from the file, passes it to Gnowee, and the updated vector replaces the corresponding variables in the MCNP input file. This approach could be expanded to other transport codes, like GEANT4 [61] or Serpent [59], to allow for their adoption into COEUS. It also improves usability by mimicking input formats familiar to a large segment of potential users. Adding a make file makes it easier and more repeatable

to use the software by building the dependencies and adding the appropriate environment variables. The MCNP like input file allows one to introduce the entire experimental facility and any possible source into the radiation transport code. With the new input framework, the constraints definition changes from v1.0. The constraints are included in the definition of each variable. The constraints are now defined as boundaries to each of the variable, *i.e.* for a continuous variable, the boundaries are possible lower and upper values; for a discrete variable the user defines all the possibilities for that variables, thus no need for added constraints. The constraints can be also built as functions, *i.e.* if the weight of the ETA is a constraint, the number of neutrons in a specific cell, which are defined together with the variables by identifying which elements in the MCNP input file they correspond too. For the weight it will be density and volume, for the number of neutrons it will be flux tally in a cell and its volume, etc. The user can determine any constraint to the desired variables within the limitation of the simulation code, here MCNP, used.

New objective functions are also investigated besides the neutron flux, such as the weight of the assembly, the number of particles, and the dose or reaction ratios in different locations. Towards this purpose, at the objective function described in Eq. 4.3, specific weights can be introduced by the user in order to maximize the efficiency in the search of the materials and dimensions for the ETA.

In v.2.0, COEUS permits user specification within the transport code input to supplement with a library of basic materials which the user is interested in modeling, removing the dependency from COEUS and PyNE.

Finally, employing the full neutron transport codes permits the user to introduce different types of tallies in a wider space range. The use of the radiation transport code input allows for full tally specification for any possible design constraints and objective functions. This will also allow for user-specified objective functions made from a combination of a multiple tallies.

In keeping with the same design philosophy, the hybrid methodology is migrated to an ADVANTG-style format to allow for user flexibility. This will allow for a wider range of ADVANTG options to be selected while streamlining the user input process. The new input system enables the inclusion of all ADVANTG options of two methods of spatial discretization: (1) predefined fixed bounds and intervals for static problems, and (2) the current variable-based bounds and intervals for dynamic problems.

COEUS also introduces an automatic ADVANTG switch to change from once-per-generation to once-per-evaluation for suitability for highly dynamic problems where the weight windows rapidly become non-ideal. The ADVANTG efficiency is also improved, as an on-the-fly assessment of uncertainty is introduced to ensure appropriate statistical significance. Moreover, the ADVANTG-generated weight windows are improved by the addition of a module, inside COEUS, that tracks the suitability of the weight windows to the generated designs.

On the Gnowee-side, modifications of Gnowee have been performed in order to have the option for future ETA to multi-objective function algorithm.

4.3.1 Input System for COEUS V2.0

The new COEUS version is a powerful and versatile tool designed to improve the efficiency of defining the environment and specifying everything that is needed to be optimized, sources and variables that are allowed to be changed:

- Input decks for optimization studies to be created quickly and easily.
- Calculations and variables to be embedded into any input deck, thus allowing for meaningful parameter specifications.
- Problems to be specified using any combination of units, and complex mathematically defined models to be created.

For the new COEUS version, two input text files are needed; one input for MCNP and one input for ADVANTG if a hybrid methodology is used. Examples of the input files can be found in Appendix B, together with specifications on how COEUS is run. The system requires only the user knowledge of running MCNP and ADVANTG and of the environment in which the ETA is located.

In addition, the user must:

- Understand the environment where building of the ETAs is desired.
- Understand which variables are of interest and that need to be optimized.
- Define the type and values of the variables, they can have discrete, continuous, binary, combinatorial or integral values.
- Set up a series of constraints chosen as fixed MCNP input. The constraints are also defined as the range of values of the variables.

All of the current limitations of v2.0 are congruent to the limitations of the radiation transport software of choice.

4.3.2 Examples of Application of Gnowee/COEUS Version 2

The first motivation behind improving COEUS is to develop a generalized design platforms for tailored neutron outputs and moderated spectra for NIF. The goal is to expand the experimental capabilities of NIF by including the measurement of nuclear reactions at energies below 14.1 MeV. This work fits well within the research of the complex reaction networks for the Nuclear Forensic Program. Possible alternative applications are investigated by using Version 2 (v2.0) of Gnowee/COEUS with the newly introduced COEUS input system. This Section outlines possible neutron applications cases that have been taken into consideration in order to predict all the possible features for COEUS. For each application, how those

examples would interact with the code and the current capabilities is defined.

BNCT

The idea of applying Gnowee/COEUS to tailor energy of neutron beams for the Boron Neutron Capture Therapy (BNCT) has originated at UC Berkeley [4], [5]. In the past, the UC Berkeley team invested a lot of efforts to study the optimal neutron beams (in terms of energy, intensity and direction) that would deliver maximum dose to a deep seated brain tumor (Malgnant Glioma) [86] while minimizing dose to healthy tissue. The goal was to design appropriate BSAs [87] to shape neutron beams from different neutron sources in order to determine the optimal neutron energy range, which could deposit high doses in the tumor cells in the brain containing ^{10}B while largely sparing the normal cells. More details are given in Chapter 8, Section 8.2.3.

For BNCT, beside the full experimental and treatment environment, the model of the patients head needed to be included, because the objective function was located there. This was a major limitation for v1.0 as a modeling of a human head and a tumor is required for the true objective function [87]. For the BNCT the goal, in fact, is to maximize the ratio of tumor-to-patient dose. Furthermore, it is indeed possible to introduce with the new version a new class of objective function, such as using the ratio of tumor-to-patient dose as objective function by introducing a new set of tallies for the optimization. Moreover, the irradiation time can now be introduced as one of the constraints. Example of ETA designed by Gnowee/COEUS v2.0 can be found in Chapter 8, Section 8.2.3.1.

Integral Benchmarking Experiments

The concept is to use COEUS v2.0 to design an ETA that develops a spectrum to highlight energies of known nuclear cross section weaknesses. The goal is to "isolate" or emphasize specific channels to avoid the issue of compensating errors and to perform an integral experiment that really shows the impact of the nuclear cross sections. The idea is to design, with COEUS, a sphere of materials to build on the concept of the pulsed sphere experiment. In this thesis, a part of this work is started with the experiments explained in Chapter 5, where an initial a set of benign, easy to field on NIF materials are investigated for nuclear data purposes. Subsequently, an optimized sphere design is made using the same materials considered in the initial experiment. An example of this design is presented in Chapter 8. This work is of particular interest towards the LLNL's stewardship priorities [7].

Isotope Production

Novel optimization methodologies could also be used for isotope separation, notably for production of medical isotopes as well as isotopes of importance for nuclear security. Isotope production [40] is a fairly large business, and from literature studies it appears that often the target designs to produce isotopes of interested are optimized by experience as well as parametric studies. The optimization methodology developed would be used to generate the appropriate stack up assembly by introducing multiple objective functions for the various fluxes such that each of the samples generates the isotopes of interest. The basic concept

is that the objective is to generate as much of isotope X as possible while avoiding other isotopes that are difficult to separate from the irradiated sample. Based on the relative cross section of the two or more reactions, there will be an optimal beam energy that is obtained by tuning the incident neutron beam with a ETA.

For isotope separation, the constraints applied are not just the size and mass of the ETA, but also the maximum ratio of undesired to desired reaction rates as the goal here is to produce the maximum number of atoms up to some contamination percentage. This last type of constraint is available with the new COEUS version, making the software favorable for such application.

Objective functions can also be the sum of the number of atoms created for each isotope (with or without preference weighting) or the ratio of more to less desired isotopes. Furthermore, it is possible that both are combined, as well. MCNP is most likely capable of achieving the majority of this work and most likely would be used, but there could be added the possibility of investigating different transport codes. A similar approach could be applied for the production of isotopes for different applications.

Radiation Shielding

Some possible interesting challenging cases within the radiation shielding design are:

- **Space shielding design** for satellites, space reactors, and future space travel, where light weight, efficient shields are required. This is one area in nuclear engineering where more advanced optimization techniques have been applied in the past, but many of these problems are still solved by a parametric study.
- **Radiation converter design**, where it is sometimes useful to convert one type of radiation into another. The geometries for these applications tend to be fairly straightforward in the traditional layered concept.

Towards both instances, the constraints tend to be mass, thickness and the cost factor, and dose threshold or a dose reduction percentage. For those constraints it is favorable to use the new version of the code, as different tallies can be implemented within the input from the user and can allow the implementation of a flux to dose conversion tally. It would also be required the use of alternative transport codes, which takes little effort to be done with v2.0.

Several other applications could be investigated, such as inverse problems, fusion blanket design and reactor design for optimizing the fuel design.

4.4 Summary and Future Work

In the current stage of the development, Gnowee/COEUS v2.0 already represents a dramatic improvement over the current spectral shaping options (*e.g.* v1.0) and potentially enables radical improvements in experimental outcomes across a wide range of applications. The new

COEUS reads the MCNP input-like file and identifies the variables introduced by the user; collects the variables information from the input file grouping them by type (continuous, discrete, combinatorial, integral), and by upper bound/lower bound; passes the variable information to Gnowee and exchanges information as in v1.0; once the optimized variables are produced by Gnowee, COEUS allocates the new values of the variables inside MCNP and ADVANTG; and runs ADVANTG/MCNP, reading the output of interest and re-iterates with Gnowee as v1.0.

The assessment of the improved Gnowee/COEUS capabilities is ongoing process, but initial applications are shown in Chapter 8. It is expected that these additional modification of COEUS' will increase the computational time needed to solve the problem. Continuing progress is made to improve run time and the number of function evaluations to enhance COEUSs ability to solve complex problems with reasonable amount of computational costs.

One future research direction could be to implement various powerful machine learning algorithms [88]. The implementation of classes of machine learning systems to several nuclear engineering fields is an exciting research focus area. For example, machine learning algorithms have been applied to explore cross section clustering of Monte Carlo solutions and for identifying sources of nuclear data uncertainties within the materials of choice in the ETA designed.

Chapter 5

Experimental Measurements

5.1 Introduction and Motivation

The experiments at the National Ignition Facility (NIF) were performed in order to validate the computational methodology that was developed during this research project and to evaluate its performance. The goal is to have a proof of platform methodology for the NIF, and other neutron generating facilities, and to design and analyze experiments that take advantage of the high neutron flux produced by tailoring its spectra for various applications.

Simulating large experimental setups such as the NIF and designing complex assemblies to shape the neutron spectra necessitates a deep understanding of the possible errors introduced by inadequacies in the software packages used for simulations, inaccuracies in the simulated models of real experimental setups, and by systematic errors from the uncertainty in the relevant nuclear observable of the materials in the surrounding environment. A knowledge of how nuclear data uncertainties propagate into the model would be beneficial and worthwhile as well. The analyzed data can be compared with simulated results to determine the future ability to model the Energy Tuning Assembly (ETA) performance.

The techniques described in the following chapter are not novel, but the full design of experiments in the NIF environment, the development of the techniques used, and their application to spectral shaping and integral nuclear data benchmarks are more thorough and nuanced than any previous spectral shaping concept.

The focus here is to design a set of integral experiments that can be fielded at the same time (*e.g.,* "ride-along") as other experiments, in the NIF Target Chamber (TC). Running an experiment at the NIF with a large material stack as in a neutron beam shaping ETAs makes it hard to identify the causes of possible differences between the modeled and measured data. This is why the initial research was performed to collect data sets from partial ETA material stacks to gain insight into nuclear data impact where the model diverges from the ETA performance. Thus, the goal is to understand the error due to the nuclear data of the materials of interest. In this way, benchmark modeling is developed, which is an efficient use of resources at the NIF and provides additional confidence in the material cross sections

(particularly for elastic and inelastic scattering).

High-yield shots at the NIF provide a unique environment with a significant fluence of neutrons, 10^{16} n/cm^2 [7], [8], delivered in hundreds of picoseconds with a mixed hard D-D, T-T, and D-T fusion spectrum, with the D-T spectrum dominating due to the higher reactivity of that reaction. The NIF has two important advantages for integral data experiments: first, the neutron source is small with limited- to no local attenuation; secondly, the target chamber is mostly empty and surrounded by borated gunnite, which minimize and has accounted "room return" neutrons. Then, the significant fluence of neutrons is another reasons to perform neutron related experiments at the NIF: it gives the possibility to shape the spectrum without losing the intensity of the detected neutrons. In one pulse, the neutron source can deliver the number of neutrons required to achieve statistically-significant counts in the diagnostical methodology used, accounting for geometric attenuation, out- scattering, and parasitic absorption that will occur in the TC, diagnostics instrument manipulator (DIM), and material stack introduced or ETA. A lower neutron output risks not meeting the minimum number of required reactions for the neutron spectrum measurements, which would lower the quality of the data gathered. Other continuous or semi-continuous sources for the same fluence require longer irradiation, resulting in competing and alternate in-growth and decay channels with introduction of significant number of delayed neutrons. The full description of the relevant parts will be described in details in Section 5.2.

5.2 Lawrence Livermore National Laboratory: National Ignition Facility

The Lawrence Livermore National Laboratory (LLNL) in Livermore, California, is home to the nation's largest, most energetic and reproducible laser facility ever built [7]: the National Ignition Facility (NIF) uses 192 powerful lasers capable of producing a maximum total of 1.8 MJ of 3 ω (351 nm) laser light in 500 TW pulses. The laser drive strikes the hohlraum walls, creating X-rays that compress the target to densities greater than 1000 g/cm^3 and temperatures approaching 100 million K [10]. This causes the D-T fuel to fuse, resulting in the release of 10^{14}-10^{16} neutrons in a pulse only tens of picoseconds wide. Some thermalization of the neutrons occurs inside the D-T fuel, providing a mainly monoenergetic 14.1 MeV source peak [89], with a less intense lower energy spectrum. The NIF initially started as a predominantly weapons related project [9], however, it was designed for a public mission as well: attaining ignition in order to further fusion energy as a viable and economical source of power for the world [10]. Through the years, the NIF has supported many types of nuclear physics experiments.

The NIF presents a 10 m in diameter clean TC, where the neutrons that leave the hohlraum [8] encounter a large evacuated space enclosed by 10 cm thick aluminum walls surrounded by 30 cm of borated concrete, which minimizes additional thermalization and room return neutrons [90]. This structure allows for a reproducible environment where low

down-scatter and room return results in minimal and well-known thermal and epithermal background, which allows for a better spectral shaping and moderation. The large documentation of all the NIF diagnostic experiments allows for preliminary predictions of the measured flux within the TC environment.

Figure 5.1 a) shows the NIF external containment with a cross section of the TC. The target bay and the chamber (along with diagnostics) are located in the far end of the facility (lower right of Figure 5.1). Figure 5.1 b) shows the TC and the several ports that are used to insert instrumentation for a different experimental set ups like the ones presented in this Chapter.

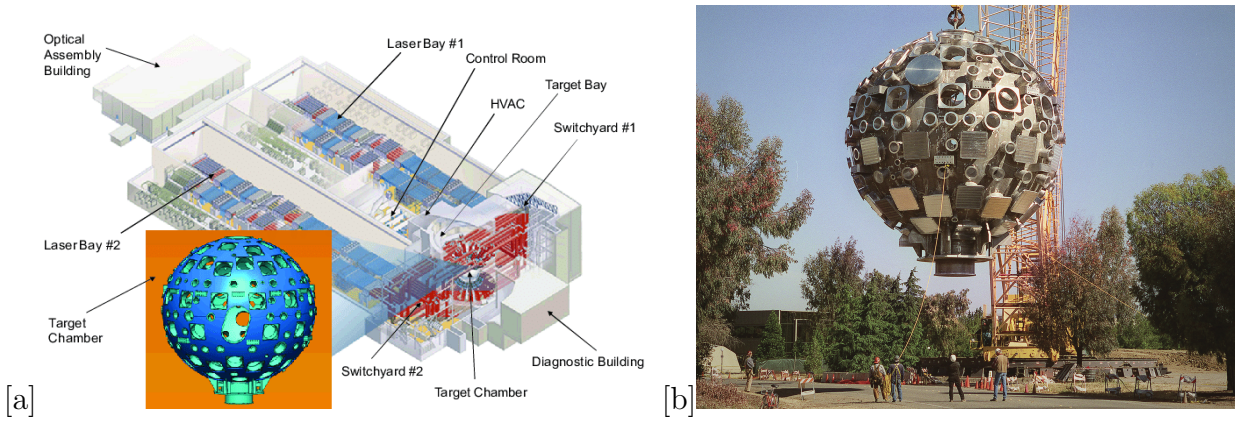

Figure 5.1: Target Bay and Chamber: a) the NIF building layout with the TC enlarged in blue. b) Close up of the target chamber with highlighted multiple ports where the experimental manipulators and detectors are inserted [56].

The blue sphere represents the inner TC (Figure 5.1) where the fuel filled target is located and the reaction occurs, while the gray ring levels extend out to a concrete bay wall. The focus in Section 5.2 is the TC and the NIF target that contains a polished capsule about two millimeters in diameter, containing a layer of cryogenic hydrogen fuel surrounding a gas-filled interior. In Figure 5.2, it is possible to see the metallic case, called a hohlraum, that holds the fuel capsule for the NIF experiments. The target handling systems in the facility precisely position the target and freezes it to cryogenic temperatures (18 Kelvin, or -427 degrees Fahrenheit) in order to solidify the fuel, which increases the density to allow for more fuel per capsule.

5.3 Experimental Set-Up

The NIF experiments are typically executed via experimental platforms [91]. A the NIF experimental platform typically consists of an integrated laser set up, target design, data analysis plan, classification level, and diagnostic configuration capable of providing well-characterized pressure, temperature, radiation or implosion-trajectory conditions. Often the

[a] 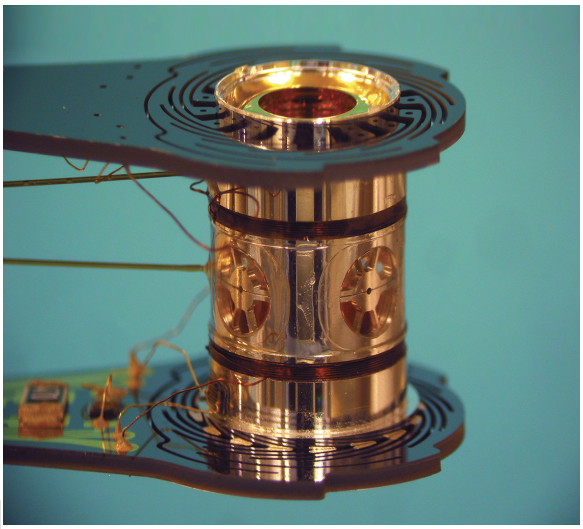 [b] 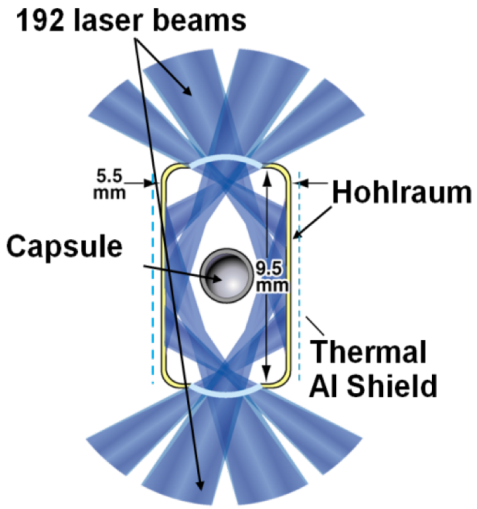

Figure 5.2: a) NIF target hohlraum. b) Schematic drawing of the target hohlraum with the openings for beam entrances and the capsule location [7].

experiment organization is costly and time intensive. Each proposal for an experiment is submitted through the NIF user office or specific programs, based on user needs; individual experiments are fielded on an available the NIF neutron yield shot. Most importantly, the experiments are allocated through accepted program proposals, *i.e.* Joint National Security Applications Council (JNSAC)/National Security Applications (NSA), High-energy density (HED) and Inertial Confinement Fusion (ICF) councils, Discovery Science. The users can select their experimental configurations in order to utilize the NIF beam time allocation in the best possible way [92]. For the approved proposals, a Diagnostic Instrumental Manipulator (DIM) or a Target and Diagnostic Manipulator (TANDM) configuration is designed, based on neutron fluence and volume requirements.

Due to time and monetary resource constraints on Ph.D. research, experiments in this work have been designed as ride-along to pre-existing shots. The neutron experiments were therefore introduced passively into the available DIMs without disturbing the already planned experiments. Ride-along experiments are designed to be executed using existing capabilities and proven shot configurations, while meeting each experiment requirements. Any NIF D-T yield shot may support additional experiments through coordination with the campaign experimental team. This includes the NIF facility neutron calibration shots as well as programmatic shots. For example, the first shot configuration available was performed during an Energetic Neutron Platform (ENP) shot, designed to examine the active electronics and test the objects under intense prompt neutron impulses. This experimental shot at the NIF had an available empty passive SNOUT configuration which was used for holding the electronics. Other experiments described in this Chapter were performed for organized shots for diagnostic purposes: to monitor the changes in neutron flux as a consequence of the silver-coated target design and to benchmark the simulation originally done.

The ride-along experimental processes described in this Chapter still went through a feasibility study which included engineering design, safety approval and the NIF post-shot analysis.

Each of the presented designs needed to satisfy the following requirements:

- To fit into the space envelope, so that their dimension, shape and weight are compatible and can incorporate features to aid alignment in the TC.
- The additional elements can be inserted and removed via the DIM side access ports and removable items such as image plates, film packs, filters, etc. can be reached.
- The required tool access is accommodated, and human factors are considered, such as handles, grips, or support areas for handling the hardware during assembly and installation.
- The cleanliness and the hazards of the materials used in the experiments need to be adequately considered. The materials for the presented experiments had no associated hazards, and thus no insurmountable hazardous material issues were foreseen, simplifying the process for the preparation of shots.

The feasibility study found that the proposed ETA design and overall experiment were low risk, and could be done at a reasonable cost [93]. This finding reduced the overall time needed for preparation and approval to 4 -6 months. It was a unique opportunity to pursue and analyze measurements from seven experiments in those four shots at the NIF within time frame reasonable for a Ph.D. The experimental set up follows the modeled design, presented in Chapter 7, and the introduction of the flux monitors which are described in detail in Chapter 6.

The proposed engineering design went through safety approval and was scheduled on pre-established shots. The materials and machining processes were already expected to pass the NIF cleanliness standards, and no insurmountable hazardous material alert was issued making this last step faster [92].

Finally, as for most of the neutron experiments, collaboration with radiochemistry and gamma spectroscopy facilities for post-shot analysis followed the experiment. Access to the removable foil pack was required within a few hours to measure short-lived fission and reaction products.

The experiments presented and designed in Chapter 7 and 8 for present and future shots include also single material, but also ETA complex stack of materials which have not yet been performed and are queued for future analysis. Those more complex designs are all passive standalone package which do not require external electrical power or modifications to existing diagnostic capabilities at the NIF, making them an ideal follow up to the presented work. For this reason, current and future beam shaping experiments will be using the equatorial DIMs: DIM 90-78 and TANDM 90-348. Both DIMs, as seen in Subsection 5.3.3, have an

ideal location for our experiments and can be used without impacting any other experimental configuration. Also, both DIMs are used typically by the radiochemistry group, which was part of this project collaboration, for holding Solid Radiochemistry debris Collectors (SRC) [17] making post-shot analysis rapid and streamlined. The two instruments that were used as part of this work are the passive SNOUTs and the large Target Option Activation Device (HTOAD) [94], as described in detail in Subsection 5.3.4, which are attached to the DIMs. The HTOAD is located on the SNOUT of the DIM 90-78, which carries the primary neutron effects experiment. The experiments are described below and for each experiment the following is emphasized: the laser configuration, the targets, the DIMs and the specific instruments used. The flux monitors and the detector studies are described in Chapter 6. To develop an accurate simulation methodology, it is important to have knowledge of the above characteristics and to use the appropriate neutron source spectrum.

The four campaigns are summarized in the Table 5.1 and labeled with their caption, shot number, date of the shot, and locations. More details are given in the sections below. The complete analysis of the results will be presented in Chapter 7 and 8.

Table 5.1: Description of the experimental campaigns.

Name	Type	Shot number	Date	Manipulator
S1	SNOUT	N180311-002	03/12/2018	TANDM 90-34
S2	SNOUT	N180715-002	07/16/2018	TANDM 90-34
S3	SNOUT	N180722-001	07/22/2018	TANDM 90-34
S4	SNOUT	N181014-001	10/14/2018	TANDM 90-34
H1	HTOAD	N180311-002	08/31/2017	DIM 90-78
H2	HTOAD	N180715-002	03/12/2018	DIM 90-78
H3	HTOAD	N180722-002	07/16/2018	DIM 90-78

5.3.1 Laser Configuration

The laser beams enter the gas filled hohlraum from the top and bottom to produce X-rays from the cylinder walls, thereby evaporating the hohlraum and its holder [16]. The X-rays penetrate the upper layers of the fuel pellet (currently designed as a Ge doped polymer [16]), heating it rapidly to the point where a plasma is formed, the rocket-like ablation of which creates an implosion inwards through the fuel pellet. The pellet collapses to an extremely dense state where, depending on temperatures, containment time and uniformity of the implosion process, thermonuclear burn will spread through the fuel, yielding varying degrees of energy production.

There are several types of laser beam methodologies used at the NIF and the main characteristics of the laser beams during the four campaigns are summarized in Table 5.2.

Table 5.2: Description of the laser configurations for each of the campaigns.

Shot	**Energy (kJ)**	**Peak power (TW)**	**Pulse length (ns)**	$\Delta\ \lambda$ ($\AA$)
S1	631	376	1.9	9.7/8.5/1.2
S2	645	317	2.4	9.7/8.5/1.2
S3	664	326	2.4	9.7/8.5/1.2
S4	815	282	3.9	9.7/8.5/1.2
H1	638	624	6	0/0/0
H2	631	376	1.9	9.7/8.5/1.2
H3	645	317	2.4	9.7/8.5/1.2

The information of the lasers for each shot described in Table 5.2 are given beforehand in order to understand the standoff requirement of the SNOUTs used. Figure 5.3 introduces a plot of the SNOUT standoff requirement during the shots with respect to the laser beams.

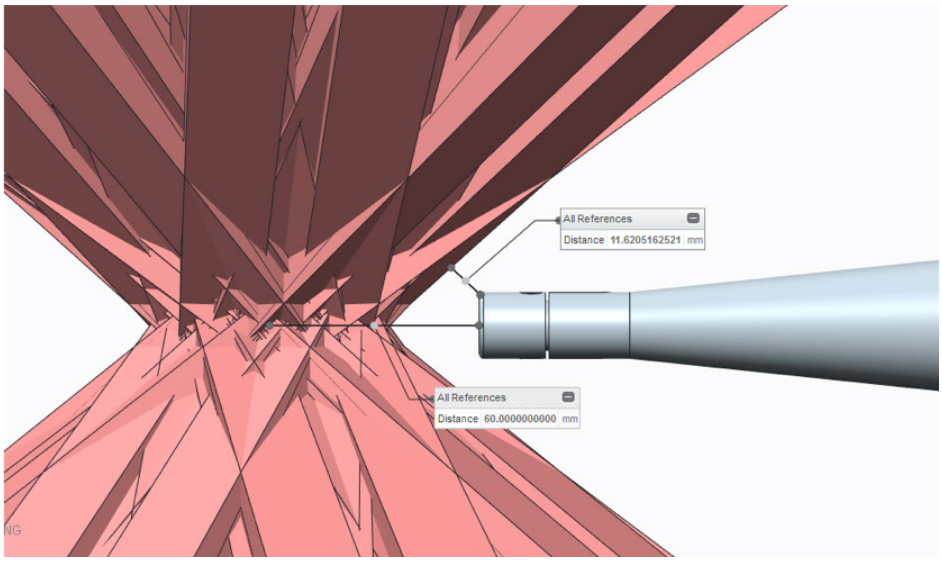

Figure 5.3: Beam clearance of the SNOUT respective to the lasers [95].

The H1 shot used a drive of 192 lasers with a 6.0-6.5 ns Bigfootx09 [9] subscale Symcap [96] pulse shaped, with a standard SymCDT capsule [96], [91] (cryogenic D-T) heated with a laser energy of 1.6043 MJ. This shot produced 450 TW more power than previous similar shots.

The SymCDT methodology for neutron source produced a total backscatter from the D-T gas-filled Symcap of 15.99 kJ. Thanks to the High Density Carbon (HDC), diamond, ablators a high D-T yield was reached but required a 10 cm standoff from the target.

For the other three campaigns, S2/H2, S3/H3 and S4, the shots used 192 lasers directly with the direct drive of exploding pusher (PDXP) [97] platform. With the direct drive, the

target downscatter is minimized and the required experimental standoff is smaller than for cooled targets which improves reproducibility between similar shots from the point of view of the neutron spectrum source. The PDXP allows up to 5 cm source standoff and makes it favorable for modeling validation. The PDXP driver uses as a target a glow discharge plasma (GDP) hydrocarbon plastic capsule (CH) filled with D-T. The PDXP is a pure 14.1 MeV D-T fusion source, the experiments utilizing laser energy depositions directly produce reliable high neutron yields using a simple, low-mass target assembly. Of all the shots that used PDXP the one with the highest laser power was S4 approaching H1, though it required a larger standoff from the source.

All shots used the Bigfoot approach which is a trade-off between high convergence and areal density, allowing for conditions that are favorable for controlling hohlraum symmetry and hydrodynamic instabilities. A Symcap capsule assembly uses an appropriate ablator thicknesses to act as a surrogate for an ignition capsule. They do not contain a fuel layer but rather a gas mixture; they serve as a surrogate to study, tune, and optimize implosion symmetry, and can be fielded over a range of temperatures from cryogenic to room temperature.

5.3.2 Target

The NIF is equipped with two target positioners (TARPOS) [7], located at 90-239 and 90-015, which are capable of holding cryogenic and non-cryogenic (warm) targets, including gas targets. The TARPOS at 90-015 is designed to handle layered targets, including those containing tritium. It is commonly referred to as cryoTARPOS, though both TARPOS systems can field cryogenic (but not layered) targets. Both TARPOS provide for positioning a target within 5 cm of the Target Chamber Center (TCC). Clearance from other positioner in the TC is required.

For the experiments here presented, the target itself is mounted to TARPOS 90-239, since the experimental DIM has a sweep angle of 180 degrees or less and is symmetric around the 90-124 positioner axis, the clearance requirements are easily met. A close up look of the configuration around the TCC is shown in Figure 5.4. For the shot N170831-001, the passive SNOUT was used, the TARPOS 90-239 and the positioner at 90-124. The positioner is at 0-0 with a TCC standoff at 10 cm, the direct drive capsule target at 90-239 with 0 TCC standoff, at 90-348 one of the passive SNOUTs used at standoff of 6 cm.

A well-designed and precisely fabricated target is one of the keys to a successful experiment at the NIF. Experimenters should discuss with target designers the design and type of target as early as possible (even before a shot date is determined), including its various components and materials, and requirements for specifications and tolerances, even if the design is only in the conceptual stage. Targets are made using a number of different resources, depending on the type of target and its components or sub assemblies. Any target to be shot at the NIF must be assembled with enough precision to be aligned in the TC. Table 5.3 summarizes some key features of the target and capsules used for the shots examined, they are also explained below.

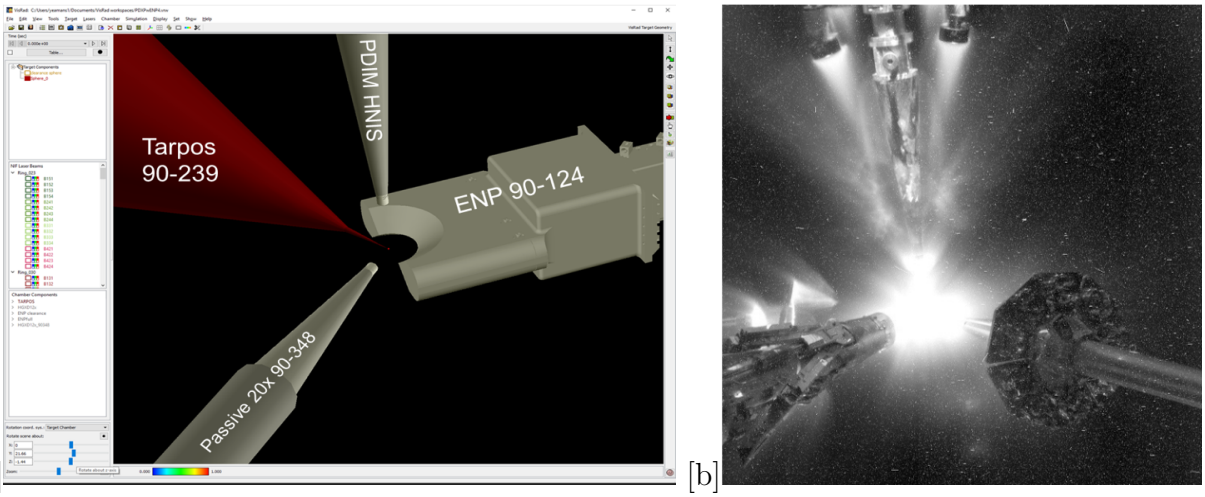

Figure 5.4: Experimental configuration close up. a) Engineering design of the Direct Drive Capsule target at 90-239, the passive SNOUT used for the SNOUT experiments at 90-348; the Energetic Neutron Platform (ENP) on DIM 90-124 taking place during the ride-along. b) Picture of the TCC during a shot [95].

Table 5.3: Target capsule details.

Name	**Shot description**	**Material**	**Diameter**	**Wall thickness**	**Coating**	**Fill pressure**
H1	N_NED_SymCDT_DT_S01a	HDC(0.25% W doped)	3 mm	18 μm	uncoat.	68 torr
S1	N_NED_ExPsh_DT_S01b	CH	3 mm	18 μm	uncoat.	5582 torr
S2	N_NED_ExPsh_DT_S02a	CH	3 mm	18 μm	Ag-0.2-0.3um	5637 torr
S3	N_Sdev_ExPsh_DT_S02	CH	3 mm	18 μm	Ag-0.2-0.3um	6138 torr
S4	N_Sdev_ExPsh_DT_S05	CH	4 mm	27.1 μm	uncoat.	6080 torr
H2	N_NED_ExPsh_DT_S01b	CH	3 mm	18 μm	uncoat.	5582 torr
H3	N_NED_ExPsh_DT_S02a	CH	3 mm	18 μm	Ag-0.2-0.3um	5637 torr

H1 used a gold hohlraum with a 5.40 mm diameter, 10.13 mm length, and a 3.45 mm light entry hole (LEH) diameter. The capsule was filled with 50% D and T 50% and 0.25% Tungsten-doped HDC [98], with a 64 μm ablator thickness.

S1, with the PDXP, used a 50:50 D-T gas-filled Symcap capsule made of CH, a commonly employed plastic-ablator, typically polystyrene, with a 3 mm shell and thickness of 18 microns. The pressure was also higher than that of the capsule used in H1. Figure 5.5 is a close up of a Symcap capsule assembly.

In S2 and S3, the laser platforms were the same and they both used a Symcap capsule and gold hohlraum, the novelty arises from the addition of a silver foam coating around the capsule. The Ag coating was between 0.2-0.3 micron at solid density, the foam had a density of 6 mg/cm^3 and was successfully adhered around an intact 3 mm of CH capsule

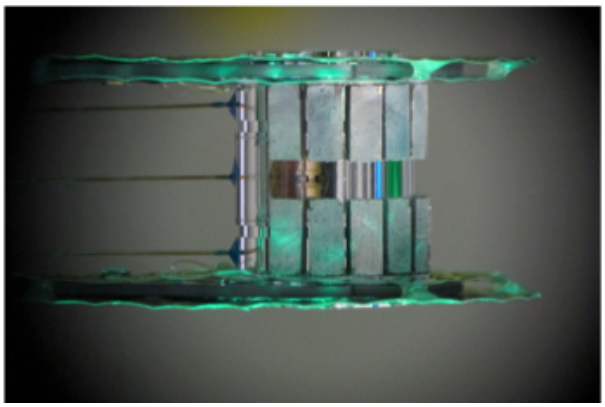

Figure 5.5: SymCDT target with mass-tamped hohlraum [7].

wall. The silver coating was to reduce the gas leakage from the capsule. For S2, the leakage rate during the shot went from 25 torr/hr to 2 torr/hr, so that the density ratio of D and T were 18% above the previous shots. The yields from the silver-coated capsule look like a statistical tie with the uncoated version at $4.1\text{x}10^{15}$ neutrons/cm^2. It goes down about 12% from the bare capsule once it is controlled for fill composition and pressure and, if any, Doppler shifting affecting the yield measurement. The mid-Z coating at the correct areal density is effective at increasing the yield, while coating at the wrong areal density substantially decreases yield. Defects that prevent the laser from directly hitting the capsule do not decrease yield substantially.

S2 had a 50:50 D-T gas filled at around ∼5500 torr at room temperature; for S3 the D-T filling was 65:35 at higher pressure and still at 293 K.

The capsule for S4 was uncoated and it was larger with a 4 mm shell diameter. The nominal capsule thickness was also higher at 27.1 μm and this shot used more energetic lasers. The primary objective in this case was to develop a high-output, well-characterized and high yield neutron and X-ray source for NSA program experiments.

5.3.3 DIM and TANDM

Within the NIF TC, a DIM is provided on a few port locations for inserting experimental diagnostics. There are currently four DIMs that provide neutron experiment platforms. The DIM is a two-stage telescoping system that positions the diagnostic package and enables exchange of diagnostics for different experiments [89]. The NIF diagnostic manipulators are used to carry ride-along experiments on neutron-yielding shots. This capability is readily accessible for collaborating groups.

The choice of the DIM for use in the ride-along experiments discussed here was based on the mechanical limitation guidelines provided by the NIF and which DIMs were available for the shots [91]. The polar DIM (0-0) was immediately rejected as it has the most restrictive exclusion zone. The three equatorial DIMs were preferable for the presented experiments:

90-78, 90-315, 90-348. The last system used is referred to as the TANDM and is used as both a target positioner and a diagnostic positioner. Usually the 90-78 is used for neutron effects experiment, and the 90-315 for holding detectors such as Neutron Imaging System (NIS)/Magnetic Recoil Spectrometer (MRS)/Co-Neutron X-ray Image (CNXI)/Neutron Activation Diagnostic Systems (NADs), described in Chapter 6[99], [89].

For the HTOAD experiments, H1, H2 and H3, the shots were performed at the DIM 90-78. DIM 90-78 is capable of a slightly closer approach than 90-315 for both TARPOS and cryoTARPOS while maintaining the same load bearing capacity. Due to 90-78 being capable of achieving the closest possible approach, any design that meets the weight and moment limitations for 90-78 will meet the limitations for the remaining DIMs. The closest approach of 60 mm and opening angle of 102.3 ° corresponds to a weight limitation of 80 kg. The outer radius is limited to a maximum of 280 mm to allow for clearance on the diagnostic load package (DLP) cart. The HTOAD has a limited volume and weight, therefore it was possible to use the 90-78.

The SNOUT used for S1, S2, S3 and S4 experiments was located on the TANDM 90-348. The TANDM has the advantage of sustaining larger weights than the rest of the DIMs, which allowed for the introduction of a larger number of materials and possible complex ETAs. The TANDM also has the same cable plant and data acquisition capability as DIM 90-78 which allows it to be used for validations.

The TANDM provides the closest possible approach to target chamber center (TCC) while maintaining the beam and TARPOS/cryoTARPOS clearances. A close approach to TCC is necessary to maximize the neutron fluence seen by the experiment and reduce the capsule neutron output required.

The requirements for the DIM chosen for the SNOUT experiments are similar to what is required for future ETA experiments: the weight limitation, the proximity to the TCC and the easy access to payload material. Finally, for any sample, the ideal retrieval time is under 2 hours, therefore it must be manually accessible from the SNOUT or ETA installed in the DIM.

5.3.4 SNOUT and HTOAD

As previously mentioned, an initial set of validation experiments has been conducted at the NIF using the SNOUTs and HTOAD instrumentation. This section will give a detailed description of SNOUTs and HTOAD instrumentation used to perform the experiments.

Since partial ETA data sets were collected here, the models can be used to gain insight into nuclear data issues indicated by divergence between the model and ETA performance. The propagation of nuclear data uncertainties into the modeled results from the NIF would also be beneficial and worthwhile.

Table 5.4 summarizes each assembly characteristics of the four campaigns performed in terms of elements inserted, distance from TCC, angular locations to the equatorial region.

Table 5.4: Experimental instrumentation details.

Name	Instrument	Volume (cm^3)	Material inserted	Distance to TCC (cm)	Angles (ϕ, ω)
S1	SNOUT	3252	Empty	6	90, 0
S2	SNOUT	3252	Empty	6	90, 0
S3	SNOUT	3252	Al T-6061 (30 cm)	6	90, 0
S4	SNOUT	3252	Al T-6061 (60 cm)	8	90, 0
H1	HTOAD	60	Empty	51	90, 48
H2	HTOAD	60	HDPE	51	90, 48
H3	HTOAD	60	SS	51	90, 48

5.3.5 SNOUT

The SNOUT is introduced in the DIM and can be easily added and removed from the port. The DIMs can hold the SNOUT in the chamber at variable distances from the target assembly. Many neutron experiments are assembled onto a single shot and for this project two DIMs were employed with two different SNOUTs configurations, 5 cm and 8 cm from TCC. Figure 5.6 shows the two SNOUT configurations that were used during the presented shot campaigns. For the H1, H2 and H3 experiments, the SNOUT used holds the HTOAD through the SRC, which is shown in Figure 5.6 a), while Figure 5.6 b) presents the SNOUTs used for the S1 to S4 experiments.

[a] 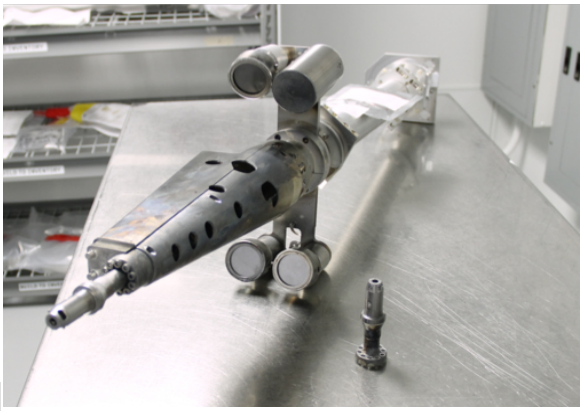 [b] 

Figure 5.6: a) SNOUT 90-78 for the HTOAD experiments. b) SNOUT 90-348 for the SNOUT base experiments [100].

The SNOUT is constructed with standard aluminum alloy, Al T-6061, which minimizes the weight for structural parts. The same shape and location would be used for future ETAs which would be located on the SNOUTs used. Due to the need for a close approach between the experiments and the TCC, the SNOUT satisfies the requirement of a conical section.

For S1, S2, S3 and S4 experiments, TANDM 90-348 carries the empty version of a SNOUT-based NED neutron spectrum tuning assembly; these experiments were designed at the nexus of something that can be built at the NIF and something that should be able to be calculated precisely.

For each of the SNOUT-focused campaigns, the idea was to introduce a level of complexity to split the different components of validation in order to be able to integrate all the sources of uncertainties that are encountered. S1 was the first SNOUT-focused shot and was used to test the flux monitor of choice and the model of a simplified 90-348 configuration as well as to see the effect of the SymcapCDT backscatter effect [96].

Within the S2 experiment, as explicitly presented in Chapter 6, the foil materials selection choice was expended from the lessons learned from S1.

For the S3 to S4 experiments, the idea was to be able to introduce the material of study inside the SNOUT and to reconstruct the size, in case the modeled assemblies required it, maintaining the same DIM configuration and standoff from the TCC. In S3 and S4, there was the an added complexity of introducing a tube of aluminum inside the tube section of the SNOUT. The description of each of the SNOUT sections of the assembly is presented below.

From the experiment, the product nuclei, mass of target sample, and total independent yield was measured as given in Chapter 6.

5.3.5.1 Assembly Description

Snouts usually have the dimensions of 50 to 100 cm and are attached to the detectors; the material of construction is mainly Al T-6061 with components of stainless steel in either grade 409 or 304. The engineering design of the SNOUT used for the ride-along experiments S1, S3 and S4 is shown in Figure 5.7.

The SNOUT used (AAA10-111922) is composed of five main components: a nose cap which contains the pinhole of few millimeters, a nose cone approximately 30 cm long, a basket which contains the spool with the TOAD, a tube of approximately 70 cm and the kinematic base at the end. Ideally, the tube and cone diameters can be increased and extended in order to accommodate larger stack of materials within the weight limitation of the DIM. The pinhole, basket and kinematic base can allocate TOAD filters with activation foils inside. Table 5.5 indicates the name, distance from TCC, length and ID for the main components. A 4 π distribution with an average yield of 3x10^{15} neutrons/cm^2 per each shot is expected for the source.

The material of choice was inserted inside the tubes in the S3 and S4 experiments, and was made to consist of elemental materials for simplicity and a straightforward relationship to the nuclear data. For practical considerations, the library used consisted of a few compounds and alloys (Al T-6061, LiF, high density polyethylene (HDPE), deuterated HDPE, Stainless 409, and boron carbide).

To maintain consistency, the SNOUT configuration materials, standoff, and densities were identical among the experiments. The only variation between the experiments S1 and

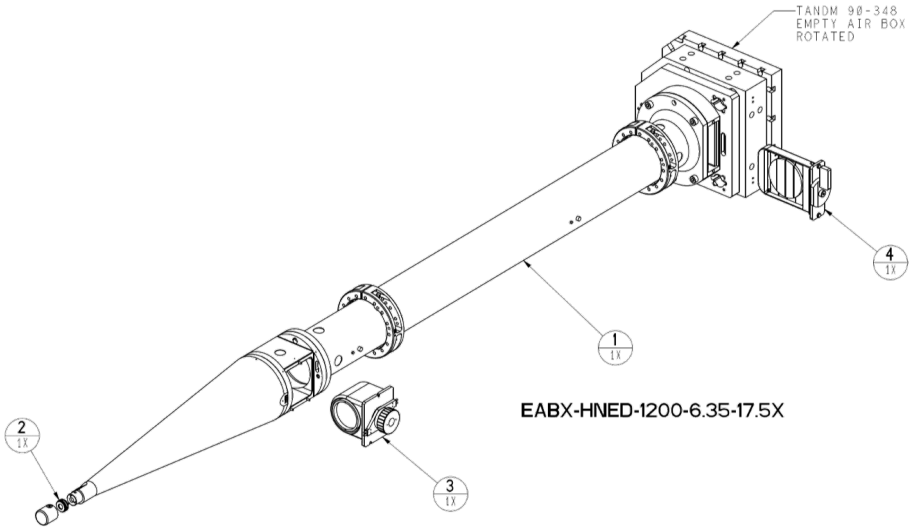

Figure 5.7: Engineering Design graphic of the SNOUT in DIM 90-348.

Table 5.5: SNOUT assembly elements.

Name	Type	Material	Distance TCC	Length	ID (cm)
AAA14-110241	Nose cap	Ta	6.043 cm	0.857	0.635
AAA10-104233	Cone Assy	Al T-6061	6.9 cm	19.93	5.25
AAA10-109067	Spool assy	Al T-6061	4.1 cm	5.1	5.25
AAA09-111599	Filter basket	SST, A2-70	47.01 cm	6.043	4.3
AAA14-113881	Tube	Al T-6061	69.0 cm	68.9	5.25
AAA09-114230	Kinematic base	Al T-6061	110.0 cm	5.1	5.25
AAA11-106528	Kin. base filter	SST, A2-70	118.12 cm	1	5

S2 were the type of foils used, and for experiments S3 and S4, the introduction of the initial material of interest. In those first experiments, an Al T-6061 cylinder (close up cylinder in Figure 5.8) was introduced inside the tube section. For a deeper understanding, the cylinder size changes from 30 cm in length in experiment S3 to 60 cm in experiment S4.

In the future, instead of performing experiment with individual materials placed inside of SNOUTs, an ETA assembly would be placed near the source instead of a SNOUT, by satisfying the NIF scoping studies requirements. Some examples of possible ETA to design are given in Chapter 8. This ETA would be used instead of the SNOUT, maintaining the characteristics for standoff distance, length and shape. The idea is to build a pulsed sphere-like experiment at the NIF as an optimized sphere of materials and to prove the capabilities for cross section evaluations. The ETAs in the NIF are designed to be fielded as a SNOUT replacement for a DLP mounted on either 90-348 TANDM or where the HTOAD will be located in 90-78 DIM. A close approach to TCC is necessary to maximize the neutron fluence

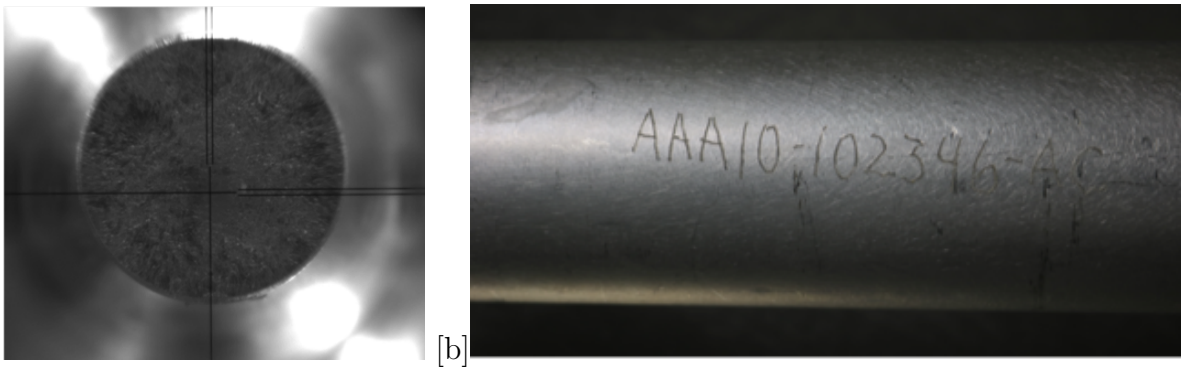

Figure 5.8: Two cross sections views of the Al T-6061 cylinder inserted in the SNOUT tube.

seen by the experiment and reduce the required capsule neutron output. As in the case of SNOUTs, the ETAs are passive, standalone packages and require no power or modifications to existing diagnostic capabilities at the NIF.

5.3.6 HTOAD

The HTOAD has been built by the NIF radiochemistry group as a larger version of the TOADs in order to contain the materials of interest for this study, as shown in Figure 5.9.

The HTOAD is mounted in the place of one SRC, usually on position of the DIM (PDIM) Aux2, on the SNOUT at the DIM 90-78 as visible on top right of Figure 5.6. The use of the SRC diagnostic platform at the NIF has allowed the development and implementation of the TOAD assembly for fielding materials of interest inside the NIF chamber during high yield neutron shots as ride-along diagnostic. The SRC collectors are located 50 cm from TCC and their ride-along diagnostic nature made them ideal for this work. DIMs can hold the SNOUT along with the collector in the chamber at variable distances from the target assembly.

The goal of the HTOAD experiments was primarily to assist with the development of a robust MCNP model for future HTOAD activation experiments. Combining the results from the H1, H2 and H3 shots, there is sufficient experimental data available to validate MCNP models for the radiochemistry platform at the NIF. It also allows us to validate the MCNP simulation for a single material or for stack of materials in the HTOAD that will help us to develop benchmarks to determine various uncertainties for the future development of ETAs at the NIF. The design of future experiments should be driven by this type of simulation.

5.3.6.1 Assembly Description

The HTOAD is made out of 300-series stainless steel, specifically 304, which minimizes ablation to the outer case of material viewing the target directly. The HTOAD holds almost 160 cm^3 of material and includes a polyethylene sleeve for neutron downscatter studies. The

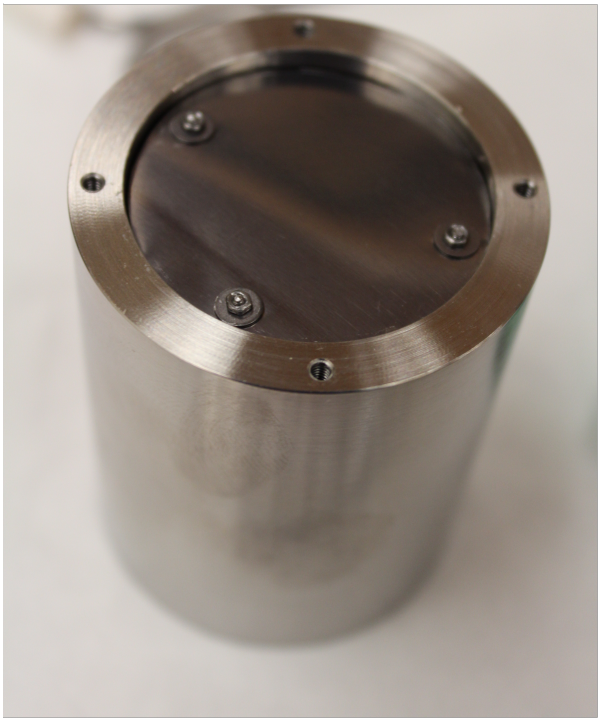

Figure 5.9: HTOAD container that is used to field several grams of material or multiple foil stacks.

HTOAD has a 49.5 mm internal diameter with a length of 69.8 mm and thickness of 1.14 cm.

The distances from the TCC of all the above-mentioned DIM components holding the HTOAD used are summarized for clarity in Table 5.6.

For the sake of the experimental validation, the HTOAD was used in three different configurations: empty (H2), filled with high density polyethylene (H1) and filled with iron (H3). The objective of the experiment was to further examine the results of the HDPE HTOAD and iron experiments by fielding a similar configuration without HDPE: an empty HTOAD. Ideally, the room-return neutrons flood the center of the NIF chamber with the same intensity, roughly independent of location, but due to configurations changing for each shot, asymmetrical scattering has an effect on where the ETA assembly can be located. For a detailed understanding of the effect of scattering neutrons within the NIF chamber, H2 was performed with an empty HTOAD.

Table 5.6: Elements of a the NIF shot containing the HTOAD and their characteristics.

	Capsule	**Hohlraum**	**SNOUT**	**SRC TOAD**	**HTOAD front**
Distance from TCC (cm)	0.1	0.5	6	50	45
Sample area (cm^2)	0.05		0.5	4.9	20
Sample Depth (cm)	0.05		0.14	0.1	8
Solid angle (msr)	200		10	2.0	10
Volume (cm^3)	0.0025		0.07	0.5	160

In all three configurations, there are four foil stacks located at 19 mm distance from TCC. The difference between the three configurations is the cylindrical material inserted inside the HTOAD container. For H2, the foils are held in place using three Ta/W (97.5% Ta, 2.5% W) threaded rods with 1.5 mm diameter. The foil stacks are scotch-taped on 3 mm Ta plates as shown in Figure 5.10. In the empty configuration, all neutrons come from the NIF D-T source and from scattering within the SNOUT, DIM and TC. From H2, it is possible to obtain an information about the thermalized neutrons in the distance and angular location in the NIF TC, the systematic errors in neutron scattering in materials inside the NIF environment as well as information regarding asymmetry in such scattering.

For the H1 and H3 experiments, three different cylinders are built with the foils taped on the front and back, the reasoning for this is detailed in Chapter 6. Figure 5.11 shows the position of the three cylinders of HDPE in the HTOAD for H1; the length of each cylinder is 19 mm with a diameter of 38.1 mm.

For H1 experiment, HDPE was introduced, a polyethylene $(-CH_2\text{-})_n$ with a density of 0.95 g/cm^3, which is a moderating medium that can be selected to produce the desired neutron spectrum in an ETA. The HDPE moderator blocks creation of a large low-energy neutron flux within the HTOAD.

For H3 experimental, the same carbon steel was used as shown for the HTOAD construction as in Figure 5.12. The objective was to analyze the changes into flux and reaction rates in the foils due to steel in order to study and understand the uncertainties arising from the steel, particularly data from the (n,inel) and (n,elastic) reactions. The analysis results are discussed in Chapter 7.

Figure 5.10: Tungsten rods used to hold the four foil stacks in the empty HTOAD configuration.

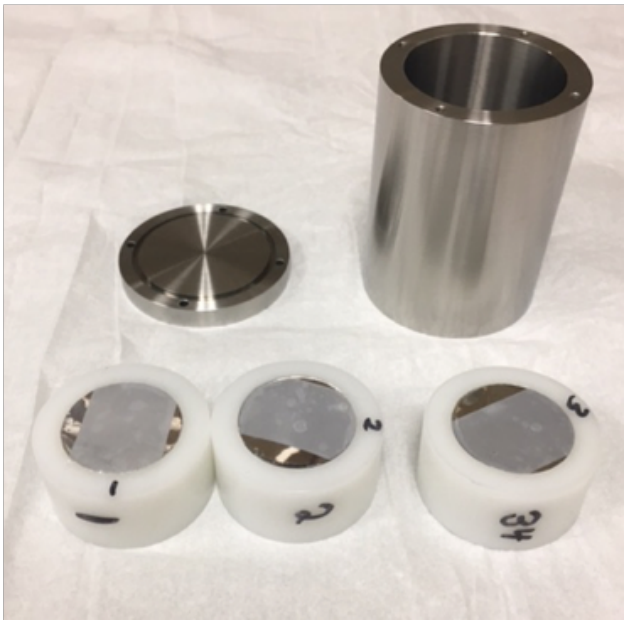

Figure 5.11: HTOAD cylinder with the three HDPE segments and the respective taped TOADs, with foils.

[a] 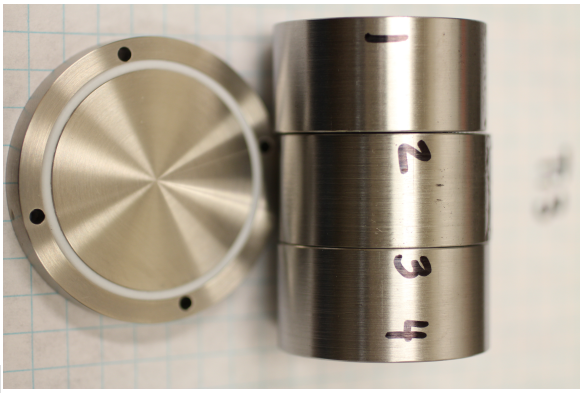

[b] 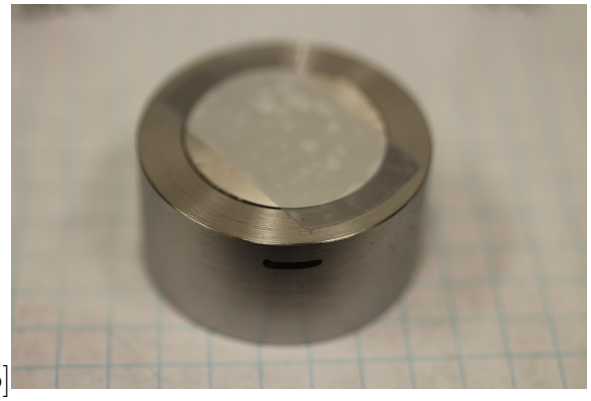

Figure 5.12: a) Three identical SS segments introduced inside the HTOAD, b) Close up to the TOAD with the activation foils taped to one of the SS segments.

Chapter 6

Neutron detection systems

This Chapter introduces the neutron detectors commonly used inside the National Ignition Facility (NIF) chamber and those used for the validation experiments described in Chapter 5.

6.1 Neutron Spectroscopy at NIF

Several diagnostic systems are required to gain meaningful information about the individual shot experiments degree of success [90]. NIF relies on a suite of nuclear diagnostics [90] to measure the neutronic output of experiments in inertial confinement fusion, high energy density physics, and fundamental sciences [90]. Below is given a brief description of the instrumentation present in the NIF chamber which is used to gather information for the presented research. In Section 6.2 more details are provided for the instrumentation added exclusively for the experiments described in Chapter 5.

- The **Neutron Time-Of-Flight (nTOF)** [101], [90], [102] provide performance metrics of absolute neutron yield and neutron spectral content (spectral width and non-thermal content) from which the implosion physical quantities of temperature and scattering areal density are inferred. The time-of-flight technique is one of the first methods employed in neutron detection and uses the time between the source generation, either measured from an accelerator beam or a chopper, and the time of detection to reconstruct the detected energy from the kinetic energy formula. Time-of-flight methods are considered the gold standard for neutron spectroscopy and can have very high measurement precision.

- Spatially distributed **Neutron Activation Diagnostic System (NAD)** [90], [102]. The NADs measure the primary D-T neutron emission with nearly identical systematic uncertainties. NAD measures primary D-T fusion neutron fluence at 20 points surrounding the target chamber using the ^{90}Zr(n,2n)^{89}Zr reaction and utilizing the 12.1 MeV reaction threshold to minimize signal from spurious neutron sources.

- A **Magnetic Recoil Spectrometer (MRS)** [103] shares few systematic properties with comparable NTOF and NAD devices and is deployed for independent measurement of the primary neutronic quantities.
- A **Neutron Imaging System (NIS)** [99] takes two images of the neutron source, typically gated to create co-registered 13-15 MeV primary and 6-12 MeV down scattered images.
- **Particle Time-Of-Flight (PTOF)** [104] measures compression-bang time using D-T or D-D neutrons, as well as shock bang-time using D^3He-protons for implosions with lower X-ray background. In concert, these diagnostics serve to measure the basic and advanced quantities required to understand NIF experimental results.

The detection system methodologies described here are necessary for the sake of the research to measure the source term and the neutron flux inside the chamber wall seen by the SNOUT and HTOAD experiments. Verification of the source term is required to understand the validation analysis. Thus, each experiment needs the information from the full nTOF suite, the NADS, NIS, and MRS to measure the source term.

6.2 Detection for the NIF Campaigns

The detection method chosen to measure the neutron spectra inside the HTOAD, the SNOUTs and future Energy Tuning Assemblies (ETAs) is called the activation foil methodology [105], [106]. The SNOUTs as the HTOAD, and the designs for future ETA assemblies, are all passive standalone packages and require no electrical connections or modifications to existing diagnostic capabilities at NIF. The foil activation method is also a passive neutron detector system that directly measures the full spectrum generated. This method uses multi-foils stacked targets [21], which are removed from the chamber post-shot and sent to off-site gamma-ray detectors to assay of the activity induced in them via (n,x) reactions. The foils are located in strategic points where information regarding the neutron flux is required. The availability and the size of the activation foils allow them to be easily fit within the experimental space.

Other advantages of using the foil activation technique [105],[21] are that the foils can be several millimeters thick without disturbing the neutron field due to their relatively low reaction cross sections, and the foils are practically insensitive to γ radiation, so they may be employed in mixed radiation fields and can be placed in high radiation environment, like the NIF TC, that would damage or degrade other kinds of instrumentation. Most importantly, foil activation depends linearly on the total particle fluence and not the time-differential flux. The disadvantages of using the activation method are the lack of live measurements (since the foils activity is measured after irradiation), the time sensitivity of the post-irradiation measurements, the absolute activity levels, and counting statistics. Finally, well-known cross sections and foil material properties are required, but not always available.

The foil activation method is specifically used to measure the volume averaged spectrum over a wide range of energies [105], but because neutrons are difficult to detect, activation is used to produce γ rays and beta particles, which are proportional to the neutron flux and easier to detect. Activation is the conversion of a stable isotope into a radionuclide by the absorption of a neutron and the formation of a product other than than the ground state of the target nucleus. In order to conserve energy, newly formed radionuclide is usually in an excited state and de-excite by energy release in the form of γ radiation. The foils, after being exposed to the neutron source, are transferred to a nuclear counting facility and the activity measured on an energy calibrated high purity germanium (HPGe) detector with known absolute detection efficiency. An HPGe detector counts γ-rays emitted from the activation foil and spectral peak analysis is performed and related to the neutron spectrum. The availability of a world-class radiochemistry facility [17] during all the NIF campaigns permitted quick and inexpensive measurements of the foils activation. A brief description of the counting facility used is found in Section 2.2.4.

6.2.1 Foil Activation Background

The way the neutron flux can be assessed from the foils is through the comparison of the measured reaction rates with those from a model of the expected reaction rates based on the calculated neutron energy distribution. The fundamental goal of activation analysis is to measure the induced activity to determine the number, N of interactions occurred in the foil during irradiation [2].

In the simplest case, the foils or wires are so thin that the probability of an interaction is small for any specific neutron. The neutron flux remains unperturbed, and the number of interactions, N, corresponds to the number of radionuclides created within the foils and is given by:

$$N_{act} = \int \phi(E)\Sigma_{act}(E)V dE. \tag{6.1}$$

Where:

- Σ_{act} is the energy-dependent macroscopic cross section (cm);
- E_{act} is the activation energy (MeV) averaged over the neutron spectrum;
- V is the foil volume (cm^3).

During a NIF shot the exposure times of the activation foils is 100-200 of hundred picoseconds (ps) and even the slowest multiple scattered neutrons arrive at the foil in a few microseconds. After exposure to the neutron flux, the foils are transferred to a counting facility for measurement of the activity. Because the activity is continuously decaying during this stage, careful account must be made of each of the times involved. The irradiated sample may not be placed in front of the energy calibrated HPGe detector immediately, so

the counting interval needs to be taking into account. The delay time is the time between the end of the irradiation and the beginning of the counting is denoted as the delay time, t_d. The counting/acquisition time is denoted as t_c. Given that most of the decay lifetimes for the activation foils of interested are an hour or longer this means that the irradiation time is $\sim$ billion times smaller than the delay time, or cool-down period. Thus, there is no time dependence in the irradiation time or decay happening during the NIF shot.

The total counts of the number of γ-rays counts of a specific energy in a given peak is given by Eq. 6.2.

$$\begin{aligned} C_i(E_i) = N[\frac{e^{-\lambda_i t_d}(1-e^{-\lambda_i t_c})}{\lambda_i} \\ \times(\frac{t_{live}}{t_c})][\frac{1-e^{-\mu(E_i)\rho_i x_i}}{\mu(E_i)\rho_i x_i}] \times [\epsilon(E_i) \times BR(E_i)] + B, \end{aligned} \tag{6.2}$$

where:

- i is the index number of a γ-ray peak;
- E_i is the ith measured gamma-ray's energy in the HPGe detector (MeV);
- N is the number of isotopes in the activation foils to emit γ at E_i [#];
- $\epsilon(E_i)$ is the HPGe detector's absolute detection efficiency for γ at E_i;
- *BR(E_i)*is the the absolute intensity (branching ration) of γ at E_i with BR(E_i) [s^{-1}];
- λ_i is the decay constant of the activated isotopes that emit γ at E_i with *BR(E_i)* [s^{-1}];
- t_d is the delay time between the end of the irradiation and the start of the counting [s];
- t_{live} is the live counting time [s];
- t_c is the real counting time [s];
- $\mu(E_i)$ is the material dependent mass attenuation coefficient as a function of photon energy E_i [$\frac{cm^2}{g}$];
- x_i is the activation foil's thickness [cm];
- ρ_i is the activation foil's density [$\frac{g}{cm^3}$];
- B is the number of background counts expected.

Counting systems are subject to several correction factors to be able to arrive at N from the observed counting rate. Due to the random nature of radioactive decay it is important to take into consideration the energy-dependent total detector efficiency, which is defined as the total number of γ counted, C, in the detector divided by the total number G of γ escaping the foil (Eq. 6.3).

$$\epsilon(E_\gamma) = \frac{C(E_\gamma)}{G(E_\gamma)}. \tag{6.3}$$

Then, the ϵ represents the overall counting efficiency, the measured absolute efficiency can be expressed as:

$$\epsilon_d(E_\gamma) = F_{d,\gamma} G_d(E_\gamma) E_d(E_\gamma), \tag{6.4}$$

where:

- $F_{d,\gamma}$ is the peak summing correction factor for a γ-ray characteristic of a given nuclide at some distance d from the detector
- $G_d\ (E_\gamma)$ is the energy dependent geometric correction factor accounting for the efficiency difference between a volume source and a point source
- $\mathcal{E}_d\ (E_\gamma)$ is the intrinsic energy-dependent efficiency of the detector at a distance d.

The overall counting efficiency is influenced by many factors: a geometry factor corrects for the fraction of the radiation that is not subtended by the detector, a counter-window factor corrects the number of beta particles or γ absorbed or scattered by the detector window and the counter intrinsic efficiency.

Other correction factors include: (1) the time correction factor, f_{time}, to take into account decay of the activated isotopes during transfer and counting, (2) the dead time correction, (3) the spectroscopic factor, f_{spec}, to account for the branching ratio (BR),(4) the absolute detection efficiency, (5) the f_{self}, a correction factor for γ self-attenuation in the foil, and (6) the coincident summing correction factor.

The combination of all of these correction factors, ϵ, can be calculated by simulating the whole set-up and specifying the number of beta or γ-rays reaching the detector. The intrinsic efficiency is determined experimentally using calibration sources of known intensity. All of the correction factors are combined to adjust the measured activity. If each factor is accounted for, the measured counts can be adjusted to accurately reflect the true activity.

6.2.2 Foil Materials

An important part of this neutron detection methodology is research into the appropriate foils to best reproduce the flux that is detected in the SNOUT and HTOAD. Foils choice is made in terms of material, dimension and geometry. The foils can be cut very thin and

small. With smaller foils it is possible to get more detailed information and the perturbation upon exposure to the neutron flux is smaller. But small foils also mean lower foil activity and therefore lower accuracy in the flux determination. The same cost-benefit analysis is needed to determine the material type and areal dimension.

The effects that need to be taken into consideration in the decision to pursue specific foil geometries and properties are the following:

- Flux depression caused by the presence of the foil in neutron field due to different neutronic properties from the media in which the neutron flux is measured.
- Self-shielding caused by the shielding of the inner part of the foil by its outer part.
- Self-absorption is caused by the absorption of the radiation which is emitted from the inner part of the foil by its outer layers.

In terms of the type of material chosen for the activation foils, there are a number of physical and nuclear properties to consider, including the cross sections, foil composition, half-life of the induced activity, and the type of decay radiation.

The properties of the activation materials play an obvious part in determining the physical environment in which they may be exposed. Materials in gaseous or liquid form are very difficult to employ, therefore almost all activation detectors consist of metallic foils or wires that can be cut to the desired dimensions. Very high purity of the material is often required to avoid interference from other neutron-induced reactions.

To achieve a high degree of sensitivity, materials are chosen that have a large cross sections for a neutron-induced reaction and each activation foil must have a unique cross section to span the range of the neutron spectrum being measured. The threshold energies of all foils should cover evenly the energy range of interest in the unfolded neutron energy spectrum. Meanwhile it is important to keep the neutron absorption probability small enough to avoid perturbing the flux during measurement. The uncertainties of cross section must be as small as possible as well (IRDFF-90 [34]).

The half-life of the induced activity should be neither too short nor too long; long half-lives require the use of long irradiation times (not the NIF case), very short half-lives can lead to difficulties in transferring the foil to the counter.

6.2.3 Irradiation Foil Sets

The analysis of the foils, from the campaigns discussed in Chapter 5, require the use of the radiochemistry and γ spectroscopy facilities for post-shot analysis to measure the neutron spectrum obtained. The foil packs are required to be removed from the TC within 2 to 6 hours to measure short lived reaction products.

The validation calculation requires a measurement of the product nuclei, the mass of target of the sample, and total independent yield. Those measurements are then compared with the reaction rates and the neutron spectra simulated from neutron transport physics.

The comparison is also performed against the analytical calculation of the reaction rates from the spectrum expected by the NTOF measurements and using the XS from IRDFF.

For the NIF campaigns, the foils were chosen following the practical guidelines from Section 6.2.2 and the availability in the standard NIF NAS. These are: aluminum (Al), indium (In), zirconium (Zr), gold (Au), titanium (Ti) and nickel (Ni). Table 6.1 gives information on the foil materials investigated.

Table 6.1: Description of the activation foil materials, natural abundance of particular nuclide and induced activity half-life.

Elem.	**Nat. abund.**[%]	**Reaction**	**Half-life**	γ**Energy [keV]**	γ **Abund. [%]**	**Thresh. [MeV]**
^{90}Zr	100	^{90}Zr(n,2n)^{89}Zr	78.4 hrs	909.15	100	12.10
^{58}Ni	67.9	^{58}Ni(n,2n)^{57}Ni	35.6 hrs	1378	81.7	12.43
		^{58}Ni(n,p)^{58}Co	70.9 days	811	99.45	0
^{197}Au	100	^{197}Au(n,2n)^{196}Au	6.18 days	356	87	8.11
		^{197}Au(n,γ)^{198}Au	2.7 days	411.8	95.6	0
^{115}In	95.7	^{115}In(n,n')^{115m}In	4.5 hrs	336.2	45.8	0.336
		^{115}In(n,γ)^{116m}In	54.3 min	1293.6	84.8	thermal
^{27}Al	100	^{27} Al(n,α)^{24} Na	14.9 hrs	1368.6	99.49	3.25
		^{27} Al(n,p)^{27} Mg	9.5 min	844	71.8	1.896
^{48}Ti	73.7	^{48} Ti(n,p)^{48} Sc	43.7 hrs	983.5	100	3.9
^{47}Ti	7	^{47} Ti(n,p)^{47} Sc	3.35 days	159.4	68.3	0.81

Aluminum has some ideal characteristics for experiments with D-T and D-D neutron sources as it occurs as one isotope of mass number 27 which has good reaction cross sections for fast and thermal neutron reactions. Zirconium and indium are ideal for the D-T reaction due to large (n,2n) cross sections above 9 MeV. Indium also has a large cross section at $<$ 1 MeV, extensive experimental experience at NIF, high availability for laboratory testing, the 54 minute half-life of ^{116m}In, which lends itself to multiple laboratory experiments in a condensed period of time, and ^{115m}In's large thermal neutron cross section of 162 barns. Nickel has a broad cross section for an (n,p) reaction between 3-13 MeV.

The cross sections of the reactions from Table 6.1 are shown in Figure 6.1. The Figure 6.1 a) shows some limitations of the foil pack used for the measurements. In general, there is overlapping and high sensitivity in the areas of high neutron flux as shown in Figure 6.1 b). However, there is a gap in the 10 eV to 100 keV region. This region is below the threshold reactions and above the highly sensitive thermal region for the (n, γ) reactions. This means

that the unfolded spectrum in this energy range is limited by the limited reaction sensitivity and is highly uncertain.

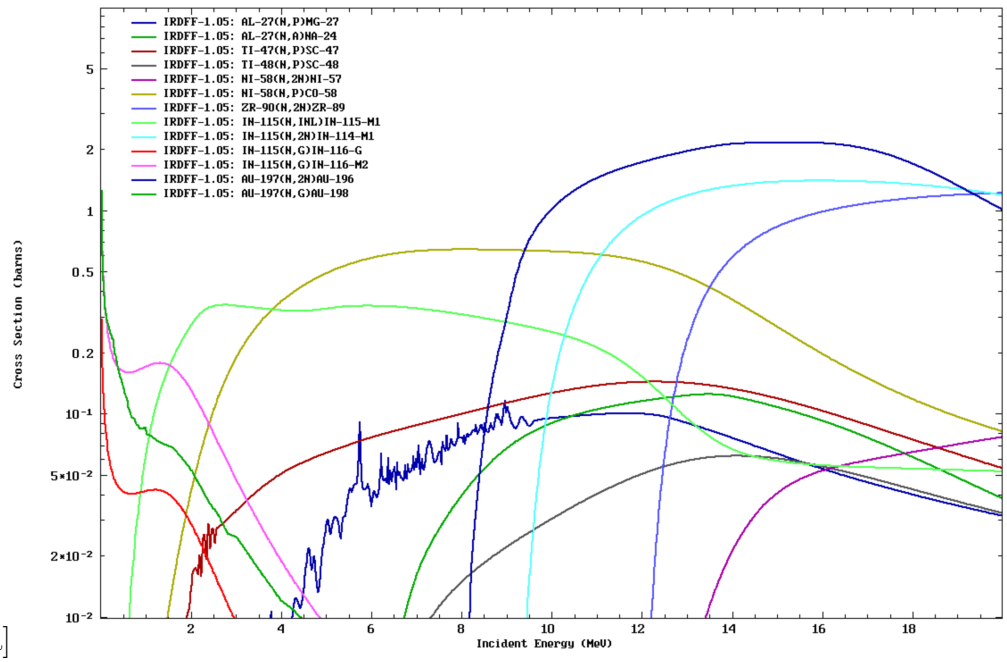

[a]

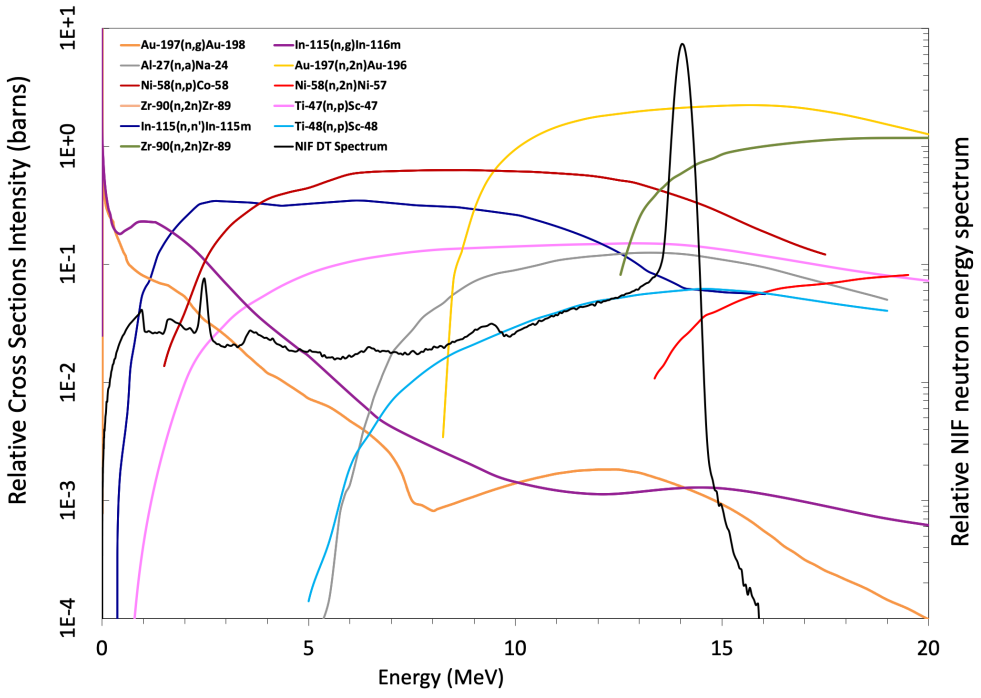

[b]

Figure 6.1: a) IRDFF v1.05 cross section data for the reactions used, b) Cross sections compared to the neutron spectrum at NIF (in black).

Usually the foils used have a diameter around 50 mm but it varies with the distance from the TCC. The thicknesses used have ranged from $0.1 - 5$ mm, more details for each foils stack used are given in Section 6.2.4.1 and 6.2.4.2. Foils are then sealed inside the TOAD, which is removed after a shot for processing.

6.2.4 HPGe Counters

The foil samples inserted in the chamber after each shot are removed and transported to the nuclear counting facility at LLNL for γ counting with HPGe detectors. Figure 6.2 shows the HPGe facility in the NIF radio-chemistry laboratory at LLNL with a close up of the detector.

An HPGe γ-ray spectrometer is a semiconductor-based detector. The decay of the product nuclei produced in the activation reactions normally involves the emission of either β particles or γ-rays. Gamma rays counting is often preferred because the penetrating nature of the radiation minimizes the effects of self-absorption within the sample. Furthermore, it is far easier to perform energy spectroscopy with γ-rays.

Precise experimental knowledge of the irradiation efficiency, ϵ_{irr}, beyond that attainable by modeling is necessary to produce meaningful results. For each of the experiment diagnostic description there will be a representation of the efficiency for the counting.

6.2.4.1 Activation Foils for the HTOAD Campaigns

Each of the HTOAD in campaigns H1, H2 and H3 included four stack of foils located at 19 mm of distance and each foil stack consists of four foils with a total of 16 foils per campaign. Table 6.2 gives the detailed distances of the foil stacks from the TCC. Each of the block contain the same foils and same dimensions. Between the different campaigns, the changes to the foils include the setup the foils are inserted in the HTOAD cylinder but this does not affect the neutron flux detected.

Table 6.2: Foil pack distances to the TCC. It is difficult to put an uncertainty on those measurements as their relative distance is within <0.5 mm and absolute distance from TCC is model based.

Foil Stack	**Distance (mm)**
Stack 1	512.3
Stack 2	529.3
Stack 3	548.3
Stack 4	566.3

In H2 experiment, the cylinder is empty and the foils are taped together using tungsten rods. In the rest of the HTOAD, for H1 and H3 experiments, the foils are located inside of a special sealed sample container: a target option activation device (TOAD). The TOAD has

[a]

[b]

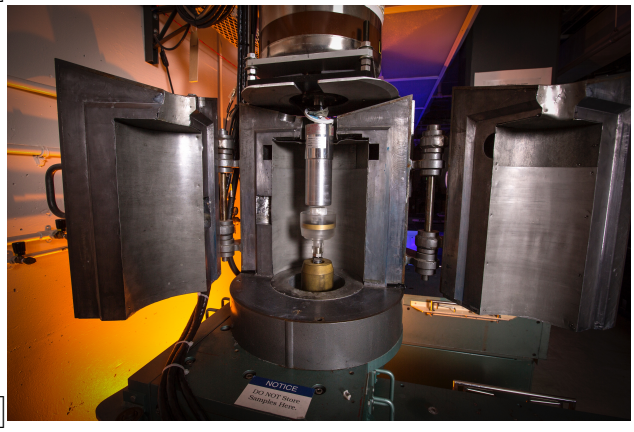

Figure 6.2: a) HPGe room at LLNL, b) HPGe detector.

been developed to field materials of interest directly and they are scotch-taped on 3 mm Ta plates. Foils are sealed inside the TOAD, which is removed after a shot for processing as shown in Figure 6.3. In each case the foils are separated with Q_l foils.

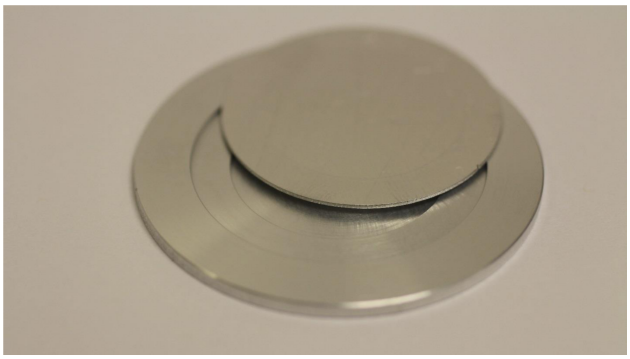

Figure 6.3: Picture of a TOAD. The foils are inserted inside a TOAD.

The foil materials correspond to the ones from the NAS standard: Al, Au, Zr, In. Figure 6.4 is a picture of the foils taken before the NIF shot.

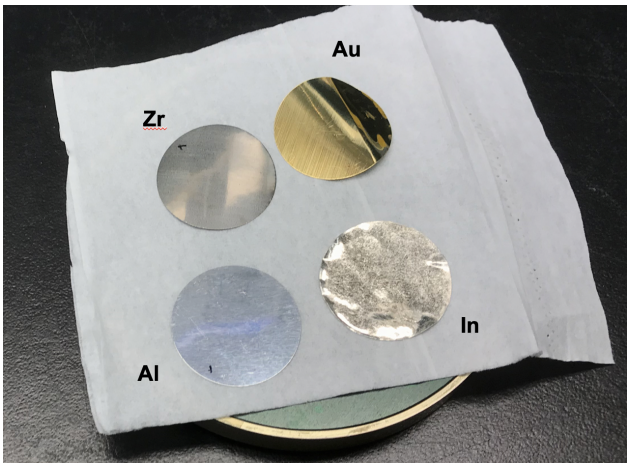

Figure 6.4: Some of the HTOAD foils.

The sizes of all the foils inserted pre-irradiation for all the 3 campaigns are given in Table 6.3. During the manufacturing the foils might suffer irregularities and slight dimensional changes, thus Table 6.4, Table 6.5 and Table 6.6 provides for each campaign the masses, areas and area densities of all the foils.

Table 6.3: Foil pack dimensions inside the HTOAD.

Foil elem.	**Diameter [mm]**	**Thickness [mm]**	**Density (g· cm^{-3})**
Au	50	0.6	19.3
Zr	50	5	6.59
Ti	50	30	4.83
In	50	40	7.15

Table 6.4: Foil packs inside the HDPE HTOAD.

Foil	**Mass (g)**	**Area (cm^2)**	**Areal density (g/cm^2)**
In-1	0.340	5.00	0.068
In-2	0.335	5.09	0.066
In-3	0.335	5.00	0.067
In-4	0.338	5.03	0.067
Ti-1	0.291	4.98	0.058
Ti-2	0.287	4.85	0.059
Ti-3	0.286	4.81	0.059
Ti-4	0.282	4.79	0.059
Zr-1	0.081	4.86	0.017
Zr-2	0.083	4.94	0.017
Zr-3	0.082	4.84	0.017
Zr-4	0.080	4.79	0.017
Au-1	0.939	4.85	0.193
Au-2	0.921	4.83	0.190
Au-3	0.940	4.85	0.194
Au-4	0.926	4.84	0.191

For the HTOAD the counting is performed using the radiochemistry counting facility seen in Figure 6.2 with the co-axial HPGe XP/3 ORTEC detector [17]. The spectral analysis of the samples counted on HPGe multichannel analyzer systems was performed using the LLNL code GAMANAL [107].

For each of the HTOAD campaigns an efficiency data is given at a specific distance from the detector surface. The distances of the foils counted in the detector are given in Table 6.7. The efficiency curve for the stacks is seen Figure 6.5.

In the H2 campaign with the empty HTOAD, it is expected to see the consistency with the (n,2n), (n,p) and (n,α) reaction channels being dominated by 14.1 MeV neutrons and the production of radionuclide consistent with $1/R^2$ where R is the radius. While with the HDPE and iron case in H1, H2 it is possible to analyze the effects of those materials in the neutron detection.

6.2.4.2 Activation Foils for the SNOUT Campaigns

In the SNOUT, the foil stacks are located at different heights and locations as each location in the TC is a unique neutronic environment. The foils are located in three locations along the SNOUT as seen in Figure 6.6, at 7 cm, 41 cm and 110 cm.

Table 6.5: Foil packs inside the empty HTOAD.

Foil	Weight (g)	Area (cm^2)	Areal density (g/cm^2)
In-1	0.370	5.11	0.072
In-2	0.395	5.02	0.079
In-3	0.386	5.03	0.077
In-4	0.389	5.10	0.076
Ti-1	0.296	4.88	0.061
Ti-2	0.293	4.91	0.060
Ti-3	0.301	4.93	0.061
Ti-4	0.293	4.93	0.059
Zr-1	0.086	5.01	0.017
Zr-2	0.084	4.95	0.017
Zr-3	0.079	4.83	0.016
Zr-4	0.085	5.00	0.017
Au-1	0.929	4.95	0.188
Au-2	0.941	4.75	0.198
Au-3	0.936	4.91	0.191
Au-4	0.929	4.86	0.191

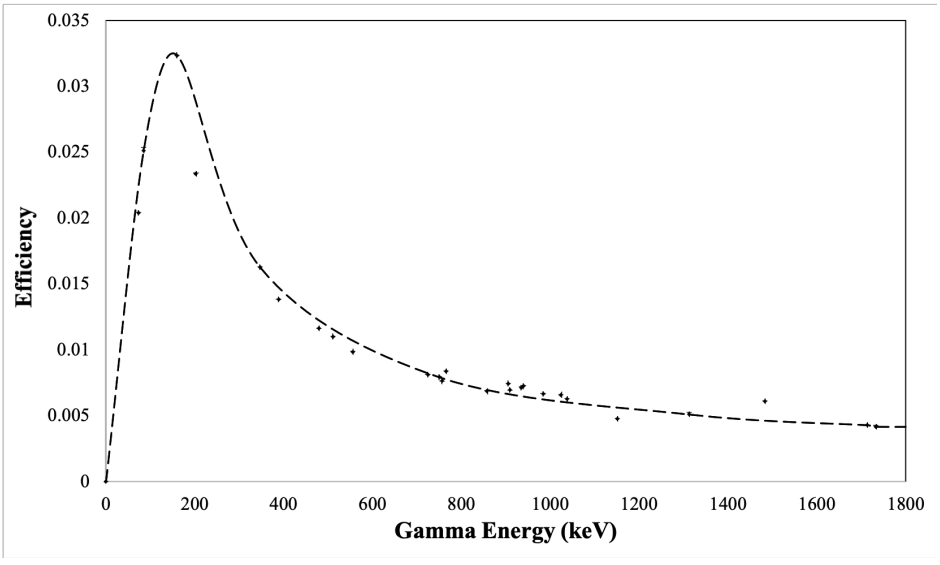

[a]

Figure 6.5: Efficiency HPGe efficiency calibration performed at 18 cm from the detector for the HTOAD foil packs.

Table 6.6: Foil packs inside the Iron HTOAD.

Foil	**Mass (g)**	**Area (cm^2)**	**Area density (g/cm^2)**
In-1	0.4823	5.12	0.094
In-2	0.4840	5.10	0.095
In-3	0.4847	5.07	0.096
In-4	0.4708	5.03	0.094
Ti-1	0.2952	4.97	0.059
Ti-2	0.2974	4.99	0.060
Ti-3	0.2955	5.01	0.059
Ti-4	0.2963	4.98	0.060
Zr-1	0.2683	5.04	0.053
Zr-2	0.2676	4.93	0.054
Zr-3	0.2715	4.97	0.055
Zr-4	0.2663	5.01	0.053
Au-1	0.9381	4.88	0.192
Au-2	0.9406	4.86	0.194
Au-3	0.9291	4.87	0.191
Au-4	0.9411	4.85	0.194

The foil pack of SNOUT is constant through each of the four campaigns, in order to maintain consistency in the experiments and to ensure the only changes in the environment are due to adding a different material within the SNOUT. Also, the eventual goal is to use the SNOUT as an ETA which would be located between the sets of foils. The dimension of the foils changes at different distance to the TCC; due to the variation in distances, the size increases as the flux decreases with $1/R^2$.

The selected foils were changed between S1 and the rest of the campaigns, as a lesson learned from the first shot. The foils are chosen to allow for the best unfolding of the spectrum, the efficiency and the statistics though with compromises for the cost, availability and dimensions. The cross section used for the reaction channels are the same for the HTOAD, the IRDFF v. 1.05, and the elements chosen are: Al, Au, In, Ni, and Zr.

The foils are separated by thin Al foils, incorporated in the counting samples, the filters are taped on the plate using polyimide (Kapton^{TM}) film tapes with acrylic pressure sensitive adhesive LLNL component. In this way the foils are easily located in the pinhole array inside the nose cap, filter basket, and kinematic base.

Table 6.8 represents the location, distance and type of the foils chosen for S1.

For the experiments S2, S3 and S4, extra foils are added to the pack to highlight an additional reaction (see Table 6.9).

Table 6.7: Foil locations in the XP/3 detector.

HTOAD campaign	Foil packs	Distance detector to window [cm]	Distance midpoint of source [cm]	Header distance [cm]
H1	1	0.81	5.75	4.93
	2	0.81	5.75	4.93
	3	0.81	5.75	4.93
	4	0.81	5.75	4.93
H2	1	0.81	5.75	4.93
	2	0.81	5.75	4.93
	3	0.81	5.75	4.93
	4	0.81	5.75	4.93
H3	1	0.81	5.75	4.93
	2	0.81	5.75	4.93
	3	0.81	5.75	4.93
	4	0.81	5.75	4.93

Plot in Figure 6.7 shows the efficiency curve for the stacks in the SNOUT shot campaigns.

Three sets of activation foils were irradiated during the SNOUT experiment. The first set was irradiated to provide source spectrum information and measurements. The second foil set was irradiated to record the frontal effects of the backscattered neutrons from the materials inserted in the SNOUT. The third foil set was irradiated to measure the background effect of the empty tube cases as well as the ETA sample cavity to measure the ETA modified spectrum.

6.3 Unfolding Analysis

Unfolding seeks to solve the inverse problem to determine the unknown incident energy-dependent neutron flux given a set of measurements and a known detector response function [106]. Mathematically, this is formulated as:

$$M_i = \int R_i(E)\phi(E)dE \quad \text{and} \quad i = 1, ..., M, \tag{6.5}$$

where:

- M_i is the measured value of the detector system for the ith channel;
- $R_i(E)$ is the energy dependent response function for the i^{th} measured channel;
- $\phi(E)$ is the incident neutron energy spectrum.

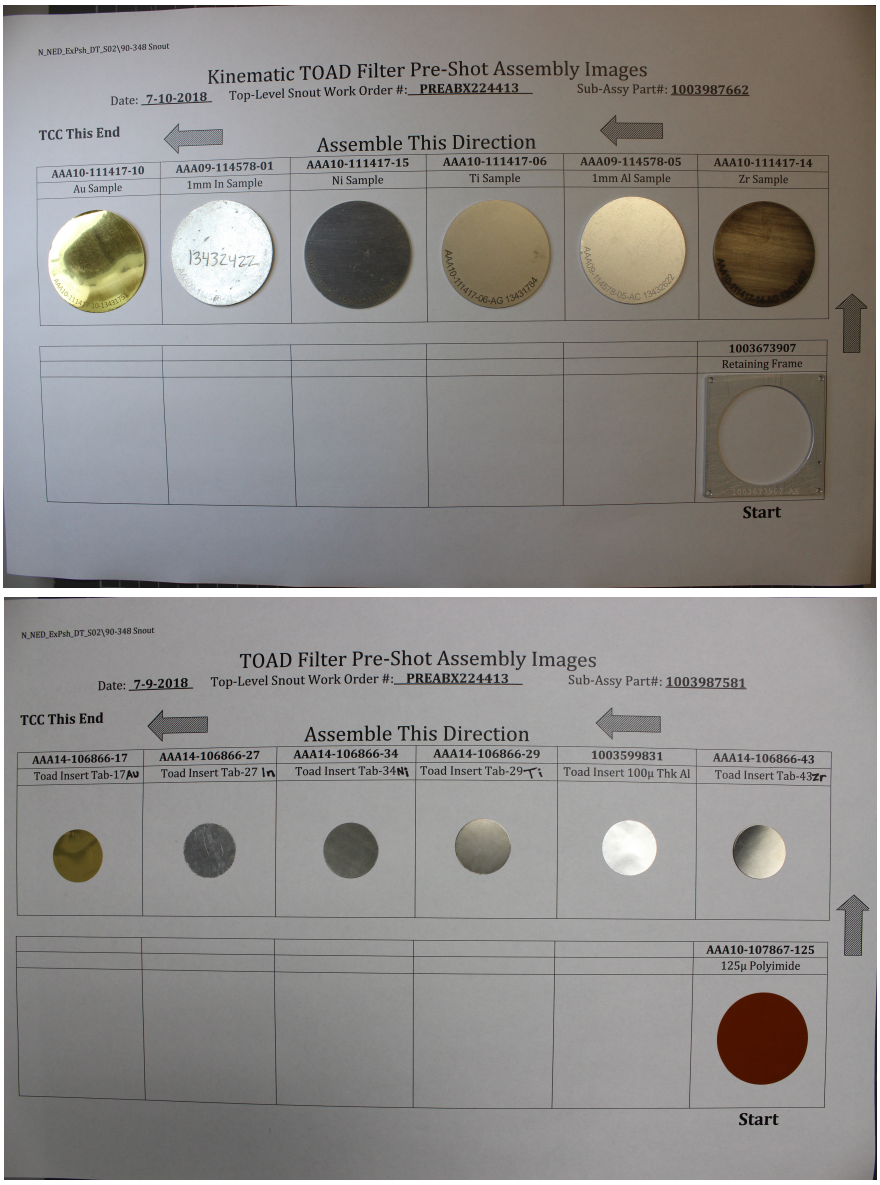

Figure 6.6: Picture of the foils inserted inside a SNOUT. The foils sizes change based on the location: a) foils inside the kinetic base, b) foils inside the pinhole.

In the forward version of the problem, R(E) and ϕ(E) are known and M has a unique solution.

In the inverse problem, $\phi(E)$ is unknown, and Eq. 6.5 has no unique solution due to the degeneracy created by representing a continuous function with a finite number of measurements [106]. An approximate transformation of Eq. 6.5 can be made to the linear matrix equation:

Table 6.8: Activation foil characteristics of the foil packs used inside the SNOUT for S1.

Location foils	Standoff	Reaction prod.	Thickness [mm]	Mass (g)
kinematic base	110	^{196g}Au	0.1	3.733
kinematic base	110	^{198}Au	0.1	3.733
kinematic base	110	^{115m}In	1	14.35
kinematic base	110	^{116m}In	1	14.35
kinematic base	110	^{89}Zr	1	12.555
kinematic base	110	^{54}Na	1	5.393
basket	41	^{196g}Au	0.1	0.9393
basket	41	^{198}Au	0.1	0.9393
basket	41	^{115m}In	1	0.4189
basket	41	^{116m}In	1	0.4189
basket	41	^{89}Zr	1	0.2626
basket	41	^{54}Na	1	0.132
pinhole	7	^{196g}Au	0.1	0.148
pinhole	7	^{198}Au	0.1	0.148
pinhole	7	^{115m}In	1	1.182
pinhole	7	^{116m}In	1	1.182
pinhole	7	^{89}Zr	1	1.008
pinhole	7	^{54}Na	1	0.042

$$\overrightarrow{M} = \mathbf{R}\overrightarrow{\phi}, \tag{6.6}$$

$$\begin{pmatrix} M_1 \\ M_2 \\ . \\ . \\ . \\ M_M \end{pmatrix} = \begin{pmatrix} R_{11} & R_{12} & \cdots & R_{1N} \\ R_{21} & R_{22} & \cdots & R_{2N} \\ \vdots & \vdots & \ddots & \vdots \\ R_{M1} & R_{M2} & \cdots & R_{MN} \end{pmatrix} \cdot \begin{pmatrix} \phi_1 \\ \phi_2 \\ . \\ . \\ . \\ \phi_N \end{pmatrix}, \tag{6.7}$$

were M is the number of measurements and N is the number of neutron energy groups. Eq. 6.7 has no unique solution when $N > M$, and often not for $N < M$ due to the correlations between the response functions. Instead, Eq. 6.7 is often solved using iterative minimization approaches such as the method of least squares, or χ^2, which is given by:

$$\frac{\chi^2}{n} = \frac{1}{n}\sum_i^M \frac{(\sum_j^N R_{ij}\phi_j^g - M_i)^2}{\sigma_i^2}. \tag{6.8}$$

Table 6.9: Characteristics of the Ni and Ta foils used inside the SNOUT for S2, S3 and S4 shot campaigns.

Location foils Mass (g)	**Standoff**	**Reaction prod.**	**Thickness [mm]**
kinematic base 17.57	110	^{57}Ni	1
kinematic base 17.57	110	^{58}Co	1
kinematic base 3.834	110	^{48}Sc	1
basket 0.408	41	^{57}Ni	1
basket 0.408	41	^{58}Co	1
basket 1	41	^{48}Sc	1
pinhole 0.131	7	^{57}Ni	1
pinhole 0.131	7	^{58}Co	1
pinhole 0.321	7	^{48}Sc	1

In Eq. 6.8, *n = (N-1)*, the number of the degrees of freedom, and σ_i is the uncertainty of the *i-th* measurement [106]. These methods are often modified to account for the non-negative flux requirement, smoothness of the solution, and the addition of *a priori* information. Each of these modifications, if done properly, is useful in overcoming the degeneracy of the solution space to unfold spectra that are consistent with TOF measured spectra.

One limitation of the direct application of minimization or goodness of fit methods is the difficulty in assessing the uncertainty of the unfold [108]. Many computer programs have been developed to solve spectrum unfolding problems using variations of the basic mathematics described above [108]. Each code differs in the treatment of the uncertainty and the requirement for *a priori* information, such as a guess of starting spectrum. In Section 6.3.1, STAYSL is discussed in the context of unfolding for neutron activation.

Table 6.10: Foil locations in the XP/3 detector.

SNOUT campaign	Foil packs	Dist. detector to window [cm]	Dist. midpoint of source [cm]	Header dist. [cm]
S1	pinhole	0.81	5.75	4.93
	basket	0.81	5.75	4.93
	kinematic base	0.81	5.75	4.93
S2	pinhole	0.81	5.75	4.93
	basket	0.81	5.75	4.93
	kinematic base	0.81	5.75	4.93
S3	pinhole	0.81	5.75	4.93
	basket	0.81	5.75	4.93
	kinematic base	0.81	5.75	4.93
S4	pinhole	0.81	5.75	4.93
	basket	0.81	5.75	4.93
	kinematic base	0.81	5.75	4.93

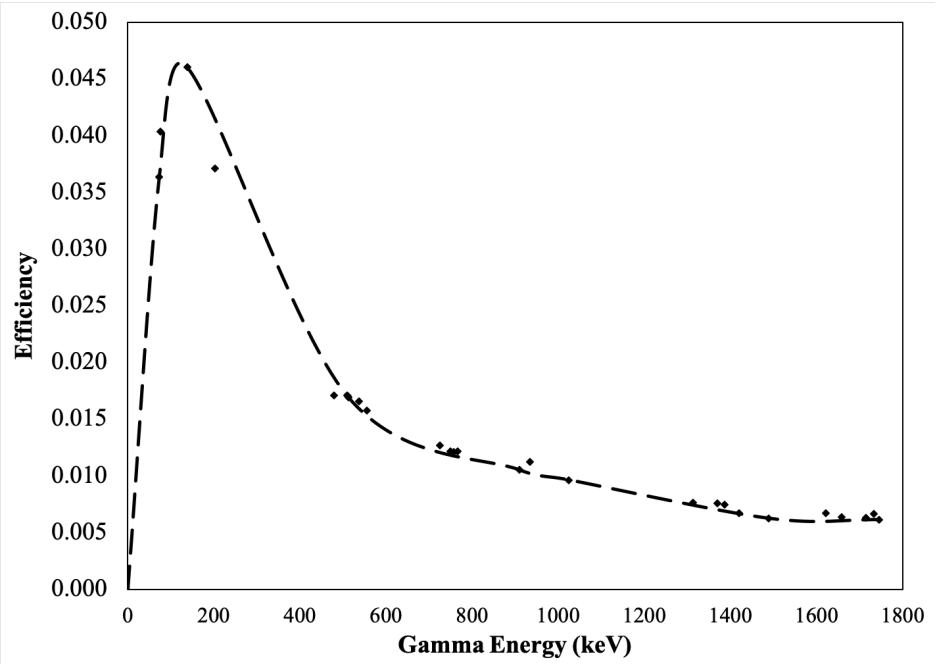

[a]

Figure 6.7: Efficiency HPGe efficiency calibration performed at 18 cm from the detector for the SNOUT foil packs.

6.3.1 STAYSL

The foil activities were used with the underlying IRDFF nuclear data to unfold the neutron spectrum using STAYSL Suite v1.2.0, developed by Pacific Northwest National Laboratory (PNNL) and available from RSICC [109]. STAYSL determines the incident neutron flux using a generalized least-squares to perturb an initial spectrum guess adjusted based on a χ^2 comparison of the measured activities rates and their uncertainties and the activities calculated from an adjusted flux [110]. The χ^2 statistic used by STAYSL for the least-squares minimization is given as:

$$\chi^2 = \begin{pmatrix} P & -\overline{P} \\ A^\circ & -\overline{A} \end{pmatrix}^\dagger \cdot \begin{pmatrix} N_P & 0 \\ 0 & N_{A^\circ} \end{pmatrix} \cdot \begin{pmatrix} P & -\overline{P} \\ A^\circ & -\overline{A} \end{pmatrix}, \tag{6.9}$$

A° is the foil activities, P is the neutron flux convoluted with the cross section:

$$P = \begin{pmatrix} \phi \\ \Sigma \end{pmatrix}, \tag{6.10}$$

N_P is the co-variance matrix from the flux and nuclear data convolution, and N_A is the activity co-variance matrix:

$$N_P = \begin{pmatrix} N_\phi & 0 \\ 0 & N_\Sigma \end{pmatrix}. \tag{6.11}$$

In the χ^2 function, P and N_P are introduced since a solution is desired: the value of $\overline{P}$, which minimizes χ^2, to be the most likely value based upon the *a priori* knowledge of $\overline{P}$ given by P and N_P. STAYSL utilizes data from the IRDFF v1.05 library because this library has an increased level of benchmarking for dosimetry applications.

STAYSL required an initial spectrum guess for the neutron flux, which is expected to be a close approximation to the true spectrum and is obtained from a radiation transport model. The spectrum utilized in the NIF experiments is the MCNP-calculated neutron fluence in the zirconium foil with the captured systematic uncertainty. The zirconium foil used for the neutron yield fluence is the one in the pinhole of the SNOUT and in the first foil pack for the HTOAD. The activities produced for the foils are often degenerate, where an infinite number of spectra could provide the same endpoint. The initial spectrum allows for a physics-and modeling-based result to guide the overall result.

Sub-modules allow for the calculation of neutron and γ self-shielding (SHIELD), corrections for a time-varying flux (BCF), and re-binning of the nuclear data into arbitrary energy groups structures (NJOY99/NJpp). The software package comes with pre-compiled cross section data in the STAYSL PNNL 140- group, 69-group (WIMS/EPRI-CPM), 129-group (for 14.1 MeV source), 175-group (VITAMIN-J), and 640-/725-group (SAND IIa) energy grid structures. For the NIF experiments, the ideal group is the 129-energy-group cross section data.

The primary limitation in unfolding neutron spectra from foil activation is that there is limited information available. For example, in the proposed foil pack, there is a maximum

of ten different response functions. This is compensated for by providing additional *a priori* information to the unfold process in the form of a realistic spectrum guess. An alternative approach is to use detection systems that contain a more dynamic response as the possible use of the CVD [22] diamond inside the SNOUT experiments.

Chapter 7

Improvements and Experimental Validation of the Monte Carlo Model of the Target Chamber

The first part of this Chapter describes the improvements in the Monte Carlo model of the full National Ignition Facility (NIF) Target Chamber (TC) in preparation for the experimental validation and design of future ETA using Gnowee/COEUS. The full MCNP NIF TC model was further expanded to replicate the NIF campaigns described in Chapter 5 in order to produce a high-fidelity neutron spectra distribution inside of the TC. The simulations of the full NIF model are used as sources for designing optimized ETA for nuclear engineering applications at NIF. The second part of the chapter introduces the measurement results of the experiments performed and described in Chapter 5. The results presented have a two-part outcome. First, the measurements at the SNOUT and HTOAD levels are analyzed and described, featuring the development of a proof-of-platform design system for performing measurements exploiting NIF SNOUTs and HTOAD for nuclear engineering applications. The status of the design will be discussed and the implications for future work will be explored. Second, the measurements are compared to the expected result of the MCNP and COEUS simulations. The comparisons contribute to the process of validation and verification of the modeling software package used for designing optimized ETAs in NIF. Providing accurately verified and validated MCNP modeling is crucially important for predicting the overall performance of an ETA system for future experiments at NIF and other facilities. Verification of the simulations is also performed and presented here between MCNP and SCALE.

7.1 Improved Simulation of NIF Experiments

As described in Chapter 4, the code package/suite used for simulations is MCNP, which is also the chosen radiation transport engine for the optimization software package COEUS.

The MCNP versions used in this work are first MCNP5, for the oldest model of the NIF TC, and second MCNP6, for all the other simulations, with the libraries ENDF/B-VIII and IRDFF v. 1.05. The IRDFF v.1.05 library is needed due to cross section data shortcomings in ENDF/B-VIII, especially for the activation foil cross sections.

While the MCNP software has been extensively benchmarked and can be trusted, experimental validations are still needed in order to increase confidence in the computational results and the modeling of a complex environment such as NIF. This is especially true when intending to validate the optimization package Gnowee/COEUS which implements MCNP as a radiation transport code. This section describes the improvements in the MCNP NIF TC modeling and their fidelity to corresponding experimental setups and gives justification for the models designed. The analysis begins with determining the level of geometric detail required for the full TC transport simulations and all the contribution here done to previously existing models. NIF is highly complex due to the effects of room return neutrons, rendering correct modeling crucially important. Therefore, this step of the Ph.D. work was of high importance for the design process in the present and future experiment setup at NIF and for the validation process of the Gnowee/COEUS software package.

This section describes the model fidelity calculations and justifies the models designed. The analysis begins with determining the level of geometric detail required for the full TC transport simulations. The discussion is followed by the description of the experimental section, of SNOUTs/HTOAD and ETA.

7.1.1 Full MCNP Model of NIF Target Chamber

In MCNP the user determines the appropriate details in order to achieve the desired accuracy and precision in the simulations result. One advantage of the Monte Carlo method, as previously discussed, is the fact that the simulation can model the true geometry and physics of the system. As mentioned in Chapter 4, the goal of this approach is to take advantage of COEUS v.2.0, where the ETA is optimized within the entire experimental facility to account for the contribution of any room-return effect on the optimization. Ignoring the wall's composition and the full DIMs structure may adversely impact the neutron scattering rates in the system. If the models used do not accurately capture the physical neutron flux, all other calculations will be incorrect; therefore, significant efforts have been undertaken to ensure simulations are as accurate as possible. Neutron scattering in different instruments inside the target chamber and in the chamber wall considerably shifts the neutron spectrum to lower energies.

This models fidelity, however, does come at a huge computational expense. As fidelity increases, utilizing more computational resources to perform the calculation is of greater importance. Thus, work has been performed to improve statistics and runtime of the model.

An initial version of the full model of NIF Facility TC has been inherited by the NIF modeling group in the LLNL Computational Engineering Division. The MCNP input file for the full 3D model of NIF TC is a complex file with thousands of lines written by several contributing authors, which increased its complexity and reduced its clarity. The MCNP

model has often been tailored to specific NIF campaign configurations. Thus, many elements that were present in Chapter 5 were not modeled previously. Time was spent to understand, improve and expand older NIF MCNP models to the shots performed here. Also, a goal is to make the complex input file a more user-friendly and efficient designing tool. Figure 7.1 presents a cross section view of the MCNP NIF TC, using the visualization software Moritz [111]. The elements external to the concrete TC walls have no impact on the results to this work as no collections of neutron particles is needed outside the walls for the presented experiments.

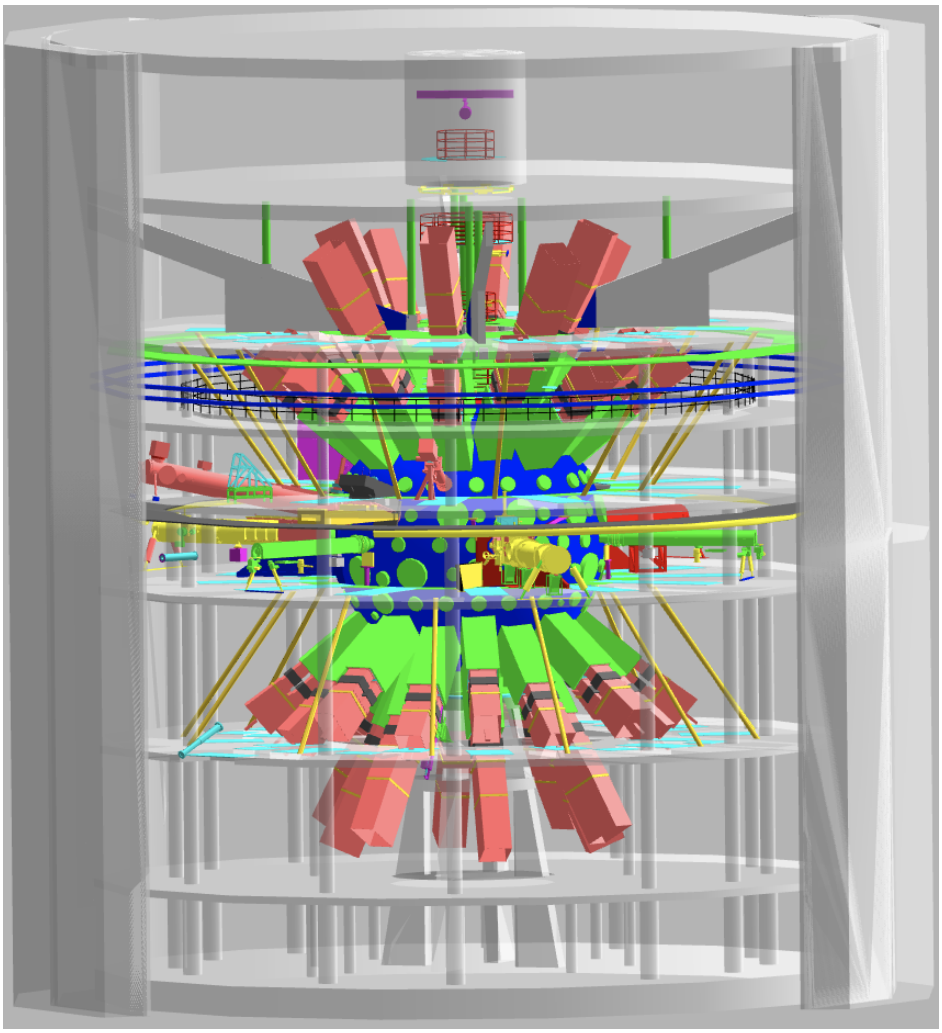

Figure 7.1: MCNP geometry of the NIF facility used as starting point to model the HTOAD and SNOUT campaigns. The geometry includes the target chamber sphere with all the ports and inserted manipulators.

The characteristics of the NIF TC represented in Figure 7.1 are summarized and categorized following an MCNP input structure file, thus starting with geometry materials, followed

by the source and tallies description, etc. The main characteristics of the NIF TC for all shot configurations are best summarized by describing the used geometry and materials, the neutron sources, tallies, and the variance reduction techniques.

7.1.2 Geometry and Material Modeling

The starting MCNP5 model of NIF included a limited number of internal elements needed for the shots, such as the CryoTARPOS, the equatorial DIMs 90-78 and 90-315, but lacked the other manipulators and elements described in Chapter 5. In Section 5.3.4, specifically in Figure 5.4, it is possible to see two elements missing in any previous modeling: the passive SNOUT element on the TANDM 90-348 and the ENP at 90-124. Thus, the need for adding and contributing to the NIF TC modeling by adding both manipulators was identified. The manipulator elements have been added as the SNOUTs, the HTOAD and all the neutron detectors used for the shots. Those components were available as CAD design by the NIF ELM-U system (pictures of the main components are collected in Appendix B). Those elements are described below.

The main TC geometry, including the TC walls, reflectors, CryoTARPOS, the DIMs and TANDM presence are constant for all of the shot configurations of this thesis. In order to facilitate the design procedure, a main file with the most common TC elements throughout the four campaigns is maintained as one file while the specific DIMS/SNOUTs/HTOAD for a shot are contained in a set of external files which are inserted in the main file by the calls created with a Python script. In order to simplify the MCNP input modifications for various design procedures, a NIF MCNP Input Generator has been developed to automatically generate MCNP readable files with minimum user interventions. It allows the users to define the shot configuration by choosing the DIMs/TANDM of interest and available experimental set-up (SNOUTs types/rags/HTOAD/Energetic Neutron Platform (ENP) platform etc.). More elements could be added in the future, but are outside of the scope of this thesis. The user calls or deletes with the Python script the elements of interest, which are then assigned to the main MCNP input file. The element needed is inserted by the code by providing to the TC input the cell, surface and correct transmutations information. The transmutation input provides the right coordinates and the adjustable angles and distances from the TCC. This also allows the users to only change few elements from a pre-made MCNP input file without dealing with a complex NIF TC input file. This is particularly useful for performing quick design optimizations with common available shots. Additionally, it is important to highlight that the newly improved MC model of the NIF TC runs on MCNP6 for all the simulations, indicated in the work also as MCNP.

- The TC is modeled as a set of concentric spheres with the first wall panels on the inside, followed by the chamber wall and gunite shield, which is a common used Los Alamos concrete material containing only fine particles. The model includes a 550 cm radius spherical target chamber consisting of a 10-cm thick aluminum (Al-5083) wall covered by 40 cm of shotcrete (concrete shielding), all concrete floors with openings

between the chamber and the target-bay wall to allow beams to be configured for both indirect (current mode), and direct drive operation, as featured in Figure 7.2.

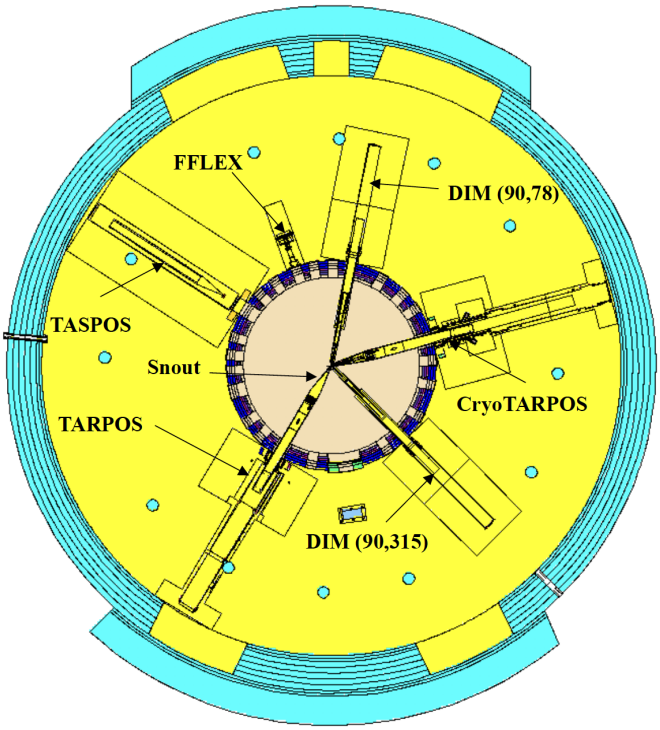

Figure 7.2: Cross-section view of the MCNP Model of the NIF spherical internal target chamber including the walls, the DIMS, TARPOS and CryoTARPOS inserted through the ports and the external walls of the NIF facility. The most internal environment is characterized by vacuum, while the yellow corresponds to air.

The concrete used for the NIF walls of the TC is estimated to be standard Los Alamos concrete composition [112] along with other material compositions used. The stainless steel 409 first wall panel assemblies are modeled in several layers with appropriate densities to preserve the total mass of the panels. The first wall panels extend from 4.63 m from Target Chamber Center (TCC) to the inner surface of the aluminum (Al-5083) chamber wall at 5 m from TCC. The effective thickness of the panels is equivalent to 1 cm of solid steel. The 10 cm-thick chamber is followed by 40 cm of gunite shield.

- The Cryogenic Target Positioner (CryoTARPOS) and the Target Positioner (TARPOS) are used to handle cryogenic and warm (room temperature) targets, respectively. The spherical coordinates for the CryoTARPOS are: θ=90° and ϕ=15°. The positioners are modeled in great detail as extended into the TC during a shot. This configuration is used to calculate the neutron flux spectrum experienced by all parts of

the positioners. Special attention is given to parts associated with the cryogenically-cooled payload since they will be exposed to the highest neutron flux during a shot and therefore can be expected to exhibit the highest post-shot residual activity. The majority of components in the two positioners are composed of either aluminum alloys (mainly Al-6061-T6) or different types of steel (*e.g.* SS-303, SS-304, A36, etc.), with some bronze and copper components being used in the cryogenic cooling system built into the CryoTARPOS payload package. Figure 7.3 gives the close-up overview of the CryoTARPOS inside the TC.

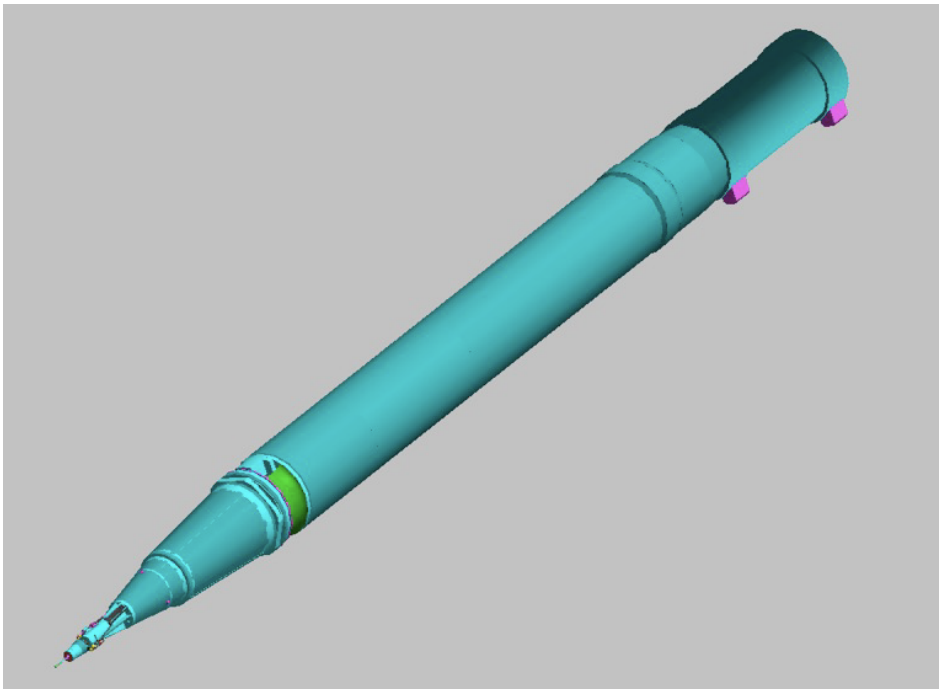

Figure 7.3: MCNP modeling of the CryoTARPOS inserted in the chamber.

- DIMs and a TANDM are used to hold experiments inside the NIF TC as seen in Chapter 5, and have been newly added and further expanded during this work. Such contribution will help for predicting doses, neutron fluxes and reaction rates in experiments including those manipulators. An example of their modeling is shown in Figure 7.4. Besides the two manipulators that included the experiments, a third DIM is present during the shots, the 90-24, with an ENP in the proximity of the TCC. Both the DIM 90-24 and the ENP models are missing in the initial MCNP version, and thus both have been newly modeled and introduced in the simulations due to the large effects the ENP has on neutron scattering at the TCC level. The position of the third DIM is θ=90° and ϕ=24° and can be seen in Figure 7.4.

  The main material characteristics for the DIMs and TANDM are summarized in Table 7.1.

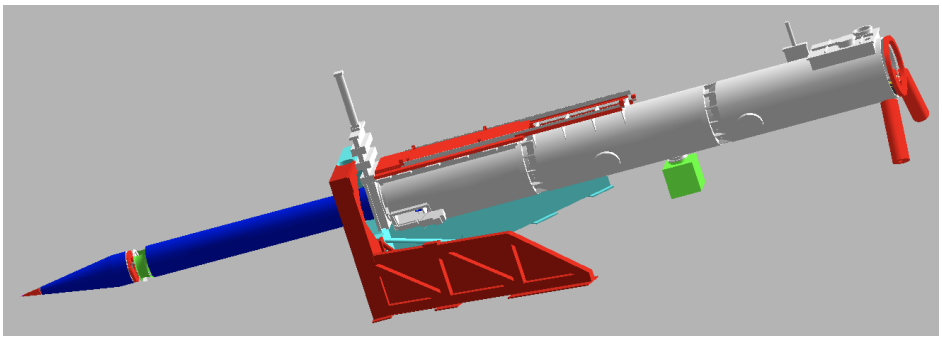

Figure 7.4: Example of the complexity of the MCNP model of the NIF DIMS, here TANDM 90-348.

Table 7.1: DIM and TANDM materials of interest.

Element	**Material**	**Density [g/cc]**
Covering materials	Al-6061 [Al 95.8-98.6% Cr 0.04-0.35% Si 0.4-0.8%, Mn max 0.15%, Zn max 0.25% Ti 0.15%, Mg 0.8-0.12%, Cu 0.15-0.4%]	2.7
Bolts	Stainless Steel 304 [C 6.08%, Si 1%, P 0.05%, S 0.03%, Cr 17-20%, Mn 2.0%, Fe 60%, Ni 8-13%]	7.84
Rags	Stainless Steel 303 [0.06%C , 0.05%S, 0.04% P, Mn0.35%, Fe 99.75%]	7.872

7.1.3 Source and Particles

Too often in experiment design, in order to accelerate the simulation timing or to simplify the design, as for the TN+PFNS ETA [6], the neutron source used for MCNP is a point mono-energetic Gaussian D-T neutron source of 14.1 MeV at (0,0,0) coordinate location. However, since the first comparison with the experimental data, such approximation has shown to be incorrect as scattering occurs at the TCC level, inside the target itself. The most adapted source applicable for most NIF shots is the Appelbe source approximation [113]. Appelbe uses relativistic kinematics to derive an expression for the energy spectrum of neutrons produced by fusion reactions in deuterium and deuterium tritium thermal plasma. The derivation does not require approximations and the obtained expression gives the exact shape of the spectrum. The high-energy tail of the neutron spectrum is shown to be highly sensitive to the plasma temperature. The changes in the spectrum are associated with different yields which are presented here for all campaigns.

In order to prove that the approximated Appelbe source is a good approximation of neutron flux spectra, the simulation results are compared with the neutron flux spectrum

measured using the NIF NTOF detectors [101]. An important factor in calculating the right neutron flux is the determination of the deuteron stopping power within the target, as this determines the energy of the deuteron as a function of depth as well as the total depth of implantation. The lower the stopping power, the further the implantation which increases the total reaction volume within the target and increases the predicted lower energy neutrons. Figure 7.5 shows the Appelbe and the measured flux spectrum from the Neutron Time Of Flight (NTOF) detectors [102]. These fluxes are very different from a monoenergetic 14.1 MeV neutron source.

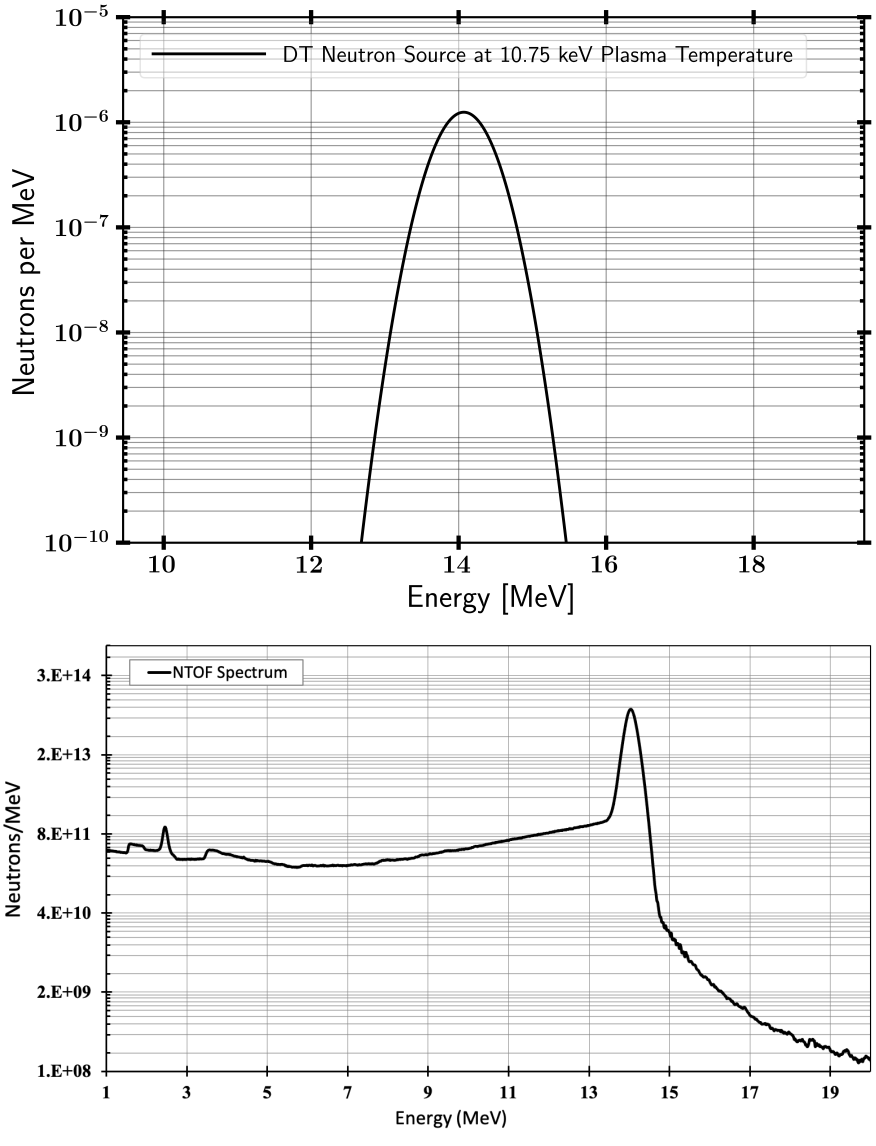

Figure 7.5: Neutron source spectra comparison between the a) Appelbe distribution and the b) NTOFs measured neutron flux from the detector.

As expected, Figure 7.5 shows how the measured flux from the NTOF has more thermalized neutrons then the one predicted by Appelbe. The Appelbe neutron flux is considered to be a good prediction for the initial design simulations and for when NTOF results are not available.

7.1.4 Tally/Detection System

Performing full NIF core simulations with all the SNOUTs, HTOAD and ETA characteristics and elements is complex and time intensive. It is efficient, then, to construct a 2-step process: first, the full 3D MCNP NIF TC simulation is run to generate the surface neutron sources around regions of interest, and second, the MCNP simulation is run only for the regions of interest with now known neutron surface sources. These auxiliary surfaces are built around the instruments of interest, and they play the role of surface neutron sources. These surface neutron sources are a more realistic representation of the neutron energies and spatial distributions inside the TC, *i.e.* the source includes the contribution from wall-returned neutrons. In this case the experiments are located in two different locations in the TC, at the extremes of DIM 90-78 and TANDM 90-348 and both are surrounded by cylindrical surfaces, and have a front and back surfaces. Step-1 records the neutrons crossing the surfaces by simulating the full NIF TC model. These surfaces permit collection of information of neutron energies from the front, back and side of the TC. The neutron recording is performed using surface tallies and the SSW or "Surface Source Write" card from MCNP. The MCNP run using the SSW card produces a file "wssa," which defines the three surface tallies as surface sources. Additional information needed for recording the surface fluxes are the surface crossing estimator F1 and the surface flux F2 tally; the surface direction using the option 0 or 1 for the cosine "C". The neutron flux information on the surface is given *per* cm^2, *per* area of the tracked surface. Then, step-2 uses those surfaces as sources for each the SNOUT, HTOAD and for designing future ETAs. This two step approach significantly reduces the simulations times.

7.1.5 Uncertainties and Variance Reduction for the Full Model

Running a full TC core simulation is computationally expensive and time-intensive, especially when improved statistics are needed at the level of the detector systems. As predicted, simulating a full NIF TC represents a huge problem due to the thousands of planes, macrobodies, foils, surfaces, and isotopes that must be tracked within a $\pm$ 1% statistics on reaction rates at the activation foils level. For a 3D simulation of the neutron flux at a point of interest in the TC, more than 9 million histories must be run to achieve good statistics, taking up to 168 hours to complete a full NIF calculations on a LBNL Savio using 8 threads. Assuming perfect speedup, about 1500 core processors are required to reduce the execution time to one hour for the full 3D NIF TC model. To further improve the statistics of the flux in the foils, the first tendency is to increase the number of histories or particles, which further increases the running time. Furthermore, determination of statistical uncertainty on

the final results is likewise difficult. Thus, there is a need for introducing variance reduction (VR) techniques.

Different VR techniques are used throughout the MCNP NIF TC model, for example at the level of the concrete walls geometry, where splitting is used as it is a largest section of heavy material. The SNOUTs, HTOAD and ETA use varying importance values throughout the cells of increasing importance inside of the detector system. Instead, the number of collisions in the SNOUTs or HTOAD is increased at the region closest to the activation foils or CVD diamond by increasing cell importance. The farther the TC elements are from the detectors of interest, the lower their importance will be. This allows for the simulation to focus and track particles that are going in the preferred direction, eliminating particles that travel into regions that in the end will likely not contribute to the results.

7.1.6 Importance of An Accurate Full 3-D MC Model of NIF TC

The model inaccuracies in the simulation deck are the first source of error to consider and possibly eliminate. To do so, it is important to optimize the full MCNP engineering design by including parts that are the most relevant to a neutron transport simulation as the neutron source, detector used, and precise material composition. As an example, to assess the source uncertainties, the comparison of the predicted neutron flux and the measured one is performed at the level of the pinhole for well-known reaction in Zr or Au foils, which are often used as reference at NIF. At the pinhole level, the effect of the source neutron flux is predominant, and less backscattering is perceived than on the rest of the foil locations. In addition, the effects of the other experiments inserted in the TC, such as ENP, can be observed due to their proximity and effects to the TCC and the source. Next, to understand the effect of neutron thermalization due to the room-return effects, the analysis in Section 7.3 is focused on the activation foils with lower energy threshold at the basket and kinematic base level.

Figure 7.6 and Figure 7.7 show the effect of the background of scattered neutrons at the TCC level and the fluxes for each energy ranges of the neutron scattering in the chamber. In the next section, the effects of the room return are showed by comparing the simulation results with and without the densities of all the NIF TC elements.

It is possible to see in Figure 7.6 how the TC elements affect the overall neutron flux, from 10% to more than 20%, for neutrons at energy level below 5 MeV.

Figure 7.7 shows also the effect of the scattered neutrons (and gamma) from the chamber wall into the source itself, and the large difference in results it yields in the lower energy range. Thus, it is important to make sure that the room-return effects are correctly handled by not introducing systematic errors due to incorrect material location or characteristics, which could influence the results. The closer the material is positioned to the system flux monitor, the greater effect this will have on the results.

As mentioned in the tally paragraph, the standard modeling in this work is performed in two steps: (1) the simulation is performed for the full NIF TC inserting a set of three surfaces (the front, back and cylindrical surface) around the SNOUTs and HTOAD elements,

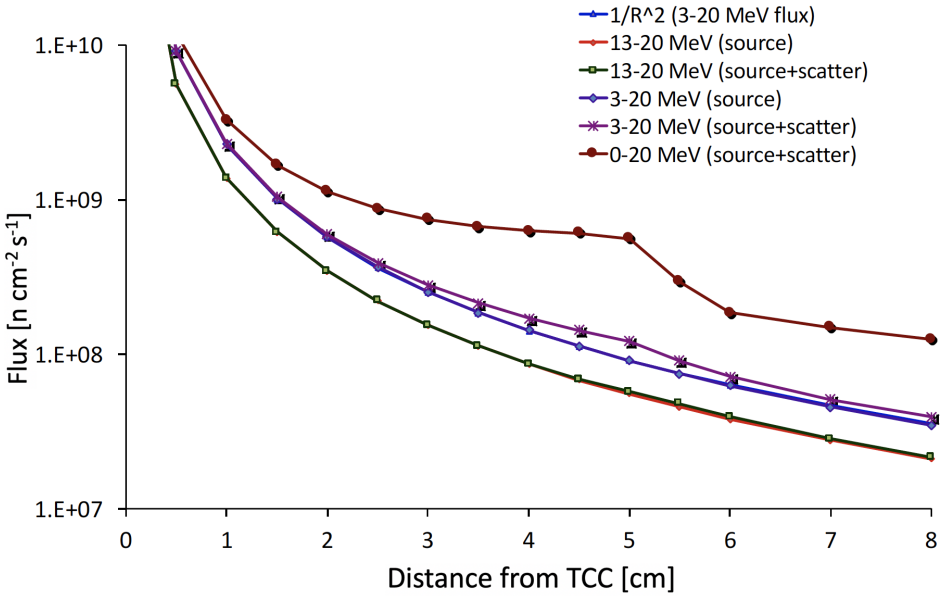

Figure 7.6: Scattered and source neutron fluxes at different distances from TCC for several energy ranges.

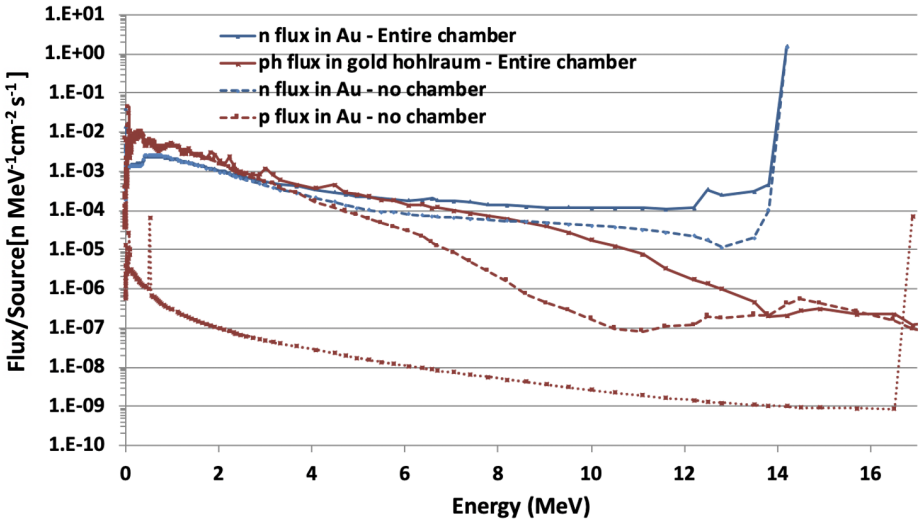

Figure 7.7: Simulated neutron and gamma fluxes inside the gold hohlraum with and without the full NIF chamber.

creating a SSW file; (2) the SSW file is used to simulate surface sources for the modeling of regions of interest inside TC. In order to ascertain the quality of the methodology, the comparison between the averaged flux in the middle foil stack at the basket for the SNOUT (shot S1) is shown in Figure 7.8.

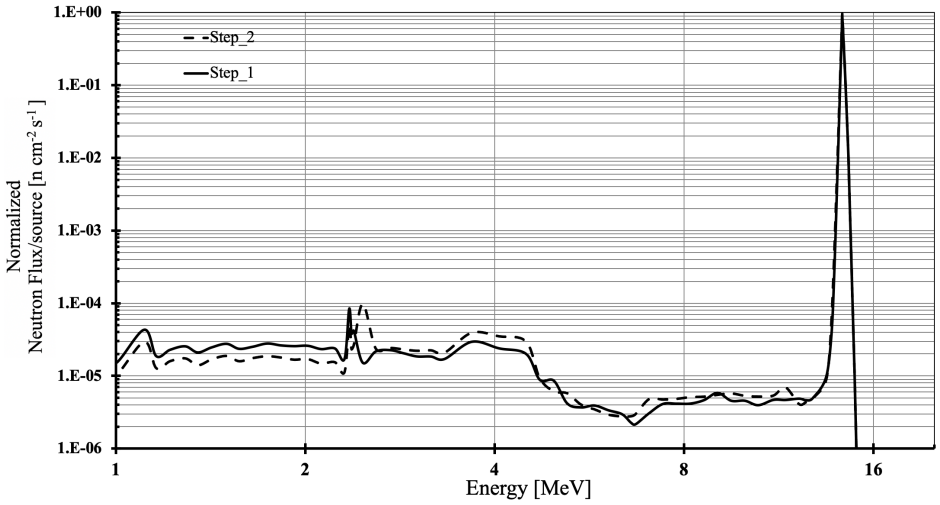

Figure 7.8: Neutron source spectra comparison between 1 and 2 step modeling for the foil stack in the basket.

Figure 7.8 shows a slight softening of the neutron spectrum in the 1-step process representing 5% of the total number of neutrons. Neutrons that backscatter off the delimiter back into the cylindrical area or across the tally surface are not counted due to the breakup of the simulation into two stages. The effects are compensated before and after the 2.5 MeV peak and the variation of the spectrum overall does not change above 1%. Overall, the distributions were close, which indicates that the two-step method did not introduce large uncertainties.

7.2 Experiment Modeling: SNOUT/HTOAD

The main focus of the validation experiments and future ETA experiments is the design of specific instrumentation that supports the experiments described in Chapter 5: the SNOUT located on the TANDM 90-348 and the HTOAD located on the RAGS on the SNOUT 90-78. Effort is invested on properly modeling those two new instruments, which was not available previously. This addition significantly improved the full 3D MCNP model of NIF TC, and will simplified the design modeling of future experiments.

7.2.1 Geometry and Material

The first elements of interest are the SNOUTs. Figure 7.9 a) represents the SNOUT used as support for the HTOAD in the H1 to H3 shots, while Figure 7.9 b) represents the SNOUT used in the S1 to S4 experiments. Proper modeling of the masses and densities is crucial, as any error introduced has a large effect on the final results. Figure 7.10 shows a close up of the HTOAD located on the RAGS of the SNOUT in b).

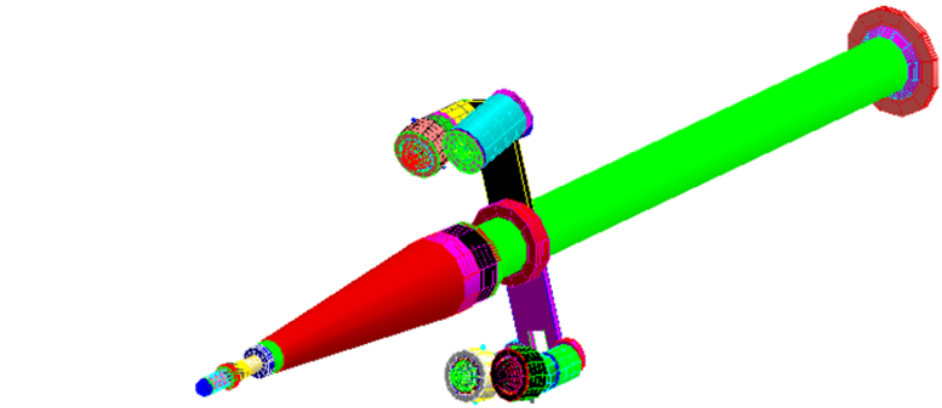

[a]

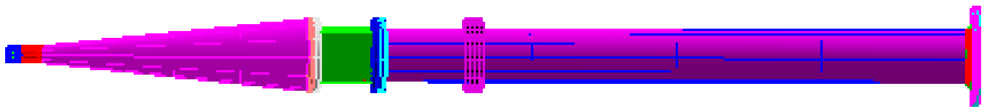

[b]

Figure 7.9: 3D Moritz display of the MCNP modeling of: a) the SNOUT used on DIM 90-78 with the SRC including the HTOAD; b) the SNOUT used on TANDM 90-348.

For such close-up modeling, it is important to determine and properly design the bolts, as these constitute dense materials near the point of flux measurement, and are made of materials denser that the activation foils. The other objects and materials of interest are the foils themselves and the material inserted inside the HTOAD and SNOUT for study. The main materials are summarized in Table 7.2.

It is possible to predict that the simulation results will predominantly be affected by the correct composition and density of the materials above listed and specifically their nuclear data cross sections. The goal of the experiments is to isolate and consider at the end only the uncertainties from the nuclear data.

7.2.2 Source and Particles

The main neutron source used for all the MC runs is the same as described in Section 7.1.1. The 2-step methodology is used for the HTOAD and SNOUT simulations, where the neutron source information are generated at step 1 by simulating the whole TC. The neutron

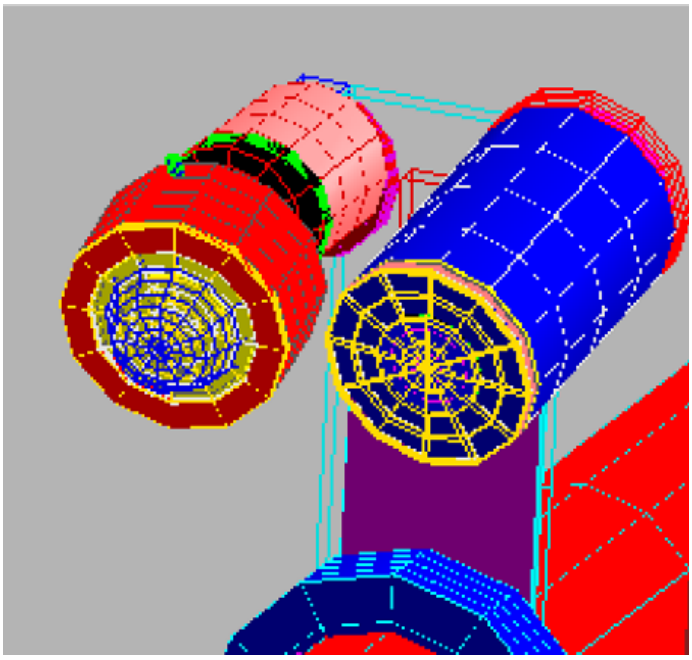

Figure 7.10: 3D Moritz display of the MCNP modeling of upper side of the RAGS, where the blue cylinder represents the HTOAD external view.

Table 7.2: SNOUTs and HTOAD's elements with respective density and composition.

Element	**Material**	**Density [g/cc]**
Material Insert in the HTOAD	High density Polyethylene (HDPE) [C at 9.5%]	0.9
SNOUT	Al-T6061	2.7
Foil Stack	Ta [90%, W10%]	16.6
	In	7.31
	Au	19.3
	Ni	8.9
	Zn	7.1
	Zr	6.5
	Ti	4.5
	Al	2.7

crossing the surfaces are recorded in a "wssa" file, with the SSW (Surface Source Write) card available inside MCNP. At step 2, the neutron source is read from the "wssa" file using the SSR card (Surface Source Read) [54], which sends source neutrons from the defined surfaces around the HTOAD and SNOUT inward. The SSR file reads in the formatted file "wssa"

that contains all of the particle histories that cross defined surfaces. The surfaces source probability distribution functions generated from the MCNP SSW card will also be used for the SCALE model [20].

7.2.3 Tally/Detection System

For the simulation focusing on the HTOAD and the SNOUTs, it is important to record the neutron (flux information) and define data (energy, etc.) at the detectors level or in specific location of interest. In order to perform the validation analysis, it is necessary to tally the neutron flux and to extract the reaction rates in the activation foils as well as the neutron flux in the CVD detector. The measured quantity here is the neutron flux expressed per source neutrons and per unit energy (MeV), specifically using the MCNP **F4** tally. The **F4** tally records the average neutron flux in a cell, in units of neutrons/cm^2, *e.g.* the cell can be the activation foils or around the SNOUT and HTOAD walls. F4 accounts for the volume of the cell, where the flux is collected and the neutron scattering effects are recorded. In order to extract the reaction rates, a flux estimators times a cross section is used by introducing the FM card. With the FM card the user assigns the correct microscopic cross section per flux estimator for each of the foils in order to have the correct reaction rates for the energy groups of interest. An example of FM card for the ^{90}Zr(n,2n)^{89}Zr is **FM4 (-0.5145 716 16)** where **4** is referred to the corresponding tally **F4**, **-0.5145** is the atomic density of the material **m716** (^{90}Zr) and **16** is the MT number, which corresponds to the (n,2n) reaction. The FM card provide the reaction rate as **(neutron flux from F4)* (atom density of material) * (σ)**. Examples of MT number and relevant reaction types used are summarized in Table 7.3, the resulting reactions rate are given in units of reactions/cm^3 per source neutrons.

Table 7.3: Reaction Type and the MT number, for the FM card of MCNP.

Reaction	**MT**
(n,2n)	16
(n,n')	51
(n,γ)	102
(n,p)	103
(n,np)	28

The tallies also provide information on number of collisions, absorption, energy deposition, boundary crossings.

Even though time didn't allow for inserting a CVD diamond detector during a shot, the detector has still been modeled as a diamond cell. The cell of interest is tallied using the pulse tally **F8** in order to calculate the energy deposition in the detector crystal. The standard **F8** tally is a pulse-height tally and the energy bins are no longer the energies of scoring events, but rather the energy balance of all events in a history. It is important to point out that the **F8** tally fails in accounting correctly the neutron-photon coupled calculations, as MCNP

does not include nuclear level decay schemes. Keeping this in mind, the focus of this work is exclusively on the neutron flux, and thus this choice is satisfactory.

7.2.4 Uncertainties and Variance Reduction for the Full Model

In terms of reducing statistical uncertainties, the VR technique used in this step for the 2-step modeling is the hybrid methodology of coupling MCNP with ADVANTG. ADVANTG is compatible with all MCNP features and can handle one or more cell tallies (**F4, F6, F8**), surface tallies (**F1** and **F2**), point-detector tallies (**F5**), and Cartesian mesh tallies (FMESH). ADVANTG modeling requires the meshing of the system geometry, the meshes becoming more frequent and cells smaller closer to the detector foils. MCNP is then provided with the weight window map, also full unbiased simulations should be done to compare with the ones using ADVANTG. The tallies of interest for our ADVANTG modeling is **F4** for the activation foils and **F8** for the CVD diamond detector. The size of the geometrical meshing decreases linearly when getting closer to the activation foils and diamond detector.

It is important for modeling uncertainties to consider the effect of the masses and correct location of the instrumentation, as adjustments are often needed after the shots,. In order to understand the effect of properly modeling the SNOUT and HTOAD, an analysis is performed by introducing and removing the material densities in the SNOUTs and HTOAD and compare for each case the neutron fluxes in the activation foils. Thus, the simulations performed are with:

- all cells at zero density;
- the measurement sample cells at real density, everything else in the universe at zero density;
- everything in the universe at real density.

Table 7.4 presents the comparison of the above three cases in terms of produced nuclides from the reaction rates in the foils located in the SNOUT, for shot S1, and at all three locations.

The largest changes come from the presence of scattering along elements on the two SNOUTs, less so from the density of the foils itself.

Besides validation, verification is an important step in the approach, and is performed between two MC codes. The verification is needed as SCALE is used together with MCNP in order to represent the cross sections uncertainties propagation in the ETAs. Table 7.5 presents examples of relative differences in the comparison of reaction rates in the foils reactions, running the same model of empty SNOUT (S1 shot) in SCALE and MCNP.

From Table 7.5 it is possible to see the MCNP and SCALE results for this test case do not match completely, but the relative errors fit with the verification seen in previous studies [114]. The supported theory of discrepancies between SCALE and MCNP comes from the

Table 7.4: Nuclides produced for three density cases in the reference SNOUT S1 case.

Stack location	Nuclide produced	No dens.	Partial dens.	Full dens.
kinematic	^{196g}Au	3.20E-08	2.42E-08	2.24E-08
	^{198}Au	1.61E-08	5.42E-10	2.92E-10
	^{115m}In	2.44E-09	4.17E-11	2.25E-11
	^{116m}In	1.88E-08	6.68E-11	6.06E-11
	^{89}Zr	9.92E-09	1.12E-08	9.89E-09
basket	^{196g}Au	2.10E-07	2.06E-07	2.02E-07
	^{198}Au	1.93E-08	7.61E-10	6.00E-10
	^{115m}In	1.40E-08	1.71E-10	1.68E-10
	^{116m}In	5.11E-08	2.44E-08	1.84E-08
	^{89}Zr	7.36E-08	7.42E-08	7.35E-08
pinhole	^{196g}Au	9.81E-06	9.74E-06	9.73E-06
	^{198}Au	6.54E-08	2.41E-08	2.41E-08
	^{115m}In	6.57E-07	5.35E-07	5.34E-07
	^{116m}In	1.64E-07	8.42E-08	7.49E-08
	^{89}Zr	3.03E-06	3.05E-06	3.02E-06

fact that just SCALE considers the propagation of uncertainties. The last uncertainties that will be of focus in the thesis, in Section 7.3 is the one from the nuclear data.

7.3 Measurements and Comparison

The primary objective of this section is the validation and verification of the simulation results by comparing them with the experimental measurements described in Chapter 5 and 6.

The first measurement of interest is the neutron yield in 4π for each of the shots. As presented in Chapter 5, the target capsule frequently changes between shots, as the capsules can be coated and the size can change, which can modify the final neutron yield. Furthermore, it is important to know the correct yield in order to have the final absolute values of foils activity. The yields for the shots are summarized in Table 7.6.

7.3.1 Measurements and Comparison of Three HTOAD Campaigns

The measurements in the three HTOAD campaigns are performed at the location of each of the 4 neutron activation foil stacks. The HTOAD campaigns include: one empty HTOAD

Table 7.5: Comparison of the nuclides produced in the three foils packs (SNOUT S1) using MCNP and SCALE.

Stack location	Nuclide produced	MCNP	SCALE Sampler 252-Group	Percent change rel. to MCNP
kinematic	^{89}Zr	9.92E-09 ± 0.13%	2.28E-08 ± 4.8%	1.8
	^{196g}Au	3.20E-08 ± 0.13%	2.86E-10 ± 2.6%	-1.8
	^{198}Au	1.61E-08 ± 0.08%	2.27E-11 ± 2.3%	1.2
	^{115m}In	2.44E-09 ± 0.13%	6.02E-11 ± 3.4%	-0.6
	^{116m}In	1.88E-08 ± 0.08%	1.08E-08 ± 4.7%	9.5
basket	^{89}Zr	9.92E-09 ± 0.05%	2.04E-07 ± 4.8%	1.0
	^{196g}Au	2.10E-07 ± 0.05%	5.93E-10 ± 2.6%	-1.2
	^{198}Au	1.93E-08 ± 0.12%	1.69E-10 ± 2.3%	1.0
	^{115m}In	1.40E-08 ± 0.10%	1.83E-08 ± 3.4%	-0.3
	^{116m}In	5.11E-08 ± 0.10%	7.95E-08 ± 4.7%	8.2
pinhole	^{89}Zr	7.36E-08 ± 0.06%	9.81E-06 ± 4.8%	0.8
	^{196g}Au	9.81E-06 ± 0.13%	2.39E-08 ± 2.6%	-1.0
	^{198}Au	6.54E-08 ± 0.08%	5.39E-07 ± 2.3%	0.9
	^{115m}In	6.57E-07 ± 0.05%	7.48E-08 ± 3.4%	-0.2
	^{116m}In	1.64E-07 ± 0.05%	3.21E-06 ± 4.7%	6.2

Table 7.6: Neutron yield from Zirconium foils exposed to the unmodified spectrum for H1.

Shot	Shot Number	D-T neutron yield
H1	N170831-002	4.25×10^{15}
S1, H2	N180311-002	3.73×10^{15}
S2, H3	N180715-002	3.88×10^{15}
S3	N180722-001	3.88×10^{15}
S4	N181014-001	3.56×10^{15}

campaign and two campaigns with the inserted materials of interest, high density polyethylene (HDPE) and stainless steel (SS). The selection of these materials comes from their frequent use in most ETA designs, as HDPE softens the neutron spectra and SS is used as coating for many NIF instrumentation. The first shot performed, N170311-002, utilizes an HTOAD filled with the HDPE material, which together with the SS campaign, will be compared to the empty HTOAD case. For understanding the influence on the flux and reaction rates of the inserted material, the empty HTOAD is used as a reference. The latter provides information on the effects of scattered neutrons and on the possible experimental and modeling errors, without including the extra material complexity. Also, a comparison will be

performed for foils between the empty HTOAD and the empty SNOUT experiment. Such comparison will provide the different effects of room return in two different locations inside the TC, attesting also the asymmetry in scattering inside the TC where different locations record neutrons with different energy ranges.

In Figure 7.12 the two graphs a) and b) present the normalized measurements of the activation products in each of the foils inside the HTOAD experiment filled with with HDPE (Figure 5.11).

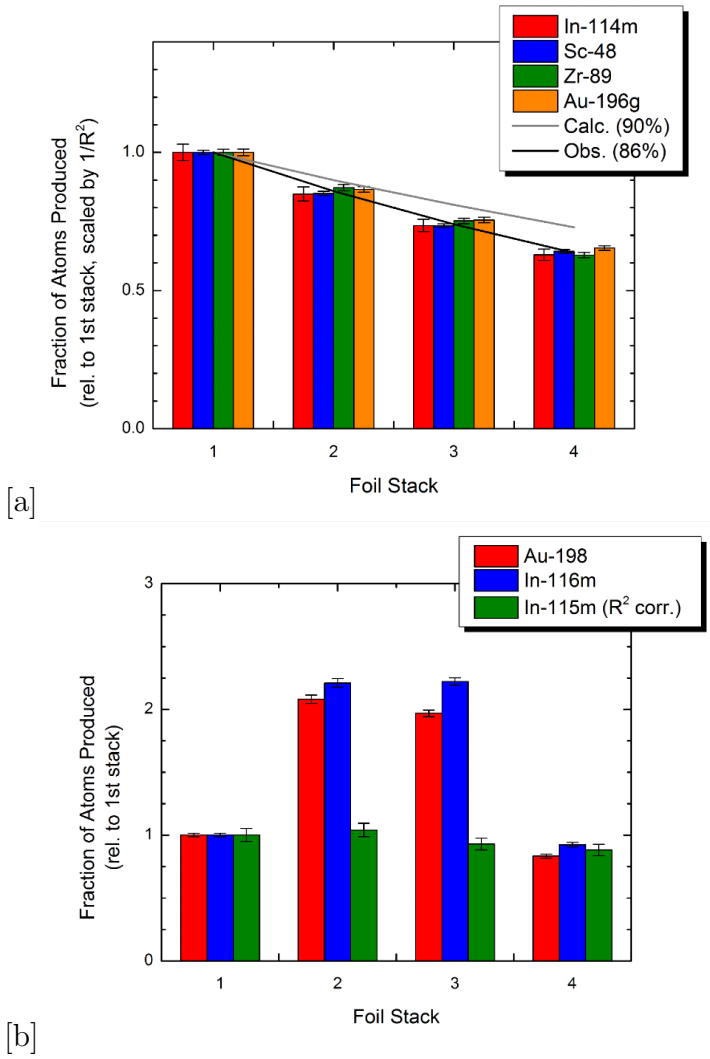

Figure 7.11: Radionuclides produced in the foil stack for the HTOAD with HDPE inserted from a) by 14.1 MeV neutrons ; b) by low energy neutrons.

Figure 7.11 underlines the decrease in the 14.1 MeV predominant radionuclide production from stack 1 to stack 4, caused by the softening of the neutron spectra through the HDPE material. The scattering cross sections at 14.1 MeV for the HDPE can be used to account

for the decrease in the activation products, as almost 86% of the 14.1 MeV neutrons are transmitted through the HDPE per stack level. The observed percentage of transmitted neutrons is slightly lower than the predicted one presented in [115] and shown here in Figure 7.12, which presents HDPE transmission versus material thickness.

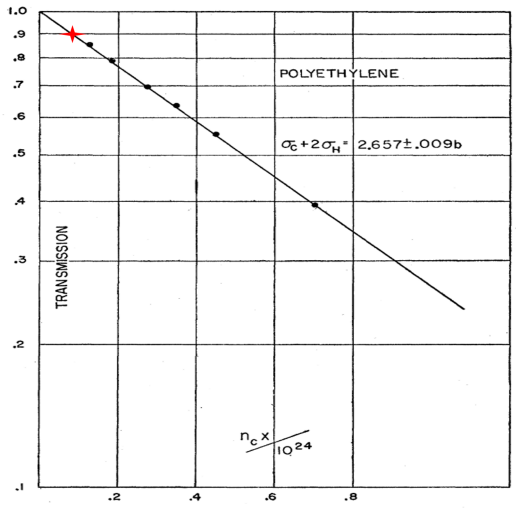

FIG. 3. Polyethylene transmission *vs* scatterer thickness in units of number of carbon atoms/cm².

Figure 7.12: Total Cross Sections for for polyethylene for 14.1 MeV Neutrons [115].

The products of capture reactions and to some degree of the (n,n') reaction products in the 2-10 MeV range, are enhanced in the center of the HTOAD and visible in the production of ^{196}Au and ^{116m}In, especially.

Figures 7.13 a) and b) present the normalized fraction of produced atoms measured in each of the foils for the empty HTOAD case. In Figure 7.13 a) a predominance of the (n,2n), (n,p) and (n,α) reaction channels with the interaction of neutrons at 14.1 MeV is shown. The nuclides produced are: ^{114m}In, ^{48}Sc, ^{89}Zr and ^{196g}Au and their production is consistent with $1/R^2$, where R indicates the radius distance from TCC. Figure 7.14 b) shows the behavior of the low-energy neutrons by reporting the production of ^{198}Au, ^{116m}In and ^{115m}In. The behavior of the same radionuclides production is relatively consistent throughout the empty HTOAD with some minor effects from local scatter at the front and back foils versus the middle foil stacks.

Furthermore, Table 7.7 presents the comparison between the two cases by showing the investigation of the different ^{198}Au/^{196g}Au ratio. While the ^{197}Au(n,γ)^{198}Au reaction has a metastable state, the contribution to the observed decays from metastable state feeding of the ground state during the counting period was negligible. The gold ratio used without HDPE is usually 0.1, which is relatively constant from shot to shot, ranging from 0.08-0.12.

The gold ratio is often used as a standard value to understand the presence of low energy neutrons. The proximity of the golden foils to the HDPE sees the increase of the ratio

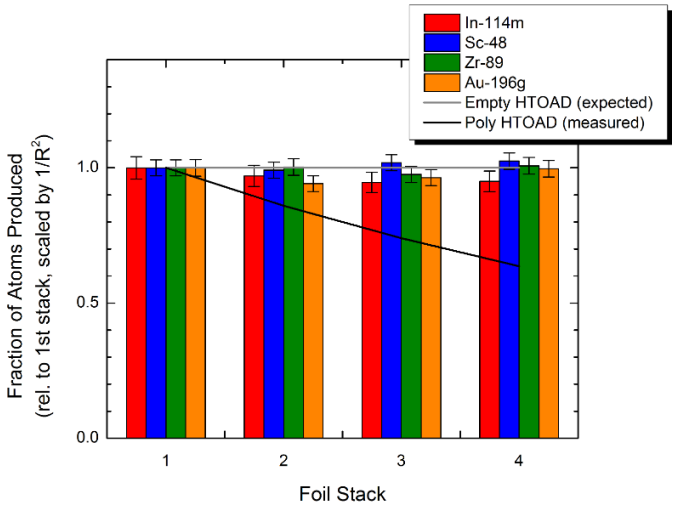

[a]

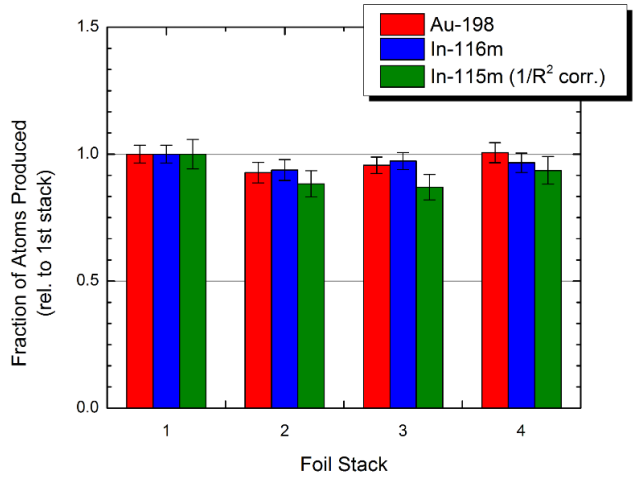

[b]

Figure 7.13: Radionuclides produced in the foil stack for the empty HTOAD case from a) by 14.1 MeV neutrons ; b) by low energy neutrons.

Table 7.7: Observed ^{198}Au/^{196g}Au ratios in the foils inside the empty and HDPE HTOAD.

Foil stack	**Empty**	**HDPE**
1	0.119	0.53
2	0.129	1.38
3	0.138	1.58
4	0.147	0.84

through (n,γ), where the effects of the HDPE on the down-scattered lower-energy neutrons is severe. The interplay of lower-energy neutrons with the HDPE is complicated.

In the absence of HDPE, the ^{198}Au production should be the same in each foil, while ^{196g}Au production falls off with R^2. Room-return neutrons flood the center of the NIF chamber with the same intensity, roughly independent of location and increase the ^{198}Au production rate for the last foil stack in the empty HTOAD. The HTOAD can contain enough HDPE to affect the incident neutron spectrum but not significantly. Activation of ^{89}Zr and ^{196g}Au caused by 14.1 MeV neutrons falls off more quickly than expected from $1/R^2$ behavior.

Figure 7.14 presents the radionuclide production for the third HTOAD experiments using SS.

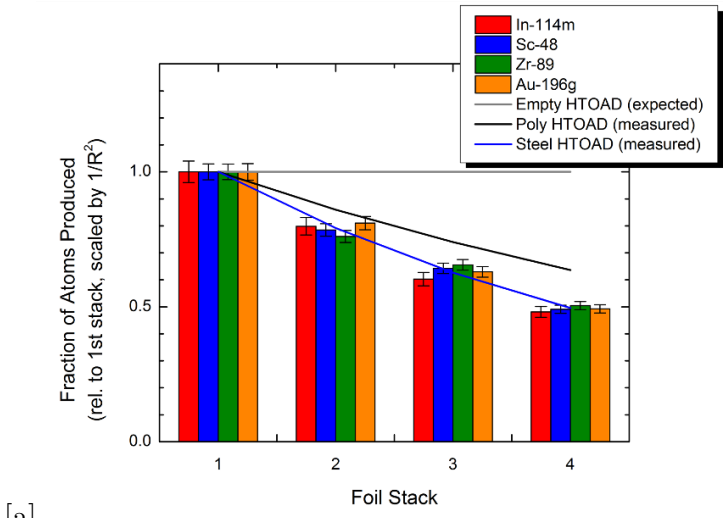

[a]

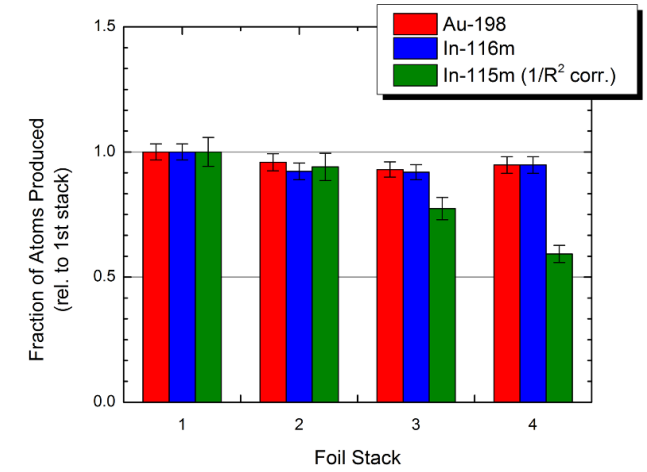

[b]

Figure 7.14: Radionuclides produced in the foil stack for the HTOAD with stainless steel inserted from a) by 14.1 MeV neutrons ; b) by low energy neutrons.

In the SS the (n,γ) reaction predominantly dominates in the high energy range, but its

effects are not seen below thermal energies.

The measurements and the simulations are compared by analyzing the integral activation reaction products with given information on the statistical uncertainty from the MCNP values, the measurement uncertainties and the relative difference between the measurements and the computed results. Table 7.8 presents the comparison of the HDPE-fill HTOAD case, Table 7.9 for the empty case and Table 7.10 for the SS case. The counting of ^{48}Ca nuclides in the Ti foils counted in the first experiment resulted in bad statistics and consequently it is not considered for the other two tables.

Table 7.8: Comparison of the nuclide produced in the foils exposed to the unmodified 14.1 MeV D-T source spectrum for the HDPE filled HTOAD.

Foil pack	**Nuclide type**	**MCNP nuclides produced**	**% change rel. to observed**
Pack 1	^{89}Zr	8.35E+07 ± 2.8%	0.3
	^{116m}In	3.30E+07 ± 5.7%	5.1
	^{115m}In	6.37E+07 ± 3.2%	4.2
	^{196g}Au	4.30E+07 ± 4.1%	0.2
	^{198}Au	5.98E+07 ± 2.8%	0.1
	^{48}Sc	1.75E+07 ± 2.9%	2.8
Pack 2	^{89}Zr	4.37E+07 ± 2.9%	1.3
	^{116m}In	3.11E+07 ± 5.7%	5.3
	^{115m}In	6.32E+07 ± 3.5%	4.8
	^{196g}Au	4.84E+08 ± 3.1%	1.8
	^{198}Au	6.17E+07 ± 2.8%	1.3
	^{48}Sc	1.37E+07 ± 2.9%	2.8
Pack 3	^{89}Zr	3.76E+07 ± 2.9%	1.3
	^{116m}In	2.56E+07 ± 5.7%	5.0
	^{115m}In	6.75E+07 ± 3.2%	4.2
	^{196g}Au	3.76E+08 ± 3.0%	1.4
	^{198}Au	6.42E+07 ± 2.8%	1.8
	^{48}Sc	1.12E+07 ± 3.0%	3.1
Pack 4	^{89}Zr	2.90E+07 ± 3.7%	2.7
	^{116m}In	1.96E+07 ± 5.7%	5.8
	^{115m}In	7.43E+07 ± 3.4%	6.2
	^{196g}Au	2.94E+08 ± 3.1%	1.1
	^{198}Au	6.99E+07 ± 2.8%	2.0
	^{48}Sc	8.58E+06 ± 3.0%	3

Table 7.9: Comparison of nuclide produced from foils exposed to the unmodified 14.1 MeV D-T source spectrum for the empty HTOAD.

Foil pack	**Nuclide type**	**MCNP nuclides produced**	% **change rel. to observed**
	^{89}Zr	1.77E+07 ± 3.0%	0.1
	^{116m}In	5.16E+07 ± 3.5%	1.7
	^{115m}In	1.88E+07 ± 5.8%	2.2
Pack 1	^{196g}Au	5.66E+08 ± 3.1%	-3.3
	^{198}Au	5.28E+07 ± 2.9%	0.8
	^{48}Sc	1.64E+07 ± 2.9%	2.8
	^{89}Zr	1.78E+07 ± 3.1%	3.3
	^{116m}In	5.16E+07 ± 4.3%	4.1
	^{115m}In	1.66E+07 ± 5.8%	4.8
Pack 2	^{196g}Au	5.33E+08 ± 3.1%	4
	^{198}Au	5.22E+07 ± 2.9%	1.1
	^{48}Sc	1.63E+07 ± 3.0%	2.8
	^{89}Zr	1.73E+07 ± 3.0%	3.3
	^{116m}In	5.75E+07 ± 3.4%	4.5
	^{115m}In	1.63E+07 ± 5.7%	5.2
Pack 3	^{196g}Au	5.45E+08 ± 3.1%	3.8
	^{198}Au	5.78E+07 ± 2.9%	1.8
	^{48}Sc	1.67E+07 ± 2.9%	3.1
	^{89}Zr	1.79E+07 ± 3.0%	0.6
	^{116m}In	6.09E+07 ± 3.9%	3.1
	^{115m}In	1.76E+07 ± 5.8%	1.3
Pack 4	^{196g}Au	5.64E+08 ± 3.1%	4.1
	^{198}Au	6.49E+07 ± 2.9%	2.8
	^{48}Sc	1.68E+07 ± 3.0%	3.4

The analysis here is set at different levels: to assess the abilities to model the NIF TC using the comparison with the empty HTOAD level; to gain information on the analysis of the neutron flux through the materials of interest (HDPE and SS) to see how effectively each material can be used to modify the neutron spectra inside the HTOAD; and to assess the type of foils stack needed to unfold the entire neutron spectra. Both materials have been of high interest for the ETA, for the HDPE for its ability to soften the neutron spectra, and for the SS as an ideal material for coating the ETAs in an environment as harsh as NIF. From the comparison of the empty HTOAD, seen in Table 7.10, the majority of the reactions in

Table 7.10: Comparison of the nuclides produced from foils exposed to the unmodified 14.1 MeV D-T source spectrum for the SS-filled HTOAD.

Foil pack	**Nuclide type**	**MCNP nuclides produced**	**% change rel. to observed**
Pack 1	^{89}Zr	5.74E+07 ± 2.9%	0.3
	^{116m}In	6.37E+07 ± 3.2%	4.8
	^{115m}In	3.30E+07 ± 5.8%	5.2
	^{196g}Au	5.97E+08 ± 3.1%	-0.2
	^{198}Au	5.98E+07 ± 2.9%	0.1
	^{48}Sc	1.75E+07 ± 2.9%	2.8
Pack 2	^{89}Zr	4.37E+07 ± 2.9%	3.3
	^{116m}In	6.32E+07 ± 3.5%	5.1
	^{115m}In	3.11E+07 ± 5.7%	4.8
	^{196g}Au	4.84E+08 ± 3.1%	-1.8
	^{198}Au	6.17E+07 ± 2.9%	1.5
	^{48}Sc	1.37E+07 ± 2.9%	3.2
Pack 3	^{89}Zr	3.76E+07 ± 2.9%	3.3
	^{116m}In	6.75E+07 ± 3.2%	4.5
	^{115m}In	2.56E+07 ± 5.8%	5.2
	^{196g}Au	3.76E+08 ± 3.1%	-1.4
	^{198}Au	6.42E+07 ± 2.8%	1.8
	^{48}Sc	1.12E+07 ± 3.0%	4.1
Pack 4	^{89}Zr	2.90E+07 ± 3.1%	3.2
	^{116m}In	7.43E+07 ± 3.5%	-7.8
	^{115m}In	1.96E+07 ± 5.8%	5.2
	^{196g}Au	2.94E+08 ± 3.1%	-4.1
	^{198}Au	6.99E+07 ± 2.8%	1.0
	^{48}Sc	8.58E+06 ± 3.0%	6.2

the foils match the simulated results.

However, problems are encountered at the foils where there is isomer isotope production following elastic and inelastic scattering.

It is important to mention that the comparisons that are by default performed with ENDF/B-VIII were improved by almost 10% by using the IRDFF v1.50 library instead. The ENDF/B-VIII library is mainly used for the NIF simulations and it presents the largest errors as the metastable isomer states are not accounted for [32]. The Indium reaction rates for the production of ^{115m}In and ^{116m}In and the ^{196g}Au, for example, are larger in the HDPE

case as more neutrons reach thermal ranges. With less thermalization, iron still presents the largest uncertainties especially for the gold (n,2n) reaction.

SS is composed of several elements, primarily ^{56}Fe and ^{54}Fe, for which improved inelastic scattering cross sections are needed over a wide range of neutron energies to provide data where none-to-little exists and to meet targeted-accuracy application-driven uncertainty margins, which might effect the comparison of the measurements with the simulated results [40].

There are large discrepancies of above 5% between the evaluated data libraries and the experimental information, which goes beyond the magnitude of measurement errors. Further differences are seen in the (n,γ) reactions where the initial source term is not well-defined. In both HDPE and iron, the largest differences are in the epithermal region where the (n, γ) reactions are the most sensitive to small changes in the overall flux.

7.3.2 Comparison of Measurement Results for Four SNOUT Campaigns

Three sets of foil irradiation measurements are performed during the SNOUT campaigns: (1) pinhole foils with direct exposure to the D-T neutron source; (2) foils at the basket; (3) foils placed in the kinematic base, in order to evaluate the neutron scattering in the DIM and the room return effects. The evaluation at all three locations is important even for future ETAs where the foils in the kinematic base will record the neutron changes in the tailored spectrum. The direct exposure foils are used to obtain an unfolded neutron spectrum that is used as the starting source spectrum in subsequent MCNP models to predict experimental performances. One of the goals is to determine how the neutron flux possibly changes at different locations inside the TC, thus the interest in comparing the results of the SNOUT with the HTOAD located in different points of the TC surface. The SNOUT experiments defined as reference cases, as for the HTOAD, are the empty SNOUTs and the analysis is performed afterwards with an inserted material of interest.

There are four campaigns of SNOUTs. The first two, S1 and S2, use an empty SNOUT with two different foils sets. Those two cases will first be compared to the simulation, followed by the comparison with the other two shots that used an aluminum cylinder inside. For the empty SNOUT designs, it is of interest to perceive the influence of a well-defined source and of the full NIF TC model. Table 7.11 presents the comparison of the MCNP results versos the experimental results at the pinhole, basket and at the kinematic base for S1. Table 7.10 presents the number of nuclides N_0 produced in each foil subdivided by the mass of the foil and the corresponding shot yield (Table 7.6). The measurement errors are also included.

The changes in the flux between the three measurement locations in Table 7.11 can be explained in the empty SNOUT, as the scattering along the SNOUT becomes the predominant effect which can cause the slight increase in relative error. The kinematic base effects of the DIM and NIF TC are evident in the higher measured activation for Au and In, which is consistent with the previous conclusions that thermal and near thermal contamination due

Table 7.11: Comparison between the nuclides produced in the foils exposed to the unmodified 14.1 MeV D-T source spectrum for the S2 empty SNOUT shot campaign.

Foils Location	**Isotope**	**N_0/n/g measured with err.**	**Rel. Err.[%]**
kinematic	^{196g}Au	3.20E-08 ± 1.6	7.29
	^{198}Au	1.61E-08 ± 1.2	-5.3
	^{115m}In	2.44E-09 ± 1.2	9.9
	^{116m}In	1.88E-08 ± 1.6	-7.1
	^{89}Zr	9.92E-09 ± 1.5	2.4
basket	^{196g}Au	2.10E-07 ± 1.2	2.5
	^{198}Au	1.93E-08 ± 1.2	-1.9
	^{115m}In	1.40E-08 ± 1.2	5.5
	^{116m}In	5.11E-08 ± 2.8	-4.2
	^{89}Zr	7.36E-08 ± 1.1	1.0
pinhole	^{196g}Au	9.81E-06 ± 1.3	0.3
	^{198}Au	6.54E-08 ± 5.3	0.25
	^{115m}In	6.57E-07 ± 0.7	2.4
	^{116m}In	1.64E-07 ± 2.0	1.3
	^{89}Zr	7.36E-08 ± 1.1	0.5

to room return is higher than expected. The most significant difference between the calculated and measured activation occurred at the kinematic position. The measured activation is mainly lower than expected.

The validation analysis shows that the errors between the simulated and measured reactions increase significantly when moving further from TCC, up to 7%. The results in the pinhole are well represented in the simulation, and the basket sees the same neutron flux as the HTOAD with slight differences that are likely the result of asymmetric scattering in the environment. Comparing the results with the empty HTOAD, the differences between the HTOAD front foils and the baskets of the SNOUT, both located around 50 cm from the TCC, shows the effects of the different angular locations and coatings. The asymmetry of the HTOAD flux compared to the SNOUT accounts for a decrease of 2-3% of the flux intensity at 14.1 MeV.

One of the sources of variation investigated stems from the effects of the scattering cross section of aluminum. The uncertainties of the points of reference using the unfolded spectrum using STAYSL also must be assessed. For the unfolding, the same rules as for the HTOAD are used: the χ^2, the self-shielding correction and the $1/R^2$ correction. Figure 7.15 presents the first of the unfolded spectra as compared to the simulated spectra used for testing the methodology at the pinhole location.

In the pinhole foils, the STAYSL unfolding represents the simulation just above the 1

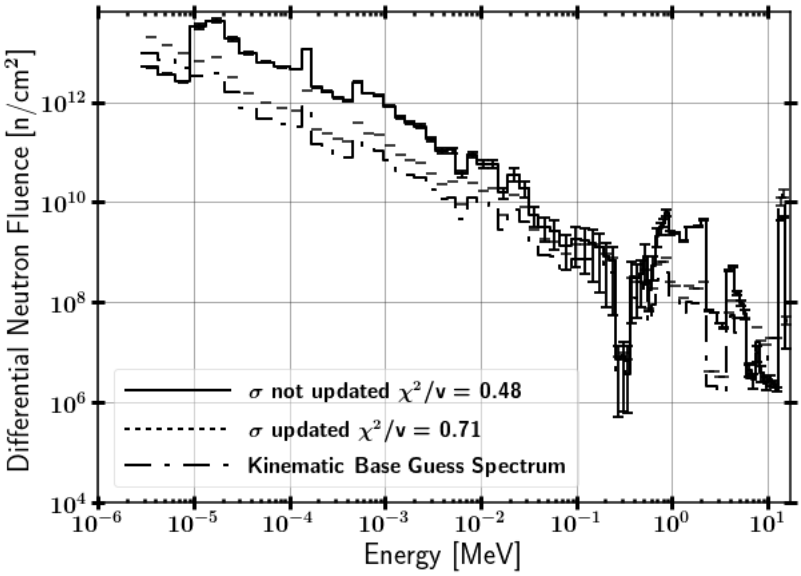

Figure 7.15: Unfolded spectrum using STAYSL and the MCNP predicted spectrum.

MeV region within the 10%, which is introduced as a standard requirement for successful STAYSL unfolding . Several detailed analyses come into play to perform the correct spectrum unfolding procedure at the basket and kinematic region. One way to reconstruct properly the spectrum from the foil activation is by expanding the set of foils in S2, by introducing more materials and increasing the reactions available for the unfolding. By improving the unfolding the comparison with the MCNP flux could be improved too in order to determine the spectra for the basket and kinematic regions.

To satisfy the first request of increasing the foils material range, in addition to understand how different types of shots can affect the design and understand how possible it is to model different shot conditions, a S2 experiment is been performed and is used for comparison. Table 7.12 presents the comparison of the MCNP results versus the experimental results at the pinhole, basket and at the kinematic base locations for S2.

As it is expected, the differences in shots S1 and S2 are noticeable, due to a lower intensity of 14.1 MeV neutron source and the presence of scattered neutrons at the pinhole level for the presence of the ENP experiment at the 90-124 DIM. The comparison with MCNP is affected by the source changes as well, which in this case proves the importance of the quality of modeling. The comparison is consistent with the ones from S1, differences larger than systematic measured errors are present in the isomers and indium. For S2, new difficulties appear in the nickel foil, as indicated by the large underestimation of the simulated results for the production of ^{58}Co by (n,p) reaction. Questions are initially raised by the quality of the measurements of the foils by the HpGe counter, as nickel is often used as an activation foil for standard spectroscopy and is found in many steel alloys.

In order to confirm the initial analysis of the ^{47}Ni(n,p) reaction, an investigation was

Table 7.12: Comparison between the produced nuclides in the foils of the SNOUT, exposed to the unmodified 14.1 MeV D-T source spectrum for the S2 empty shot.

Foils Location	**Isotope**	**N_0/n/g measured with err.**	**Rel. Err.[%]**
kinematic	^{196g}Au	3.20E-08 ± 1.6	5.1
	^{198}Au	1.61E-08 ± 1.2	-7.5
	^{115m}In	2.44E-09 ± 1.2	10
	^{116m}In	1.88E-08 ± 1.6	-7.4
	^{89}Zr	9.92E-09 ± 1.5	3.2
	^{24}Na	3.01E-09 ± 4.6	-6.8
	^{47}Ni	2.40E-10 ± 4.0	3.1
	^{58}Co	1.20E-08 ± 2.5	27
basket	^{196g}Au	3.20E-08 ± 1.6	2.2
	^{198}Au	1.61E-08 ± 1.2	-3.5
	^{115m}In	2.44E-09 ± 1.2	4.5
	^{116m}In	1.88E-08 ± 1.6	3.4
	^{89}Zr	9.92E-09 ± 1.5	1.3
	^{24}Na	3.01E-09 ± 4.6	-4.4
	^{47}Ni	2.40E-10 ± 4.0	1.0
	^{58}Co	1.20E-08 ± 2.5	28
pinhole	^{196g}Au	3.20E-08 ± 1.6	0.4
	^{198}Au	1.61E-08 ± 1.2	0.25
	^{115m}In	2.44E-09 ± 1.2	2.5
	^{116m}In	1.88E-08 ± 1.6	1.4
	^{89}Zr	9.92E-09 ± 1.5	0.7
	^{24}Na	3.01E-09 ± 4.6	0.4
	^{47}Ni	2.40E-10 ± 4.0	0.1
	^{58}Co	1.20E-08 ± 2.5	28

performed by using the same foil on the other two programmed shots, S3 and S4, to see if the same effect reappears. Keeping the ^{58}Co isotope produced from STAYLS unfolding reactions, the resulting spectrum for the first two locations, basket and kinematic base, is shown in Figure 7.16. Due to the presence of more available reactions and improved guessed spectrum the STAYSL unfolding spectra matches the spectra comparison at the kinematic base. The comparison is however worse in the pinhole and basket. Those last differences shows the effect of the ^{47}Ni(n,p) reaction at 14.1 MeV and the effect of ^{47}Ni(n,p) reaction is decreasing in the kinematic region due to softer neutron spectrum at the kinematic base. Also, those uncertainties presented in S1 are one of the reasons that it was decided to insert the same Aluminum alloy (Al-6061) into the SNOUT as it is used for the SNOUT coating

in S3 and S4. Adding Al-6061 material slab in a known and previously validated simulation model, would allow to focus the analysis on the uncertainties introduced by this specific material.

An approach to better understand the effect of Aluminum cross section uncertainties, seen also in Figure 2.10 is to perform different MCNP simulations, by changing the transport cross sections, to record the effects of the Aluminum scattering cross sections on the final result.

This type of testing is interesting to see how the matching with the unfolded spectrum is improved with the changing of the transport cross sections. Several cross sections are used from various libraries and are compared to the STAYSL-PNNL Spectral Adjustments [110], which can be seen in Figure 7.16, for a) the basket and b) the kinematic base.

Even though changes in the spectrum are evident, not much improvement can be seen using various libraries.

The other two shots are performed with two different sizes of Al alloy stacks, the results of which are presented in Table 7.13 and Table 7.14. The analysis here considers details of neutron spectrum changes in the Aluminum block.

The flux at the pinhole is not affected by the material inserted, in both experiments the ENP was present so they can be referenced to the S2 experiment also in terms of foils used. It is possible to see how inserting the material at two different Aluminum lengths changes the flux considerably. Considering the pinhole and the basket, the changes to S2 are small yet visible, the result of back scattering are visible due to the (n,2n) reactions. In the kinematic base, it is possible to see a 14% error in the comparison of the ^{115}In(n,n') as more thermalized neutrons are present. The indium foil, especially the (n,n') reaction, has decent overlap with the same activation energy range for ^{58}Ni(n,p) and is consistent with the model.

As was previously the case, the same problem occurs with the ^{58}Ni(n,p) reaction, for which the measurement value is 15% lower than the expected one with a 2.5% relative error (at $\chi^2 = 29$). The ^{58}Ni(n,2n) results, on the other hand, agree well with the modeled results. As the problem is consistent for all three measurements, it is clear the problem lies in the nuclear data libraries. A likely cause of simulation and measurement comparison error for the (n,p) reaction is the excessively-small uncertainty in the IRDFF v1.05/ENDF/B-VIII cross sections at around 14.1 MeV, which don't match, as is shown in Figure 7.17.

The unique aspect about the experiments performed here versus most other nickel activation experiments presented, including those featured in the EXFOR library, is the overwhelming prominence of the flux at 14.1 MeV. Figure 7.18 also presents the experimental data from the EXFOR library for ^{58}Ni(n,p) reaction. While a lot of data exists at 14.1 MeV, the spread in values is over 14%, more likely around 30% and far outside each measurement's uncertainties as seen in this work. The most probable explanation for improvement with the IRDFF data is that they took a weighted average and assigned a small uncertainty reflective of the number of measurements assuming errors average out to the right value, while ENDF/B-VIII assigned an appropriately large error bar.

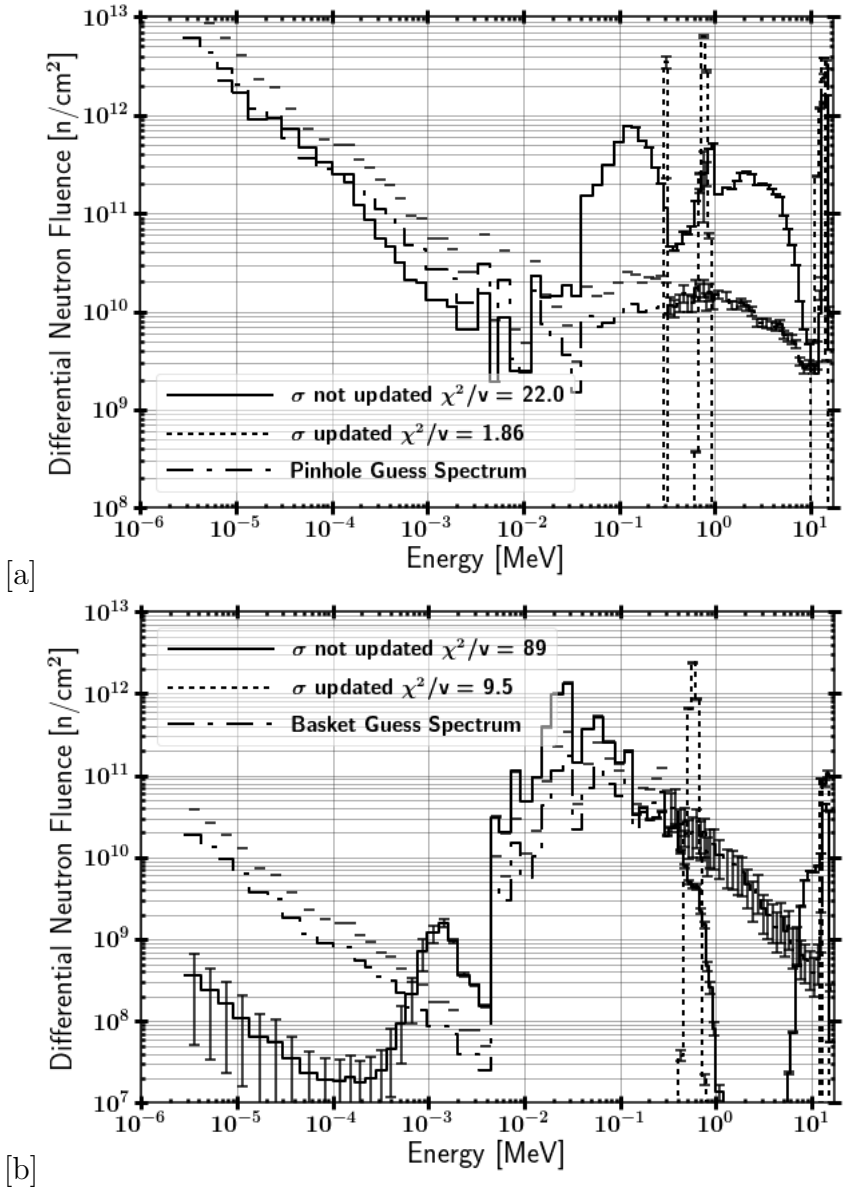

Figure 7.16: STAYSL unfolding spectrum and MCNP spectra at a) basket and b) kinematic base region.

It is also important to mention that at ENDF/B-VIII, the cross section starts at 812 keV for nickel and indium, as if 100% of the reactions produce the isomer, while in IRDFF, the cross section starts at 500 keV. This introduces a very small effect since the cross section is small between 500-812 keV, but it is still appropriate to consider in the comparison. The influence is also quite low for S4 especially below 10^{12} neutrons at the kinematic base.

Furthermore, considering that ^{58}Co has a metastable state with a 9.1 hr half-life, the measurements of the ^{58}Co samples for S3 and S4 were performed after 2 weeks for ^{58}Co and

Table 7.13: Comparison between the produced nuclides in the foils of the SNOUT, exposed to the unmodified 14 MeV D-T source spectrum for the S3 shot with the inserted Aluminum slab of 30 cm.

Foils Location	**Isotope**	**N_0/n/g measured with err.**	**Rel. Err.[%]**
kinematic	^{196g}Au	3.20E-08 ± 1.6	9.5
	^{198}Au	1.61E-08 ± 1.2	10
	^{115m}In	2.44E-09 ± 1.2	6.9
	^{116m}In	1.88E-08 ± 1.6	5.8
	^{89}Zr	9.92E-09 ± 1.5	2.9
	^{24}Na	3.01E-09 ± 4.6	0.4
	^{47}Ni	2.40E-10 ± 4.0	1.8
	^{58}Co	1.20E-08 ± 2.5	27
basket	^{196g}Au	3.20E-08 ± 1.6	2.2
	^{198}Au	1.61E-08 ± 1.2	-3.5
	^{115m}In	2.44E-09 ± 1.2	4.5
	^{116m}In	1.88E-08 ± 1.6	3.4
	^{89}Zr	9.92E-09 ± 1.5	1.3
	^{24}Na	3.01E-09 ± 4.6	-4.4
	^{47}Ni	2.40E-10 ± 4.0	1.0
	^{58}Co	1.20E-08 ± 2.5	28
pinhole	^{196g}Au	3.20E-08 ± 1.6	0.4
	^{198}Au	1.61E-08 ± 1.2	0.25
	^{115m}In	2.44E-09 ± 1.2	2.4
	^{116m}In	1.88E-08 ± 1.6	1.4
	^{89}Zr	9.92E-09 ± 1.5	0.7
	^{24}Na	3.01E-09 ± 4.6	1.4
	^{47}Ni	2.40E-10 ± 4.0	0.1
	^{58}Co	1.20E-08 ± 2.5	28

used the ground state half-life to correct due to decay back to the activities at the time of the shot, considered t=0. The 2 weeks waiting period weren't introduced in the counting during S2, thus the results might feel the effects from different isotopes of nickel that can produce, with thermal capture, ^{58m}Co. The thermal capture cross section is very high (140,000 barns) and even the ground state is unusually high (1650 barns).

It is possible to see how the aluminum effect in the flux is decreased, as the more thermalized are the neutrons, fewer (n,γ) reactions are present. The aluminum cylinder thus increases the neutrons in the flux ranging from 2-5 MeV which could be useful for several isotope separation studies.

Table 7.14: Comparison between the produced nuclides in the foils of the SNOUT, exposed to the unmodified 14.1 MeV D-T source spectrum for the S3 shot with the inserted Aluminum slab of 60 cm.

Foils Location	**Isotope**	**N_0/n/g measured with err.**	**Rel. Err.[%]**
kinematic	^{196g}Au	3.20E-08 ± 1.6	6.96
	^{198}Au	1.61E-08 ± 1.2	-10
	^{115m}In	2.44E-09 ± 1.2	14
	^{116m}In	1.88E-08 ± 1.6	-9.8
	^{89}Zr	9.92E-09 ± 1.5	2.5
	^{24}Na	3.01E-09 ± 4.6	6.4
	^{47}Ni	2.40E-10 ± 4.0	2.4
	^{58}Co	1.20E-08 ± 2.5	18
basket	^{196g}Au	3.20E-08 ± 1.6	2.2
	^{198}Au	1.61E-08 ± 1.2	-4.5
	^{115m}In	2.44E-09 ± 1.2	6.5
	^{116m}In	1.88E-08 ± 1.6	-3.7
	^{89}Zr	9.92E-09 ± 1.5	1.0
	^{24}Na	3.01E-09 ± 4.6	4.4
	^{47}Ni	2.40E-10 ± 4.0	-1.4
	^{58}Co	1.20E-08 ± 2.5	27
pinhole	^{196g}Au	3.20E-08 ± 1.6	0.5
	^{198}Au	1.61E-08 ± 1.2	0.75
	^{115m}In	2.44E-09 ± 1.2	-2.5
	^{116m}In	1.88E-08 ± 1.6	1.4
	^{89}Zr	9.92E-09 ± 1.5	0.75
	^{24}Na	3.01E-09 ± 4.6	2.4
	^{47}Ni	2.40E-10 ± 4.0	0.1
	^{58}Co	1.20E-08 ± 2.5	28

Figure 7.19 presents the flux comparison for each location of all the SNOUTs for all the SNOUT shots. The ratio for the unfolded spectrum comparison for S3 are shown in Figure 7.20 and using all the reactions provided besides the Ni(n,p) reaction, which proved to give a poor flux reconstruction for all three locations.

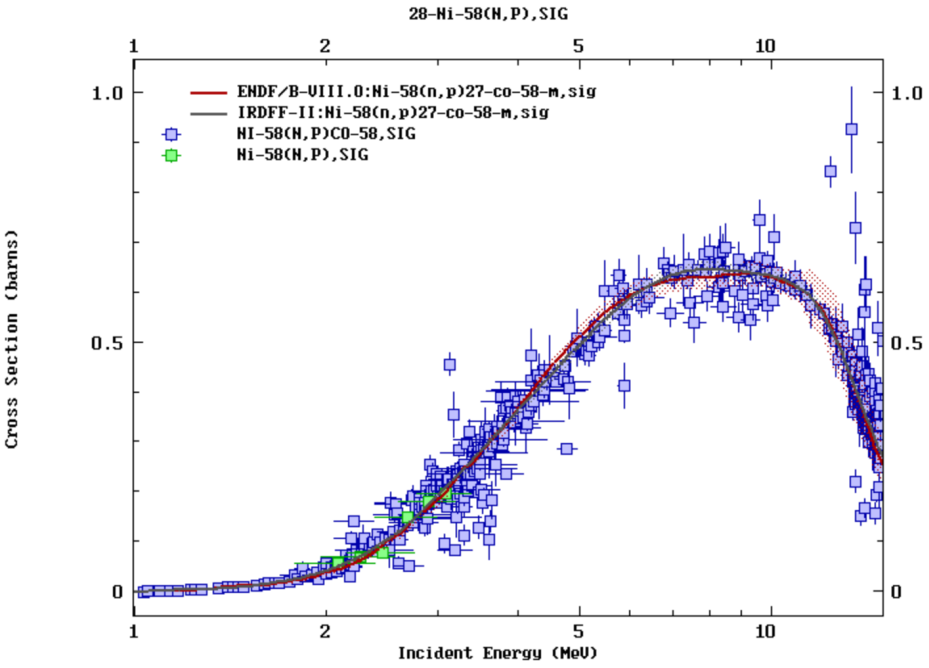

[a]

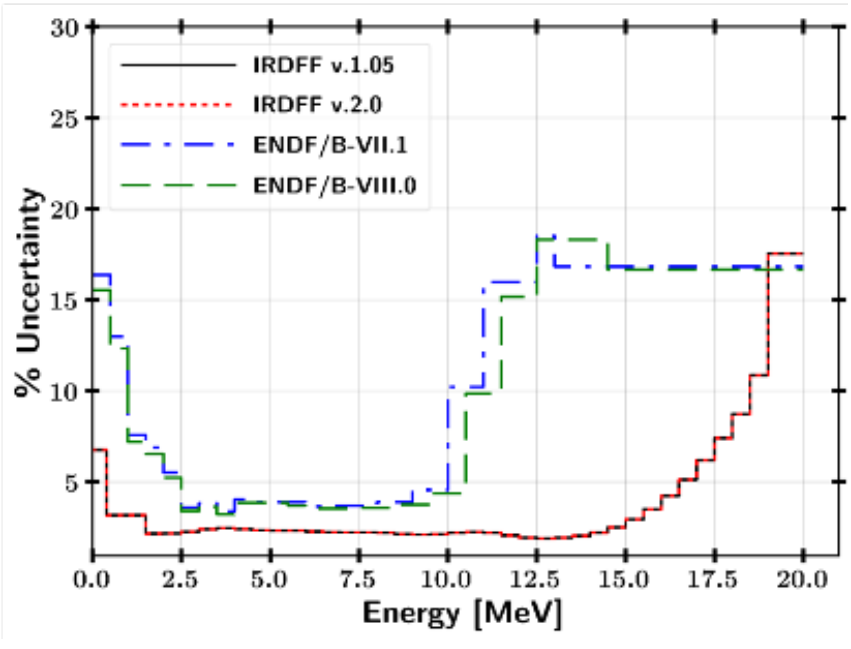

[b]

Figure 7.17: a) Nickel nuclear data in the ENDF/B-VIII and IRDFF v2.0 library data. b) Uncertainties % for ENDF/B (both -VIII and -VII) and IRDFF (both v1.05 and v2.0) for ^{58}Ni(n,p)^{58}Co

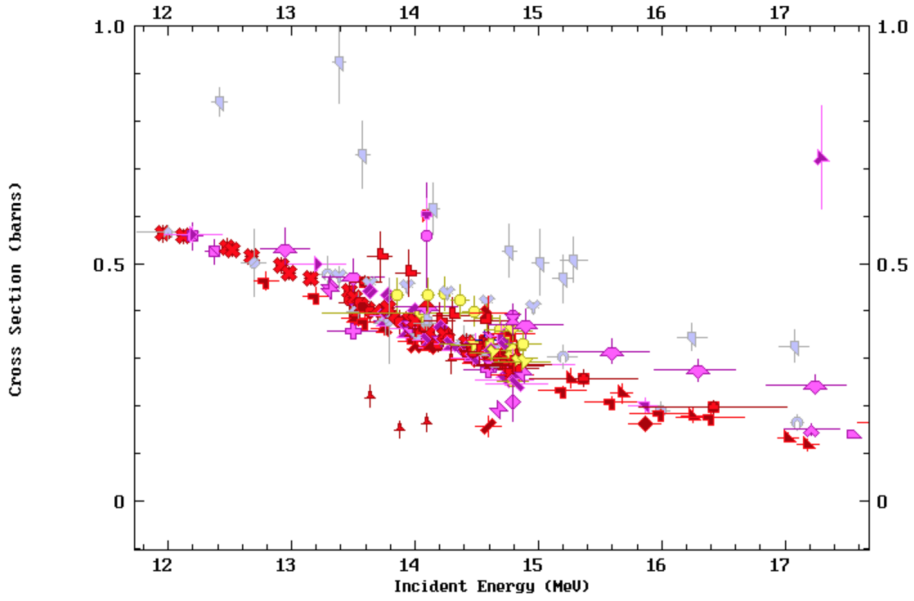

Figure 7.18: EXFOR data for ^{58}Ni(n,p)^{58}Co reaction at 14.1 MeV

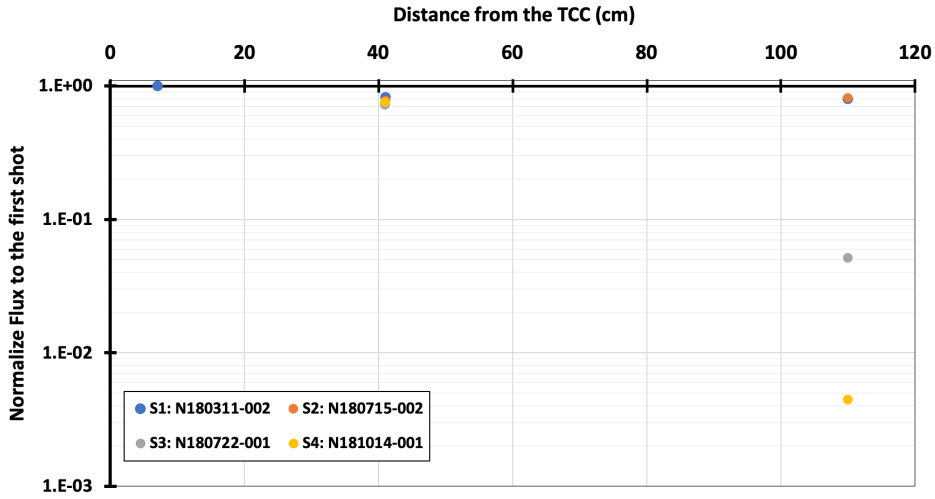

Figure 7.19: Normalized fluxes for shot S2, S3 and S4 to the flux from the S1 shot in the SNOUT at all three locations.

7.3.3 Summary of the Results and Conclusion

This work seeks to validate the ability to model the ETA using COEUS with MCNP, a challenging proposition given the weighted impact of component cross sections on the resulting spectrum modification that could highlight nuclear data deficiencies. The concept is to have a robust, fully-benchmarked method for designing future experiment possibilities at

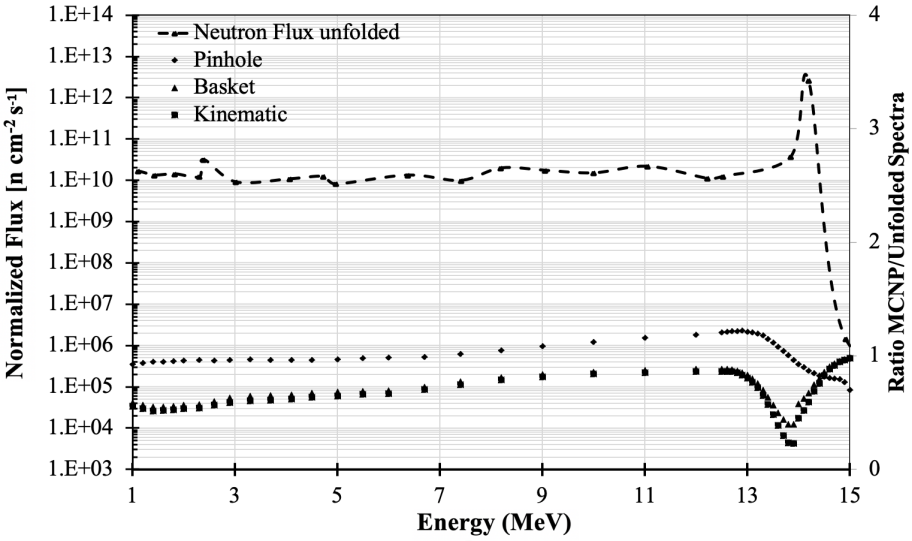

Figure 7.20: Ratios of difference of the STAYSL unfolded spectra to the MCNP spectra for all three locations used in S3.

NIF. The goal was to run those experiments in possible NIF locations for future ETA. For a full ETA, it is difficult to record in the simulated results the contribution of the propagated nuclear data uncertainties and on all the systematic errors, hence the idea to consider and integrate the possible sources of errors one at the time when designing simple experiments. Towards this end, the initial steps performed included collection of data sets from partial material stacks to gain insight into nuclear data impact. The initial experiments described in this chapter are set up to test this methodology. The MCNP simulation models the experimental SNOUT and HTOAD performance remarkably well over a large energy range and several orders of magnitude in response. The largest discrepancies between the model and the STAYSL unfolded spectrum are in the 10 eV to 10 keV region, where the activation foil pack had limited sensitivity and coverage. Few nuclear data uncertainties have been identified, which would be highly useful to consider for future ETA and nuclear data measurements, such as for aluminum and nickel. The remaining discrepancies will most likely disappear with more precise nuclear data information. Other discrepancies found were consistent with the conclusion from the first set of experiments, in which room return, extra neutrons returning to the experiment from scatter off the walls, and other components of the room were found to deliver a larger thermal flux than expected. Results from spectrum characterization were generally consistent with the expected effects, except for the activation level in the nickel foil. Importantly, this work validated the ability to model the NIF neutron spectrum produced at various locations, which allows for the use of foil activation spectroscopy requiring an a priori spectrum to be used to unfold the neutron energy spectrum. Also, the simulation development work on this project was performed with the intent of providing a modular and extensible modeling framework for different types of designs in

the NIF TC that can be widely used for the future. An additional objective of this work was to develop a validated experimental proof-of-concept platform for measurements performed in a short time and relatively inexpensively.

In Chapter 8, several ETA designs will be presented using the modeling methodologies validated here. Those ETA will be inserted instead of the SNOUTs on TANDM 90-348 with the same TC effects seen here. The NIF modeling is then already determined, and COEUS will be used to predict optimal ETA designs for a few chosen objectives.

Chapter 8

COEUS V2.0 Application: Examples of ETA Designs inside the National Ignition Facility

The previous chapters in this dissertation outlined the problem definition of neutron tailoring (Chapter 1), the physics behind it (Chapter 2), the modeling methodology (Chapter 3), and the further development of the optimization approach used (Chapter 4). The experiments used for validation of the methodology are presented in Chapter 5 and Chapter 6, including an introduction of all the important instrumentation that is available at the National Ignition Facility (NIF) for neutron spectra tailoring experiments. The described experiments have then been used to validate the modeling capabilities and simulations introduced in Chapter 7. In this chapter, the newly developed and validated modeling framework is tested by designing optimized neutron spectra tailoring assemblies for specific applications. The chapter outlines some of the modeled Energy Tuning Assembly (ETA) inside the NIF, describing how the runs are performed with respect to the objective spectrum, variables and constraints. A brief description is presented on how the process of converting a model of optimal Energy Tuning Assembly (ETA) design into an engineering design at the NIF is performed for future deployment, while learning from past mistakes. The chapter is organized into three major sections. Section 8.1 describes the feasibility study that has to be done in order to build the ETAs at the NIF, which provides the possible constraints needed. Section 8.2 moves to introduce some of the possible applications of COEUS v2.0 and Section 8.3 covers several examples of ETA designs that were developed.

8.1 Applications

Informed by the experience of all the modeling work presented in Chapter 7, and the newly improved optimization code Gnowee/COEUS v2.0, a series of ETA designs within the NIF is here introduced, for tailoring the D-T spectrum to a series of applications. The ETA

designing process in a facility like the NIF goes through a series of steps that highlight the contributions and importance of the work that has been performed throughout this research.

The first step to design an ETA is to determine the correct single or multiple objective functions for the needed application. These functions can include the neutron flux, the reaction rate, a detector response, etc. As described in Chapter 4, the newly developed version of COEUS provides a set of possible objective functions, and a lot of work has been performed in order to generalize the optimization methodology. This new capability overcomes the v1.0 limitation of defaulting the neutron spectrum at the ETA window exit as an objective function. Now, with the second version, the user has the possibility to have the objective function located anywhere in the modeled space.

Furthermore, it was important to have a detailed understanding of the geometric configuration of the ETA. This is a crucial and newly introduced step described in Chapter 7. Previously, the ETAs were designed in empty space using an approximate point source at a fixed location. Since the goal for this work is to optimize an ETA in a realistic experimental environment, the detailed MCNP input of the NIF target chamber (TC) was included in the COEUS input model. This allowed to record all neutron contributions from room scattering and from a realistic neutron source. In order to satisfy this step, a detailed model of the NIF shot campaigns has been further developed and improved. Chapter 7 introduces the new model including the added DIM and TANDM (90-124, 90-348) and the experimental instrumentation (SNOUTs and HTOAD), the added flux monitors (foil packs), all of which is essential for future ETA campaigns. The design framework has also been improved in terms of efficiency, due to the volume of simulations that has been performed for each shots. In order to speed-up simulations, a two-step MCNP methodology has been developed. The first step collects, in terms of surfaces, all the neutrons approaching the SNOUTs and HTOAD and uses them subsequently as surface neutron sources for simulating only the HTOAD, SNOUTs or ETA, without the need of including the rest of the full 3D model of the NIF TC in the simulation. This methodology has been verified and it drastically improves the running time and the statistics inside the detectors.

Moreover, it was crucial to understand and qualify the accuracy of the simulation results. The first campaign at the NIF had provided invaluable information on the NIF experiments when dealing with the neutron spectrum. Additionally, Chapter 7 provides a validation of both MCNP and COEUS modeling performance, providing information on the type and amount of uncertainties in both the experiments and the simulations. Thanks to this validation, it is possible to provide a level of confidence on the prediction of the final results for future ETA designs. The only unknown in the results predicted by the ETA optimization will be the propagation of the cross section uncertainties within the ETA materials. For this purpose, the design result output from Gnowee/COEUS is not definitive. One more step is performed by remodeling the "ideal" ETAs with SCALE Sampler to assign the appropriate uncertainties from nuclear data to the final results. In case of large uncertainties, the goal is also to further reiterate the optimization in order to eliminate any material contributing to the largest uncertainty.

The main step, which is the focus of this Chapter, is running the full model with

Gnowee/COEUS to design the ETAs for various applications. The new code version has a MCNP-like input file where the NIF variables in the input can be defined as discrete, continuous, binary, etc. The constraints of the variables can be defined as upper and lower boundaries for continuous variables, as a list of values for discrete variables, etc. More constraints can be in the form of a mathematical function, *e.g.* the weight of the assembly, for which it is important to provide the correct correlation of geometry and density variables. In order to provide the correct constraints it is important to go through the NIF feasibility study in designing an ETA, which is presented in the following section. In this chapter, the type of variables and all possible values are detailed for each application as well as the NIF TC source spectrum and the objective information.

In a final step, outlined as the future work, a series of definitive experiments and shot configurations for the ETA of interest is proposed. It is fundamental here to weigh the different resulting ETA layouts against material, manufacturing costs, and regulations. The code, in fact, provides more than one optimal design, which can be used to determine, for example, the overall cost of each possible ETA, affecting the choice of the "optimum" final design.

8.2 Energy Tuning Assembly Design at the NIF

This Chapter provides several optimization examples, and describes how COEUS V2.0 can be used within the NIF environment. Although the new development in the objectives and constraints for this optimization were discussed in Chapter 4, Section 4.3, some of the key parameters are mentioned here to aid in the discussion. The new version of the code will greatly accelerate the pace of development in many areas of nuclear engineering that need neutron spectra with specific desired characteristics: detector calibrations, the study of radiation damage to different materials, cross section measurements, material science, design of targets for production of medical isotopes, medical applications such as BNCT or various shielding applications. The NIF, in fact, is a unique source of neutrons with a very high flux output and a monoenergetic 14.1 MeV neutron source peak, and could be thus utilized in many applications requiring strong source of fast neutrons..

8.3 Feasibility Study at the NIF

In this section a few important feasibility guidelines for building any instrumentation on the DIMs are summarized. It was found out that the DIMS (especially DIM 90-78 and TANDM 90-348) are the most ideal location for placing new instrumentation or ETAs. Any designed experiment at the NIF needs to meet the robust engineering standards of the NIF. As an example, it is critical to avoid or mitigate unconverted 1 W laser light impinging on the ETA case and either scattering into the NIF optics or causing ablative recoil that could physically damage the ETA.

- In order to avoid interfering with the optics of the laser, there is a minimum standoff requirement consisting of a standard 10 mm standoff between TANDM positioner payloads and the 1 W beams. An additional 0-5 mm might be needed if the ETA is inserted as a new payload and not in the pre-existing SNOUT, and the positioner precision can only be determined with certainty by fielding the final design. If the ETA is inserted in VisRad together with the ENP, as it is often seen in the shots in Chapter 5, it is important to consider the 10 mm radius sphere of the TCC. It is also important to keep clear from the polar direct drive exploding pusher (PDXP). The standoff of any load in the TANDM has to be 7-10 cm from the TCC, the TANDM itself 48 cm.

- Another mechanical consideration to consider is the conical opening angle determined by the entrance angle of the beams with the PDXP pointing. There is an exclusion zone from the laser exclusion zone and the positioners (TarPos/CryoTarPos) sweepout to the conical opening angle. Other groups have used slightly more conservative beam point models to determine the acceptable envelope of 72.1 degrees for equatorial instruments. The target itself is mounted to TARPOS 90-239 and there is likely to be an additional experiment mounted on the other DIM. If a sweep angle of 180 degrees or less, symmetric around the 90-124 axis is sufficient, the clearance requirements are easily met.

- The ETA will be loaded in the NIF target bay. Payloads under 10 kg can be loaded manually as done with the SNOUT. In the likely event that the payload is over 10 kg but not more than 100 kg, the payload will be loaded with lifting equipment. The DIM and TANDM require the ETA to not go beyond 100 kg.

- The materials which are used to encase the ETAs need to follow the NIF guidelines. Two options are given: 300-series stainless steel, which is a good choice for the outer case to minimize ablation of material viewing the target directly; or standard aluminum construction alloys as for the SNOUTs, *e.g.* Al T-6061, which are good for structural parts that do not face TCC to keep the weight down. Guidelines are also given in the various examples in terms of materials inserted in the ETA. It is possible that no insurmountable hazardous material should be used, besides such that are following encasing guidelines. Generally, materials that are not desirable are gases or materials with a low melting point, but also reactive, or materials that are too expensive.

- Within the NIF guidelines, activation of the ETA needs to be less than 5 mR/hr at 1 ft and 1 hour after a 10^{15} neutrons/cm^2 shot.

The applications presented here for ETA designs have been constrained by the above pre-existing feasibility study. The study has been presented within this work as a part of the HTOAD and SNOUT experiments described in Chapter 5 and will be used consequently for the ETAs. As seen throughout this initial step, the options are to position the ETA inside pre-existing HTOAD and SNOUTs or as a stand-alone diagnostic load package (DLP) on

the TANDM 90-348 and DIM 90-78. It was evident, for example, the available sizes of the HTOAD could not fully shift the spectrum peak or perform complex tailoring. However, the HTOAD could be used to place a combination of materials optimized to increase the number of neutrons in the specific energy range. An other option would be to build an alternative HTOAD to place inside the SRC, consequently reducing the spectrum slightly to have peaks at energy ranges below 14.1 MeV so as to study iron scattering between 8 and 10 MeV. The SNOUT gives more opportunities, due to its length, to insert more materials and it can be modified in size to fit the requested ETA.

8.3.1 Designing of ETAs as Integral Benchmark Designs for Neutron Activation Studies

The initial idea is to design integral experiments in order to recreate monoenergetic fluxes at energies below 14.1 MeV. The goal is to highlight energies of known data weaknesses by isolating specific energy channels. This would be an efficient use of the resources at the NIF because of the large need of having more semi-integral and differential experiments and is in line with the national security and counter-proliferation LLNL mission. Integral benchmarks are used for data validation. The nuclear data community relies on an extensive set of benchmark experiments, such as criticality or fusion nuclear shielding experiments, to test new evaluations of cross section databases. However, integral experiments should be avoided for the adjustment of general-purpose libraries. One such set of experiments came out of the LLNL pulsed-sphere benchmark experiments program. During the last 33 years, numerous high energy pulsed-sphere experiments have been designed, in which small, medium, and large spheres of different materials were pulsed with a burst of high-energy neutrons [116]. Measured time-dependent detector responses at distant locations provide a benchmark by which various neutron transport codes and cross section libraries may be judged. The radius of spheres is designed to be an integer number of mean free paths for 14.1 MeV neutrons and the various tested materials (*e.g.* ^{6}Li, ^{7}Li, Be, C, N, O, Al, ^{235}U, ^{238}U, ^{239}Pu, Fe, etc.). Pulsed Spheres have been used for multiple nuclear data efforts, because they are sensitive to elastic and inelastic scattering cross sections. Our goal is to recreate the pulsed sphere experiments inside the NIF with full sensitivity and uncertainty analysis for sources of experimental uncertainty, like the neutron intensity, room return effects, and material effects and size of the sphere to be included within one step with Gnowee/COEUS. The latter will include all the variables of the design and constraints in one single calculation, where a series of materials are studied for the sphere in various configurations. The LLNL pulsed sphere experiments studied a series of materials in various configurations. Sometimes, identical materials in different geometric configurations were used to investigate pulse spectrum behavior resulting from attenuation through various thicknesses of the material.

In this Chapter, the idea is to design an optimized ETA to sufficiently modify the NIF neutron spectrum for integral benchmarking experiments in order to identify discrepancies indications on needed nuclear data adjustments at several energies. The initial example

focuses on structural materials as Al, Fe, Ni, etc., which have isotopes that have been prioritized by Nonproliferation and Homeland Security funding agencies. Systematic experimental campaigns based on a set of these isotopes will greatly facilitate this need, thus the interest in using the NIF for such applications as well, especially focusing on the inelastic scattering cross sections over a wide range of neutron energies [40].

8.3.1.1 ETA Design Simulations and Results for Aluminum

The material of interest is here aluminum (Al) and the goal to design experiments to look into specific cross sections at different energies range. For Al, neutrons between 6 and 10 MeV are produced from 14.1 MeV source neutrons by elastic and inelastic scattering, the last has shown to introduce the largest uncertainties in the results. Al based alloys are used (together with stainless steel) as the main material for building manipulators and covering the instrumentation inside of the NIF TC. The presence of both materials at 14.1 MeV can affect part of the neutron thermalization in the chamber because of their large scattering cross sections (Chapter 2). Thus, there is the need to understand and analyze the quality of the nuclear data at different energy ranges. As shown in Chapter 7, the effect of aluminum-based alloys present in the NIF TC on the thermalization of 14.1 MeV neutrons was visible. Thus, it is important to determine the accuracy of Al scattering cross sections for various energy ranges. An example of possible ETA that can be inserted inside the NIF for such studies is introduced here. By using the prescribed process discussed here, the future user might be able to design ETAs to obtain different energy ranges.

The initial prospect was to design ETAs that could be inserted in the NIF TC in a short time frame, thus the need to constrict the ETA design inside two of the instrumentation seen in Chapter 7, the SNOUT and HTOAD with little to no engineering modification. It is, in fact, of interest for the NIF research group to be able to have a couple of ETA designs and predicted fluxes to build for future experiments. This could be possible thanks to the efforts and contribution of the work performed in this thesis, which will allow future users, or those with limited knowledge in simulation, to run and simulate an ETA of interest following the summarized steps presented [15].

In Chapter 7, in fact, the full 3D MCNP model of the NIF TC for the shot configuration of interest was further developed, and successfully validated through a series of initial experiments. The latter is extremely important in performing integral benchmarking types of experiments. In this type of experiments, the NIF chamber is considered as a "clean" room, which means the environment is proved to be well validated, documented, controlled and known at the time of the experiment. This requirement has been partially satisfied in Chapter 7, where the validation identified and quantified the discrepancies expected from the measuring point location, the room return effects, the scattering in the NIF chamber, and the SSR source file so that the only remaining unknown discrepancies left for those new experiments are mainly determined by the materials of interest.

The ETA designs are performed using the 3D detailed model of the NIF introduced with COEUS v2.0. The initial objective function of the first ETA example is to reproduce the

neutron spectra with energy ranges of 8-10 MeV in the aluminum target located at the end of the ETA. The Gnowee/COEUS v2.0 for the application input was designed using, as a source, the full cylinder surfaces, "wssa" file, as seen in Chapter 7 specifically created for the S3 shot campaign. This shot configuration was chosen, as the source, due to the frequency of recurrence for such shot type for ride-along typo of experiments. The manipulator chosen for the ETA location is the TANDM in 90-348 as it has been already used in this work and because it can handle heavier weights. The initial required shape for the ETA of interest is predominantly cylindrical in order to be located inside of the SNOUT tube. In such a way, it is possible to provide an experimental set-up that have been previously tested and that have passed the NIF feasibility studies. In the future, the ETA designs optimized for actual monoenergetic integral benchmarks, would have to be of spherical shape as for the pulsed sphere experiment, [116] in order to provide equal probability for neutrons to reach the material of interest.

The variables in the MCNP input-like files are: the location of the ETA inside the TC; the distance of the assembly from the TC; its dimension as radius and length of the ETA and the location of the Al sample of study; and the number, size and type of the materials inserted in the ETA and their densities. The variables used and described are bounded so to satisfy any possible constraints for physical or experimental reasons. Experimental constraints are mainly identified in the NIF feasibility study. A brief summary of the constraint characteristics is listed below.

- The ETA dimensions are constrained based on its shape and dimension. If the goal is to insert a cylindrical shaped ETA inside the SNOUT cylinder, the standoff is approximately 40 cm from the TCC with a maxim length of 100 cm and a maximum diameter of 50 cm if the element is inserted inside the cylinder. If the ETA geometry of interest is conical then a standoff of 8 cm from the TCC is accepted, the length is limited to 40 cm if inserted inside the SNOUT, but 140 cm if it is a load by itself. If the assembly is conical then the opening angle has to follow the constraints from the NIF feasibility study.

- The number of material elements inserted is constrained to a maximum of 10, more materials might increase the difficulties in building the assembly.

- The neutron source is defined using the "wssa" file previously created by simulating the full NIF TC in the MCNP model as it was done in shot S2. This is one of the new capabilities of COEUS v2.0. It is very important for the sake of the optimization in tailoring neutron spectra that all thermalized neutron contributions are considered as well as all the possible uncertainties that can come along. In the initial application of the first version of the optimization code, it was shown [117] that the assumptions of a 14.1 MeV point source located in the empty NIF environment introduced large errors in designing optimal ETAs.

- The objective function here is defined as a neutron flux with a peak of energy ranging 8 to 10 MeV.
- A list of materials is provided here as deterministic variables, the chosen materials taking into consideration their costs and availability for manufacturing. The list consists of a few compounds and alloys: Al T-6061, LiF, high density polyethylene (HDPE), deuterated HDPE, Stainless Steel 409/304/303, boron carbide (cobalt salt), and every naturally occurring element. Of all the materials available in libraries like PyNE, those that are gases, with low-melting point, expensive, and/or reactive are removed. Modifications can be made to the material list in the future to remove or add any desirable materials.
- The weight is constrained to 100 kg, which is the TANDM weight limitation.
- The neutron flux monitors used are the neutron activation foils, which are set to be inserted at the exit of the assembly. The flux will be simulated at the level of the Al samples as well.
- The minimum neutron flux intensity at the sample level (the Al) has to be around 6.86 10^8 n/cm^{2}s.

Gnowee/COEUS v2.0. simulations require an appropriate set up for the ADVANTG code, with the size of the meshing smaller closer to the detector system, and larger when farther from the sample. COEUS's task is to collect and provide to Gnowee all the given variables, grouping them by name, typology (continuous, discrete, binary, etc.), upper and lower boundaries, and all the values of the discrete variables given by the user in the input file.

COEUS v2.0 is then ran on a High Performance Computing (HPC) cluster, the UC Berkeley Savio cluster in this case, to generate the relevant ETA design for the specific energy range flux. The optimization run computed almost 5000 designs during 62 hours (wall time). The final result provides a time history of the top designs associated with the number of objective function evaluations and their associated fitness value. An example of the fitness curve shape is shown in Figure 8.1.

Since COEUS is a population-based optimization code, it returns the final set of n designs and their associated fitness for each optimization. The number of designs is decided by the user, in this case they are 25. This complete set of designs, along with the stored time history, can be useful when transitioning from a computer model to an engineering design. When stepping into the engineering design, it is important to evaluate some trade-offs that are not captured in the optimization, *i.e.* material costs and availability. Figure 8.2 introduces the snapshot of the top design optimized for delivering a neutron spectrum ranging between 8 and 10 MeV that could be inserted inside of a SNOUT, with all the given constraints for the TANDM 90-348.

The resulting flux that reaches the 1-cm-thick and 50-mm-radius aluminum sample is seen in Figure 8.3.

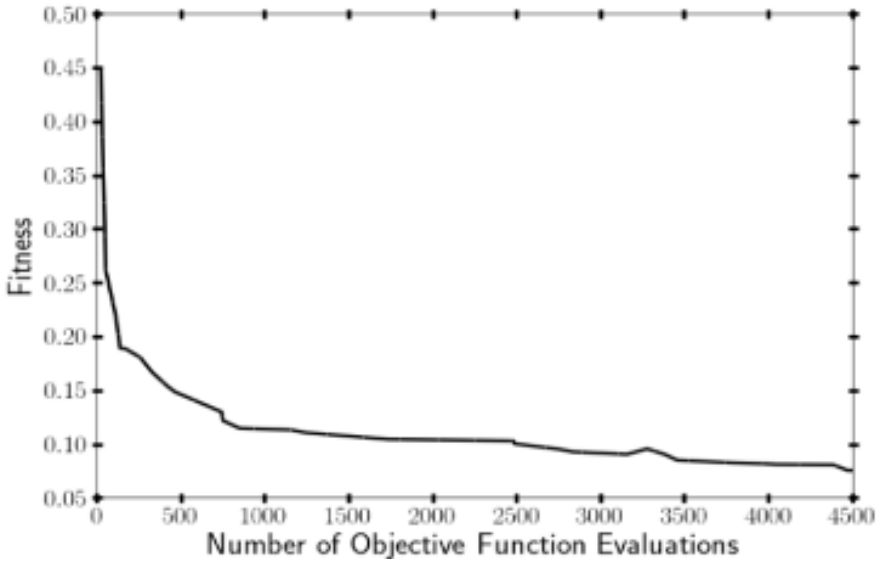

Figure 8.1: Fitness curve for the optimization at 8-10 MeV objective spectrum.

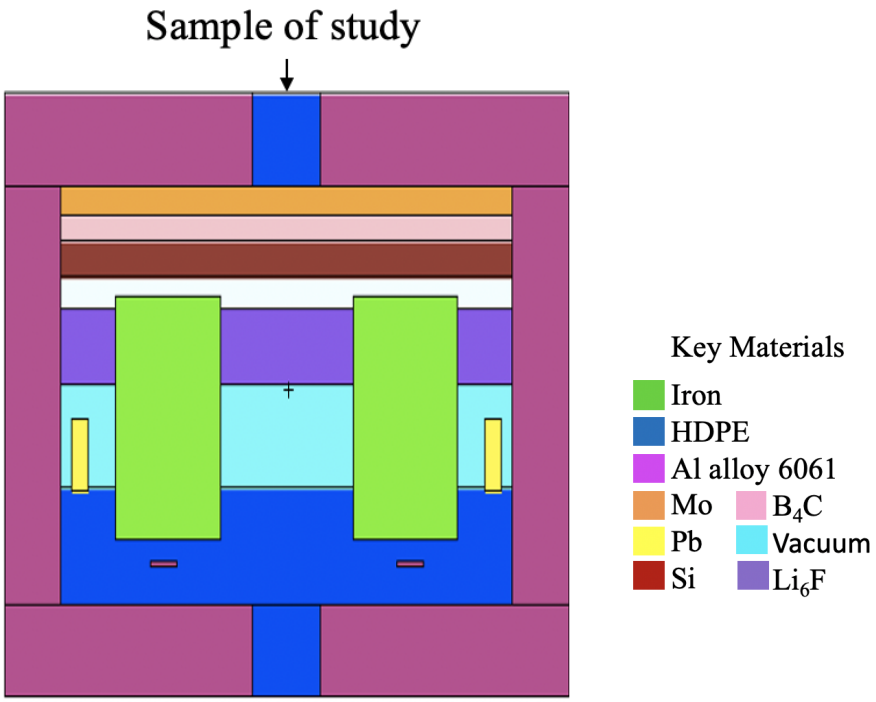

Figure 8.2: ETA produced by COEUS to reproduce an objective neutron flux peaking at an energy range of 8 to 10 MeV.

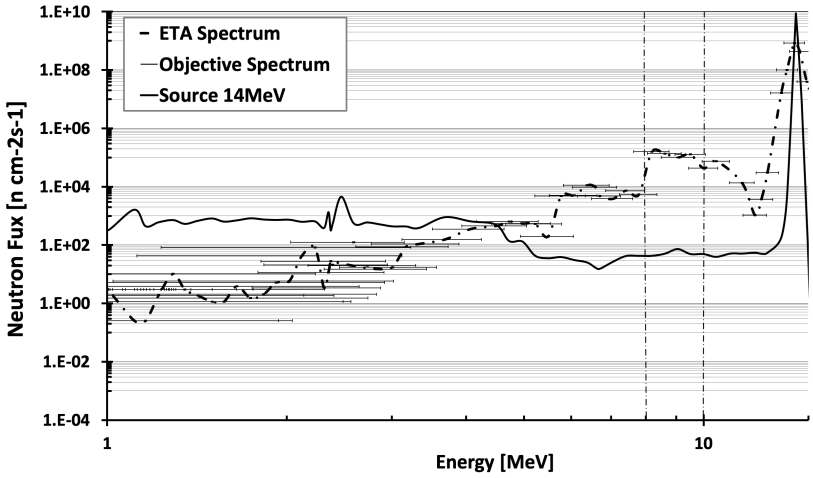

Figure 8.3: A comparison of the modeled ETA flux spectrum achieved across the foil pack and the small energy range objective spectrum and the initial source of 14.1 MeV.

The ETA model in Figure 8.2 is required to be cylindrical, the optimized dimensions have a length of 35 cm and a radius of 7 cm. Both the dimension and the weight are imposed by the NIF and that is the limiting factor for the spectral shaping performance (especially for the energy peaks at and below 10 keV as seen in the BNCT application). Additionally, the constraint on mass limits makes the atom density the key factor on the choice of the materials to remove neutrons from the 14.1 MeV peak.

For this spectrum, there is the physics goal constraining the performance to the 8-10 MeV range. The presence of mainly mid- or low-Z moderators resulted in a higher flux in the 8-10 MeV range due to the low-energy scatters required by neutrons to populate this region, mainly elastic and inelastic scattering in materials as aluminum and nickel, HDPE polyethylene, carbide materials and Lithium. Besides these materials, the need for a clean 8-10 MeV range has introduced few high-Z elements in order to further reduce the 14.1 MeV neutron spectra and in return to populate the energy region below 1 MeV.

In the interest of future experiments at the NIF that remove the 14.1 MeV neutron peak, alternatives to the SNOUTs are needed. Removing the SNOUT limiting weight and size constraints might allow for heavier materials. For this reason and for the sake of providing to the user the capabilities of the optimization software, an ETA has been designed with the objective of a 10 MeV monoenergetic spectra. For such run, the shape, size and weight of the SNOUT has been removed. The only remaining constraints are the TCC geometry standoff requirements and the limits due to the MCNP input file. The resulting ETA and normalized spectra are available in Figure 8.4

The goal here is to further remove the 14.1 MeV neutrons, besides low- to mid-Z elements seen before there is a larger component of heavy nuclides as of Bismuth and Lead, which, also, cause a removal of neutrons at 10 MeV due to the (n, 2n) reactions. The dimensions of the assembly are slightly increased and the chosen shape is the conical one in order to be

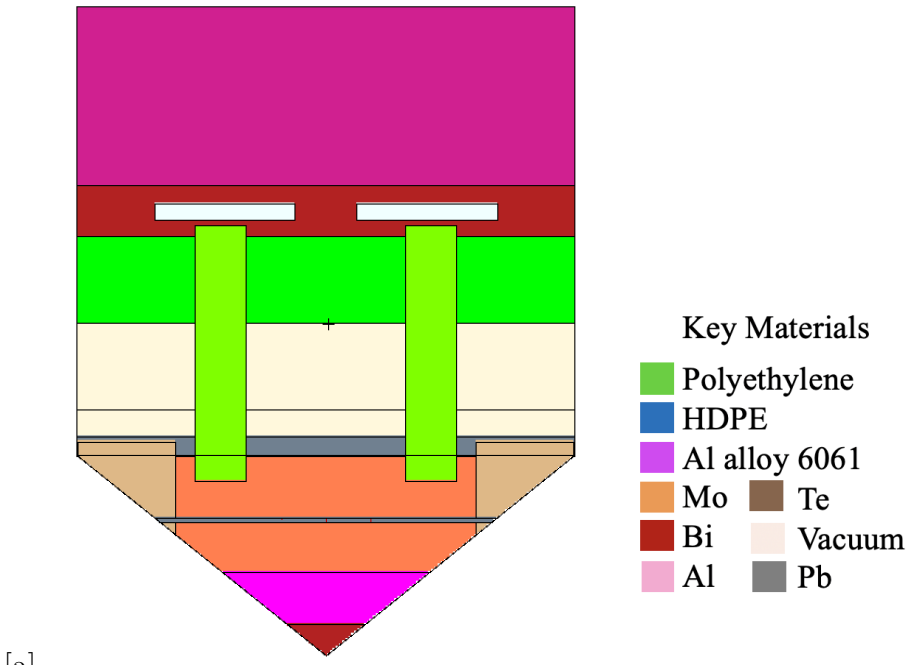

[a]

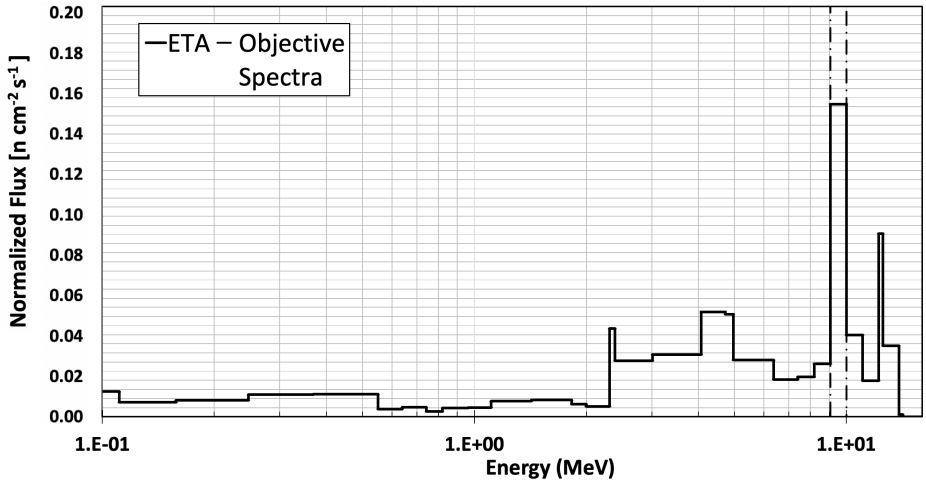

[b]

Figure 8.4: a) ETA produced by COEUS to reproduce a monoenergetic neutron spectrum of 10 MeV; b) Normalized continuous energy MCNP neutron flux per source strength and comparison to the objective of 10 MeV peak.

located as close as possible to the source. The conical shape allows to the ETA to be closer to the TCC by withing the opening angle requirements.

It is worth noting that the fitness is larger for this case than for the first example, 1.95 vs 1.7 due probably to the difficulty approaching a monoenergetic flux. The largest uncertainties are located for energies between 0-100 keV, has minimal effect on the resulting distribution

because the neutrons in this bin account for less than 5% of the overall spectrum achieved in the ETA. A non-negligible statistical uncertainty is though present around the 10 MeV peak and below 1 MeV with a calculated 10% in standard deviation. The increase in the fraction of neutrons below 10 keV is due to the introduction of low- and mid-Z materials, that are ideal for an elastic scattering perspective and enable the design to meet the NIF weight constraints. It is of significant interest to study the 8 to 10 MeV region as it is populated by neutrons with neutrons at energies produced mainly by inelastic scattering. The example shown in Figure 8.4 points out that it is possible to obtain more extreme spectra shifting if imposed constrains are lifted, thus demonstrating the enhanced ability of COEUS V2.0 to tailor neutron spectra.

8.3.2 Production of Iron Isotopes

Another element of interest is Iron, particularly Fe-56, which is also in the CIELO library [37] as a high-priority nucleus of study. Improved evaluated nuclear data are needed to create accurate ENDF-formatted files for general purpose transport applications, *e.g.* criticality, shielding, and activation like seen in the Aluminum case. Innovative reactor systems require improved inelastic scattering cross section data to meet target accuracy demands. New measurements and evaluations are needed in the 0.5-20 MeV range to reduce uncertainty down to 2-10% (depending on region). Substantial differences currently exist in data libraries, *e.g.* below 2 MeV the differences between JEFF-3.1 and ENDF/B-VII.1 reach 28%. Thus, it would be of interest to determine if similar integral benchmark using ^{56}Fe could be designed with Gnowee/COEUS.

Besides this initial application possibility, an additional example application of interest was investigated, using the same methodology for generating a specific Iron isotope. The isotope of interest is ^{60}Fe, for which production of neutrons below 14.1 MeV is needed. Through a series of experiments, the Radiochemistry Group at the NIF found that more Fe-60 is produced by neutrons below 10 MeV. Thus, a small ETA could be placed inside of the HTOAD to reduce the neutron spectra from 14.1 MeV to below 10 MeV. The objective here is to increase the number of atoms of ^{60}Fe in the sample. ^{60}Fe has a half-life of 1.5x10^6 years $\pm$ 20% and was found in deep sea sediments at a well determined depth. This has been interpreted as being due to the solar system passing through the remnant of a supernova explosion about 3 million years ago. ^{60}Fe arises in neutron reactions only as a secondary product from:

- ^{58}Fe(n,γ)^{59}Fe(n,γ)^{60}Fe
- ^{59}Co(n,p)^{59}Fe(n,γ)^{60}Fe
- ^{59}Co(n,γ)^{60}Co(n,p)^{60}Fe, etc.

At this time, the idea at the NIF is to explore the use of second-order reactions to produce ^{60}Fe, subsequent to the production of ^{59}Fe, during the same irradiation; thus, providing low-

energy neutrons to the sample is needed. The two interesting reactions in this case are ^{58}Fe(n,γ)^{59}Fe ($t_{1/2}$ = 45.1 d) and ^{59}Fe(n,γ)^{60}Fe ($t_{1/2}$ = 1.5x10^6 y). ^{58}Fe is the most neutron-rich stable isotope of iron but with low natural abundance of 0.28%. Isotope production via (n,γ) reactions is favored by lower energy neutrons than when production is via (n,p). The ^{59}Co cross section is also higher at neutron energies below 1 MeV. During a 14.1 MeV shot yielding 10^{16} neutrons, 3.6x10^9 atoms of ^{59}Fe will be produced. Assuming a cross section of about 1 mb for ^{59}Fe(n,γ), the total subsequent production of ^{60}Fe is 1x10^6 atoms. It was shown by experiments from the Radiochemistry group at LLNL, with a collection efficiency of 1%, that just 3 atoms of ^{60}Fe are present in the final sample. Thus, more ^{59}Fe production is needed to extract ^{60}Fe by increasing neutrons below 10 MeV. The intention behind spectrum tailoring is to devise means of producing a sufficiently intense flux of low-energy neutrons to increase the rate of ^{59}Fe(n,γ) production, in order to subsequently extract more ^{60}Fe nuclides.

8.3.2.1 ETA Design Simulations and Results for ^{60}Fe Production

The list of variables considered and their associated constraints are listed below:

- The main irradiation position option available for ride along experiments is at the SRC position which is distant nominally 50 cm from the TCC, inside the HTOAD seen in Figure 8.4. The HTOAD subtends approximately a 3.7x10^{-4} of solid angle from the TCC. The HTOAD has a volume of 65 cm^3, and an inner diameter of 4 cm, subtending approximately 3.7x10^{-4} of solid angle. It is possible to mount from gram-sized metal foils inside TOADs up to 100 grams sized samples inside the HTOAD with an inner diameter of 4 cm. The HTOAD size can be increased ideally further increase with the boundaries of a maximum length of 15cm and a maximum weight of 25 kg.

- The number of material elements inserted are constrained to 6 including the sample of interest, as more materials will increase the difficulty in building the assembly.

- In th BNCT case, the source is calculated using the full realistic model of the NIF and not just a point source.

- A set of materials is given similarly as for the first benchmark case seen in the previous Section.

- The objective function here changes from the previous cases. The objective is for a HTOAD to hold enough of a Co salt to produce around 3.6x10^9 atoms of ^{59}Fe.

The HTOAD-ETA design is shown in Figure 8.5.

The resulting amount of ^{59}Fe(n,γ) reactions matched well with 3.74x10^9 nuclides of ^{59}Fe in order to have 3600 atoms of ^{60}Fe. The ETA run to match the objective is faster than for other cases, less than 12 hours of running wall time, and less than 1000 designs have been evaluated. Most of the run time has been spent in order to improve the statistics in the

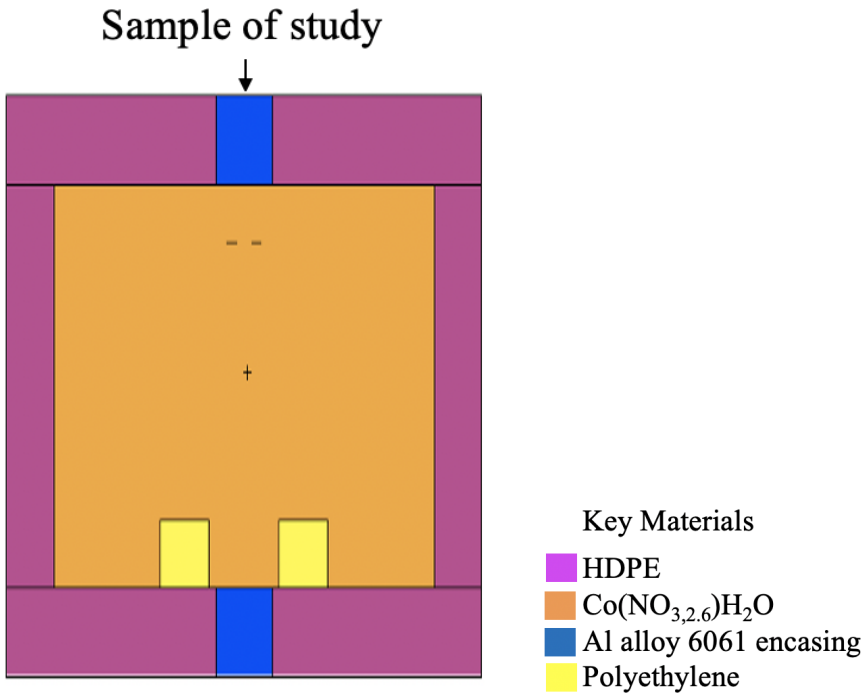

Figure 8.5: ETA produced by COEUS to reproduce an objective notional of ^{60}Fe production.

samples of Iron in the HTOAD as the neutron flux reaching the sample is 10^7 less than the source flux.

The ETA's dimensions are 5 cm for the radius and 10 cm for the length. The ETA proposed is slightly larger than the standard HTOAD, but still easy to build to fit in the SRC of the SNOUT. The material composition chosen for the ETA of interest is made of a HDPE cup inserted inside the HTOAD, which has been previously used as a combination of a cup of HDPE and the compound of $Co(NO_3)_{2.6}H_2O$, a cobalt salt, alternated with polyethylene elements. The lack of high-Z materials to thermalize the neutron spectra is a consequence of the weight and size limitation imposed. The construction of the HTOAD also utilizes a placement of Aluminum foils to trap recoils from the target foils, then the target foils and their trailing Al foils are counted together. An even further interesting exercises for the COEUS v2.0 code, and for future experiments, would be to increase the ^{59}Fe isotope production as carrier-free. In this way an ETA for isotope separation can be designed by starting with a target other than iron. A few guidelines on how the isotope separation can be performed with COEUS v2.0 is seen in Appendix C.

8.3.3 Application in Boron Neutron Capture Therapy

One of the most interesting and complex applications mentioned here is the use of Gnowee/ COEUS v2.0 for Boron Neutron Capture Therapy (BNCT) spectral shaping. BNCT is a

well-studied medical treatment used for many forms of cancer that has shown some promise in improving patient outcomes [5]. For the purposes of this report, the specific treatment considered a brain tumor known as Malignant Glioma [86].

BNCT is an alternative method to traditional cancer treatments and combines both the pharmaceutical and radiological approaches necessary to achieve highly selective tumor cell death. In particular, glioblastoma multiforme is an aggressive form of cancer of the brain's glial cells that presents an obstacle to traditional radiation therapy and surgery due to its propensity to develop microscopic tendrils, originating from the main tumor mass, which penetrate normal brain tissue. This form of cancer affects 7,000 Americans annually and is 90% fatal, usually within 10-12 months of diagnosis. The isotope ^{10}B, which has a high thermal neutron cross section, is selectively delivered to the tumor cells. The area is subsequently irradiated with neutrons, which deposit high doses in the tumor cells containing ^{10}B while largely sparing the normal cells. Because the human body and tissue mainly consist of water (a moderator from a physicist point of view) and the tumor is usually located several centimeters into the body, the neutron beam from the outlet of a treatment device should be epithermal (optimal range of 1-20 keV, depending on the depth of the tumor).

In the case of aggressive tumors, such as glioblastoma multiforme, it is crucial that the radiation treatment start as soon as possible, and that the optimal neutron beam characteristics are tailored to each patient case. It is also possible to have a single radiation treatment session (instead of 5 to 6 weeks of radiation treatment sessions) of less that 1 hour if all treatment parameters are optimized, including the optimal energy range of the neutron beams. The neutrons interact with the light nuclei of the tissue and are moderated down to the desired thermal energy range by the time they reach the tumor site. The cells with high amounts of boron (the tumor cells) will receive significant dose from the thermalized neutrons, while the healthy tissue receives much lower doses. In early 1990s, patients suffering from glioblastoma multiforme took part in clinical BNCT trials conducted at the Brookhaven National Laboratory's Graphite Research Reactor and the Massachusetts Institute of Technology's Research Reactor [5]. However, results from both studies were disappointing, due to a number of factors including less-than-optimal neutron beam characteristics and lack of a sufficiently tumor-selective ^{10}B compound. After the U.S. clinical trials were abandoned in 1991, clinical experimentation continued in other parts of the world, including Japan. One of the main reasons for the failed clinical trials in the United States was related to the less-than-optimal neutron beam characteristics, which the nuclear department team at UC Berkeley was able to show: several Ph.D. theses and related papers were published in late 1990s and early 2000s [118],[87].

One of the first optimization methodologies that was developed for tailoring neutron beams for such applications was a one-dimensional code, SWAN [119], developed at the UC Berkeley. Thus, most of the studies involved parametric optimization methodologies which were accomplished by Monte Carlo simulations on a large number of beam shaping assemblies in order to identify the optimal cases [87], [118]. In addition, the optimal methodology for one patient with a particular location and shape of tumor will not work for a different patient with a different location and tumor size. This unnecessarily limits the design space in ways

that can drastically impact the overall performance of the BNCT design as well as for other applications requiring shaping of the neutron spectra. An alternative methodology for BNCT is proposed here, using the Gnowee/COEUS to optimize the neutron energy spectra to be delivered to the tumor by maximizing the ration of tumor dose over tissue dose (12.5 Gy-equivalent)[87]. The nature of the metaheuristic algorithm makes the search routine problem independent and thanks to the newly improved v2.0 COEUS, the software package can be applied to such medical application.

8.3.3.1 ETA Design Simulations and Results

As for the previous ETA designs, the ETA for the BNCT is designed by locating it within the NIF chamber and it is designed to fit in the TANDM 90-348, either inside the SNOUT or in the DLP.

In the BNCT application, besides providing the opportunity for the new optimization software package to simulate an ETA of interest, the unique possibility to verify the optimization methodology towards previous methodology is given, using the same objective function. This type of study can be performed for all optimization applications, but there have not been many past optimization examples of complex BSA or ETAs in the NIF environment that could be used as benchmarks. The reference design used for the verification is [87] where the assembly and resulting flux are seen in Figure 8.6. This flux is calculated at the exit of this ETA, which should more accurately be referred to as Beam Shaping Assembly (BSA). The starting source for this work and the reference case is a monoenergetic D-T neutron spectrum of 14.1 MeV. It is important, however, to consider that there are changes in the facility's environment where the ETA or BSA are located for the two examples. For the ETA designed in this work, the assembly is ideally located inside the NIF TC and records the effects of the room return neutron scattering, which helps increase the number of neutrons at lower energies. Also, the NIF irradiation is prompt in hundreds of picoseconds, which is unique and not guaranteed in any other facility.

For the verification analysis, the comparison is performed at the level of the normalized neutron flux "per source strength" ($\frac{n \times cm^{-2} \times s^{-1}}{source\ n}$) and both methodologies use MCNP5 for the neutron simulation at the assembly window and inside of the tumor for consistency.

Table 8.1: BSA material from Ref. [87].

Region	Material
yellow	Lithiade Polyethylene
green	Lead
Pink	40% Al-60% AlF_3
Light blue	Iron
Orange	Bismuth

As for the previous ETA applications, the initial designs are made following a set of imposed constraints and an objective function and they are listed below:

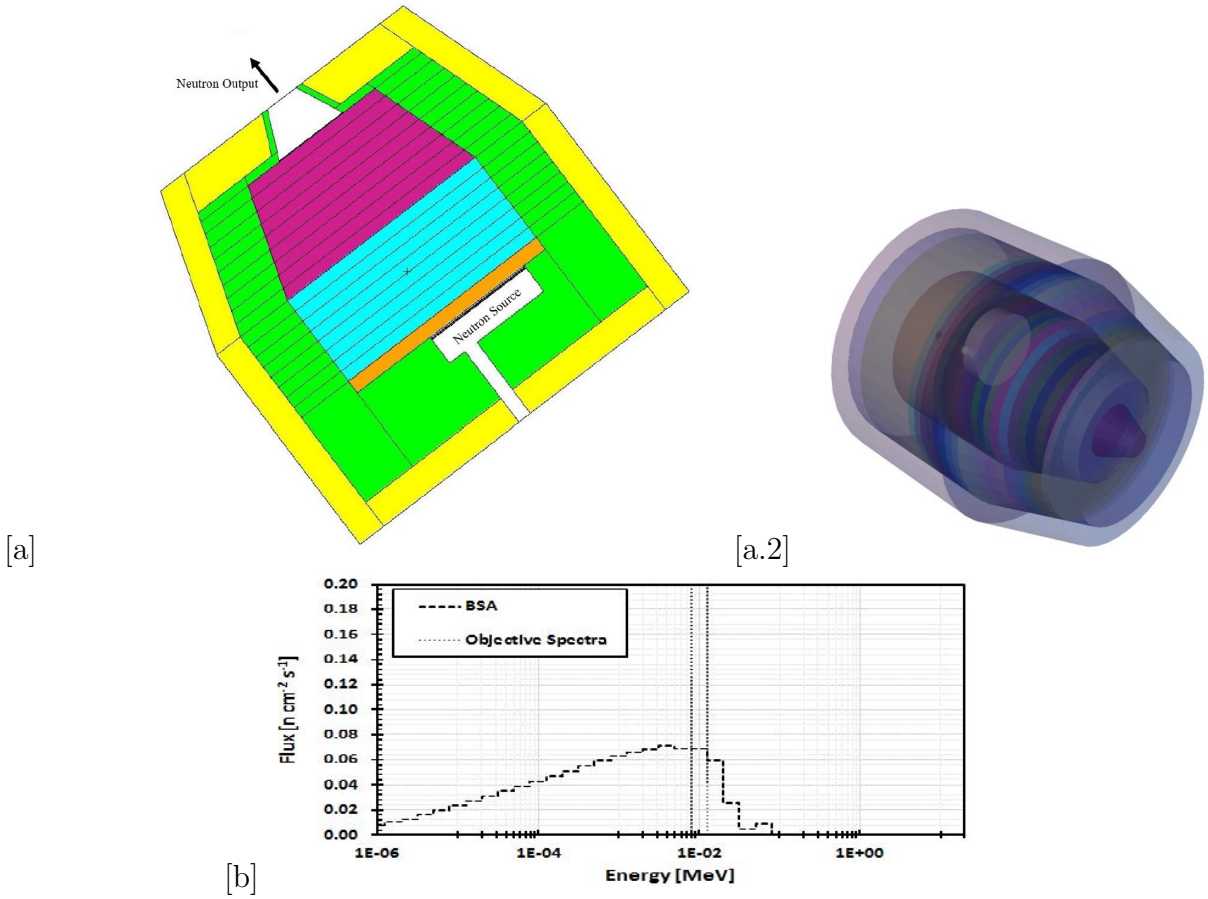

Figure 8.6: a) Schematic drawing of Dr. Verbeke's BSA design. Each color represents a different material, and the lines represent zones, or cells, of the design and presented in Table 8.1. b) represents the 10 keV monoenergetic neutron spectrum produced, the neutron flux is divided by source neutrons [87].

- The ETA dimensions are constrained to a maximum length equivalent to the 8 cm standoff from TCC up to 140 cm, and to a maximum radius of 50 cm.
- The number of material elements inserted are constrained to 10, adding more materials will increase the difficulty in building the assembly.
- The neutron source for the ETA comes from the SSR file created, "wssa", created while simulating the full NIF modeling as in the shot S2. The source for the BNCT utilizes the full realistic NIF model and not just a point source.
- The two objective functions are: the neutron spectra at the assembly exit, which is required to match the reference seen in Figure 8.6; and the ratio of tumor dose over patient normal tissue dose: D_t/D_p that needs to be maximized.

- The weight is constrained to 100 kg for the TANDM limitations.
- Activation foils are set to be inserted at the exit of the assembly in order to detect the flux, which will be used for the spectrum unfolding in the corresponding experiment and comparison with the COEUS v2.0.
- Minimum neutron flux intensity at the foils level of 6.86×10^8 n/cm^{2}s. No neutrons with energies above 40 keV at the patient skin are allowed for both objective functions.

From the previous experience it has been seen that for extreme neutron flux tailoring, neither the SNOUT nor the HTOAD are big enough, thus the limitations are studied. Also, the NIF guidelines are used here in order to build MCNP input-like file for COEUS, but due to the geometrical shape, there is no effective feasibility study available at the moment for the BNCT assemblies.

The current analysis is performed at two levels in order to compare the ETA with the BSA of reference. The BSA of reference is modeled following the limitation of having a quasi monoenergetic neutron flux at the exit of the ETA. The 10 keV limit [87] has been defined following few previous step analysis and simulation that starts from the dose maximization in the tumor respectively to the healthy tissue one. It has been identified that the ideal neutron spectrum at the tumor level is centered around 8 keV, and by performing further simulation it was identified that the flux at the BSA window is 10 keV instead. In the second part of the analysis, the goal is to optimize the ETA based on the neutron flux inside the head tumor, removing what before used to be a series of MCNP runs. Thus, one big advantage of the new methodology is demonstrated.

As a first step, COEUS is verified by comparing the neutron flux at the ETA window exit with the BSA by optimizing the assembly to the monoenergetic 10 keV spectrum. A comparison between the two assembly is also drawn. In the first part of the analysis, as mentioned, the results of the simulations with the new COEUS v2.0 are compared with the reference design flux of the ETA shown in Figure 8.6. For COEUS, the objective is located at the end of the assembly. COEUS is then run to generate an ETA given the starting source spectrum.

The resulting ETA designs and respective flux are presented in Figure 8.7 and Figure 8.8.

In the comparison with the ideal objective spectrum and the ETA referenced flux, it is possible to see that the ETA accomplishes a significant shift from a 14.1 MeV mono-energetic source and tries to match well the objective peak spectrum. The flux is driven towards the creation of as many 10 keV neutrons as possible.

The reference BSA is more or less of cylindrical shape with an outer diameter of 140 cm and a height of approximately 140 cm, while the new ETA is smaller with a length of 110 cm and a radius of 45 cm. The ETA has a reduced dimension from the original referenced case, expanding its use in more facilities in the future. This example shows how an automatic optimizations provides the possibility to reduce the assembly size while taking materials into consideration simultaneously. The ETA achieves to shift foor a much higher fraction of the

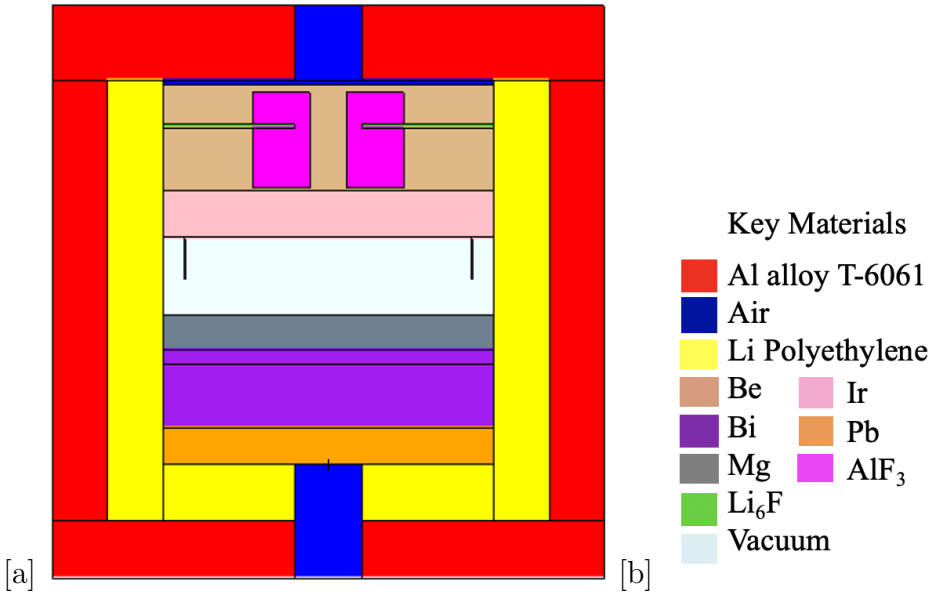

Figure 8.7: a) ETA produced by COEUS to reproduce an objective notional of 10 keV spectrum.

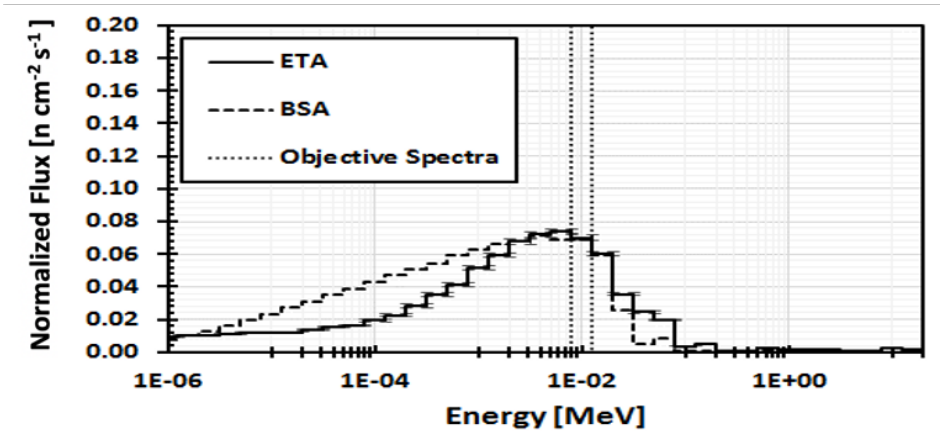

Figure 8.8: Normalized continuous energy MCNP neutron flux per neutron source strength compared with the objective function and the design in Figure 8.6.

flux (> 15%) in the 10 keV bin than the BSA design. It assessed fitness, of around 1.71, which was better than the 1.86 for the BSA design. The disagreement with the reference case is especially at the level of the spectrum tale, below 10 keV and > 40 keV, which includes the lowest fraction of the neutrons present.

Furthermore, the most impressive improvements are the quality of the shifted spectrum in a run of less than a week, with almost 5000 function evaluations. However, due to a large statistical uncertainty associated with the evaluation of the 10 keV bin for this ETA design,

there is a need of a computational running time that is increased compared to the previous application examples, using an HPC machine such as Savio [84] with multiple cores.

In the second part of the analysis, instead, the BNCT optimization is treated as an integral problem that includes the model of a patient's head, with a maximum normal tissue dose of 12.5 Gy-equivalent. Thus, the second analysis includes maximizing the D_t/D_p at the tumor level, which is required for finalizing the ETA optimization. The optimization process proceeds by testing different constraints and FOM: such as minimizing the dose to skin and healthy tissues and maximizing the dose to the tumor, which requires a spectrum of almost 8 keV inside the tumor region and the removal of neutrons with energies > 40 keV. The dose conversion factors are presented in Figure 8.9.

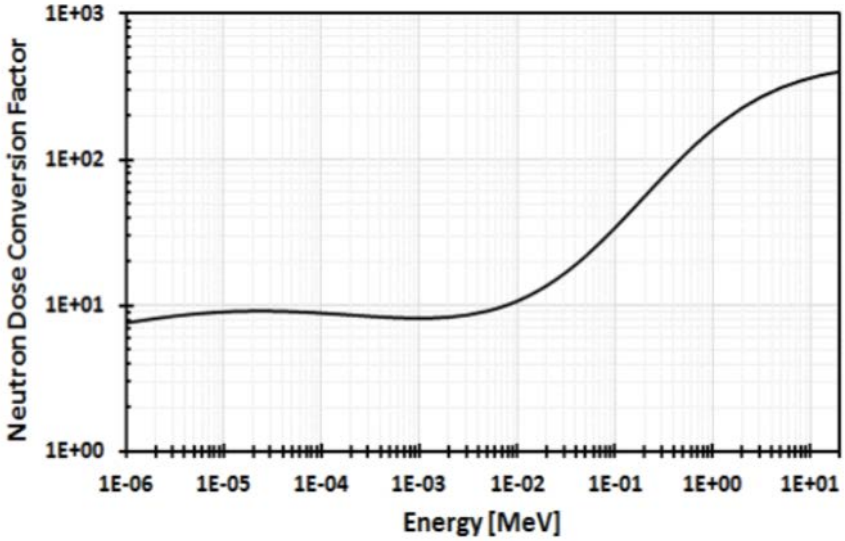

Figure 8.9: Dose Conversion Factor from neutron flux [87].

It is, in fact, necessary to remove neutrons above 40 keV as they are dangerous for the patient and as it boosts neutrons reaching the tumor.

As mentioned before, the new automatic optimization methodology optimizes the ETA considering the full environment space including the head, thus controlling the effects of the neutrons in the entire environment. This distinction is important because there is no guarantee that the spectrum will achieve a given dose ratio that is not degenerate. The advantage of having the whole NIF simulation might also increase the intensity of the BNCT lower energy source. Figure 8.10 shows the addition of the lithiated polyethylene head sphere model. The head is inserted following the same guidelines that have been used in the reference case, *i.e.* at 11.5 cm from the ETA surface of interest. The sphere has a 7.5 cm radius, an inner sphere at a depth of 8 cm from the head sphere, and with a 1-cm-radius representation of the tumor towards which neutrons will focus.

Thus, thanks to the newly improved COEUS version, it is possible to introduce several components in the optimization: the neutron generator or source of neutrons (*i.e.* the

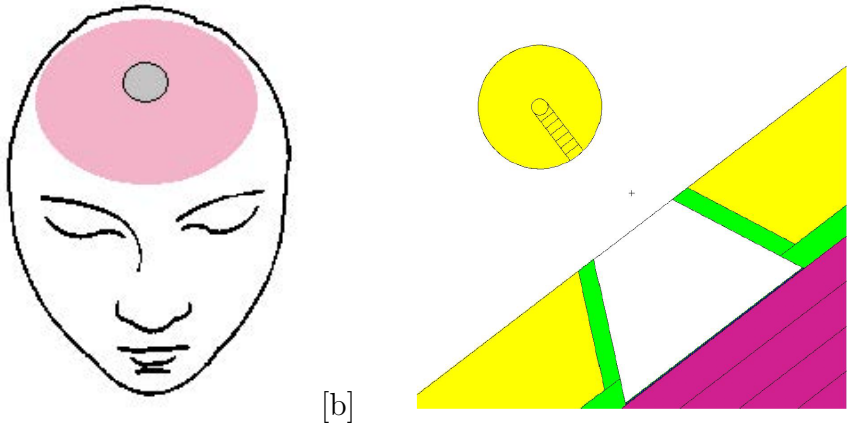

[a] [b]

Figure 8.10: a) Representation of the tumor location at 8 cm depth used to determine the 10 keV flux at the end of the reference ETA. b) shows the addition of the polyethylene head sphere model to the output of the ETA for the full model in COEUS v2.0. The little sphere shows the binning for use in conjunction with cell-flux tallies from MCNP.

NIF), the phantom head located apart from the ETA where the objective function is located and the ETA that ensures that the neutron energy flux is tailored providing an adequate energy output for the neutrons. One more step to be added in the future to improve the optimization, is a mechanism for the delivery of Boron to the tumor region. Thus, with Gnowee/COEUS v2.0 it is possible to include within one single run all of the optimization issues existing in the BNCT optimization: the ETA must be able to output into the tumor a neutron spectrum in the range of 8 keV accounting for the production rate of neutrons, the amount of neutrons lost in the moderation process inside the environment, and to allow for sufficient capture in Boron while at the same time reducing unwanted interactions inside of the head. Furthermore, the use of ADVANTG for the simulation provides the flexibility to improve the statistics in the various regions according to the dimensions of the geometry accelerating the running time.

The new resulting ETA is shown in Figure 8.11, while the normalized flux is presented in Figure 8.12, which is compared to the normalized flux, per neutron source strength, calculated inside of the tumor region using the reference BSA and compared to the objective spectrum.

The run has computed more than 6500 designs over 8 days, and as seen in Figure 8.11, shifts the neutron spectra extremely to 8 keV. The assembly has a height of 110 cm and an outer radius of 50 cm, which is larger than the one seen previously in Figure 8.7. Dimensions are still kept below the sizes of the reference design. The spectrum in the ETA is highly monoenergetic with more than 20% of the neutrons reaching 8 KeV, more than in the reference case (12%), which is another improvement.

One point to consider is that the number of neutrons reaching the tumor is hardly within the limit of 6.86×10^8 n/cm^{2}s, due to the ETA larger dimensions and the large number of

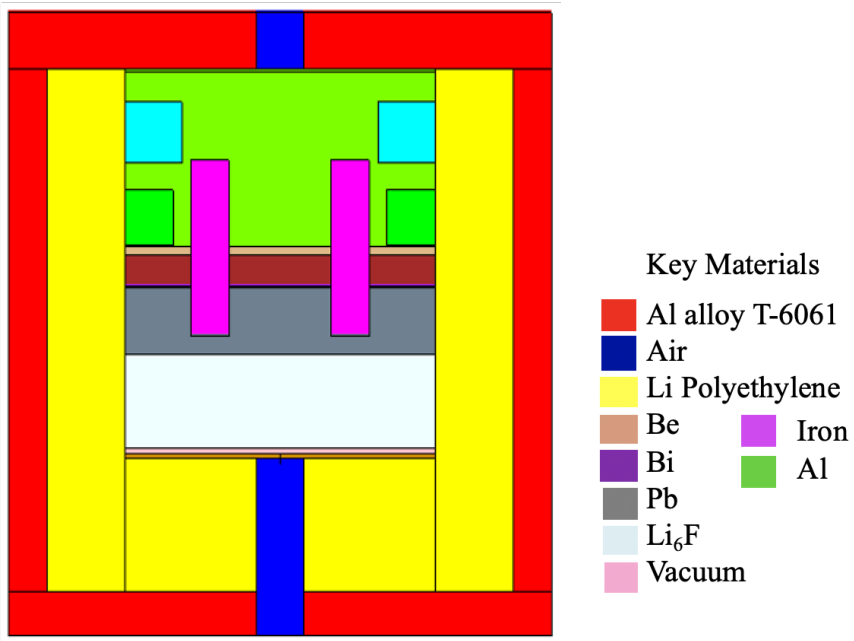

Figure 8.11: Cross-sectional view of the ETA.

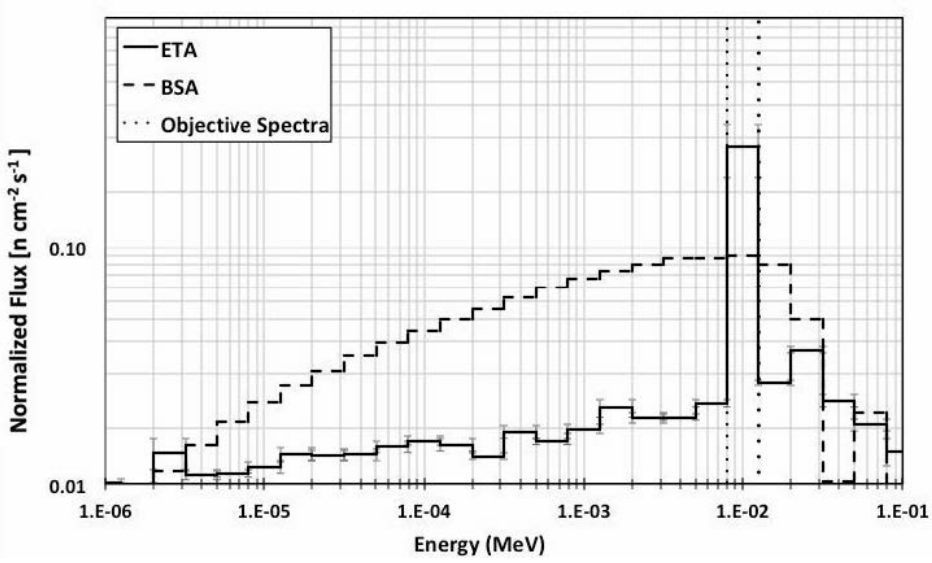

Figure 8.12: The normalized neutron flux inside of the tumor from the ETA, BSA and objective function.

neutrons dissipating in the space. This is important to mention since for different facilities with different neutron source output, such constraints should be taken into consideration. In addition, the weight reaches the 100 kg due to the size and high atomic density material chosen, which might make the assembly difficult to be inserted in alternative locations inside

the NIF or facilities.

The result and the comparison with the previous methodology is a successful representation of the methodology: the possibility to integrate a full system of a possible experimental set-up in order to tailor the neutron energy to a specific objective function maintaining limitation of numbers of neutrons, etc. New enhancements can been seen in the ETA design process as the objective function can be located inside the tumor and not just at the ETA exit window. Modeled results show promise for developing novel neutron spectra and capabilities. Gnowee/COEUS could be easily improved with minor modification to consider alternative neutron sources. As it is possible to see the assembly has been optimized in order to have a fully monoenergetic flux at 8 keV where neutron above 10 keV are eliminated.

Future studies could take advantage of the improved capabilities of COEUS v2.0 in order to add more details in the modeling and optimization, such as adding design constraints on the irradiation time and new FOM possibilities. The irradiation time is a function of the total dose delivered to the location of tumor required to kill cancer cells so this can be formulated as a minimum number of reactions, given specified source strength.

8.4 Summary and Future Experimental Configurations

This research leveraged and expanded upon the concept of previous beam shaping assemblies (BSAs) and moreover on the first ETA design example for the TNF application. The primary limitation with the BSA designed with the parametric approach that dominated the literature was the intensive user labor. Therefore, to maximize the utility of this research, a parametric point design approach was discarded in favor of formal optimization techniques with Gnowee/COEUS to design ETAs. However, the first version of the Gnowee/COEUS developed for TNF applications was limited to specific geometries, neutron source spectra, objective spectra, etc., even though the algorithm *per se* is problem independent. The largest improvement and contribution to the optimization is the added abilities to COEUS v2.0 to integrate a full MC model of the NIF environment and different objective functions. It has been shown through validation that the effects of the room-return neutrons are not negligible, as well as consideration of the possible measurement and simulation errors are important contributions to the final result. Several examples of ETA designs are presented in this Chapter, but many more could be developed as the design platform has been validated for the NIF. Also, such modeling framework could be easily applicable to other neutron generator facilities.

The applications described in Chapter 8 are examples and descriptions of how COEUS v2.0 can be used at the NIF or other locations. The proposed experimental ETA, designed with the new COEUS v2.0 and considering the lessons learned, has also undergone a scoping study at the NIF. The customized ETAs were designed to produce narrow energy ranges of 8-10 MeV for Integral benchmarking designs, or for isotope increase production, as for the

increase ^{60}Fe . Those spectra showed the various applications and capabilities available with the new COEUS v2.0 and that can be inserted in the experimental instrumentation seen in Chapter 7 with little engineering modification. Also, the application went a step further by introducing possible ETA designs to reproduce more extreme tailoring of the spectra, by reproducing a monoenergetic 10 MeV spectrum and the BNCT's 10 keV or 8 keV highly monoenergetic spectrum. Those last cases cab be inserted inside the NIF facility as DLP with more engineering manufacturing.

The presented applications and resulting ETAs presented in Chapter 8 introduce important contributions and can be used to highlight the success of the design framework developed from different points of view. First, this application shows the capability to successfully optimize an ETA within a complex system such as the NIF, providing satisfying results and impressive flux shifting. The applications presented in Chapter 8 are the first examples of applications with newly improved version 2 of the optimization code package.

Then, another contribution output from presenting the experiments of Chapter 7 and the design of the ETAs in Chapter 8, is to present and affirm the possible expanded capabilities of the NIF facility, which could contribute to a wide range of applications in the nuclear engineering field. In fact, starting from the introduced applications, any future application can be reproduce and tuned in a short time framework. It was seen that for all of the presented designs, it takes less than a week to run and reproduce an ETA of interest. In the modeling framework, the only time-consuming step is to run the full NIF modeling, which runs for a week- 10 days, but thanks to the implemented two-step methodology, there is no need to run the full model more than once during the optimization studies or experimental modeling.

During this research, due to constraints on the available time to complete this thesis, it wasn't actually possible to build an ETA of interest to insert inside the NIF chamber, for performing further validation. It is important, however, to be able to assess the quality of the predicted results without the need to run ETA tuning for the validation purposes, due to the time and cost to run any type of experiments at the NIF. This further justifies and highlights the importance of the work that has been performed in Chapter 7 for simplified experiments. Furthermore, it was possible to perform verification of the Gnowee/COEUS v2.0 methodology for the BNCT application by comparing the resulting assembly and flux of interest with the design methodology used in the past in the UC Berkeley Department of Nuclear Engineering [87]. From the verification it is possible to see that the new code is able to optimize a stack up of materials inside the ETA that satisfies the highly peaked monoenergetic flux requirement at the exit of the assembly and inside a tumor. Due to the complexity of neutron interactions with materials and the complex dependence of the reaction with the neutron energies, doing manual parametric study is not only time-consuming but also impossible to produce the most optimal ETA design. The effects in the neutron spectrum of the simultaneous consideration of multiple changing variables are in fact missing in the enumerative methodology. Thus, with the new methodology, the range of possibilities in designing ETA is wider and can both save in time and workforce for designing new tailored spectra.

The new version of the code will thereby greatly accelerate the pace of development in many areas of nuclear engineering that need neutron spectra with specific desired characteristics: detector calibrations, study of radiation damage in different materials, cross section measurements, materials science, design of targets for the production of medical isotopes, or medical applications such as BNCT or various shielding applications. The development of a generalized and validated optimization software COEUS v2.0 will enable to expand upon the capabilities of the neutron generators at a fraction of the cost in terms of manpower and research effort rather than building and designing alternative facilities. Furthermore, Gnowee/COEUS v2.0 is a great improvement from the enumerative optimization methodology, as the effect of all the variables and constraints on the neutron energy and direction path are accounted in a single run. There is no need for manual analysis of single material characteristics, sensitivity analysis, etc., that beyond being just time intensive is also more prone to human errors and require special user abilities. Moreover, the improved and validated framework has the advantage of accessibility.

It can be seen throughout this Chapter that limitations to ETA models are often imposed by the facility constraints or the material availability, more so than by the software itself. The possibility to recreate, within those constraints and in a relatively short amount of time a high-fidelity modeling for neutron tailoring, is unique. For example, what took months of workforce for designing a BSA (or "manual ETA") for BNCT application [87], now takes less than a week. Also, the metaheuristic algorithm allows to consider the cross interaction of the variables. Gnowee/COEUS framework developed herein also allows for a user with limited knowledge of the optimization methodology/cross section or MC characteristics, to design an ETA for the objective function of interest.

In the first two applications, no comparison is performed with alternative methodologies, but code verification can be done at the level of the BNCT application. The BNCT resulting designs are compared with the results from previous studies at UCB where enumerative methodologies were used [87]. It is possible that the successful optimization methodology will speed up breakthroughs in the biomedical field of targeted cancer therapies and in the commercialization of neutron beam production facilities. The metaheuristic software package enables the expansion of the capabilities of a neutron generators at a fraction of the cost in terms of manpower and research effort rather than building and designing alternative facilities. In addition, the new optimization methodology improved extensively respectively to the enumerative methodology that have been performed. The variables that influence the energy and path changes of the neutrons are considered in one single run, without the need for sensitivity or parametric study of each material or dimension.

Inside the NIF, the ETAs are designed to be mounted inside the SNOUTs and HTOAD, as a separate DLP, on the 90-78 DIM or 90-348 TANDM. Thus, the experience from the experiments presented in Chapter 7 serves to facilitate the design process, thanks to the newly developed MCNP model of the 3D NIF TC, and the experimental set-up. It presented in Chapter 7 that the proposed ETA designs are aimed to be "ride-along experiments with low risk and have a reasonable cost. Building preliminary designs might require the refining of the conceptual design, once it assessed the key sensitivity affecting the performance and

costs of the identified optimized design. It follows experimental analysis which will be no different from the one seen in Chapter 7 for this work.

Chapter 9

Conclusions and Future Directions

9.1 Conclusion

In numerous research fields there is an interest in accurate and efficient methodologies that can be used to tailor available neutron spectra to the specific application needs, including detector calibrations, study of radiation damage in different materials, cross section measurement and validation, materials science, design of targets for the production of medical isotopes, or medical applications such as Boron Neutron Capture Therapy (BNCT). Neutron sources with energies needed for those and other applications often do not exist. The main goal of this dissertation is the development of an efficient optimization software tool for tailoring neutron spectra produced in various neutron generating facilities, including the National Ignition Facility (NIF), for various applications. Specifically, a proof-of-concept platform has been developed and applied at the NIF to efficiently and accurately design various Energy Tuning Assemblies (ETA) to mimic neutron energies of interest to national security applications. ETAs are assemblies designed by the optimization package to produce the desired exit neutron spectra, by optimizing the number of neutrons having a specific direction and energy. The developed platform is general enough to be applied at other neutron generating facilities and for other applications within nuclear science and engineering. The dissertation research included specific design steps: identification of the neutron transport simulation code package, *i.e.* MCNP; further development of a fast and efficient optimization methodology for tailoring neutron energy, *i.e.* Gnowee/COEUS; development of experiments for validation of optimization tools; use of the optimization package for specific ETA designs; and performing simple ETA experiments and/or comparing optimized ETA designs with previously published results. Previous ETA research has shown particular difficulties in designing and assembling materials to customize the neutron spectra using neutron filters or neutron thermalization using low-Z moderators. A primary limitation in the past ETA design procedures was a very slow and time-consuming parametric study approach. Thus, there was a need for a more coherent, generalized, and efficient optimization methodology, that would allow for an automated (or a "black box") approach to optimal choice of materials and geometric

configurations. The UC Berkeley developed software package Gnowee/COEUS is based on the metaheuristic optimization approach, solved this problem. The ETA design process resembles a complex multidimensional and multi-variable optimization problem, and currently similar optimization methodology applicable to neutron energy tailoring does not exist.

This dissertation first introduces the initial version of the optimization code that was developed to design an optimal ETA transforming a monoenergetic 14.1 MeV neutron flux at the NIF into a thermo-nuclear prompt fission spectrum (TN+PFNS). Gnowee/COEUS uses a hybrid metaheuristic framework based on a set of diverse and robust heuristics, which appropriately balances diversification and intensification strategies across a wide range of optimization problems. Use of Gnowee has previously demonstrated superior flexibility and convergence characteristics over a wide range of design spaces. COEUS on the other hand builds and performs radiation transport of ETA designs based on Gnowee's permutations of design space variables to evaluate ETA design performance against the objective spectrum. The radiation transport is conducted with a hybrid approach that uses ADVANTG to perform adjoint Denovo deterministic transport calculations. ADVANTG develops weight windows for speeding up stochastic MCNP transport calculations. COEUS takes advantage of the embarrassingly parallel nature of metaheuristic optimization and Monte-Carlo methods.

Although the original version of Gnowee/COEUS was able to produce successful ETA designs and to mimic TN+PFNS spectrum, it had limitations. These restrictions mainly involved the use of the COEUS code, which was problem-oriented and not as generic as the algorithm. This dissertation presents the efforts undertaken in order to increase the applicability and use of COEUS towards wider applications. The new version of the code includes a newly-developed user input method. The proposed method uses a modified MCNP input deck as the primary user input definition for COEUS. The new input deck improves the usability by mimicking input formats familiar to a large segment of potential users. This approach allows the ETA geometry to be generalized within the boundaries of the radiation transport code itself. The ETA design can now be simulated inside the full NIF Target Chamber (TC) model, thus having a detailed MCNP model of the configuration is fundamental. It was crucial during this research. to understand and model the NIF TC accurately in order to obtain a high fidelity optimization that includes all the neutron's contribution from room-effect and a realistic source spectrum. Chapter 7 highlights the contribution to the NIF MCNP model: the newly added DIM and TANDM (90-124, 90-348), the SNOUTs and HTOAD, and the flux monitors (foil packs). In addition, several improvements are made to the original MCNP model of the NIF TC by introducing an efficient two-step design methodology and the MCNP/Denovo coupling as a variance reduction technique. Furthermore, thanks to the improved COEUS, it is possible to consider a realistic neutron source, instead of a monoenergetic 14.1 MeV point source. Those newly-added COEUS capabilities allows the ETA design process to overcome the large sources of errors present in the first version of the code.

A new class of constraints and objective functions has been added in the improved code, which allows for incorporation of user-defined function and methods. The updated con-

straints and objective classes are based on the Gnowee classes perform the same basic functions, and benefit from the tally flexibility allowed by the newly MCNP deck user input method. The constraints are defined either as upper and lower boundary values for continuous variables, or as a list of possibilities for discrete variables. More constraints can be added as mathematical function, *i.e.* the weight, the density, the total volume, etc. Additionally, the new variable definition input system allows the user to define any material library of interest for COEUS, removing the hard-coded dependence on PyNE [85].

In the same user-friendly philosophy for the new COEUS version, the user input file for ADVANTG has been migrated to an ADVANTG-style input format. This system allows for a wider range of ADVANTG options to be selected, while streamlining the user input process. Additionally, the efficiency of the ADVANTG-generated weight windows is improved by the addition of a module that is used to track the suitability of the weight windows to the generated designs.

Finally, the use of the MCNP-like input allows for full tally specification for any possible design constraints and objective functions. In the new input file version, the variables are defined for the ETA directly within the NIF MCNP mode and are defined as a list. The variables can be any element within the MCNP file and can be identified as discrete, continuous, binary, or combinatorial.

The main focus of this dissertation is the generalization and flexibility in terms of choosing the variables of interest, including the geometry and the constraints. The newly-improved code gives the ability to simulate realistic neutron sources, including the room-return effects, as well as to employ user-defined materials. The expansion of the code allowed the design of different ETAs of interest in the investigated NIF environment, at the SNOUT level for the TANDM 90-348 and at the HTOAD level on the DIM 90-78. It also made it possible to design spherical and cylindrical ETAs to reach the energies of 8-10 keV for cross section analysis, for monoenergetic spectra inside tumors in the case of BNCT studies, or for specific isotope production. Documentation, version control, testing, verification, and validation are indispensable parts of software development. These processes are followed meticulously to ensure high-quality open source codes that promote open science and reproducible research.

Following development of the code, a set of experiments was performed at the NIF for validation. A series of integral experiments was designed and inserted in the TC using ride-along shots with the available instrumentation, the HTOAD and the SNOUTs on DIM 90-78 and TANDM 90-348. The focus was to design a set of experiments which could be performed efficiently at the NIF and that could be reproducible in other facilities as well. The campaigns were successful, and improved the understanding and capacities of the modeling framework developed for future ETA experiments at the NIF. Both the SNOUT and the HTOAD can be used as the ETA encasing by stacking materials of interest in a controlled environment. The latter is achieved after properly validating MCNP modeling of the NIF environment and comparing the simulation results with the empty HTOAD and SNOUT campaigns. The MCNP code is used to model the full NIF target chamber with three-dimensional neutron transport, with explicit geometrical double heterogeneity, and continuous energy nuclear data which gives the highest fidelity of the final results. In addition, to facilitate the full

NIF modeling, an input maker code was developed in Python including all the available components that could be necessary for this type of experiment, for nuclear engineering applications and for inserting ETAs. The main effort in the initial MCNP modeling was focused on the extraction of meaningful information from the MCNP simulations of the full NIF TC, in order to properly reconstruct sources for the ETA analysis. Some of the statistical counting uncertainties and modeling errors in previous models are so large to mask nuclear data uncertainties. Large discrepancies can be the result of inaccurate modeling or uncertainties in the experimental data. Consequently, the goal of this work was to address these problem areas, as well as ensure that the experimental data used in evaluations have realistic uncertainties. Improving the uncertainties on the modeling and on experimental data was the first step in isolating the effect from the cross-section uncertainties.

Several initial validation experiments, at the NIF, produced satisfactory results. Material and geometrical properties used in MCNP are sufficiently well-modeled, and results show that the NIF 14.1 MeV spectrum can be modified with few of the essential materials, such as High Density Polyethylene (HDPE), Iron, and Aluminum. In the first experiments, those with empty SNOUT and HTOAD, there are differences between the measured and simulated results. These differences are expected due to the position of the measuring point as well as the effects of room return, scattering inside the NIF TC, and inside the SNOUTs and HTOAD. It is important for the MCNP modeling to be consistent, complete, and realistic. In this dissertation, all three aspects are addressed, and several quantification of uncertainty are presented.

Since partial ETA data sets are collected, models are used to gain insight into nuclear data issues where the model diverges from experimental ETA performance; propagation of nuclear data uncertainties into the modeled results of the NIF would be beneficial and worthwhile. For example, it was found that some nuclear data are inadequate for a well-know nuclear reaction ^{58}Ni(n,p)^{58}Co within the Nickel activation foils. Large effects on the comparison of the simulated results to the measurements from poorly-known inelastic neutron scattering cross sections for Aluminum and Iron are identified. Neutrons between 4 MeV and 10 MeV recorded on the foils are produced by elastic and inelastic scattering and largest errors are present in this energy range. Accurate consideration of those uncertainties will allow for realistic evaluation of the impact of each uncertainty in the uncertainty propagation for full ETA models. Cross-section uncertainties in the modeling are provided using SCALE code, where the models of the SNOUTs and HTOAD are being reproduced. The research featured here has included the modeling and design of the experiments as well as the data analysis of the results, which will be the same for all ETA experiments; hence, it was important to categorize all possible uncertainties and errors that can affect final results.

Also, it is important to consider that the flux comparison performed using the PNNL unfolding code, STAYSL, which introduces uncertainties in the nuclear data, and could be improved in the future by adding other detectors for direct flux detection. Uncertainty analysis characterizes the spread of the response function, and sensitivity studies compute the contribution of an individual parameter on the uncertainty. This aligns with the interest of determining only uncertainties from nuclear data propagation. Overall, these efforts in

quantifying uncertainties in the neutron transport simulations by simple ride-along validations experiments are useful for future designs. The output desired from the ETA designed with Gnowee/COEUS coupled with SCALE are *i.e.* the resulting flux or reaction rate, and they have only the uncertainty information of the nuclear cross sections uncertainties.

The examples of application of COEUS v2.0 are described in Chapter 8 are specifically designed to be used at the NIF, but the same design methodology can be applied for other facilities. The proposed experimental ETA, designed with the new COEUS v2.0 has undergone a scoping study at the NIF. The customized ETAs are designed to produce a narrow energy range between 8-10 MeV for integral benchmarking designs, for isotope production, *i.e.* increase of ^{60}Fe production. Those tailored spectra show the various applications and capabilities of the new COEUS v2.0. The ETA designs here optimized can be inserted in the experimental instrumentation with little engineering modification, as seen in Chapter 7. Also, more complex applications are: performing ETA designs to tailor the 14.1 MeV neutron spectrum to reproduce a monoenergetic 10 MeV spectrum and 10 keV and 8 keV neutron spectra. The two last applications are performed within the BNCT research framework with the goal of designing more complex DLP to insert at the NIF. These applications and resulting ETAs are summarized in Chapter 8, confirming Gnowee/COEUS v2.0s performance for a wide range of applications.

Another contribution from both the experiments performed and the ETA designed for future experiments is the possibility of expanding the use of the NIF facility. It is demonstrated how designing experiments using the SNOUTs, HTOAD or ETAs can take less than a month. In the modeling framework, the only time-consuming step is running the full NIF modeling (10 to 14 days), which is done only once thanks to the two-step methodology implemented. The time constraint of this thesis meant that it was not possible to build an ETA of interest to insert inside the NIF chamber in order to perform further validation. However, the quality of the predicted results are assessed through validation and verification in Chapter 7, where an example of verification was given for the BNCT ETA design. The neutron fluxes resulting from the Gnowee/COEUS-optimized ETA are compared with the neutron fluxes predicted with previous methodologies at UC Berkeley [87], [120]. This verification analysis shows that the newly-improved optimization code is able to tailor more efficiently the neutron flux with the designed ETAs. The new ETAs satisfy the required high monoenergetic flux peaks of 10 and 8 keV both at the exit of the assembly and inside a tumor. The complexity of neutron interactions and the high dependence of each reaction with the neutron energy makes the parametric methodologies more prone to mistakes and approximations. Thus, with the new methodology, the range of possibilities in designing ETAs is larger and can both improve time and workforce, and reduce approximations in designing new tailored spectra.

The new version of the code accelerates the pace of development in many areas of nuclear engineering that need neutron spectra with specific desired characteristics: detector calibrations, study of radiation damage in different materials, cross-section measurements, materials science, design of targets for the production of medical isotopes, various shielding applications, and medical applications such as BNCT. The development of a generalized

and validated optimization software COEUS v2.0 will expand the capabilities of the neutron generators at a fraction of the cost in terms of manpower and research effort rather than building and designing alternative facilities.

Finally, the study and the experiments performed with the SNOUTs and HTOAD revealed a new experimental capability for low risk and reasonable cost experiments. The capabilities developed in this research are unique on many levels. This research leveraged and expanded upon the previous concept of ETAs using high level optimization techniques and simple "ride-along" experimental setups at the NIF and of the previous ETA designs.

9.2 Future Work Directions

Having completed the initial goal, *i.e.* the initial COEUS generalization, there is still work that could be done as the code is made available and open to the nuclear engineering community. The current COEUS v2.0 and ADVANTG/MCNP package allows to design efficient ETAs for various neutron generator environments, which was the objective of this work. However, many features could be further expanded. Several MC codes are available for different applications, and thus there is need to create appropriate COEUS input files for each software package to broaden the current use. COEUS would gain even more usability if additional features are incorporated, a few of which are provided in this thesis by the author and other collaborators.

Releasing the source package openly has benefits to the nuclear engineering community, including providing potential users with a convenient and transparent way of obtaining the software package, as well as allowing for valuable contributions from the community. Community contributions could help with validating further the software, since more examples will be analyzed and more experiments will be compared to simulations. The initial models have been developed and compared, but further updates still need to be performed to test the full propagation of nuclear data uncertainties with SCALE by adding a few multi-materials experiments in the SNOUT.

Furthermore, for several ETA applications in the medical field, further work could be performed in defining an automatic routine to determine the type of constants and ETA weight to convert objective functions for various type of doses and to customize Figure of Merits (FOM). Also, if objective functions correspond to detector responses, it could be of interest to support different types of post-processing information. Calibration and experimental uncertainties can affect the optimization results besides the data uncertainties; seeing those details in the final results would be useful while performing the optimization. The application of the optimization software package could be expanded to the design of nuclear reactors whose complexity could be evaluated especially for Generation IV reactors, as well as for nuclear detonation detection.

Finally, powerful machine learning algorithms are now ubiquitous, open-source, and free for anyone to use. Our community is not quite prepared to use those modern tools, given the fragmented and limited databases of nuclear data that can be used at this point. But

in the nuclear field, machine learning techniques could be employed in order to improve in the areas of "learning speed", non-linear data handling, and complex feature identification. The implementation of classes of machine learning systems to the Gnowee/COEUS optimization software could record all the run designs from previous ETA and identify the best initialization design for following optimization processes. Also, genetic algorithms could be used to identify sources of nuclear data uncertainties, within existing integral benchmarking. A framework based on genetic algorithms can be implemented to identify and remove the source of largest uncertainties, which can be a material at a specific energy range. Additional useful future features could include adding MC code capability into the optimization as the neutron-photon coupling in order to record and constrain gamma spectra in space or energy.

The possibility of building and using preliminary designs of ETA inside the NIF is the next step following this work. Few ETA simulations have been designed and could be processed through experimental analysis development: engineering designs at the NIF, insertion within one of the described shots and the radiochemistry and gamma spectroscopy of post-shot analysis, all of which have been predicted and tested in this work.

Bibliography

[1] J. Chadwick. "The Existence of a Neutron". In: *Proceedings of the Royal Society of London* Series A.136.830 (1932), pp. 692–708. URL: https://royalsocietypublishing.org/doi/pdf/10.1098/rspa.1932.0112.

[2] K.S. Krane. *Introductory Nuclear Physics*. John Wiley & Sons, 1987. ISBN: 9780471805533. URL: http://books.google.com/books?id=ConwAAAAMAAJ.

[3] Peter Airey, Thomas Hinton, and John Twining. *Radioactivity in the Environment*. Elsevier, 2012. ISBN: 978-0-08-045015-5. URL: https://doi.org/10.1016/B978-0-08-045016-2.00001-1.

[4] Ehud Greenspan and Y. Karni. *BNCT Beam Quality Maximization*. Springer, Boston, MA, 2001. ISBN: 978-1-4615-1285-1. DOI: https://doi.org/10.1007/978-1-4615-1285-1_55.

[5] F. Barth et al. "Boron neutron capture therapy: realities and prospects". In: *Nuclear Science and Engineering* 70.2 (1992), pp. 2995–3001.

[6] James Bevins. "Targeted Modification of Neutron Energy Spectra for National Security Applications". PhD thesis. University of California, Berkeley, 2017.

[7] Lawrence Livermore National Laboratory. *National ignition facility*. 2017. URL: https://lasers.llnl.gov/.

[8] John Lindl. "Development of the indirect-drive approach to inertial confinement fusion and the target physics basis for ignition and gain". In: *Physics of Plasmas* 2.11 (1995), pp. 3933–4024.

[9] John D. Lindl et al. "The physics basis for ignition using indirect-drive targets on the national ignition facility". In: *Physics of Plasmas* 11.2 (2004), pp. 339–491.

[10] E.I. Moses. "The national ignition facility and the promise of inertial fusion energy". In: *Fusion Science and Technology* 60.1 (2011), pp. 11–16.

[11] D.T. Casey et al. "Measuring the Absolute Deuterium-Tritium Neutron Yield Using the Magnetic Recoil Spectrometer at OMEGA and the NIF". In: *The Review of Scientific Instruments* 83.10 (2012), p. 10D912. ISSN: 1089-7623. DOI: 10.1063/1.4738657. URL: http://www.ncbi.nlm.nih.gov/pubmed/23126915.

[12] S. Bogetic et al. "Metaheuristic Optimization Method for Neutron Spectra Shaping". In: *Transactions of the American Nuclear Society* 118 (2018), pp. 455–458.

[13] David J. Lawrence et al. "The Psyche Gamma-Ray and Neutron Spectometer: Characterizing The Composition of a Metal-Rich Body Using Nuclear Spectroscopy". In: *47th Lunar and Planetary Science Conference* (2016). URL: https://www.hou.usra.edu/meetings/lpsc2018/pdf/2114.pdf.

[14] J. Bevins and R. Slaybaugh. "Gnowee: A Hybrid Metaheuristic Optimization Algorithm for Constrained, Black Box, Combinatorial Mixed-Integer Design". In: *Nucl. Technol.* 205.4 (2018), pp. 542–562.

[15] J. E. Bevins. *Coeus V1.0*. 2017. URL: https://github.com/SlaybaughLab/Coeus/releases.

[16] *How ICF Works*. URL: https://lasers.llnl.gov/science/icf/how-icf-works.

[17] Shaughnessy D. A. et al. "Radiochemical Determination of Inertial Confinement Fusion Capsule Compression at the National Ignition Facility". In: *The Review of scientific instruments* 85.6 (2014), pp. 1089–7623. ISSN: 1089-7623. DOI: 10.1063/1.4883186. URL: http://www.ncbi.nlm.nih.gov/pubmed/24985820.

[18] X-5 Monte Carlo Team. *MCNP– A General Monte Carlo N-Particle Transport Code, Version 5*. Tech. rep. LA-UR-03-1987. Los Alamos National Laboratory, Apr. 2003. URL: https://laws.lanl.gov/vhosts/mcnp.lanl.gov/pdf_files/la-ur-03-1987.pdf.

[19] Mosher S.W. et al. *ADVANTG – An Automated Variance Reduction Parameter Generator*. Tech. rep. ORNL/TM-2013/416, Rev. 1. Oak Ridge National Laboratory, Aug. 2015.

[20] B. T. Rearden and M. A. Jessee. *SCALE Code System*. Tech. rep. ORNL/TM-2005/39, Version 6.2.1. Oak Ridge National Laboratory, 2016.

[21] Jorma Sandberg. "Determination of Particle Flux Spectra with Multireaction Activation Detectors". In: *Acta Polytechnica Scandinavica* 146 (1984).

[22] Gregory J. Schmid et al. "CVD diamond detectors for current mode neutron time-of-flight spectroscopy at OMEGA/NIF". In: *Charged Particle Detection, Diagnostics, and Imaging* 4510 (2001). DOI: https://doi.org/10.1117/12.451260.

[23] J. Turner. "Atoms, Radiation, and Radiation Protection". In: *J. Phys. G: Nucl. Part. Phys.* (2008).

[24] James J. Duderstadt and Louis J. Hamilton. *Nuclear Reactor Analysis*. New York, NY: John Wiley & Sons, 1976.

[25] International Atomic Energy Agency. *Evaluated Nuclear Data File (ENDF)*. 2018. URL: https://www-nds.iaea.org/exfor/endf.htm.

[26] C. L. Dunford. *Online Service retrieval code package written by C. L. Dunford*. National Nuclear Data Center, Brookhaven National Laboratory.

[27] James E. Turner. *Atoms, Radiation, and Radiation Protection*. John Wiley & Sons, 2008. ISBN: 9783527616985. URL: https://onlinelibrary.wiley.com/doi/book/10.1002/9783527616978.

[28] A.J. Koning and D. Rochman. "Modern Nuclear Data Evaluation with the TALYS Code System". In: *Nuclear Data Sheets* 113.12 (2012), pp. 2841–2934.

[29] H. Salmon et al. "(n,2n) and (n,3n) Neutron Induced Reaction Cross Sections above 8 MeV". In: *Acta Physica Polonica, A* 128.2B (2015), B231–B235.

[30] K. Shibata, O. Iwamoto, and T. Nakagawa et al. "JENDL-4.0: A new library for nuclear science and engineering". In: *Journal of Nuclear Science and Technology* 48.1 (2010), 1fffdfffdfffd–30. DOI: 10.1080/18811248.2011.9711675.

[31] A. Koning, R. Forrest, and M. Kellett et al. *The JEFF-3.1 Nuclear Data Library*. Tech. rep. 1. 2006, p. 30.

[32] D. A. Brown, M. B. Chadwick, and et al. R. Capote. "ENDF/B-VIII.0: The 8th Major Release of the Nuclear Reaction Data Library with CIELO-project Cross Sections, New Standards and Thermal Scattering Data". In: *Nuclear Data Sheets* 148.1 (2018), p. 142. DOI: 10.1016/J.NDS.2018.02.001.

[33] K. Shibata, O. Iwamoto, and T. Nakagawa et al. *International Reactor Dosimetry File 2002 (IRDF-2002)*. Tech. rep. 1. 2006, p. 30. DOI: 10.1080/18811248.2011.9711675. URL: https://www.iaea.org/publications/7069/international-reactor-dosimetry-file-2002-irdf-2002.

[34] L. Greenwood et al. "Testing and Improving the International Reactor Dosimetry and Fusion File (IRDFF)". In: *Tech. Rep.* (2017).

[35] M. R. Bhat. "Evaluated Nuclear Structure Data File (ENSDF), in: S. M. Qaim (Ed.)" In: *Nuclear Data for Science and Technology, Springer Berlin Heidelberg, Berlin, Heidelberg* 48.1 (1992), 817fffdfffdfffd–820. DOI: https://doi.org/10.1007/978-3-642-58113-7_227.

[36] L. A. Bernstein, D. A. Brown, and A. J. Koning et al. "CSEWG Covariance Committee, Guidance on Generating Neutron Reaction Data Covariances for the ENDF/B Library". In: *Tech. rep., Brookhaven National Laboratory* (2013). URL: http://www.nndc.bnl.gov/csewg/covdocs.jsp.

[37] D. A. Brown et al. "The 8th Major 280 Release of the Nuclear Reaction Data Library with CIELO-project Cross Sections, New Standards, and 281 Thermal Scattering Data". In: *Nucl. Data Sheets* 148 (2018), pp. 177–186.

[38] A. Koning, D. Rochman, and J.-C. Sublet et al. "TENDL: Complete Nuclear Data Library for Innovative Nuclear Science and Technology". In: *Nuclear Data Sheets* 155 (2019), p. 55. DOI: 10.1016/j.nds.2019.01.002.

[39] N. Otsuka. "EXFOR Formats Manual, Tech. Rep. January, International Atomic Energy Agency Nuclear Data Services". In: *Tech. Rep. January, International Atomic Energy Agency Nuclear Data Services* (2006). URL: https://www-nds.iaea.org/nrdc/basics/.

[40] L. A. Bernstein, D. A. Brown, and A. J. Koning et al. "Our Future Nuclear Data Needs". In: *Nuclear Data for Science and Technology, Springer Berlin Heidelberg, Berlin, Heidelberg* 69.1 (2019), 817fffdfffdfffd–820. DOI: 10.1146/annurev-nucl-101918-023708.

[41] Roy C. J. and W. L. Oberkampf. "A Comprehensive Framework for Verification, Validation, and Uncertainty Quantification in Scientific Computing". In: *Radiation Res.: Computer Methods in Applied Mechanics and Engineering* 200.25–28 (2011), pp. 2131–2144.

[42] M. Salvatores, G. Aliberti, and G. Palmiotti. "The Role of Uncertainty Quantification for Reactor Physics". In: *Nuclear Data Sheets 123* 68.73 (2015). DOI: 10.1016/J.NDS.2014.12.012.

[43] Trucano T. G., M. Pilch, and W. L. Oberkampf. "General Concepts for Experimental Validation of ASCI Code Applications". In: ().

[44] Lewis E.E. and Miller W.F. *Computational Methods of Neutron Transport*. New York, NY: John Wiley & Sons, 1984.

[45] R. N. Slaybaugh and S. C. Wilson. "Deterministic Parameter Study for Fixed-Source Calculations Using ". In: *Trans. Am. Nucl. Soc* 108 (2013), p. 441.

[46] Edward Larsen. "Chapter 10: Spherical Harmonic (P_N) and Simplified Spherical Harmonic (SP_N) Approximations to the Boltzmann Equation". NERS 644 lecture notes.

[47] George I. Bell and Samuel Glasstone. *Nuclear Reactor Theory*. Division of Technical Information, US Atomic Energy Commission, 1970.

[48] Atkinson Kendall and Han Weiminn. *Spherical Harmonics and Approximations on the Unit Sphere: An Introduction*. Vol. 2044. Springer Science & Business Media, 2012.

[49] Evans Thomas M. et al. "Denovo: A new three-dimensional parallel discrete ordinates code in SCALE". In: *Nuclear Technology* 171.2 (2010), pp. 171–200. DOI: https://doi.org/10.13182/NT171-171.

[50] Jaakko Leppan. "Development of a New Monte Carlo Reactor Physics Code". PhD thesis. Helsinki Institute of Technology, Helsinki, Finland, 2007.

[51] Paul K. Roman et al. "OpenMC: A state-of-the-art Monte Carlo code for research and development". In: *Annals of Nuclear Energy* 82 (2015), pp. 90–97. DOI: https://doi.org/10.1016/j.anucene.2014.07.048.

[52] Los Alamos National Laboratory. *Monte carlo code group*. 2009. URL: https://mcnp.lanl.gov/.

[53] Radiation Safety Information Computational Center. *Information Digest*. Tech. rep. U.S. Nuclear Regulatory Commission, 2014.

[54] H. Grady III Hughes and Michael R. James. "MCNP6 Class". In: *MCNP6 class at Alabama Agricultural and Mechanical University* LA-UR-14-21281 (2014).

[55] M. B. Chadwick et al. "ENDF/B-VII.1 Nuclear Data for Science and Technology: Cross Sections, Covariances, Fission Product Yield". In: *Applied Mechanics Reviews* 57.5 (2011), 2887fffdfffdfffd–2996.

[56] Hesham Khater and Sandra Brereton. "Monte Carlo Simulation of the Prompt Dose Environment in the National Ignition Facility during Low Yield D-T Shots Article". In: *Progress in Nuclear Science and Technology* 2 (2011), pp. 389–394.

[57] E. Brun et al. "TRIPOLI4, CEA, EDF and AREVA reference Monte Carlo code". In: *Annals of Nuclear Energy* 82.1 (2015), pp. 151–160. DOI: https://doi.org/10.1016/j.anucene.2014.07.053.

[58] D. Long et al. "MONK10: A Monte Carlo Code for Criticality Analysis". In: *Proceedings of the ICNC 2015, Charlotte, NC, USA* (2015).

[59] U.S. Nuclear Regulatory Commission (NRC). *Serpent*. 2014. URL: http://montecarlo.vtt.fi/.

[60] R.M. Bergmann and J. L. Vujic. "Algorithmic choices in WARPfffdfffdfffdA framework for continuous energy Monte Carlo neutron transport in general 3D geometries on GPUs". In: *Annals of Nuclear Energy* 77.1 (2015), pp. 176–193.

[61] S. Agostinelli et al. "Geant4– a simulation toolkit". In: *Nuclear Instruments and Methods in Physics Research Section A: Accelerators, Spectrometers, Detectors and Associated Equipment* 506.3 (2003), pp. 250–303. DOI: https://doi.org/10.1016/S0168-9002(03)01368-8.

[62] S.C. Wilson and R.N. Slaybaugh. "Improved Monte Carlo Variance Reduction for Space and Energy Self-Shielding". In: *Nuclear Science and Engineering* 179.1 (2015), pp. 22–41. URL: https://doi.org/10.13182/NSE13-109.

[63] Richard H. Olsher. "A Practical Look at Monte Carlo Variance Reduction Methods in Radiation Shielding". In: *Nuclear Engineering and Technology* 38.3 (2006), pp. 225–230.

[64] J. S. Hendricks and T. E. Booth. "MCNP variance reduction overview". In: *Variance Reduction and Photon Transport, Part of the Lecture Notes in Physics book series* 240 (2006), pp. 83–92.

[65] Wagner John C. and Haghighat Alireza. "Automated Variance Reduction of Monte Carlo Shielding Calculations using the Discrete Ordinates Adjoint Function". In: *Nuclear Science and Engineering* 128.2 (1998), pp. 186–208.

[66] John C. Wagner, Edward D. Blakeman, and Douglas E. Peplow. "Forward-weighted CADIS Method for Variance Reduction of Monte Carlo Calculations of Distributions and Multiple Localized Quantities". In: *Proceedings of the 2009 Int. Conference on Advances in Mathematics, Computational Methods, and Reactor Physics, Saratoga Springs, NY*. 2009.

[67] Madicken Munk. "FW/CADIS-Ω: An Angle-Informed Hybrid Method for Neutron Transport". PhD thesis. University of California, Berkeley, 2017.

[68] D. Campolina and J. Frybort. "Uncertainty Propagation for LWR Burnup Benchmark Using Sampling Based Code Scale/Sampler". In: *Acta Polytechnica CTU Proceedings* 14 (2018), p. 8.

[69] T. Zhu et al. "NUSS-RF:Stochastic sampling-based tool for nuclear data sensitivity and uncertainty quantification". In: *Journal of Nuclear Science and Technology* 52.7–8 (2015), pp. 1000–1007.

[70] A. Aures et al. "Benchmarking and Application of the State-of-the-art Uncertainty Analysis Methods XSUSA and SHARK-X". In: *Annals of Nuclear Energy* 101.5 (), pp. 262–269.

[71] K. J. et al. Kelly. "Utilization of MCNP6 implicit-capture simulations for quantification of systematic uncertainties from experimental environments". In: *Nuclear Inst. and Methods in Physics Research* 954.161411 (2020). DOI: 10.1016/j.nima.2018.10.089.

[72] *International Reactor Dosimetry and Fusion File IRDFF v 1.05*. 2014.

[73] Y. F. Chen et al. "Surface Dose Rate Calculations of a Spent-Fuel Storage Cask by Using MAVRIC and Its Comparison with SAS4 and MCNP". In: *Nuclear Technology* 175.1 (2011), pp. 343–350.

[74] M. Cavazzuti. *Optimization Methods: From Theory to Design*. Berlin: Springer, 2013.

[75] C. A. Floudas and C. E. Gounaris. "A Review of Recent Advances in Global Optimization". In: *Journal of Global Optimization* 45.1 (2009), pp. 3–38.

[76] Eddie Davis and Marianthi Ierapetritou. "A. Kriging Based Method for the Solution of Mixed-Integer Nonlinear Programs Containing Black-Box Functions". In: *Journal of Global Optimization* 43.2–3 (2009), pp. 191–205.

[77] Marco Dorigo. "Optimization, Learning and Natural Algorithms". PhD thesis. Politecnico di Milano, 1992.

[78] Truyen Tran, Trung Thanh Nguyen, and Hoang Linh Nguyen. "Global Optimization using Levy Flights". In: *Second National Symposium on Research, Development and Application of Information and Communication Technology* (2004).

[79] I. Fister et al. "Cuckoo Search: A Brief Literature Review". In: *Studies in Computational Intelligence* (2014).

[80] Yongquan Zhou, Xinxin Ouyang, and Jian Xie. "A Discrete Cuckoo Search Algorithm for Travelling Salesman Problem". In: *International Journal of Collaborative Intelligence* 1.1 (2014), pp. 68–84.

[81] Xin-She Yang. *Nature-Inspired Optimization Algorithms*. 1st. London: Elsevier, 2014.

[82] Xin-She Yang. *Engineering Optimization*. John Wiley & Sons, 2010.

[83] S. Lin and W. Kernighan. "An Effective Heurisic Algorithm for the Traveling-Salesman Problem". In: *Operations Research* 21.2 (1973), pp. 498–516.

[84] Berkeley Research Computing. *System Overview*. 2018. URL: `http://research-it.berkeley.edu/services/high-performance-computing/system-overview`.

[85] Anthony Scopatz et al. *PyNE: Python for Nuclear Engineering*. 2012. URL: `https://pyne.io/`.

[86] A. D. Chanana. "Boron Neutron Capture Therapy of Glioblastoma Multiforme at the Brookhaven Medical Research Reactor, A Phase I/II Study". In: *FDA IND 43317* Protocol 4 (1996). DOI: `10.1063/1.2969289`.

[87] Jerome Maurice Verbeke. "Development of High-Intensity D-D and D-T Neutron Sources and Neutron Filters for Medical and Industrial Applications". PhD thesis. University of California, Berkeley, 2000.

[88] Mario Gomez-Fernandez et al. "Status of research and development of learning-based approaches in nuclear science and engineering: A review". In: *Nuclear Engineering and Design* 359.1 (2020), p. 110479.

[89] Gary. W. Cooper and Carlos L. Ruiz. "NIF total neutron yield diagnostic". In: *Review of Scientific Instruments* 72.1 (2001), pp. 814–817. DOI: `10.1063/1.1320997`. URL: `http://dx.doi.org/10.1063/1.1320997`.

[90] Hesham Khater et al. "Development of Nuclear Diagnostics for the National Ignition Facility". In: *Review of Scientific Instruments* 77.10 (2006), 10E715.

[91] "National Ignition Facility Neutron Sources". In: *HEART Tucson, AZ, United States*. April 16, 2018 through April 20, 2018.

[92] Lawrence Livermore National Laboratory. *National ignition facility*. 2016. URL: `https://lasers.llnl.gov/for-users/shot-ri-resources`.

[93] Lawrence Livermore National Laboratory. *National ignition facility*. 2016. URL: `https://lasers.llnl.gov/content/assets/docs/for-users/2016-user-guide.pdf`.

[94] D. A. Shaughnessy et al. *Development of Platforms for Nuclear Science Experiments at the National Ignition Facility*. Tech. rep. NNSA Stockpile Stewardship Quarterly, April 2018.

[95] Charles Yeamans et al. *Engineering Design of NIF and picture shot picture*. 2018.

[96] D. Eder et al. "Simulations of symcap and layered NIF experiments with top/bottom laser asymmetry to impose P1drive on capsules". In: *J. Phys.: Conf. Ser.* 717.012014 (2016).

[97] Warren J. Garbett, Hai P. Le, and Marilyn B. Schneider et al. "Development and modeling of a polar-direct-drive exploding pusher platform at the National Ignition Facility". In: *Physics of Plasmas* 25.072710 (2018). DOI: https://doi.org/10.1063/1.5025724. URL: http://aip.scitation.org/toc/php/25/7.

[98] Marley Edward. "Using X-ray Spectroscopy to Quantify Mix and Plasma Conditions in Ignition Experiments Using W-doped HDC Capsules at the NIF". In: *APS Division of Plasma Physics Meeting 2019* (2019).

[99] Mark D. Wilke et al. "The National Ignition Facility Neutron Imaging System". In: *Review of Scientific Instruments* 79 (2008), 10E529. DOI: https://doi.org/10.1063/1.2987984.

[100] Shaughnessy D. et al. "Radiochemical Measurements of Neutron Reaction Products at the National Ignition Facility". In: *248th ACS National Meeting* (2014).

[101] Z. A. Ali et al. "Tests and calibration of NIF neutron time of flight detectors. Review of Scientific Instruments". In: *Review of Scientific Instruments* 79.10 (2008), 10E527. DOI: 10.1063/1.2969289. URL: http://dx.doi.org/10.1063/1.2969289.

[102] Charlie Cerjan. *NIF Shots*. Personal Correspondence.

[103] M. Gatu Johnson et al. "High-resolution measurements of the DT neutron spectrum using new CD foils in the Magnetic Recoil neutron Spectrometer (MRS) on the National Ignition Facility". In: *Review of Scientific Instruments* 79.10 (2008), 10E529. DOI: https://doi.org/10.1063/1.2987984.

[104] H.G. Rinderknecht et al. "A novel particle time of flight diagnostic for measurements of shock- and compression-bang times in D^3He and DT implosions at the NIF". In: *Review of Scientific Instruments* 83 (2012), p. 10D902. DOI: https://doi.org/10.1063/1.4731000.

[105] Glenn F. Knoll. *Radiation Detection and Measurement*. 3rd. Ed. John Wiley & Sons, Ann Arbor, 2000.

[106] S. P. Tripathy et al. "Activation Foils Unfolding for Neutron Spectrometry: Comparison of Different Deconvolution Methods". In: *Nuclear Instruments and Methods in Physics Research, Section A: Accelerators, Spectrometers, Detectors and Associated Equipment* 583.2–3 (2007), pp. 421–425.

[107] R. Gunnink and J.B. Niday, eds. *Computerized Quantitative Analysis by GAMMA-RAY Spectrometry. VOLUME I. Description of the GAMANAL Program*. UCRL-51061. NSA-26-045265. California Univ. and Livermore. Lawrence Livermore Lab. 1972.

[108] F. G. Perey. "Least-Squares Dosimetry Unfolding: The Program STAYSL". In: *Applied Mechanics Reviews* (1977).

[109] B. T. Rearden, M. A. Jessee, and al., eds. *User Guide for the STAYSL PNNL Suite of Software Tools*. OPNNL-22253. Available from Radiation Safety Information Computational Center as CCC-834. Pacific Northwest National Laboratory. 2013.

[110] L. Greenwood and C. Johnson. "Least-Squares Neutron Spectral Adjustment with STAYSL PNNL". In: *EPJ Web of Conferences* 106.5 (2016), p. 07001.

[111] URL: `http://www.whiterockscience.com/moritz.html`.

[112] J . A . Bucholz and C . Frankle. "Modeling and Assessment of Concrete and the Energy Infrastructure". In: *DOE Office of Scientific and Technical Information* (). URL: `https://www.osti.gov/servlets/purl/758827`.

[113] B. Appelbe and J. Chittenden. "Relativistically correct DD and DT neutron spectra". In: *High Energy Density Physics* 11 (2014), pp. 30–35.

[114] S. R. Johnson and K. T. Clarno. "Comparison of SCALE and MCNP Results for Computational Pebble Bed Benchmarks". In: *Trans. Am. Nucl.* 96.1 (2007), pp. 420–422.

[115] H.L. Poss et. al. "Total Cross Sections for 14-MeV Neutrons". In: *Fusion Science and Technology* 87.2 (1952), pp. 11–20.

[116] Richard Proocassini and Michael Scott McKinley. "Modern Calculations of Pulsed-Sphere Time-of-Flight Experiments Using the Mercury Monte Carlo Transport Code". In: *Joint International Conference on Supercomputing in Nuclear Applications and Monte Carlo (SNA + MC2010)* (2010).

[117] N. J. Quartemont et al. "fffdfffdfffdAnalysis of an Energy Tun-ing Assembly for Simulating Nuclear Weapon Environments at the National Ignition Facility.fffdfffdfffd." In: *Journal of Radiation Effects* 72 ((Accepted 2020)).

[118] Jerome M. Verbeke, Jasmina L. Vujic, and Ka-Ngo Leung. *Neutron Beam Optimization for Boron Neutron Capture Therapy Using the D-D and D-T High-Energy Neutron Sources*. Tech. rep. May 2017, pp. 257–278. DOI: `https://doi.org/10.13182/NT00-A3061`.

[119] E Greenspan et al. "SWANS: A Prototypic SCALE Criticality Sequence for Automated Optimization Using the SWAN Methodology". In: ORNL/TM-1999/274. 1999.

[120] D.L. Bleuel. "Determination and Production of an Optical Neutron Energy Spectrum for Boron Neutron Capture Therapy". PhD thesis. University of California Berkeley, 2003.

Appendix A

Reproducibility

This appendix contains the location of the input and codes written for the sake of this thesis. They are provided for the purposes of both documentation and reproducibility, that anyone with a license for the codes might be able to run them. The only *caveat* is that the MCNP input file of the full NIF model system are not accessible to the public. Thus, for those inputs it is required a formal request through the Computational Engineering Division at NIF, LLNL.

The underlying, public available, documentation presented for this research is located in an online repository at https://github.com/SandraBogetic/PHD. The main page also includes the thesis, experiment collaboration, briefs, and the models used for SCALE and MCNP. The main page also includes information on the NIF source and some mechanical drawings and pictures of NIF components and ETA. The site of the Gnowee/COEUS v1.0. and v2.0. are below provided too. Much of this work may provide useful tools to others needing to tailor neutron spectrum at NIF. The thesis and the online files provide, for future users, a process to perform ETA designs with the help of the Gnowee/COEUS design framework. Some simple modifications to the process will allow also users from outside NIF to design automatic ETAs. A list of tools that will be most beneficial for others is presented below:

- Python script for providing MCNP input files for the MCNP full NIC target chamber input files. Several Python 2.7 and 3 scripts were created to read in data files produced from MCNP and to produce NIF MCNP input files:
  `https://github.com/SandraBogetic/PHD/Python_NIF`
- MCNP Input files. In the folder are provided input files for the SNOUTs used in the S1 to S4 campaigns, the HTOAD designs for the H1 to H3 experiments. These models are in general used for the primary purpose of determining the flux distributions and reaction rates for each campaign scenario, using the rigorous particle transport methods of the MCNP code. Also, the folder provides the ETA MCNP input files used in Chapter 8:
  `https://github.com/SandraBogetic/PHD/MCNP_input`

APPENDIX A. REPRODUCIBILITY

- MCNP like-input files for COEUS v2.0:
  `https://github.com/SandraBogetic/PHD/MCNP_InputMaker`
- CAD designs for NIF:
  `https://github.com/SandraBogetic/PHD/Experiment_CAD`
- STAYSL Unfolding spectra:
  `https://github.com/SandraBogetic/PHD/STAYSL`
- COEUS:
  `https://github.com/SlaybaughLab/Coeus/`
- Gnowee:
  `https://github.com/SlaybaughLab/Gnowee/`
- New COEUS process and examples:
  `https://github.com/SlaybaughLab/Coeus/tree/NEW_COEUS`
  `https://github.com/SlaybaughLab/Coeus/tree/BNCT`

Appendix B

Experimental Procedure

Here I describe the standard operating procedure for the NIF Experimental Platforms used: the SNOUT-mounted auxiliary experiments (passive). Many neutron experiments are assembled onto a single NIF shot, the NIF diagnostic manipulators are, in fact, used to carry ride-along experiments on neutron-yielding shots and this capability is readily accessible to all collaborating groups.

The procedure used at NIF for the experiments in Chapter 7 are below summarized. The first step for performing the experiments as those in Chapter 7, is the designing of a NIF experiment that can be fielded in 6 months with available resources and known material: with MCNP and with CAD for the engineering designs. An example of the CAD 3D designs, for the SNOUTS, are shown in Figures B.1 and B.2. Then the NIF engineering office releases the engineering designs for the experiments, Figures B.3. The components designed are built in the NIF machine shop as seen in Figure B.4 there is a picture of the just built SNOUT used in Chapter 7. The main components are built in the NIF machine shop. The experimental designs then follow few steps in order to be performed at NIF:

- The experiments enter through the NIF User Office or specific programs;
- Any NIF DT yield shot may support additional experiments through coordination with the campaign experimental team. This includes NIF facility neutron calibration shots as well as programmatic.
- Experiments are designed into a diagnostic instrument manipulator (DIM) or Target and Diagnostic Manipulator (TANDM), with design based on fluence an volume requirements.
- Experiments allocated through accepted program proposals (JNSAC/NSA, HED and ICF councils, Discovery Science) can select their experimental configuration to best use the allocation.

- Optics Use. NIF is a rare laser facility operating above the optics damage threshold. A computational laser performance model helps determine the optics use per proposed laser shot in units of damage log growth;
- Shot cycle length. Allocation is usually made in user days. Neutron yield shots have lengthy neutron mitigation procedures. Typical planning is one yield shot per user day.
- Debris and Shrapnel. The experimental planning process at NIF focuses on machine safety and maintaining experimental throughput.

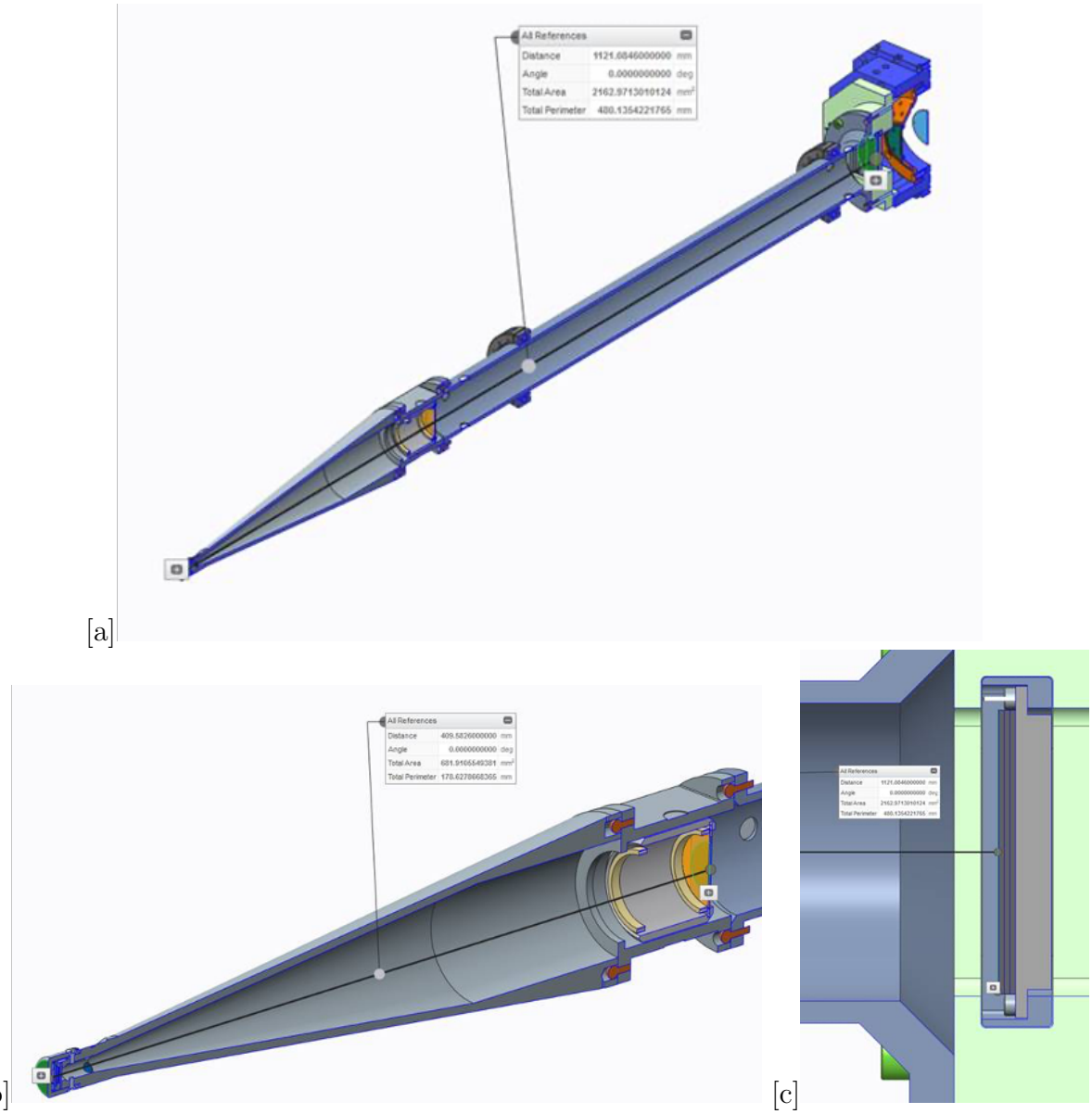

Figure B.1: CAD 3D cross section of the SNOUTs used in the 90-348 TANDM: a) of the full SNOUT; b) SNOUT cone and close up of the foil pack inserted in the basket; c) close up of the foil pack inserted in the kinematic base. The 3D CAD presents the distances of each component from the TCC.

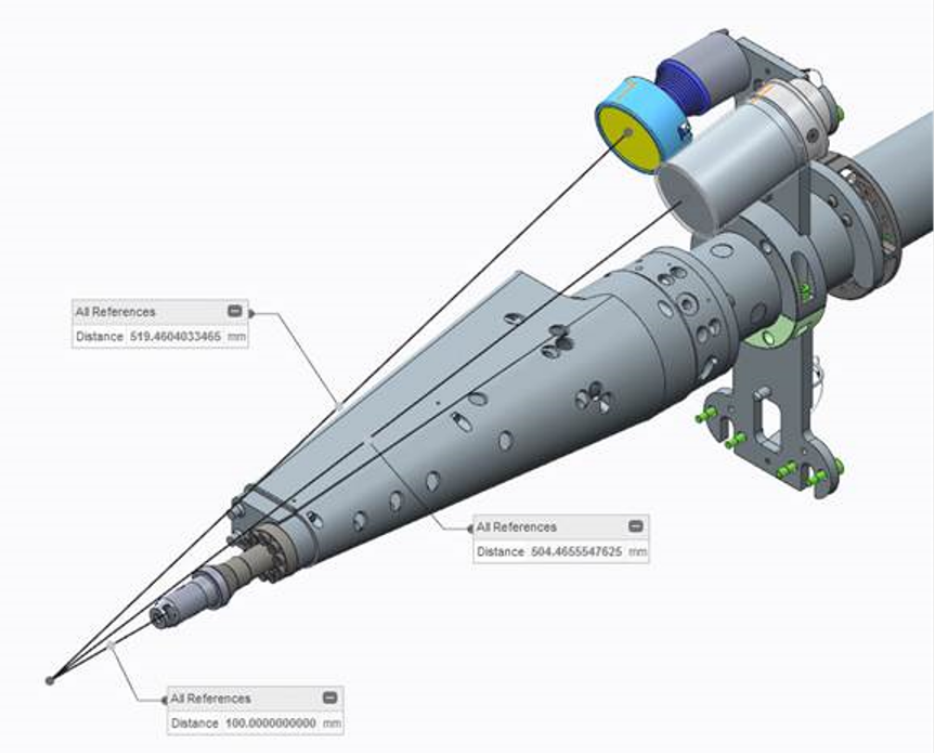

Figure B.2: CAD 3D cross section of the SNOUT's cone and SRC used in 90-78. The cone and the added SRC are the main difference with the other SNOUT. It is visible the HTOAD inserted. The 3D CAD presents the distances of each component from the TCC.

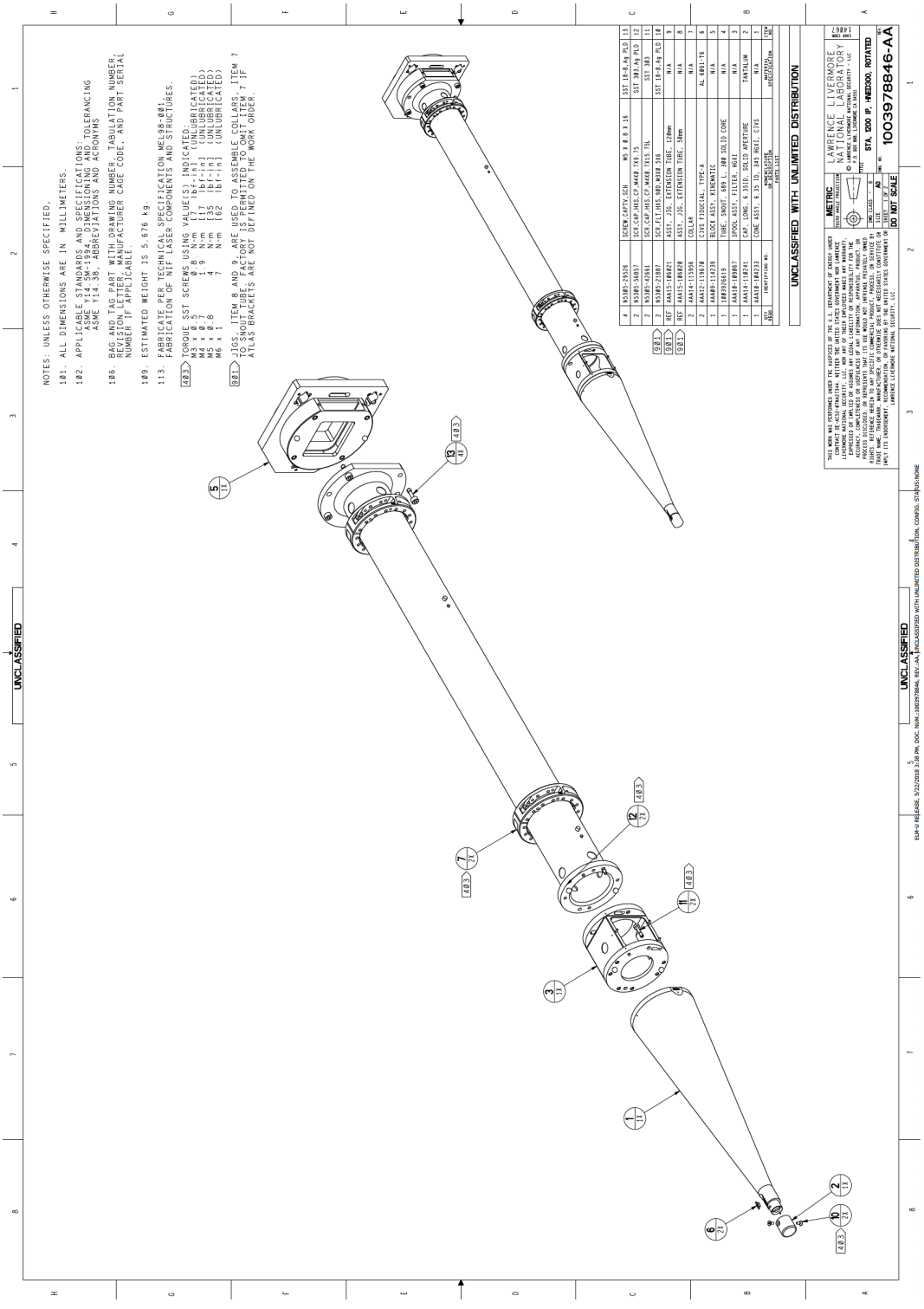

Figure B.3: Engineering drawing of the SNOUT located at 90-348

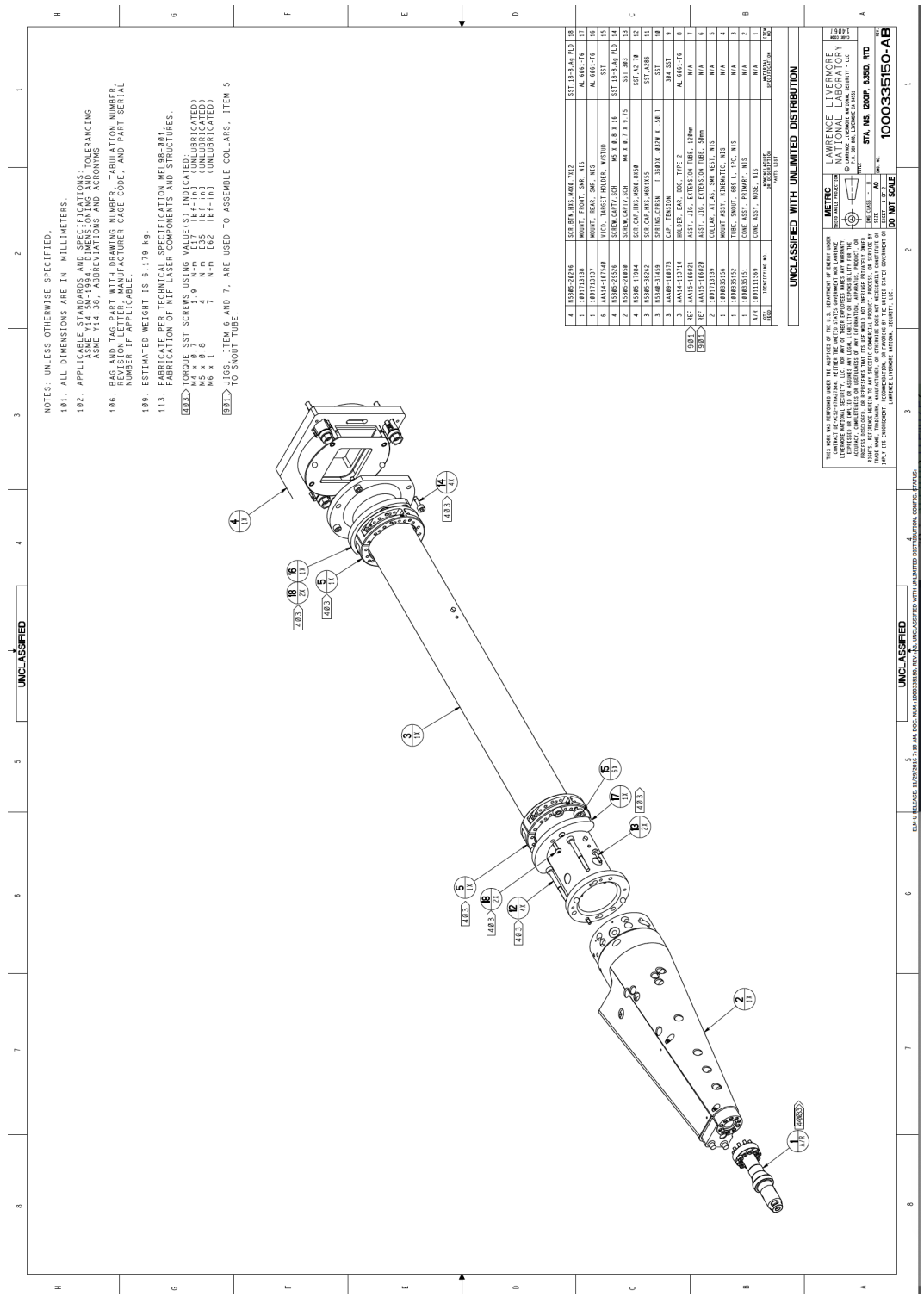

Figure B.4: Engineering drawing of the SNOUT located at and 90-78.

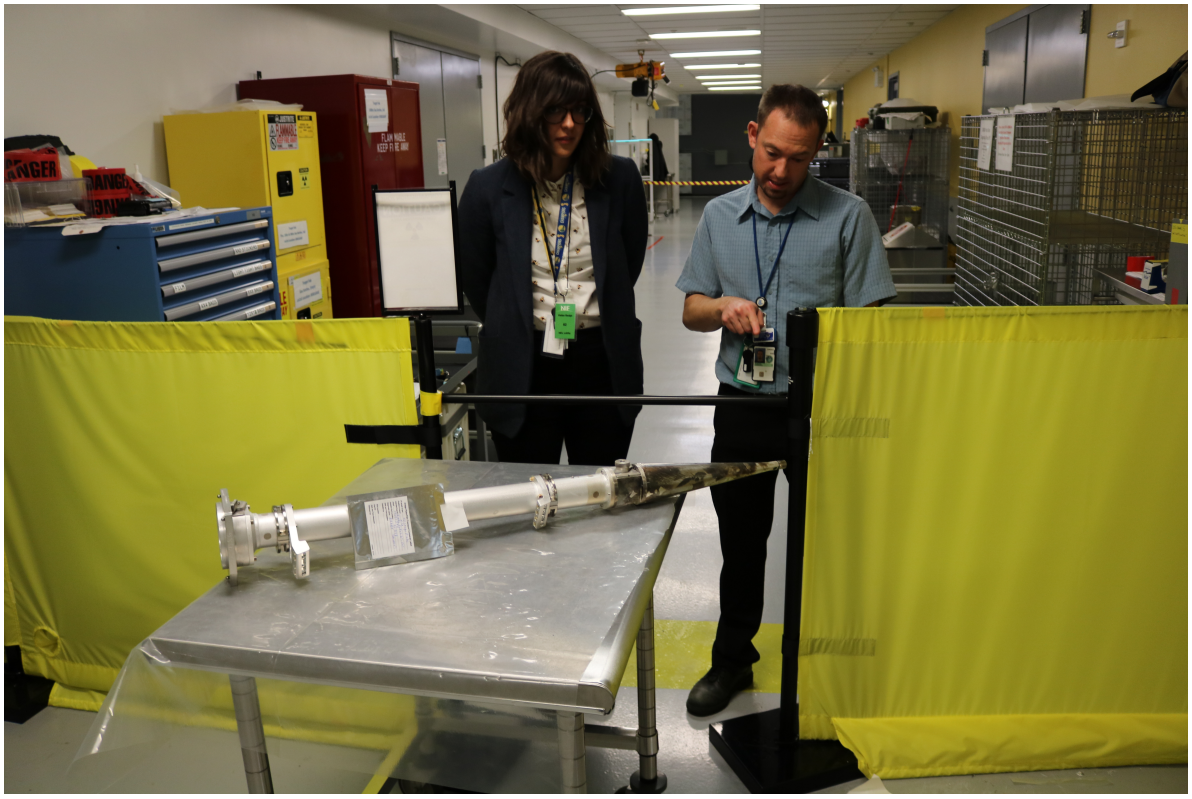

Figure B.5: Picture of the Author at the machine lab at NIF with Dr. Charles Yeamans.

Appendix C

Future Example Applications for COEUS v2.0

This chapter wants to provide an overview of few alternative application that have been investigate when further developing the code. Those examples are her given as suggestion and guidelines for user seeking to use Gnowee/COEUS v2.0 for those applications. For each example it is provided a quick overview of: the ETA geometry, the constraints and the possible objective function.

C.1 Medical Isotope Production

Medical isotope production is a fairly big business, and it appears that the target designs are usually optimized by: experience, back of the envelope calculations and parametric studies. The basic idea of this application is to generate as much of an isotope X as possible while avoiding other isotopes that are difficult to separate from the irradiated sample. Based on the relative cross-section of the two or more reactions, there will be an optimal beam energy that is obtained by a) tuning the incident neutron beam or b) degraders. Since beams is expensive and limited, often a stackup of irradiation is performed at once to generate multiple medical isotopes in sequence as the beam downshifts in energy through the irradiated sample and degraders. These beams can be either charged particle or neutrons. The goal is to automatically provide an ETA design to satisfy the requirement starting from any available source. For this type of application the needed input, implemented in MCNP or other transport codes, include the:

- **Geometry**. Typically present a stackup of layered materials. It maybe possible that a 2D matrix would also be desirable, primarily for neutron beams;
- **Constraints**. Typically there are not difficult constraints here outside of physics. Space and mass can be a limit depending on the facility. This may be more of a consideration for neutron beams than charged particles. It is also possible to incorporate

the maximum bad/good isotope ratios if the goal is to produce the maximum number of atoms up to some contamination percentage;

- **Objective Function**. The objective functions can be the sum of the number of atoms created for each isotope (with or without preference weighting) or the ratio of bad to good isotopes. It is possible that both of these will are objective functions of interest and need to be combined. Each calculation is possible to be done inside of a tally or multiple tallies, but the combination and weighting needs is handled elsewhere in post-processing by the user.

C.2 Fusion Blanket Design

Generating sustainable fusion is only half of the problem. Once that happens, to make it economically viable, the energy must be harvested and new tritium must be bred. This is typically done in a blanket that surrounds the core. For this type of application the needed input, implemented in MCNP or other transport codes, include the:

- **Geometry**. These typically are in some layered spherical or elliptical geometry. There is typically some level of symmetry, and the problem can be simplified to 1D or perhaps 2D, to accelerate the calculations.

- **Constraints**. Few constraints can be here introduced separately or simultaneously: there is typically a minimum tritium breeding ratio and energy capture rate; there could be a maximum tritium breeding ratio; and weight/size constraint.

- **Objective Function**. While there may be a lower bounds for the minimum tritium breeding ratio and energy capture rate, these are typically desired to be maximized. This problem can be treated as a multi-objective function, or the objectives can be combined into a single objective (either weighted or unweight);

The complexity of this application comes from implementing materials that can have varying weight/atomic fractions and that follow requirements/relationships dictated by materials science.

C.3 Inverse Problems

There are many applications covered under this scope that might be useful. The general concept is that there is a specific known measurement, and the goal is to know what is the source causing that measurement. This type of problem could be complicated by an intervening environment that is either known or variable. For this type of application the needed input, implemented in MCNP or other transport codes, include the:

- **Geometry**. Here the geometry can be anything. It can also be a fixed value or have variable components. The source can itself be a variable (energy, distribution, size, location, etc);
- **Constraints**. The constraints vary widely depending on the specific application, but some to consider are masses of materials, ordering of materials, types of sources, and source intensities, among others;
- **Objective Function**. This can be formulated many ways but in essence is a comparison to data measurement(s)/observation(s). This will likely require post-processing of multiple tallies. It is possible that multi-objective optimization would be an improvement, but it is believed that these can be solved with single objective optimization;

It is likely that a different code will be desired for this application, so that a new input-like file needs to be created following the rules of the desired code. A challenge for the user is to properly determine the correct objective functions and related tallies.